Table of Contents

List of Tables

Table of Figures

Table of Diagrams

List of Abbreviations

Al	Aluminium
Mg	Magnesium
Si	Silicon
Fe	Iron
Mn	Manganese
Cr	Chromium
B	Boron
Ti	Titanium
Cu	Copper
6II	Homogenized at 560°C, standard cooling
8II	Homogenized at 580°C, standard cooling
sc	Homogenized at 580°C, slow cooled
st	Homogenized at 580°C, step cooled
wq	Homogenized at 580°C, water quenched
4IIf	Homogenized at 540°C, standard cooling
6IILab	Homogenized at 560°C, standard cooling
8IILab	Homogenized at 580°C, standard cooling
vdc	Vertical direct chilled (sub contractor)
hdc	Horizontal direct chilled (own production)
Mg_2Si	Magnesium-Silicide
U2-AlMgSi	Aluminium-Magnesium-Silicide
AlFeSi	Aluminium-Iron-Silicide
HF	Hydrofluoric acid
HCl	Hydrochloric acid
HBF_4	Fluoroboric acid
R_p	Yield Point
R_m	Tensile Strength
ε	Strain
DSC	Differential scanning calorimetry
TEM	Transmission electron microscopy
SEM	Scanning electron microscopy
EDX	Energy dispersive X-ray diffraction
PSCT	Plain strain compression test
LOM	Light optical microscopy
$R_{p0.2}$	Stress at a plastic deformation of 0.2%
$R_{p1.0}$	Stress at a plastic deformation of 1.0%

1 Introduction

Because of the good strength/density ratio of Aluminium it is widely used in automotive industry. During production and extrusion, the mechanical resistance against deformation should be quiet low to reduce the demand of deformation force and deformation energy. In the final product, the mechanical properties should fulfil all demands.
To meet all requirements, an intelligent design of microstructure (grain size, precipitations, morphology, etc.) is necessary.
After casting of the billets the microstructure of the billets is dendritic. Between the dendritic arms are coarse precipitations of an Mg/Si phase (π-phase or a Mg_2Si phase) and a plate-like AlFeSi phase. Therefore it is necessary to submit the billets to a heat treatment. The first target of this treatment, which is called homogenization, is to transform the brittle, plate-like AlFeSi phase (which can cause cracks during extrusion) into a pearl-necklace distributed AlFeSi phase. The second aim is to dissolve the coarse Mg/Si phase which should be precipitated in nano-scale sized particles of Mg_2Si to increase the strength of the final product.

The main aim of this work is to obtain a tailor-made microstructure to have on one side good extrudability, which means low extrusion pressure, high extrusion speed and an absence of surface defects. Furthermore the time for heat treatment should be lowered to be able to increase the output of the furnace. On the other hand, the mechanical properties of the extruded profile should meet all requirements of standards and customers.

2 Theory

2.1 Precipitations

2.1.1 Mg/Si

Both Mg and Si are soluble at higher temperatures in solid (and liquid) aluminium, but during cooling they precipitate dependent on the cooling conditions in a different type of morphology[4,10].

Table 2.1 Different types of Mg/Si precipitations[26]

Phase	Shape	Formula	Space group	a [nm]	b [nm]	c [nm]	β	γ
GP-zone	Needle	$AlMg_4Si_6$	C2/m	1.48	0.405	0.648	105.3°	
GP-zone	Plate	Si/Mg=1	(fcc $L1_0$)	0.405				
β''	Needle	Mg_5Si_6	C2/m	1.516	0.405	0.674	105.3°	
β''	Needle	$Mg_{1.8}Si$	$P6_3$	0.715	0.715	0.405		120°
B' (C)	Lath	Mg/Si~1	Hexagonal	1.04		0.405		120°
U1 (A)	Needle	$MgAl_2Si_2$	$P-_{3m1}$	0.405		0.674		120°
U2 (B)	Needle	AlMgSi	Pnma	0.675	0.405	0.794		
β	Plate/cube	Mg_2Si	F_{m-3m}	0.6354				
Si	Plate	Si	F_{d3m}	0.5431				

At high temperatures, all Mg and Si are dissolved in the solid Al matrix. During cooling, clusters of Mg and Si are formed. These clusters transform into Guinier Preston zones (GP-zones) during cooling, which are fully coherent[4,10].
These GP-zones transform into needle shaped β''-Mg_2Si particles with a thickness of 1-2 nm and a length of ~10nm[10].
On further cooling or during holding at a temperature between 300 and 400°C cylindrical β'-Mg_2Si particles are formed, which are semi-coherent[10,14].
At temperatures higher than RT these β'-Mg_2Si particles transform into β-Mg_2Si platelets, which are fully incoherent[10].

The overall sequence of precipitation of the Mg_2Si phase is:

SSSS ➔ GP-zones ➔ β''-Mg_2Si (needles) ➔ β'-Mg_2Si (rods) ➔ β-Mg_2Si (plates)

β-Mg_2Si is fcc (CaF_2 type) with a lattice parameter a= 0.64nm[10]. β-Mg_2Si precipitates during slow cooling from 500°C to 400°C. If the alloy is cooled fast from 500°C to 400°C but slowly cooled from 400°C to 300°C, the Mg and Si is precipitated as β'-Mg_2Si[10,14]. The phases U1 and orthorhombic U2 can appear together with β'' and β', the size of these intermetallic phases is smaller than <100nm.

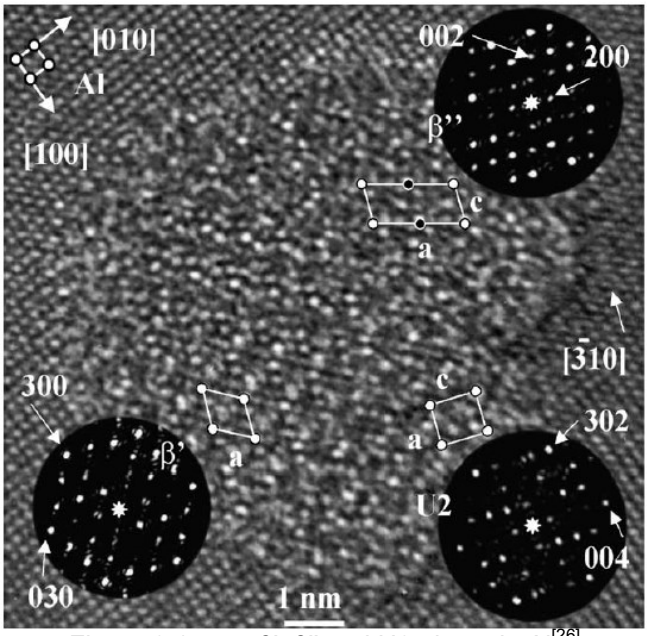

Figure 2.1 β', β'' and U2 phase in Al[26]

However the nature of the precipitations depends on the chemical composition of the alloy and the thermal history. The β' phase has the strongest hardening effect. A Mg:Si ratio of 5:6 in the alloy favours the formation of Mg_5Si_6.[26]

2.1.2 AlFeSi

AlFeSi is the common name of iron-containing phases, however the correct composition is Al(Fe,Mn,Cr)Si, because this phase also contains a significant amount of Mn and Cr in case of the alloy 6082.
There are different structures of AlFeSi intermetallics[24]:

Table 2.2 Different types of AlFeSi[24]

Intermetallic phase	Composition	Fe:Si ratio
α-AlFeSi	Al_7Fe_3Si	6
	$Al_{12}Fe_3Si$	6
	Al_8Fe_2Si	4
	$Al_{15}Fe_3Si_2$	3
β-AlFeSi	Al_5FeSi	2
π-AlFeSiMg	$Al_7FeMg_3Si_6$	1/6

During casting, Fe precipitates mainly as AlFeSi on the grain boundaries[5].
There are 3 different crystal structures associated with morphologies of AlFeSi:

monoclinic β-AlFeSi a=b=0.612 nm, c=4.15 nm, β=91°
cubic α-AlFeSi a=1.252-1.256 nm
hexagonal α'-AlFeSi a=1.23 nm, c=2.62 nm
[5, 20]

Fe is preferably incorporated in AlFeSi so that about 15% of the Si in the alloy can be lost as AlFeSi depending on the Fe content.

In the as cast billets most of AlFeSi exists as platelets with a monoclinic β-AlFeSi crystal structure on the grain boundaries[1], the particles have a length of ~10µm, the thickness is in the order of 100nm[6]. A typical β-AlFeSi particle is shown in figure 2.2.

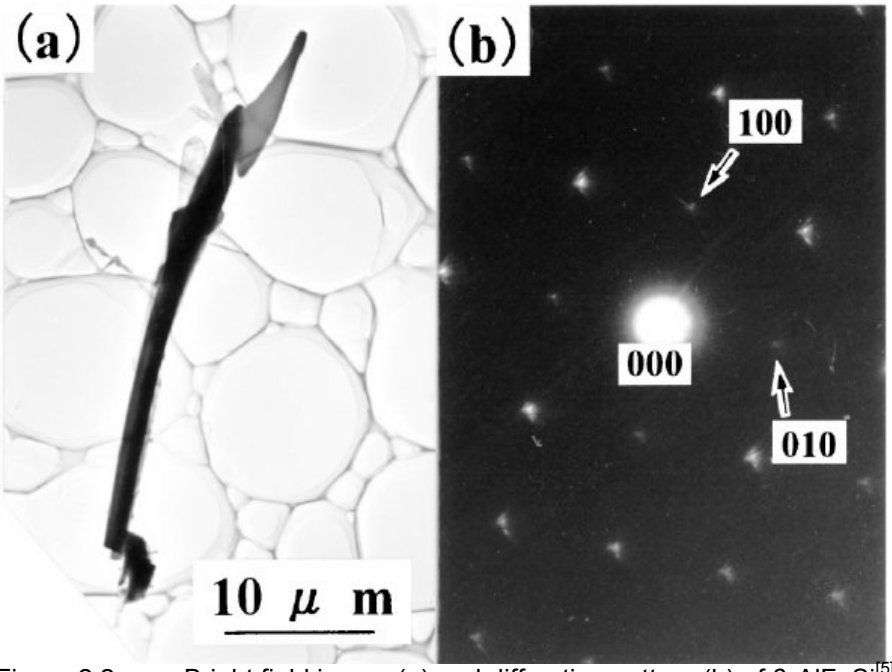

Figure 2.2 Bright field image (a) and diffraction pattern (b) of β-AlFeSi[5]

This β-AlFeSi causes deformation cracks during billet extrusion because of the small cohesion between the precipitations and the Al matrix (pick-up effect[18]). Furthermore, the monoclinic phase is very brittle, which contributes to crack formation[1]. A further reason for cracks caused by the β-phase is a stress field around the precipitations due to volume changes during precipitation[18].
During heat treatment the platelets of β-AlFeSi transform into pearl necklace distributed α-AlFeSi[1]. The transformation starts on the surface of the β platelets, the driving force for the transformation is the smaller surface energy of the α[1,18]. The reaction is diffusion controlled and responds to the Johnson-Mehl-Avrami equation[1]. The diffusion of Fe is much slower than the diffusion of Si, as a result the speed of Fe diffusion limits the transformation speed[1].

Very important for the transformation of β to α/α' is a small amount of Manganese, furthermore Vanadium accelerates the transformation[26,18].If there is no Mn in the alloy, no transformation of β into α is observed, there is only a coarsening of the β platelets[1].
An increase of 0.01% Mn content doubles the transformation speed[7]. If the Mn content is lower than 0.08%, there are no negative effects expected on mechanical properties[17]. By increasing the homogenization temperature from 585°C to 600°C the β to α transformation speed is increased by 150% [7]. If the Mn content is lower than 0.02%, the β transforms mainly to the hexagonal α', if the Mn content is higher than 0.02%, the β transforms mainly to the cubic α [1]. A typical α-AlFeSi particle is shown in figure 2.3. With increasing Mn content also the transformation speed increases, but there is no further increase at Mn contents higher than 0.2%[1]. Also Si influences the transformation speed, with a smaller Si content the transformation speed increases, but the effect is smaller than for the Mn addition[1,7]. There is no influence of the Mg content to the β to α transformation[1].

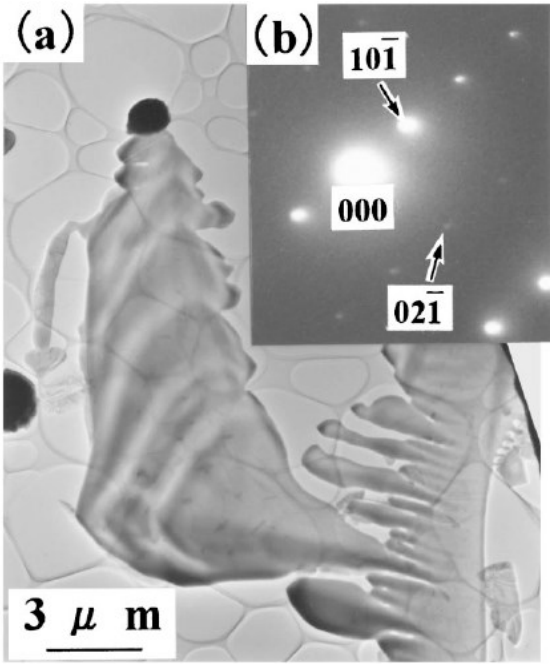

Figure 2.3 Bright field image (a) and diffraction pattern (b) of α-AlFeSi[5]

During the β to α transformation, the Si content of the AlFeSi decreases and the Fe content increases, because Fe from the matrix (and also from other precipitations) diffuses into the AlFeSi particles. As a result, the Fe:Si ratio can be used to distinguish between α and β. Furthermore, it's possible to discriminate between α and β because of their geometrical morphology, because α has a Chinese script style, β appears like needles in metallographic specimen.[6]
Al_3Fe, $AlFeSi_2$ and Al_3FeSi cannot exist in 6082 alloy as the small Fe content does not permit their formation under the given process conditions[1].

2.1.3 Si

In some cases elemental Si occurs in cast Al alloys[22]. This Si dissolves within 2 minutes at a temperature of 558°C [22]. This results in a Si rich solution of α-Al.
Especially, if the Mg:Si ratio in the alloy is low, elemental Si will be precipitated.

2.2 Homogenization Treatment

2.2.1 Purpose of the Homogenization Treatment

The main purpose of the homogenization treatment is the modification of the AlFeSi and the dissolution of the coarse Mg_2Si and subsequent precipitation of fine Mg_2Si particles. As a result of this change in microstructure the extrudability increases.
The dissolution of Mg_2Si takes place within a short time (20 min or less). However, the modification of the Si rich, brittle β-AlFeSi into the Fe rich, "ductile" α-AlFeSi determines the lower limit of the heat treatment duration.[1,6]

2.2.2 Holding Temperature during Homogenization

Most papers suggest a homogenization temperature of 580°C [1, 3, 11, 13, 16, 19], some papers suggest 585°C [5, 7, 14, 20, 21] and only few papers suggest a lower temperature (560°C) [2]. In equilibrium the following reaction starts at 576°C:

$Al + Mg_2Si + \beta\text{-AlFeSi} \rightarrow liq. + \alpha\text{-AlFeSi}$ [21]

The appearance of a liquid phase is limited to a small area (µm-size, only at the surface of the AlFeSi particles), as a result the shape of the billets remains unaffected. The reaction speed of the β to α transformation increases with the temperature. Between 585°C and 595°C (depending on the alloy composition) melting of the alloy begins:

$Al + Mg_2Si \rightarrow liq.$ [21]

If the homogenization temperature is high, generally the transformation starts and ends earlier. [4]

2.2.3 Cooling Conditions after Homogenization

Invitingly, different authors suggest totally different cooling conditions after homogenization. The content of dissolved elements in the Al matrix increases with increasing cooling rate[2].However the cooling rate should not be faster than 200°C/h, otherwise most of the Mg and Si remains in the matrix and the extrusion pressure increases due to a supersaturated solid solution. On the other hand, the cooling speed must be higher than 100°C/h, otherwise the precipitations of Mg_2Si will become too coarse.[3] Hardness measurements at room temperature show the highest hardness of water quenched samples, at slow cooling rates (cooling inside the furnace) the hardness was low.[4] In water quenched samples the extrusion pressure is high because the matrix contains most of the Mg and Si in solid solution[14].One advantage of water quenched samples is that melting of Mg_2Si cannot occur[21].
Some authors suggest a step cooling:
By quenching from homogenization temperature to 350°C and holding for 1 hour and quenching to room temperature a good extrudability (low pressure) was found. The reason for this are semi-coherent, hexagonal particles of β'-Mg_2Si. These particles are stable until the massive deformation inside the tool, there the particles dissolve within seconds and precipitate after the tool exit to give a good strength in the extruded profile. A proper temperature control is essential for this method.[14] Also good results were found at step cooling to 250°C-300°C (holding time 2h). Most of the Mg and Si precipitate as fine particles and the yield strength during extrusion is low.[3]

2.3 Calculation of the Effective Temperature during Extrusion

After cooling from homogenization temperature the billets are heated to 480-490°C in a preheating furnace. Depending on the temperature after the preheating furnace and the drop in temperature (~10K) through the transport from the furnace to the recipient the temperature directly after the extrusion machine will be between 510 and 520°C. A temperature above 500°C is essential for a good extrusion process. Approximation assuming adiabatic conditions [30].

$$\Delta T = \frac{k_{fm} \cdot |\phi_{max}|}{\rho \cdot c_p} \qquad \text{Temperature difference} \qquad (1)$$

$$\phi_{max} = \ln\left(\frac{A_1}{A_0}\right) \qquad \text{Logarithmic deformation} \qquad (2)$$

$$\phi_{max} = \ln\left(\frac{d_1^2}{d_0^2}\right) \qquad (3)$$

$d_0 = 203\,mm$ Billet diameter

$d_1 = 58\,mm$ Profile diameter

$\phi_{max} = -2.51$

$k_{fm} = 40\,MPa$ Flow stress (measured)

$\rho = 2700\,\frac{kg}{m^3}$ Density

$c_p = 897\,\frac{J}{kg \cdot K}$ Specific heat

$\Delta T = 41.4\,K$

3 Experimental Methods

The microstructure before and after the homogenization was compared with Light Optical Microscopy (LOM) and Scanning Electron Microscopy (SEM) + Energy Dispersive X-Ray Diffraction (EDX).

3.1 Chemical Composition of the used Alloys

The analyzed material was a 6082 Al-Mg-Si alloy, which is rich in Mg, Si, Mn and Cr. There is also a high iron content as a result of a high scrap rate in the melting furnace.

Table 3.1 Chemical composition of the alloys

Material	Alloy	Homog. time	Homog. temp.	Si	Fe	Cu	Mn	Mg	Cr	Zn	Ti
hdc billet	6082	04:30	560°C	1.14	0.24	0.06	0.54	0.85	0.17	0.03	0.03
vdc billet	6082	06:00	540°C	1.11	0.22	0.07	0.52	0.83	0.16	0.03	0.02

3.2 Light Optical Microscopy (LOM)

For LOM polished and etched sampled were observed. The maximum resolution is 0.5-1µm (wavelength of the optical light). Used microscope: AXIO Imager A1, Zeiss

3.2.1 Barker Etchant

For this electrolytic etching method two different methods were used:

- 5% HBF_4, Voltage 20V for 1 minute (solution 1)
- 13g boric acid, 35g HF, 800ml H_2O, Voltage 20V for 45 seconds (solution 2)
  Solution 2 gives a much better contrast in the homogenized samples.

3.2.2 Hydrofluoric Acid Etchant

To make grain boundaries and precipitations visible the polished samples were etched in 4% HF for 10 sec.

3.3 Scanning Electron Microscopy (SEM)

For scanning electron microscopy (SEM) polished samples should be used for best optical and EDX results . The maximum resolution is 10nm. The accuracy of the EDX (INCA, Energy 200, Oxford Instruments) result should be ±0.1% because of fluorescence, absorption and influences of the atomic number. Used microscope: Quanta 200 3d, FEI

3.4 Transmission Electron Microscopy (TEM)

For TEM very thin samples are needed, the material was ground, polished and dimpled to a thickness of 30µm and finally ion polished (Precision Ion Polishing System PIPS, Gatan model 691). For the observation a Philips CM12 microscope, operating at 120 kV, was used. Because of the sample holder, which consists of beryllium and copper, copper was always visible in the EDX scan, this copper content wasn't considered in the analysis.

3.5 Differential Scanning Calorimetry (DSC)

To identify the temperatures where phase transformations take place DSC experiments were done with cylindrical, 50 mg (±0.1mg) samples in a Perkin Elmer Diamond Differential Scanning Calorimeter (DSC). DSC samples with a diameter of 5mm and a height of 2mm were turned and then grounded to a sample weight of 49.9mg. These samples were heated from 50°C to 700°C with a heating rate of 20 K/min, the holding time at 700°C was 1min and then the samples were cooled down to 50°C again with a cooling rate of 20 K/min. The peaks during the cooling period are of no importance because this peaks show the precipitation and not the dissolution of the particles (and during homogenization the dissolution of the particles is important), furthermore the peaks during cooling must not be Mg_2Si and Si. It is noteworthy the DSC is calibrated for heating and not for cooling period.

3.6 Thermo-Calc

Thermo-Calc is a software package for thermodynamic and phase diagram calculations. It is possible to do equilibrium and non-equilibrium calculations (Scheil). For the calculations the TTAL5 database was used.

3.7 Plain Strain Compression Test (PSCT)

There is a linear relation between the flow stress of Aluminium and the extrusion pressure[19]. For this test samples with the dimension of 25 x 20 x 10 mm were squeezed at the average extrusion temperature of 480°C. The test was done on a Stress/Compression test machine, for preheating a tube furnace was used.
For the compression tool heat resisting steel (1.2343) was used.

For the PSCT test, the furnace was pre-heated to 700°C, the air temperature inside the furnace was 550°C during thermal equilibrium. The Aluminium specimens were placed on the top of the lower tool (figure 3.1), the distance between the upper tool and the specimen during preheating was 2mm. The temperature of the specimen was controlled during preheating. After reaching a temperature of 480°C and a waiting time of 6 minutes a pre-force of 20N was applied. Immediately after this the PSCT started, the speed of the upper compression tool was 80mm/min, which equates to a strain rate of 1 s^{-1}. The test was done to a maximum strain of 0.4.

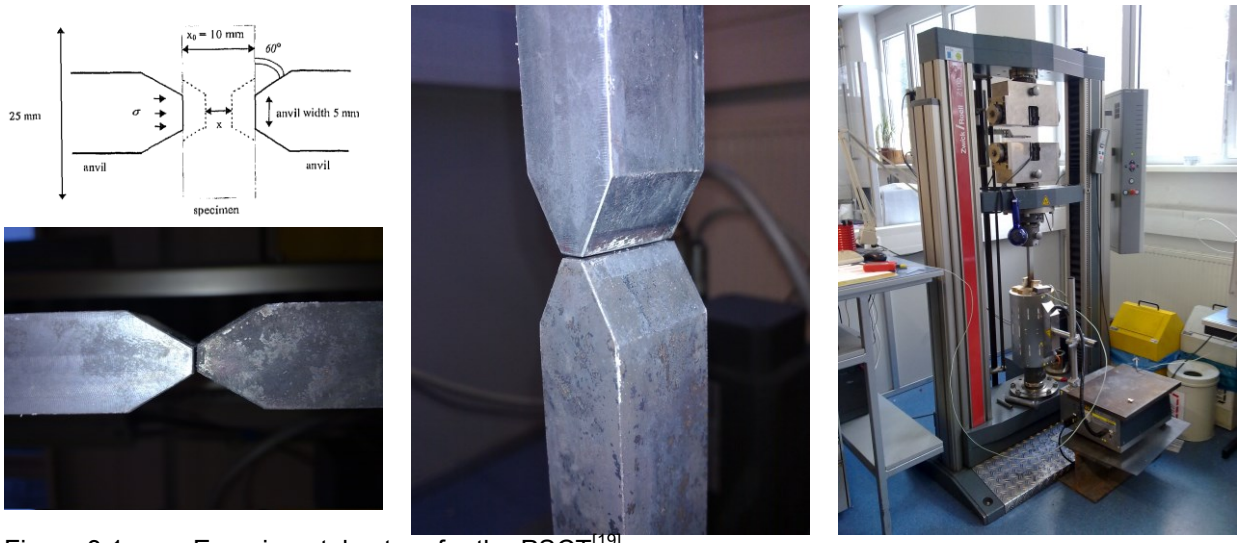

Figure 3.1 Experimental set-up for the PSCT[19]

3.8 Tensile Test

To control the mechanical properties of the extruded profile, but also for performing the PSCT the tensile testing machine Zwick (max. force 100 kN) was used.

3.9 Analyzed Profile

Normally about 2,500 kg of this profile (figure 3.2) are produced on a typical extrusion press per hour. During extrusion of the hdc billets press fleas and hot cracks appear, as a result the extrusion temperature and consequently the extrusion speed has to be lowered.

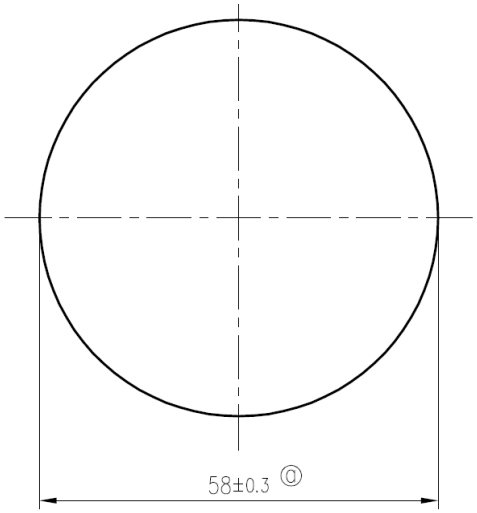

Figure 3.2 Extrusion profile (mm)

3.10 Homogenization and Cooling Experiments in the Laboratory Furnace

Target of these experiments was to find the right cooling conditions for the samples to mimic the conditions of the industrial homogenization furnace. As mechanical

forming experiment[19] with samples of a size of 10 x 20 x 25 mm each were subsequently planned, the size of the samples for the heat treatment was 52 x 52 x 15 mm, so that it was possible to prepare metallographic specimens and 3 samples for the PSCT. 7 cooling experiments were done with the following conditions:

Table 3.2 Used samples and their insulation

Experiment No.	1	2	3	4	5	6	7
Alloy	6082	6082	6082	6082	6082	6082	6082
Length [mm]	51,5	51,5	51,5	51,5	51,5	51,5	51,5
Width [mm]	51,5	51,5	51,5	51,5	51,5	51,5	51,5
Thickness [mm]	15,5	15,5	15,5	11	15,5	15,5	15,5
Insulation bottom	RT 50	RT 50	RT 50	RT 50	FT 16	FT 16	FT 16
Insulation top	---	RT 50	RT 50 while T>300°C	RT 50	FT 16	FT 16	FT 16
Insulation right side	---	---	---	---	---	FT 16	FT 16
Insulation left side	---	---	---	---	---	FT 16	FT 16
Insulation back side	---	---	---	---	---	FT 50, 10 mm air gap	FT 50 while T>300°C, then 10 mm air gap

Definitions:
RT 50…50mm thickness of the insulation, insulation starting temperature was room temperature (22°C±2°C)
FT 16…16mm thickness of the insulation, insulation temperature was the furnace temperature (560°C±5°C)
FT 50…50mm thickness of the insulation, insulation temperature was the furnace temperature (560°C±5°C)
---…No insulation was used

For the homogenization experiments, samples from the unhomogenized hdc billet were prepared.

5 heat treatments were done:

- 4h at 560°C, cooling conditions like in the production furnace
- 4h at 580°C [1, 3, 11, 13, 16, 19], cooling conditions like in the production furnace
- 4h at 580°C, slow cooling [3]
- 4h at 580°C, water quenched [21]
- 4h at 580°C, step cooled (350°C, holding time 1h) [14]

4 hours instead of 4.5 hours were applied because a reduction of homogenization time was also target of this work.

4 Analysis of the Actual Situation

4.1 Thermo-Calc Simulation

4.1.1 Overview

For the simulation equilibrium and non-equilibrium (Scheil) calculation models were used. Both for the vdc and hdc billets Thermo-Calc calculations were performed, but only the results for the hdc billets are presented, because the differences between the results of hdc and vdc billets are minimal, however the differences are mentioned for comparison at the end of the chapter.

4.1.2 Non-Equilibrium (Scheil) Simulation

The liquidus temperature is expected at 650°C, the solidus temperature at 550°C. Below 577°C β-AlFeSi exists, above 577°C only α-AlFeSi exists (figure 4.1). The precipitation of α-AlFeSi starts at 636°C and finishes at 577°C, the weight fraction at room temperature should be 1.3% (figure 4.2). The precipitation of Silicon starts at 560°C (figure 4.3). The precipitation of Mg_2Si starts at 572°C (figure 4.4). The precipitation of $Al_8FeMg_3Si_6$ starts at 563°C (figure 4.5).

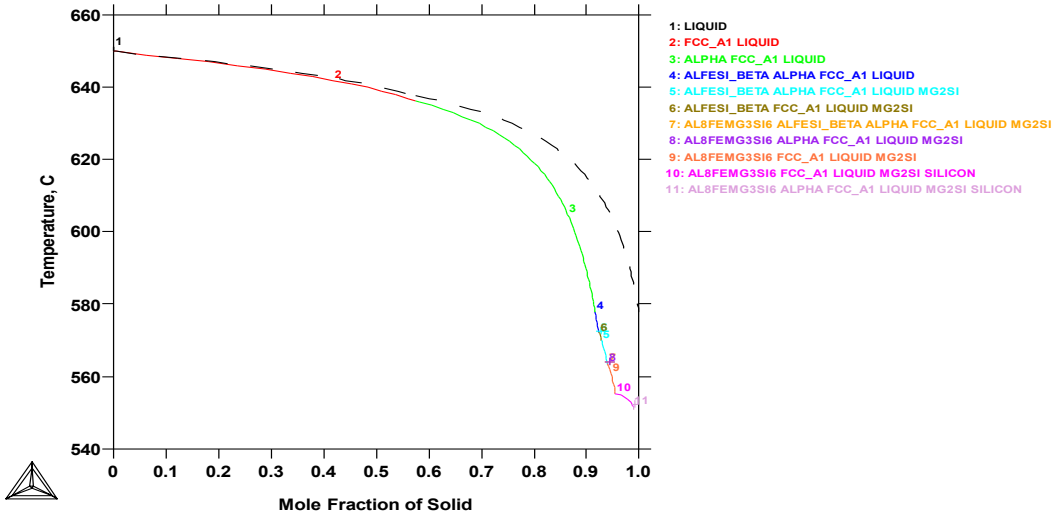

Figure 4.1 Overview 6082 alloy (Scheil), mole fraction plot against temperature

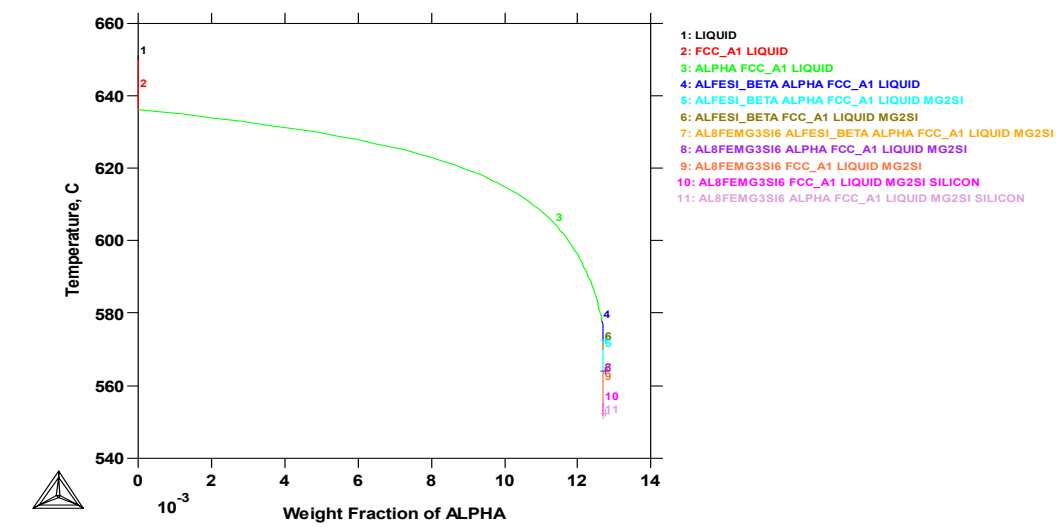

Figure 4.2 Weight fraction of α-AlFeSi

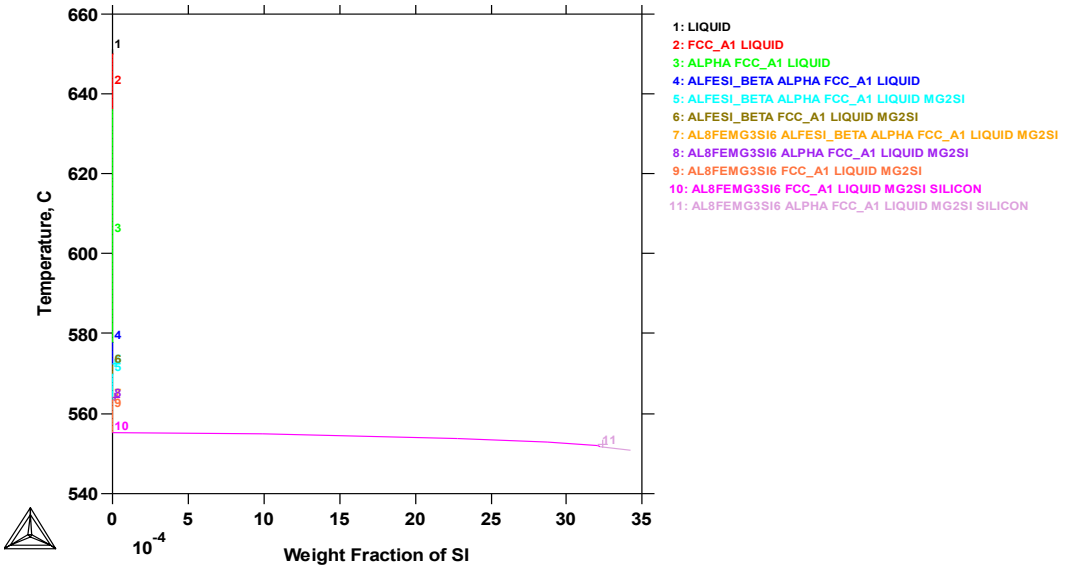

Figure 4.3 Weight fraction of Si

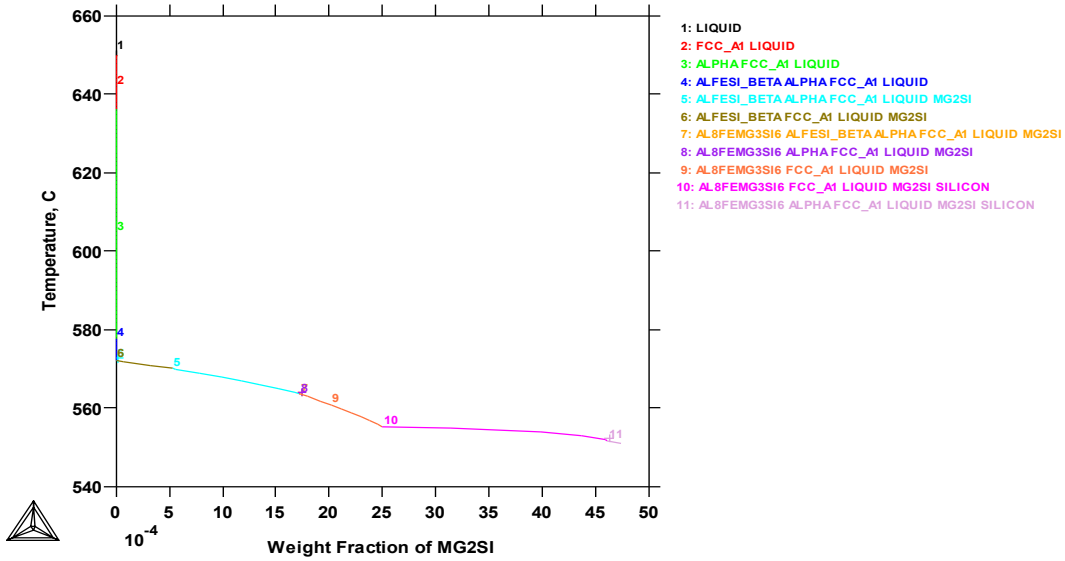

Figure 4.4 Weight fraction of Mg_2Si

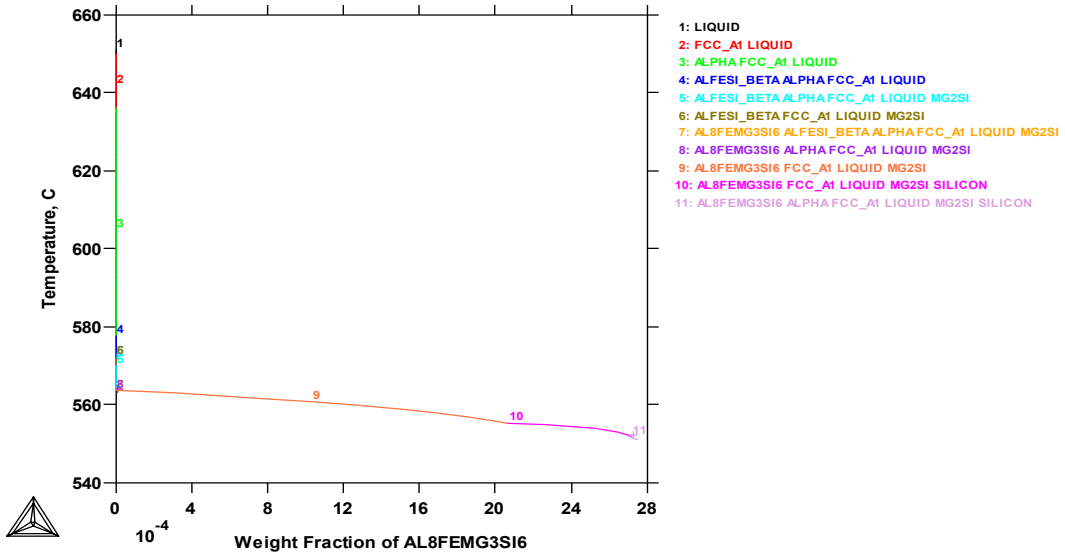

Figure 4.5 Weight fraction of $Al_8FeMg_3Si_6$

4.1.3 Equilibrium Simulation

The liquidus temperature is 650°C, the solidus temperature is 580°C (figure 4.6). The results of the equilibrium simulation are shown in table 4.1.

Table 4.1 Legend for equilibrium simulation

Phase	Number	Start of precipitation [°C]
α-AlFeSi	1	637
Mg_2Si	3	564
$Al_{13}Cr_4Si_4$	5	487
Si	6	457
$Al_5Cu_2Mg_8Si_6$	7	287
Al3M_DO22 (Al-Ti phase)	8	249

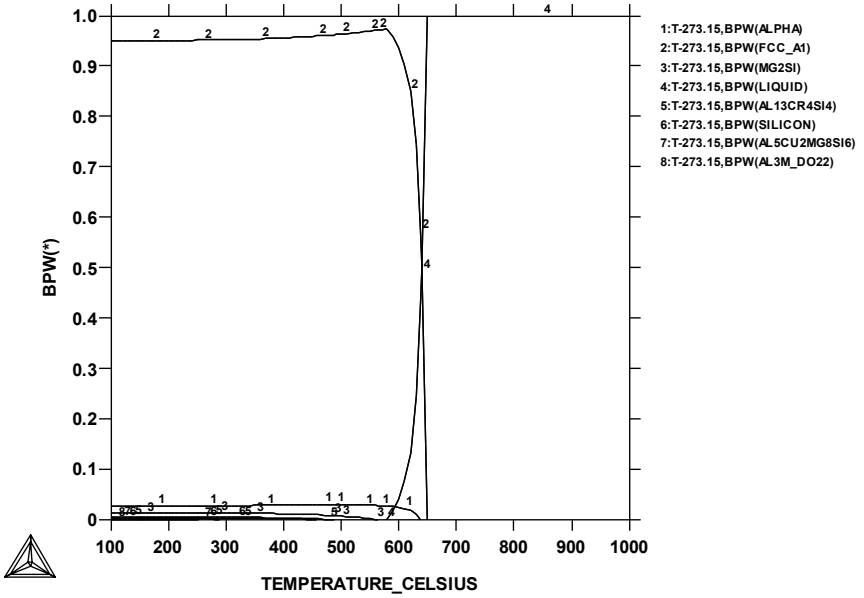

Figure 4.6 Equilibrium simulation 6082 alloy

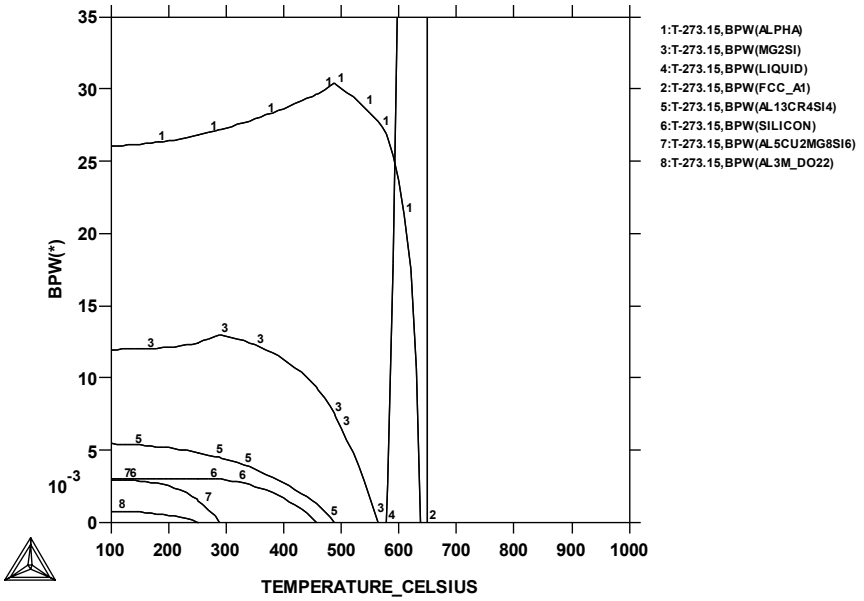

Figure 4.7 Equilibrium simulation 6082 alloy (detail)

4.1.4 Comparison of the Non-Equilibrium and Equilibrium Results

In both equilibrium and non-equilibrium simulations the α-AlFeSi phase appears, β-AlFeSi only appears in the non-equilibrium calculation because it's not stable and transforms at higher temperatures to α-AlFeSi. Both Mg_2Si and Si appear in Scheil and equilibrium calculation. However, the Si appears in the equilibrium much later than in the Scheil calculation. The reason for that is that in equilibrium calculation there is more time for the precipitation of Mg_2Si, as a result the content of Mg and Si in the matrix is lower and hence the driving force for the precipitation of Si becomes lower. In the non-equilibrium simulation also $Al_8FeMg_3Si_6$ arises, in the equilibrium calculation $Al_{13}Cr_4Si_4$, $Al_5Cu_2Mg_8Si_6$ and an unlikely but predicted Al-Ti phase can be found in the simulation.
The reason for that is that the Fe can precipitate as AlFeSi more completely in the equilibrium calculation since the diffusion of Fe requires time, as a result there is less iron available and pure Mg_2Si is formed instead of the $Al_8FeMg_3Si_6$.
In the equilibrium calculation there is enough time for the diffusion of small amounts of Cu and Cr which allows the precipitation of $Al_{13}Cr_4Si_4$ and $Al_5Cu_2Mg_8Si_6$.

Table 4.2 Comparison equilibrium and non-equilibrium simulation

	Start of precipitation [°C]	
Phase	Non-equilibrium	Equilibrium
α-AlFeSi	636	637
Mg_2Si	572	564
$Al_8FeMg_3Si_6$	563	---
Si	560	457
$Al_{13}Cr_4Si_4$	---	487
$Al_5Cu_2Mg_8Si_6$	---	287
Al3M_DO22 (Al-Ti phase)	---	249

4.1.5 Comparison of the horizontal and vertical direct chilled Billets

There is about 10% less α-AlFeSi in the vdc billets predicted because of the smaller Fe content, but the $Al_8FeMg_3Si_6$ content in the vdc billets should be slightly higher. In the hdc billets more Si should be present because of the higher Si content. However, all differences are not significant and the temperatures for precipitation and dissolution are quiet similar.

4.2 Differential Scanning Calorimetry

4.2.1 Overview

During the measurements at the production furnace a real homogenization temperature of 555°C was found. By comparing this value with the values from the literature it became evident, that 555°C is too low for homogenization, since the most publications recommend about 580°C for the heat treatment.
Therefore two experiments with the same material were performed to verify the results; both runs show exactly the same behaviour. Heating and cooling was with a rate of 20K/min.

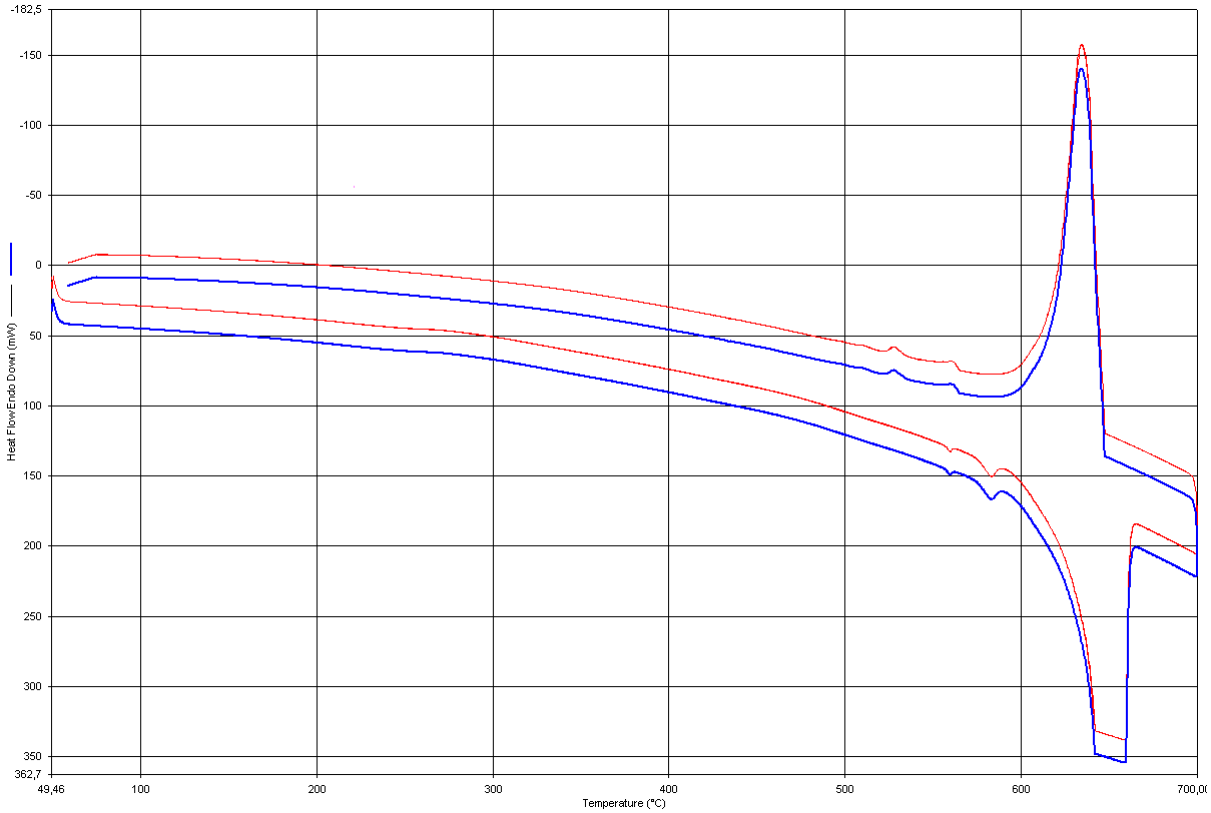

Figure 4.8 Overview of the DSC experiments (blue: experiment 1, red: exp. 2)

The lower blue and red line show the heating period of the material, the upper blue and red line show the cooling period of the material. There are very low but broad peaks at ~250°C and ~480°C during heating, most probably transformation peaks of β'', β' and β-Mg_2Si.
Because both experiments show peaks at the same position, only one experiment was evaluated.

4.2.2 Heating Period

The first peak position is 559°C (start of the dissolution at 556°C, end at 563°C), the second peak position is 583°C (start of the dissolution at 574°C, end at 590°C), the solidus temperature is 590°C and the liquidus temperature is 656°C. A comparison of the obtained data with Thermo-Calc is given in chapter 4.7.

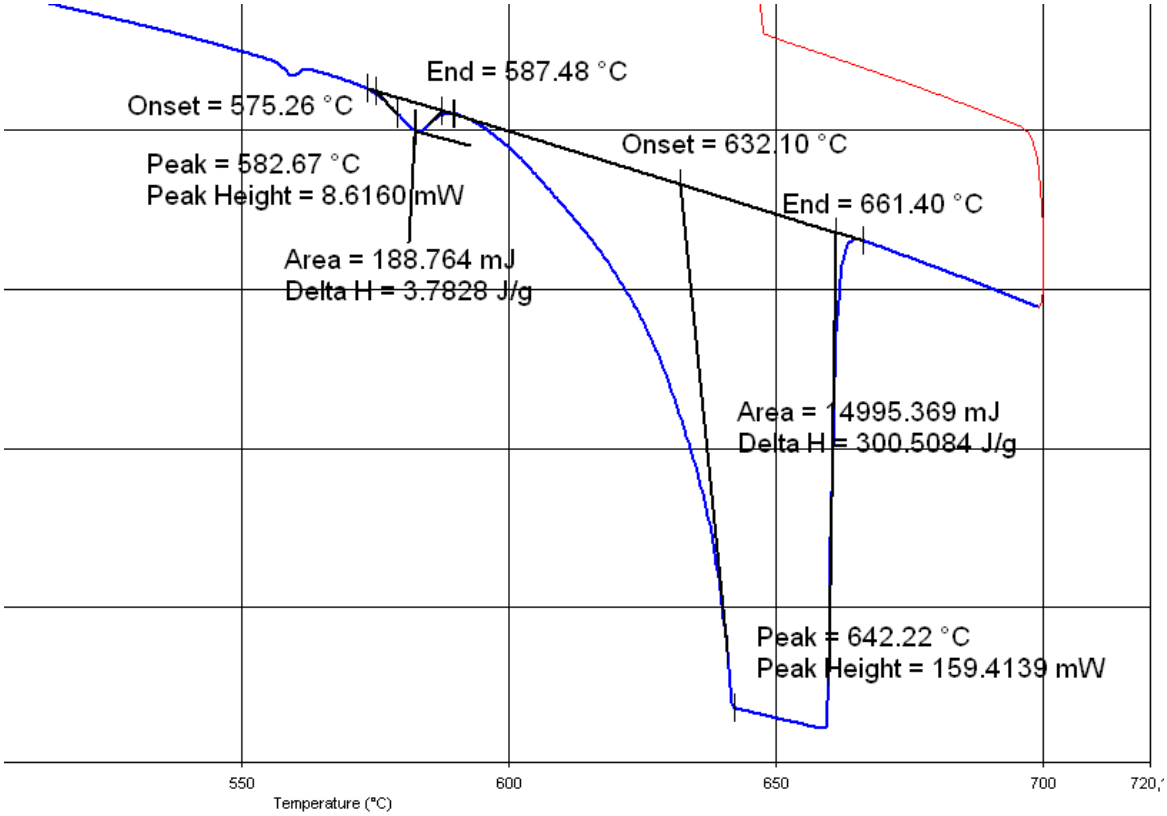

Figure 4.9 Plot of the heating period

4.2.3 Cooling Period

The left peak position is at 528°C (start of the precipitation at 536°C, end at 522°C), the middle peak position is at 561°C (start of the precipitation at 564°C, end at 554°C), the solidus temperature is 570°C and the liquidus temperature is at 648°C, supercooling in comparison with the heating period is visible.

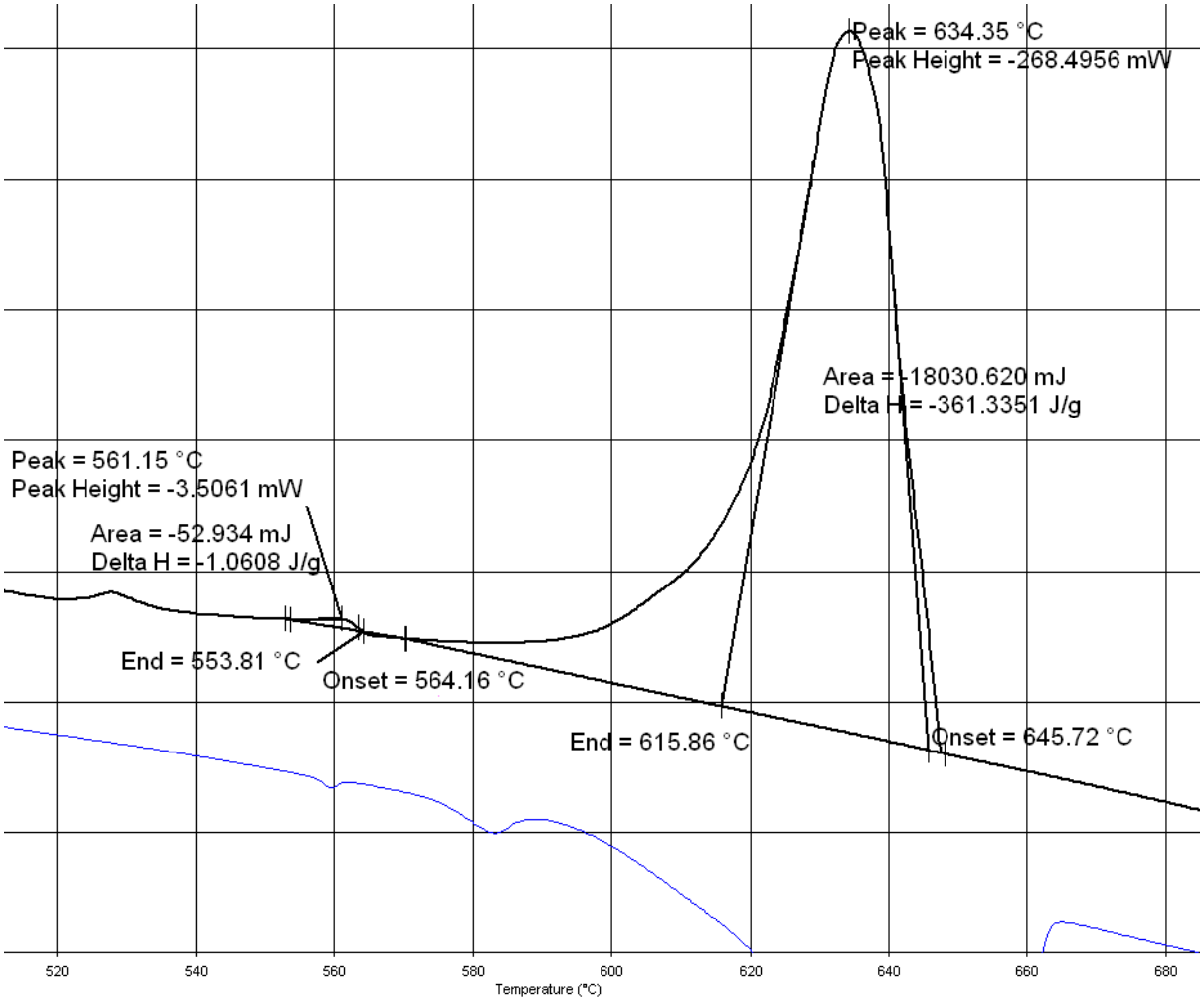

Figure 4.10 Plot of the cooling period

As the instrument is calibrated for heating the data of the cooling period is not as accurate as data for the heating period the data above wasn't used for remodelling the heat treatment.

4.3 Temperature Characteristics during Homogenization and Cooling

4.3.1 Measurement of the Temperature in the Homogenization Furnace

In order to determine the actual heating, holding and cooling conditions it was necessary to measure the temperature during the industrial homogenization treatment. The measurement was done with NiCr-Ni thermocouple (K-type).
The following characteristics were expected:

- heating to 560°C
- holding at this temperature for 4:30±0:30 hours
- cooling with fans to room temperature

The following temperature curve was measured in the core of the billet:

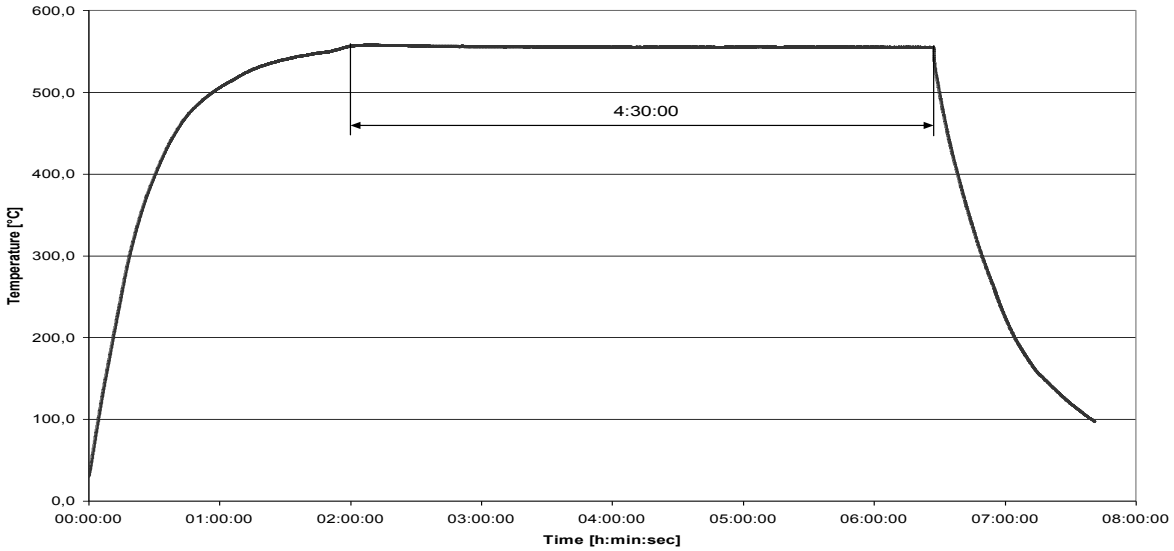

Diagram 4.1 Center temperature of the billet plot against time

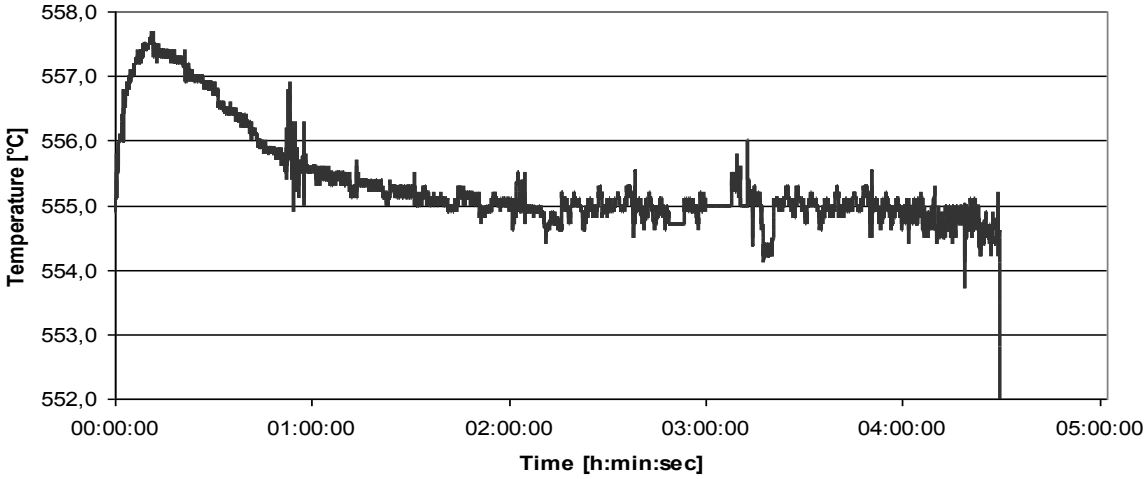

Diagram 4.2 Temperature curve during holding time plot against time (definition holding time: time between the first excess of 555°C and the first fall below 550°C)

The holding temperature is 555°C±1°C (except a small overshot of 2.5°C during the first hour). The real furnace temperature is 5°C lower than the estimated temperature. It appears, that the temperature control of the furnace works well, with a quiet small temperature deviation. This means, that billets can be heat treated quiet close to the solidus temperature without partial melting, as long as grain growth can be controlled.

4.3.2 Calculation of the Surface Temperature

As only the cooling conditions in the core of the billet were measured, it was essential to calculate also the cooling conditions on the surface.
As this problem is an unsteady heat conduction problem, an estimation can be found with the Fourier and Biot number and the Groeber-diagram [29].
For the use of the Groeber diagram it's only essential to know the properties of the material, it's not essential to know in which way the heat is released from the surface of the billet (radiation, heat conduction or convection).

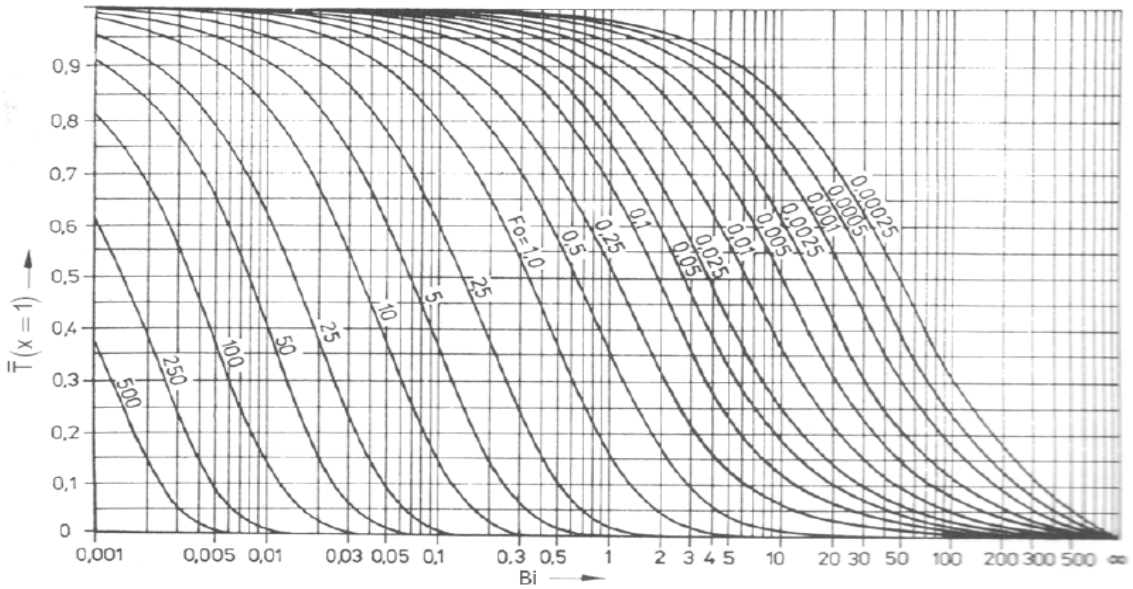

Diagram 4.3 Groeber diagram for the surface of a cylinder [29]

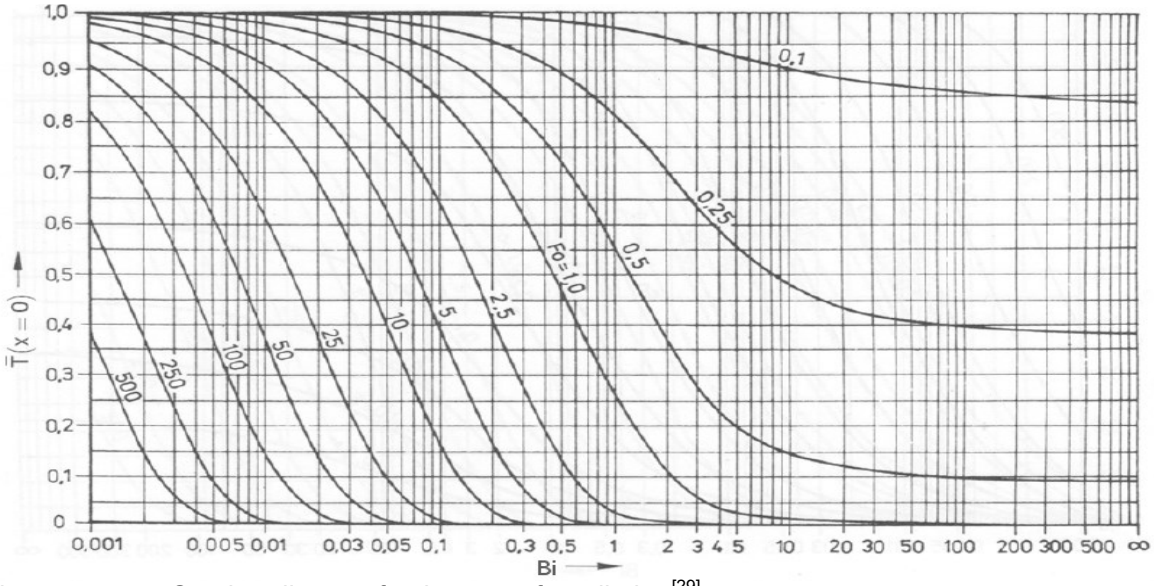

Diagram 4.4 Groeber diagram for the core of a cylinder [29]

4.3.2.1 Theory

First the temperature conductivity a, temperature T' of the core and the Fourier number "Fo" were calculated and with this data the Biot number "Bi" was calculated from the Groeber diagram for the core temperature. With this Biot number the temperature T' of the surface and finally the surface temperature T was calculated. For all material properties (a, c_p, α, λ, ρ) temperature independent values were used.

$$a = \frac{\lambda}{\rho \cdot c_p}$$ Temperature conductivity (4)

$$a = 7.0210^{-5}\,\frac{m^2}{s}$$

$$\lambda = 170\frac{W}{m \cdot K}$$ Heat conductivity

$$\rho = 2700\frac{kg}{m^3}$$ Density

$$c_p = 897\frac{J}{kg \cdot K}$$ Heat capacity

$$Fo = \frac{t \cdot a}{R^2}$$ Fourier number [ ] (5)

$$Fo = 0.0068t$$

$$T' = \frac{T - T_{fluid}}{T_i - T_{fluid}}$$ Dimensionless temperature [ ] (6)

$T_{fluid} = 30°C$ Air temperature

$T_i = 555°C$ Initial billet temperature

$$Bi = \frac{L \cdot \alpha}{\lambda}$$ Biot number (7)

α Coefficient of heat transfer [W/m²K]

4.3.2.2 Results of the Estimation

The maximum temperature difference between the estimated surface temperature and measured core temperature of the billet during the cooling process is smaller than 14°C, as a result there should be no significant difference in microstructure and mechanical properties (diagram 4.5 and 4.6). In diagram 4.7 and 4.8 the cooling rate of the center (core) and the surface of the billet is shown. The cooling of the surface starts earlier because of the thermal inertia of the core. Also the cooling rate is nearly the same both on the surface and the core. As a result all results from the analyzed samples taken from the centre of the billet are valid across the whole billet section.

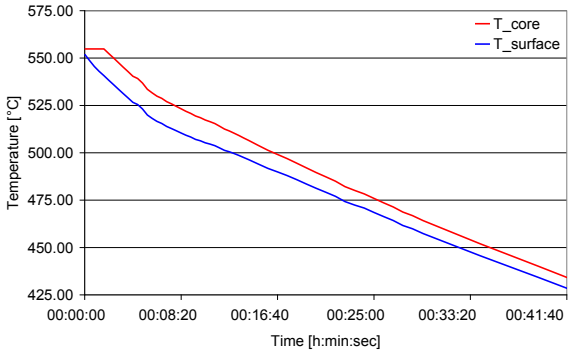

Diagram 4.5 Temperature chart (detail) of the surface and the core of the billet during cooling

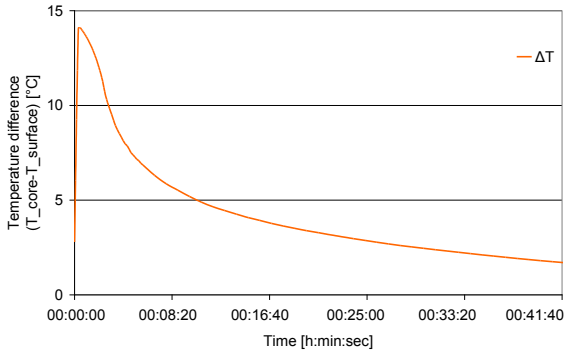

Diagram 4.6 Chart of temperature difference between the surface and the core of the billet

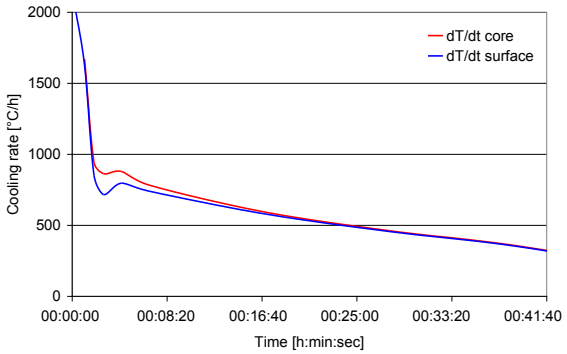

Diagram 4.7 Cooling rate of the surface and core of the billet plot against the time

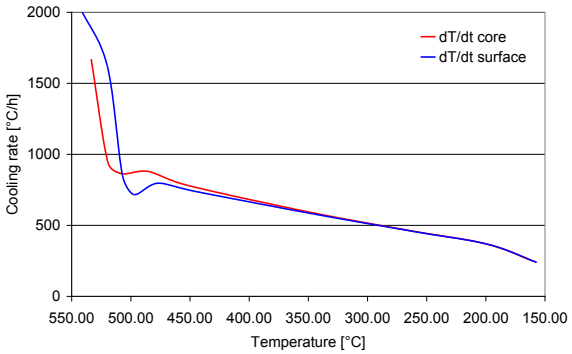

Diagram 4.8 Cooling rate of the surface and core of the billet plot against the temperature

4.4 Data from the Extrusion Machine

4.4.1 Data horizontal direct chilled Billet Extrusion

In the preheating furnace there are 6 locations (target 1-6, 1 is the last (hottest), 6 is the first in the furnace (coolest)) where the actual temperature is measured. Figure 4.11 shows a schematic drawing of the furnace with it 6 locations, diagram 4.9 shows the target temperature against time during an average extrusion process of hdc billets.

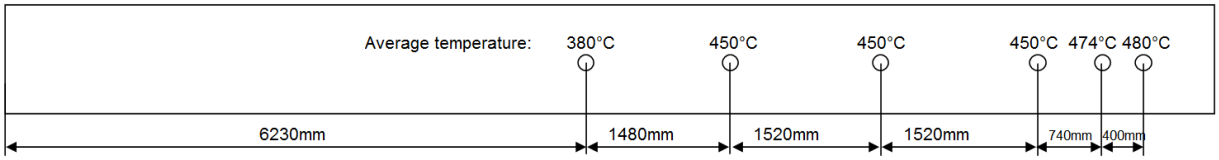

Figure 4.11 Schematic drawing of the preheating furnace

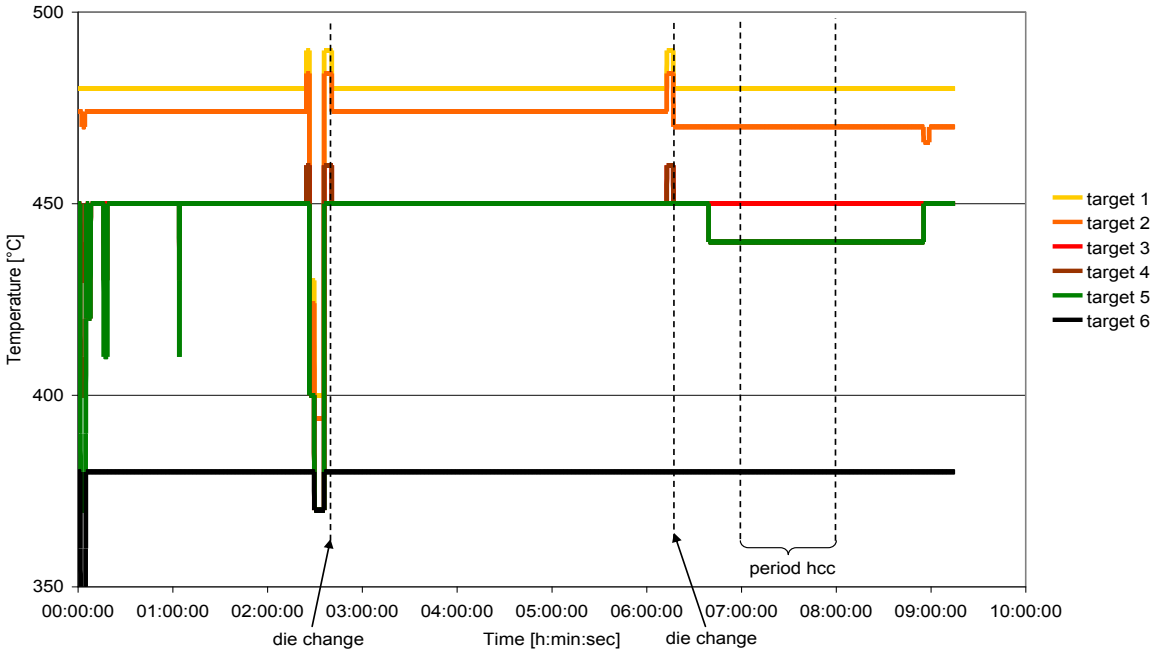

Diagram 4.9 Target temperature of the preheating furnace plot against time

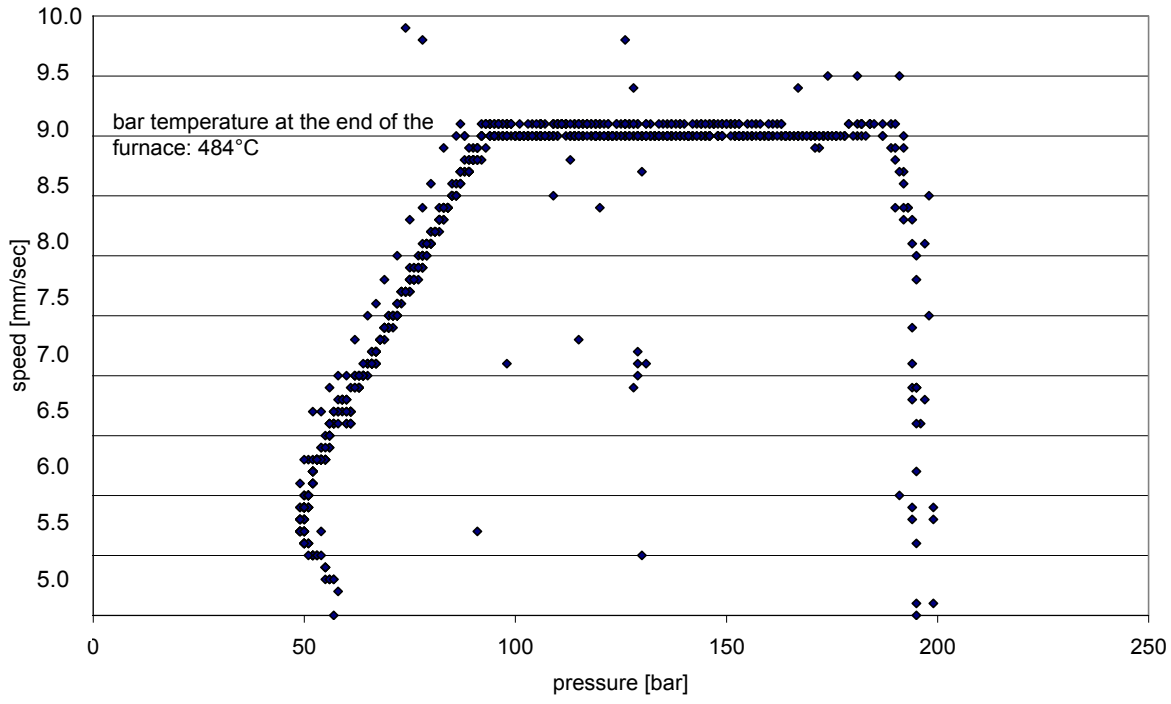

Diagram 4.10 Extrusion speed plot against extrusion pressure

4.4.2 Data vertical direct chilled Billet Extrusion

Diagram 4.11 shows the target temperature against time during an average extrusion process of vdc billets. The black line shows the target temperature at the first measurement location in the furnace, the yellow line shows the target temperature at the last measurement location in the furnace, the other lines are between this two locations.

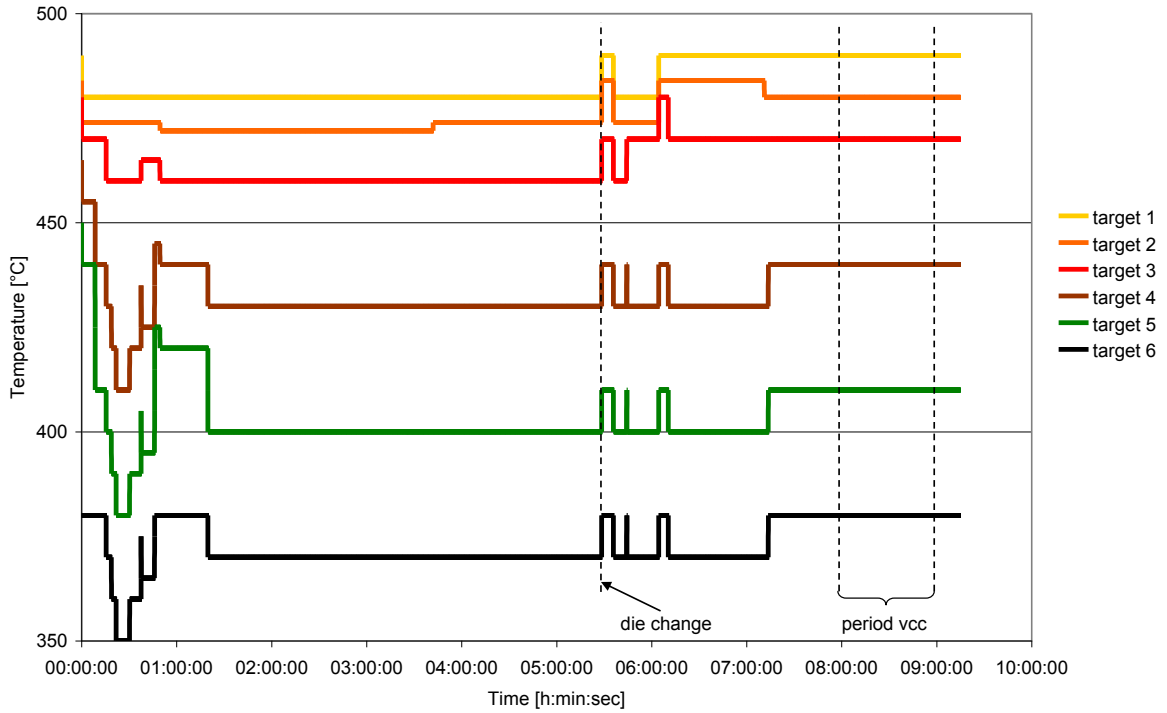

Diagram 4.11 Target temperature of the preheating furnace plot against time

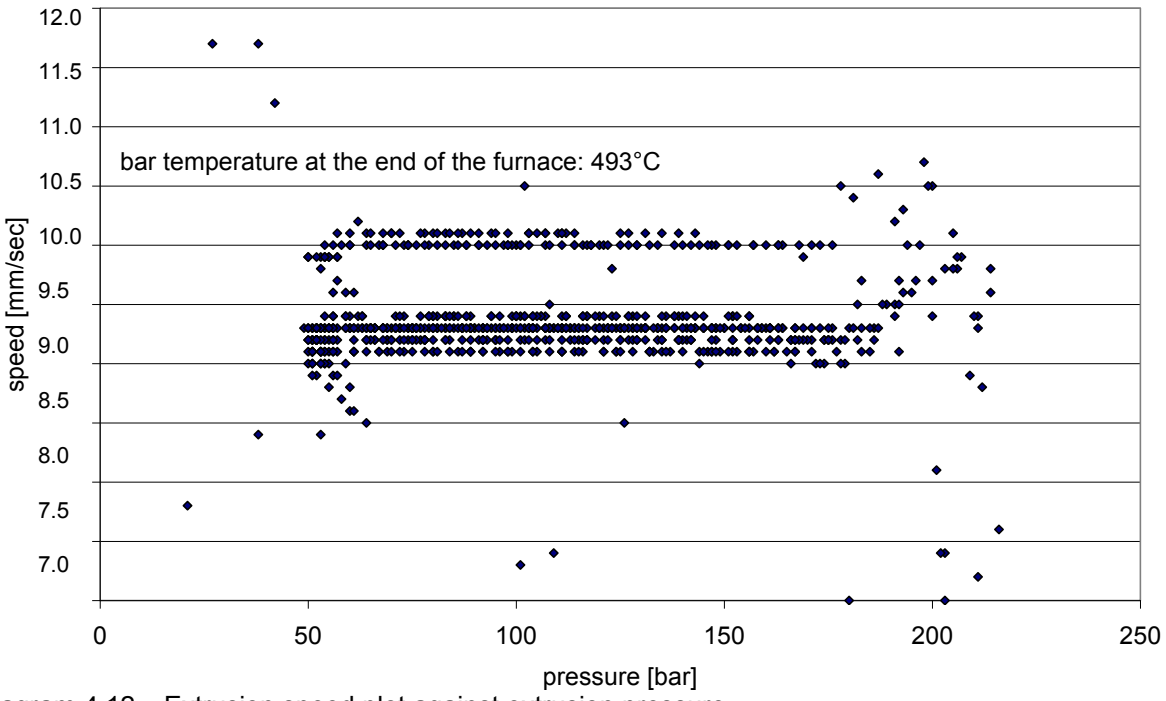

Diagram 4.12 Extrusion speed plot against extrusion pressure

4.5 Light Optical Microscopy

4.5.1 Precipitations

During the homogenization treatment the needle like β-AlFeSi transforms into the pearl necklace structured α-AlFeSi, both in the hdc billets and also in the vdc billets. Further it was found, that the Mg/Si phase from the grain boundaries dissolves during the homogenization, and subsequently precipitates inside the grains during cooling. The precipitations inside the grains are clearly visible in the etched samples.
The size of the Mg/Si particles inside the grain is smaller than 1µm (nano-scale particles), and there is a precipitation free zone at the grain boundary.
There are no significant differences between the hdc billets and the vdc billets.

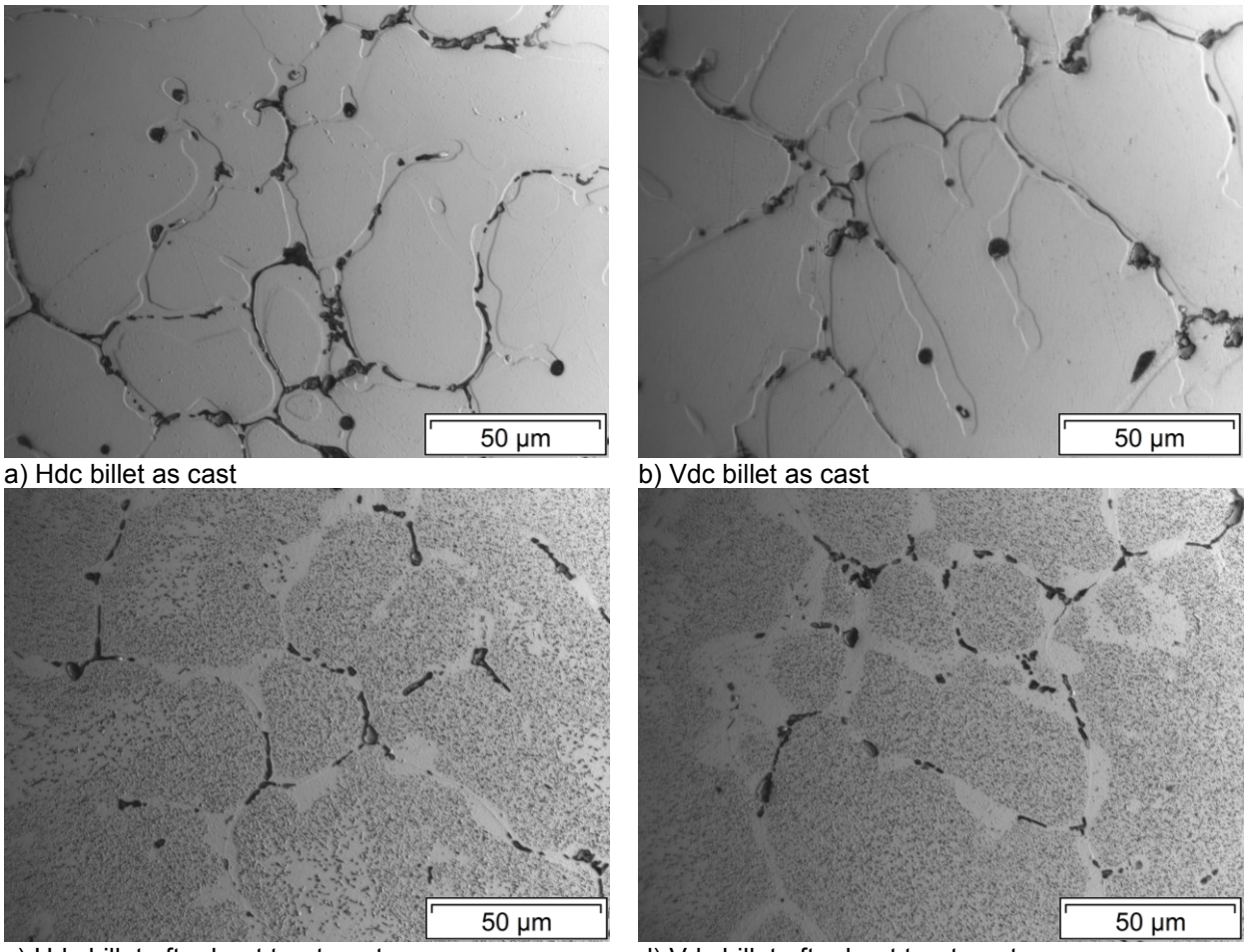

a) Hdc billet as cast
b) Vdc billet as cast
c) Hdc billet after heat treatment
d) Vdc billet after heat treatment

Figure 4.12 Comparison hdc and vdc samples (HF etched)

4.5.2 Grain Size

The grain size of the material should not increase significantly during homogenization as this would decrease the extrusion properties. In figure 4.13 the microstructure before and after the heat treatment is illustrated. By comparing the grain size of the as-cast samples and the heat treated samples grain growth at the hdc billets was visible. However, grain growth should be avoided, because the extrudability would be decreased. By comparing the microstructure, in particular the grain size, of both hdc billets and vdc billets, it is clear that the hdc billets show grain growth, in contrast to the vdc billets. The grain size of the hdc billets is smaller than that of the vdc billets before homogenization, but after heat treatment the grain size of the hdc billets is larger than that of the vdc billets. It seems that there is a decrease of grain size at the vdc samples, but there is no physical reason for that, as a result the seemingly reduction of grain size is caused by different analyzed areas, but also grain growth during homogenization can be excluded.

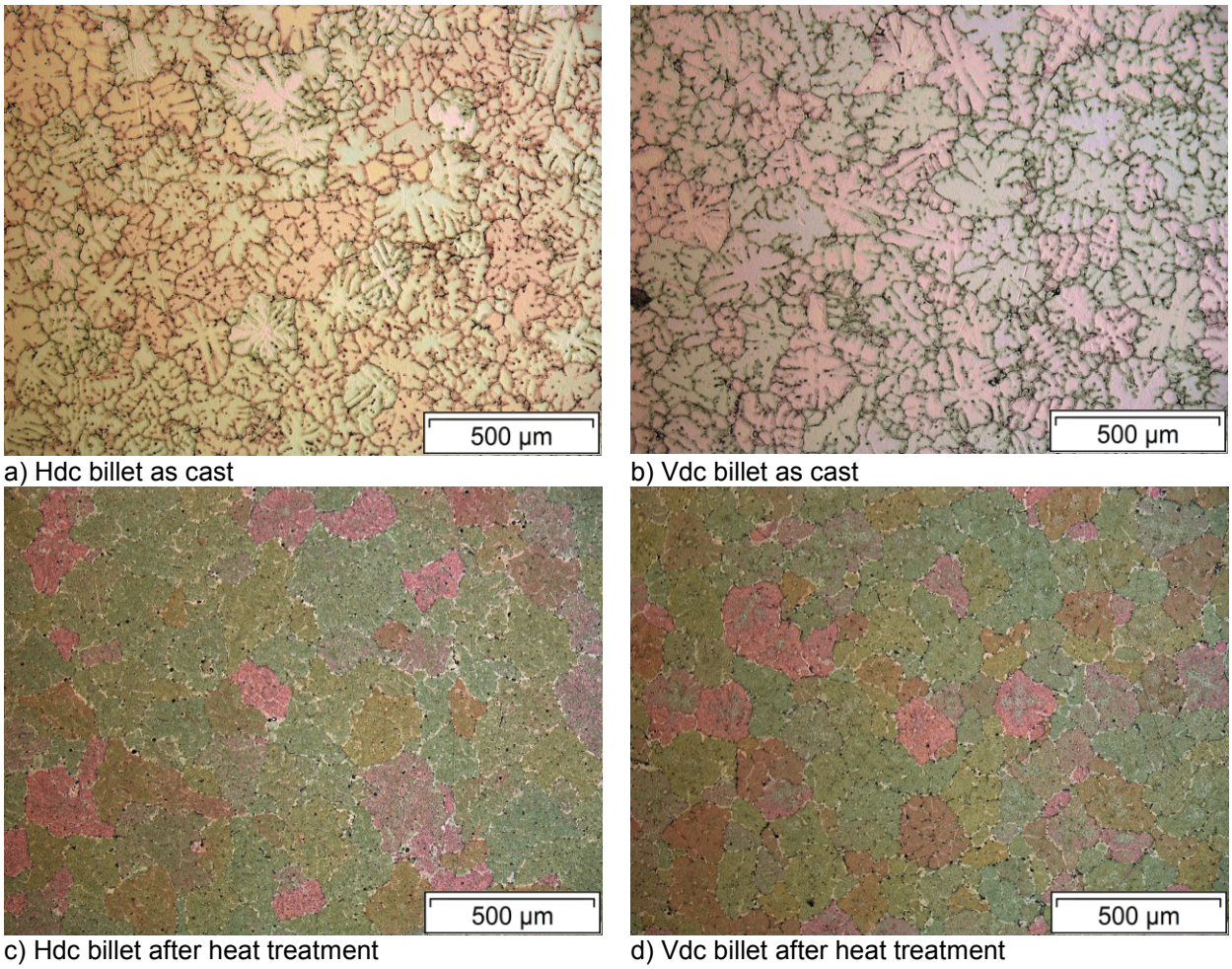

a) Hdc billet as cast
b) Vdc billet as cast
c) Hdc billet after heat treatment
d) Vdc billet after heat treatment

Figure 4.13 Comparison hdc and vdc samples (Barker etched)

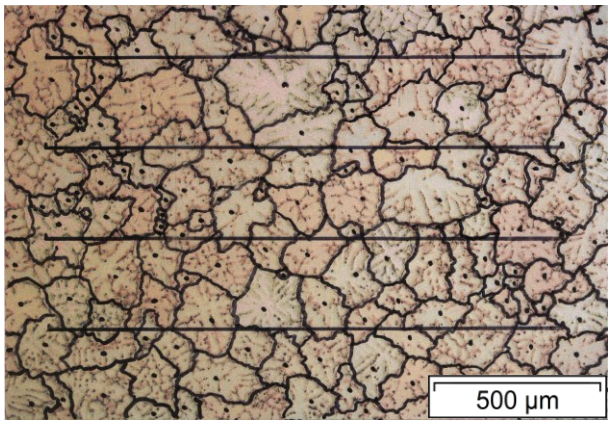

a) Hdc billet as cast

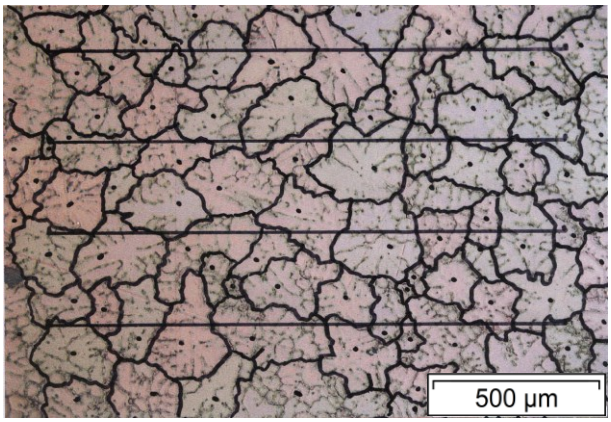

b) Vdc billet as cast

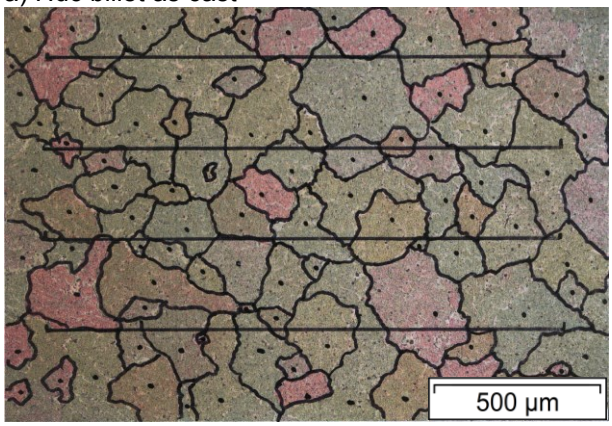

c) Hdc billet after heat treatment

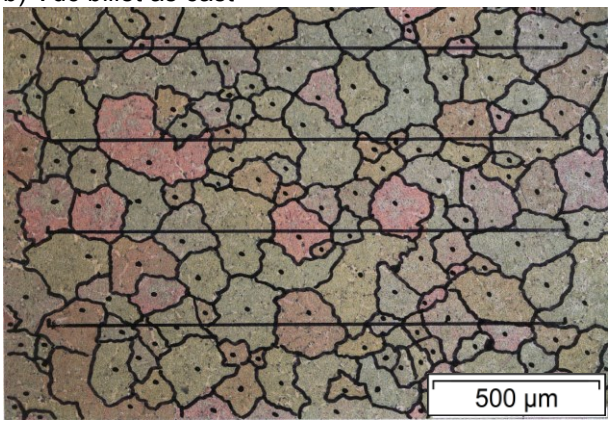

d) Vdc billet after heat treatment

Figure 4.14 Grain size comparison hdc and vdc samples (Barker etched)

Table 4.3 Grain size (line analysis)

	Grain size [µm]	
	Before homogenization	After homogenization
Hdc billet	113	136
Vdc billet	128	118

Table 4.4 Grain size (area analysis)

	Grain size [µm]	
	Before homogenization	After homogenization
Hdc billet	130	169
Vdc billet	172	132

To see the effect of time on grain growth, a sample which was homogenized 42h was compared to one which was homogenized 4h at 560°C. The grains in the 42h homogenized samples are larger, but the effect of time is not very strong.

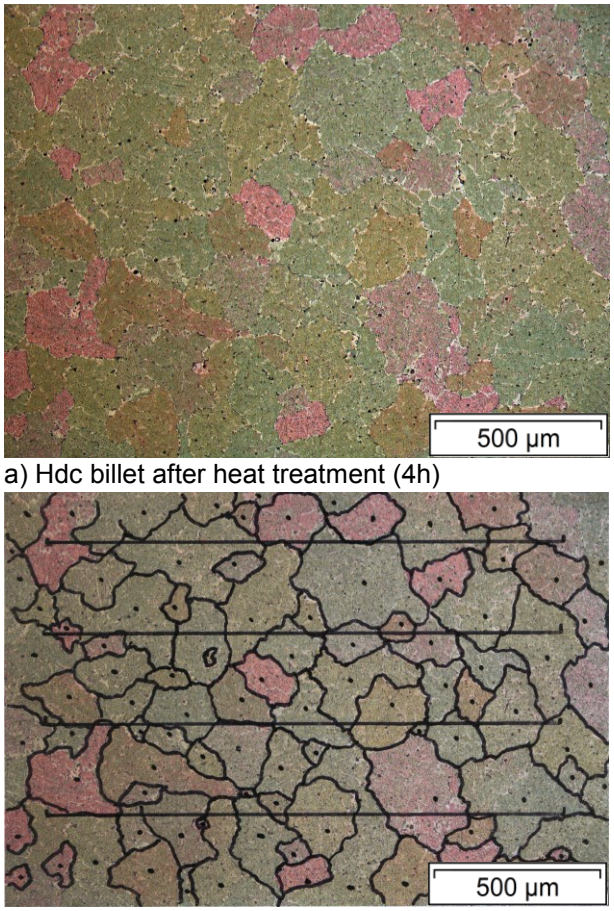

a) Hdc billet after heat treatment (4h)
b) Hdc billet after heat treatment (42h)
c) Hdc billet after heat treatment (4h)
d) Hdc billet after heat treatment (42h)

Figure 4.15 Grain size comparison hdc samples after 4h and 42h (Barker)

Table 4.5 Grain size (line analysis)

	Grain size [µm]
Hdc billet (4h)	136
Hdc billet (40h)	156

Table 4.6 Grain size (area analysis)

	Grain size [µm]
Hdc billet (4h)	169
Hdc billet (40h)	197

4.6 Scanning Electron Microscopy / EDX

During observation with the SEM a significant difference between the hdc and vdc billets was detected. There was a difference in morphology and chemical composition of the particles.

4.6.1 Unhomogenized horizontal direct chilled Billets

In the EDX area scan both a Mg/Si and a Fe/Mn/Cr/Si phase was observed. The Al content within the intermetallic phases is much less than that in the matrix and this contrast can be seen in Figure 4.16 c.

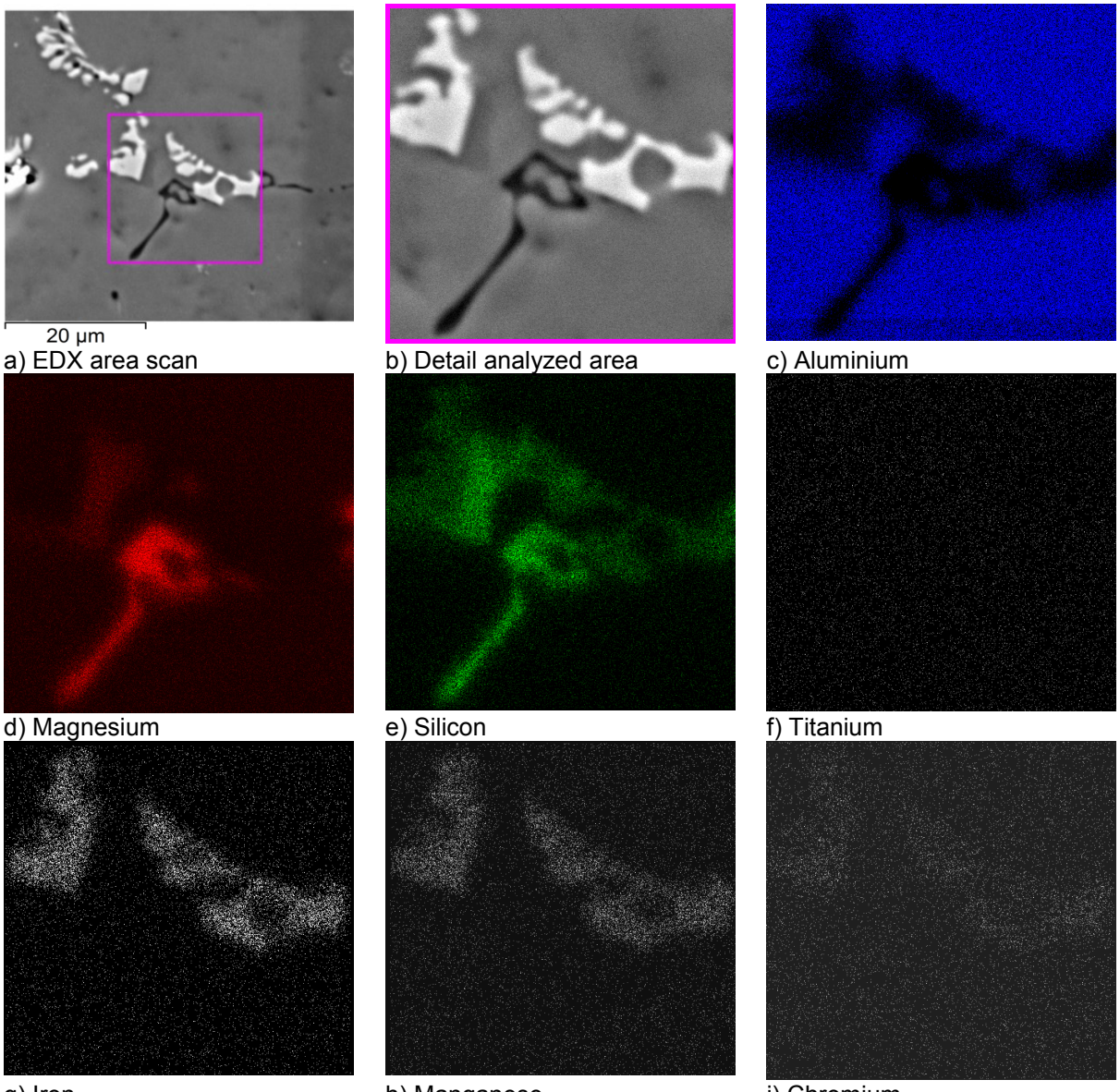

a) EDX area scan
b) Detail analyzed area
c) Aluminium
d) Magnesium
e) Silicon
f) Titanium
g) Iron
h) Manganese
i) Chromium

Figure 4.16 Area EDX analysis unhomogenized hdc billet

The matrix (EDX 1 in table 4.7) is rich in Al, the content of Mg and especially Si is low. It appears that most of the Mg and Si is precipitated. There is also a small content of Fe and Cr in EDX 1. The round grey particle (EDX 2) seems to be an Mg/Si phase. However, the Mg:Si ratio is 1.16, which is too low for Mg_2Si (the Mg:Si ratio in Mg_2Si should be between 1.73 and 2.20).
The white phase on the grain boundary (EDX 3) consists of Al, Fe, Mn, Cr and Si, and appears to be an Al(Fe,Mn,Cr)Si phase. As a result of the (Fe+Mn+Cr):Si ratio of 1.39 the phase should be a mixture of α- and β-AlFeSi. The grey phase on the grain boundary (EDX 4) consists of Mg/Si, the Mg:Si ratio of 0.89 is again too small for Mg_2Si.

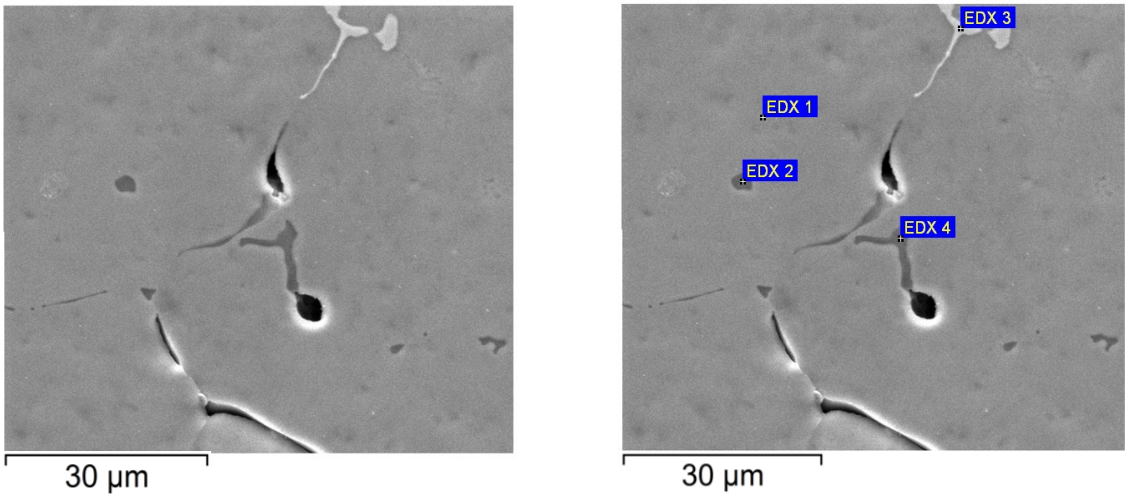

Figure 4.17 Spot EDX analysis unhomogenized hdc billet

Table 4.7 EDX results unhomogenized hdc billet

Element atom[%]	Aluminium Al	Iron Fe	Silicon Si	Magnesium Mg	Manganese Mn	Chromium Cr	Titanium Ti	Boron B
EDX 1	99.2	0.2	0.2	0.3	---	0.1	---	---
EDX 2	32.2	---	27.8	32.2	---	---	---	---
EDX 3	75.7	8.3	10.2	---	4.9	0.9	---	---
EDX 4	46.2	---	28.5	25.3	---	---	---	---

4.6.2 Homogenized horizontal direct chilled Billets

In the area scan shown in Figure 4.18 a Mg/Si, a Fe/Mn/Cr/Si and a Ti rich phase is visible. Again these phases could also contain some Al. Along the line in Figure 4.19 the Fe/Mn and the Fe/Cr ratio changes (right peak high Fe content, left peak high Mn content).

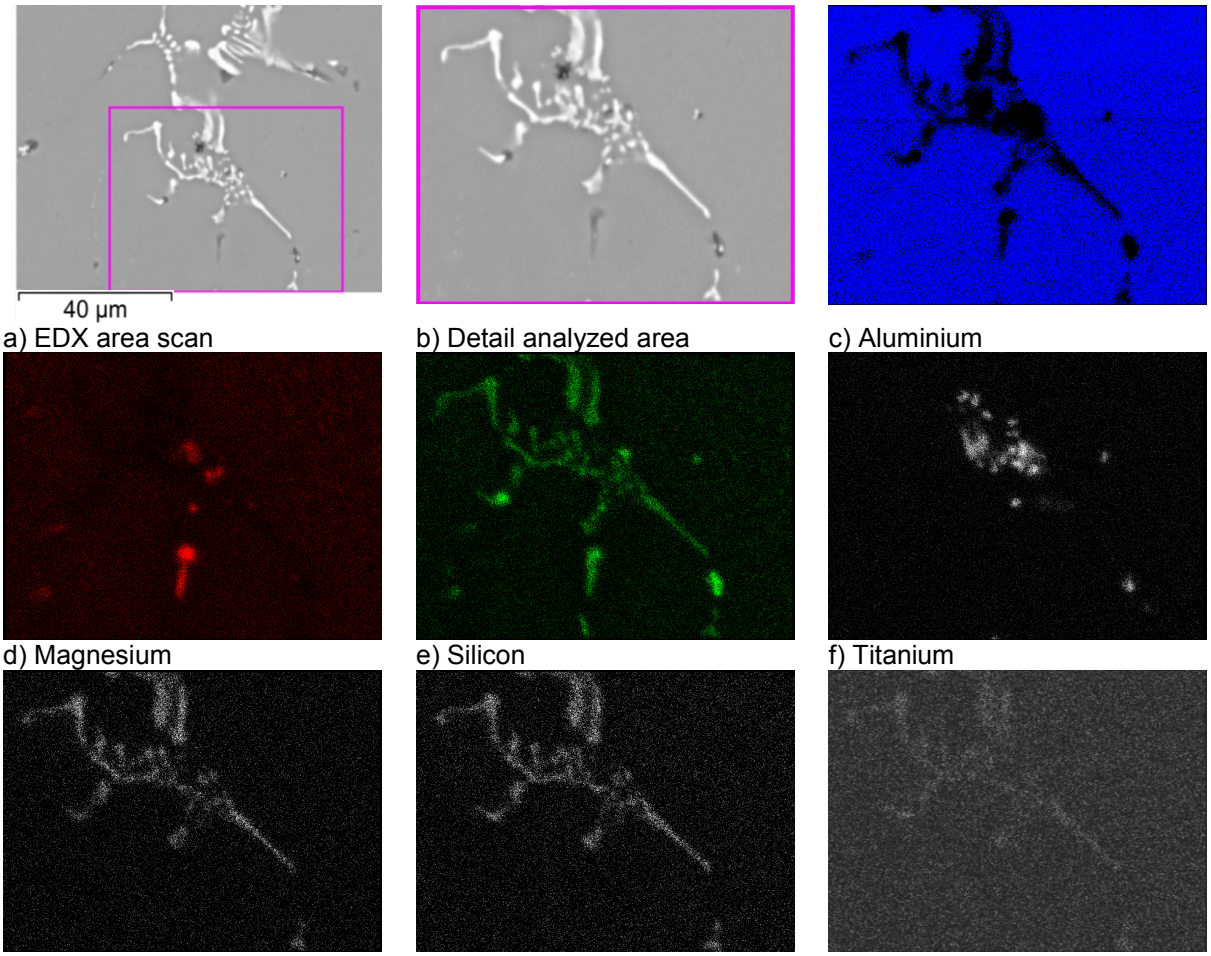

a) EDX area scan b) Detail analyzed area c) Aluminium

d) Magnesium e) Silicon f) Titanium

g) Iron h) Manganese i) Chromium

Figure 4.18 Area EDX analysis homogenized hdc billet

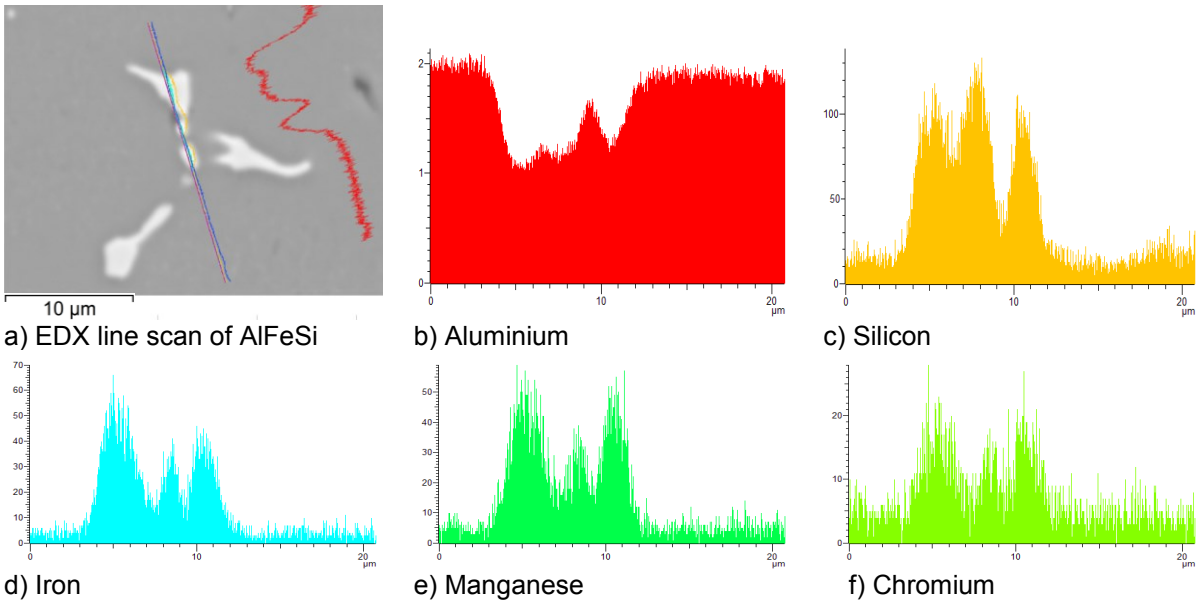

a) EDX line scan of AlFeSi b) Aluminium c) Silicon

d) Iron e) Manganese f) Chromium

Figure 4.19 Line EDX analysis homogenized hdc billet

The matrix scan EDX 1 in Table 4.8 shows a much higher Mg and Si content than prior to the heat treatment which indicates, that during the homogenization the coarse Mg/Si phase dissolves in the matrix. The Fe content decreased significantly as a result of the Fe enrichment (during β to α-AlFeSi transformation) in the AlFeSi phase. The white particle (EDX 2) consists of Al(Fe,Mn,Cr)Si, the (Fe+Mn+Cr):Si ratio is 1.37, subsequently the phase should be a mixture of α- and β-AlFeSi. EDX 3 and EDX 6 show most likely a particle of TiB_2 because of the high B content. The particle at EDX 4 contains Al(Fe,Mn)Si, the (Fe+Mn+Cr):Si ratio is 0.89, subsequently the phase should be a β-AlFeSi (this phase shouldn't occur after the heat treatment). In the particle at EDX 5 the (Fe+Mn+Cr):Si ratio is 1.30, consequential it's a mixture of α- and β-AlFeSi. The grey particles at EDX 7, EDX 8 and EDX 9 seem to consist of Mg and Si, the Mg:Si ratio in one of this particles 0.40, which is by far too low for Mg_2Si.

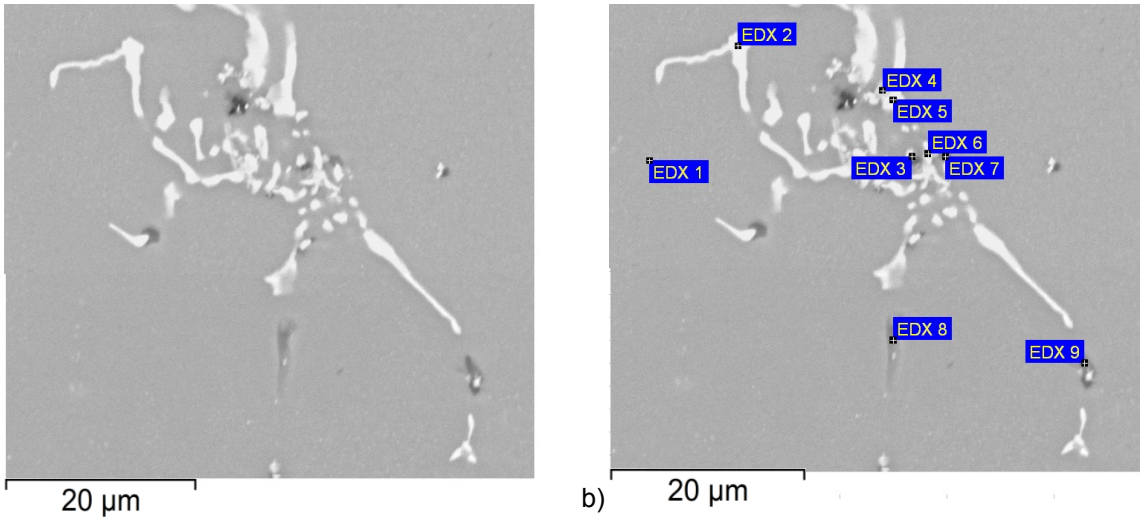

a) b)

Figure 4.20 Spot EDX analysis homogenized hdc billet

Table 4.8 EDX results homogenized hdc billet

Element atom[%]	Aluminium Al	Iron Fe	Silicon Si	Magnesium Mg	Manganese Mn	Chromium Cr	Titanium Ti	Boron B
EDX 1	97.8	0.0	0.8	0.9	0.2	0.3	0.1	---
EDX 2	72.8	9.0	11.5	0.1	5.8	1.0	---	---
EDX 3	11.5	---	0.5	3.6	---	---	10.4	74.0
EDX 4	89.0	1.8	5.8	---	3.4	---	---	---
EDX 5	76.2	6.7	10.3	---	5.9	0.8	0.1	---
EDX 6	13.6	---	0.3	---	---	---	13.7	72.5
EDX 7	71.1	---	21.0	---	---	---	7.9	---
EDX 8	78.4	---	15.4	6.2	---	---	---	---
EDX 9	51.1	---	37.1	---	---	---	11.8	---

4.6.3 Unhomogenized vertical direct chilled Billets

The matrix scan EDX 1 in Table 4.9 indicates a very low Si content but a quiet high Mg content (compared to the hdc billets). EDX 2, EDX 4 and EDX 5 show a very high Si and a low Mg content, the origin of the Al is most probably from the background, in contrast the particle consist nearly of pure silicon. The white particle (EDX 3) consists of Al(Fe,Mn,Cr)Si, the (Fe+Mn+Cr):Si ratio is 1.31, subsequently the phase should be a mixture of α- and β-AlFeSi. The particle at EDX 6 consists of Mg/Si, the Mg:Si ratio in one of this particles is 0.39, which is by far too low for Mg_2Si.

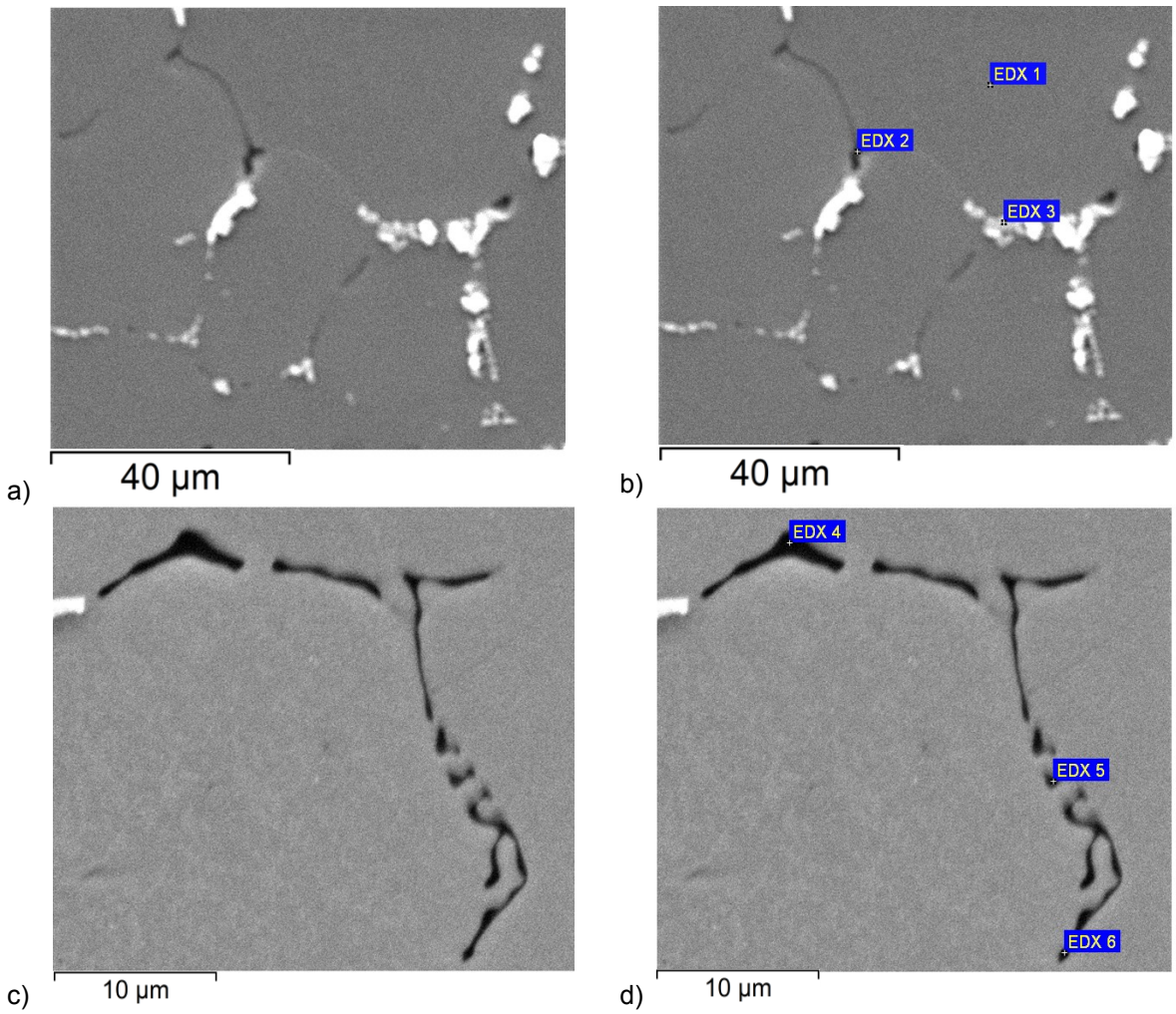

Figure 4.21 Spot EDX analysis unhomogenized vdc billet

Table 4.9 EDX results unhomogenized vdc billet

Element atom[%]	Aluminium Al	Iron Fe	Silicon Si	Magnesium Mg	Manganese Mn	Chromium Cr	Titanium Ti	Boron B
EDX 1	99.0	0.1	0.1	0.5	0.1	0.3	0.0	---
EDX 2	50.7	---	47.7	1.6	---	---	---	---
EDX 3	77.2	6.6	9.6	0.7	5.1	0.9	---	---
EDX 4	47.1	---	51.8	1.1	---	---	---	---
EDX 5	81.4	---	17.6	1.0	---	---	---	---
EDX 6	65.7	---	24.7	9.6	---	---	---	---

4.6.4 Homogenized vertical direct chilled Billets

In the area scan a „dendritic“ structure of a Al(Fe,Mn,Cr)Si particle and round particles of Mg/Si and Si were observed.

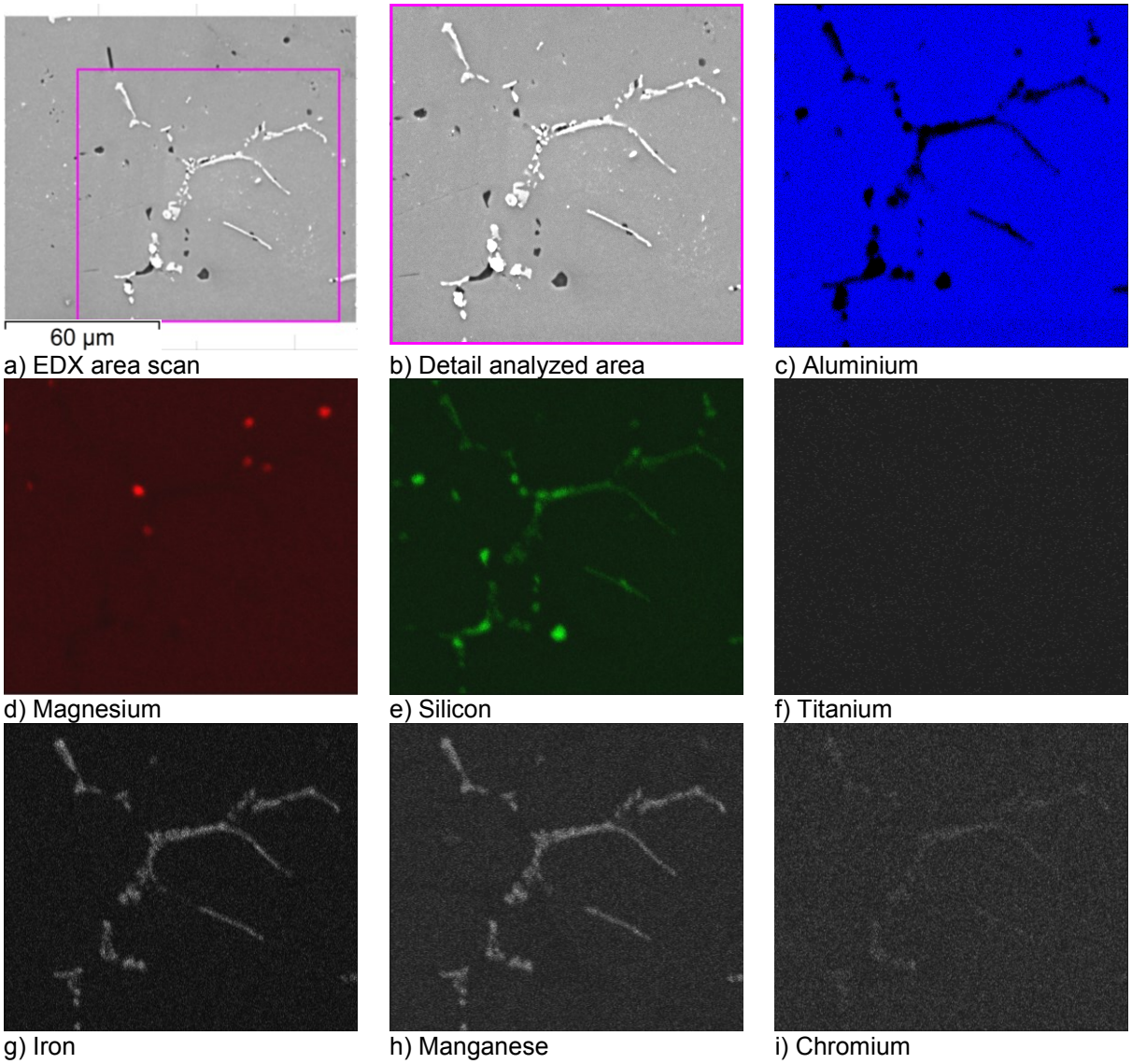

a) EDX area scan b) Detail analyzed area c) Aluminium

d) Magnesium e) Silicon f) Titanium

g) Iron h) Manganese i) Chromium

Figure 4.22 Area EDX analysis homogenized vdc billet

In the line scan (figure 4.23) an elongated particle of Si was determined. The particle is free of Mg, but on the interface of the particle an Mg rich precipitation was found.

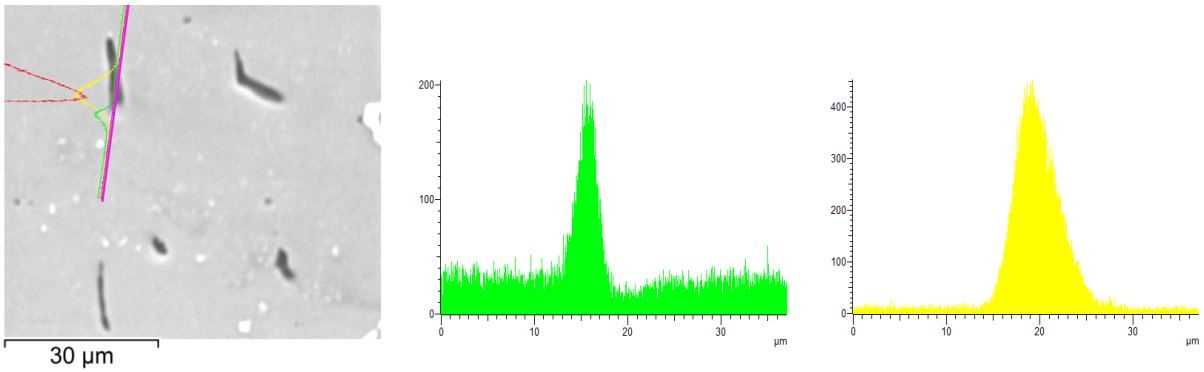

a) EDX line scan of AlFeSi b) Magnesium c) Silicon

Figure 4.23 Line EDX analysis homogenized vdc billet

In the area scan in figure 4.24 a Si particle with an Mg enrichment at the lower and right side is demonstrated.

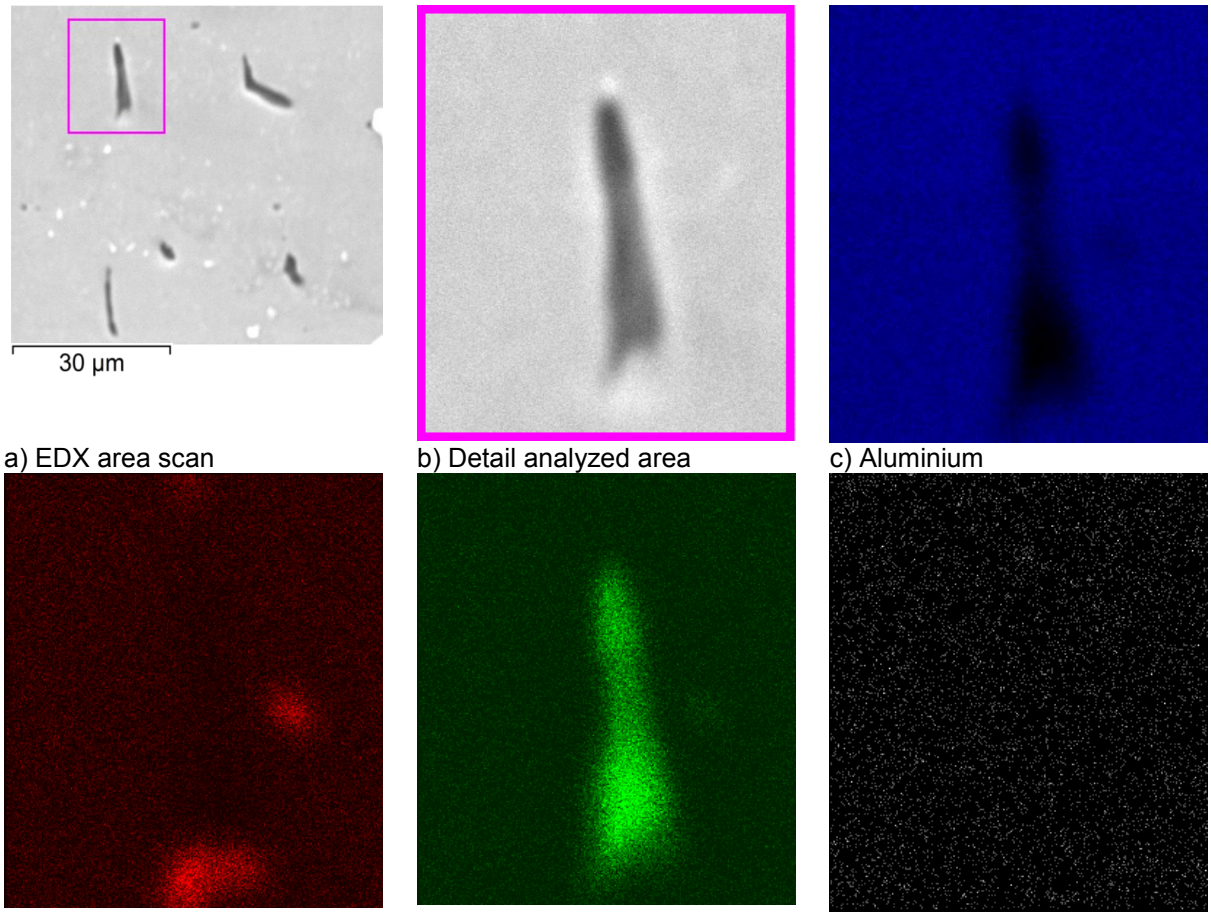

a) EDX area scan b) Detail analyzed area c) Aluminium

d) Magnesium e) Silicon f) Iron

Figure 4.24 Area EDX analysis homogenized vdc billet

In the white particle at EDX 1 in table 4.10 the (Fe+Mn+Cr):Si ratio is 1.24, it seems to be a mixture of α- and β-AlFeSi. EDX 4 shows an (Fe+Mn+Cr):Si ratio of 1.46, EDX 6 has an (Fe+Mn+Cr):Si ratio of 1.42, both particle should mainly consist of α-AlFeSi. EDX 2 and EDX 7 show a high Si content, these particles should be pure Silicon particles, the Al content is most probably from the background. EDX 5 seems to be an AlFeSi particle. In the grey particle at EDX 3 the Mg:Si ratio is 2.08, this is a typical value for Mg_2Si.

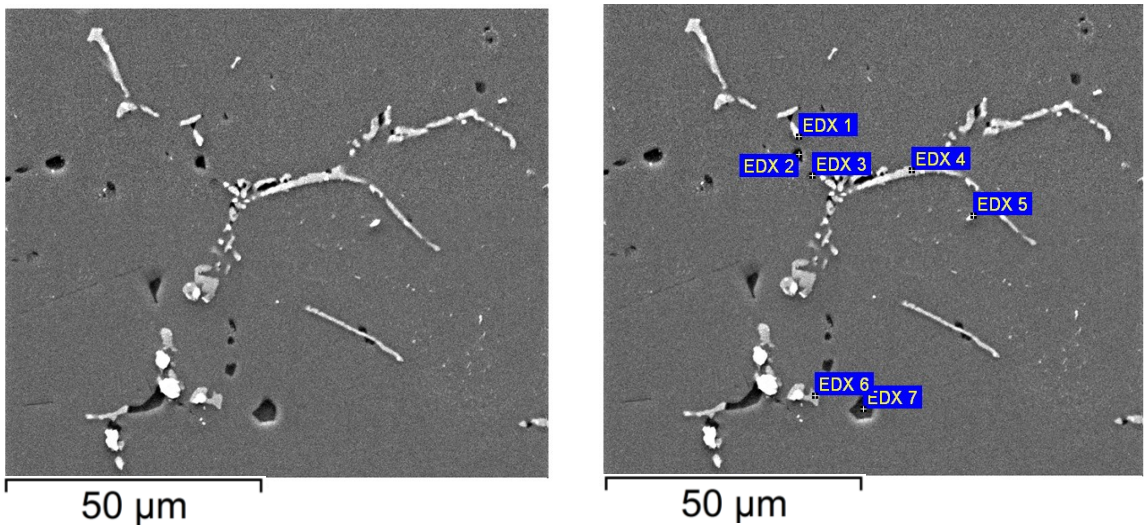

Figure 4.25 Spot EDX analysis homogenized vdc billet

Table 4.10 EDX results homogenized vdc billet

Element atom[%]	Aluminium Al	Iron Fe	Silicon Si	Magnesium Mg	Manganese Mn	Chromium Cr	Titanium Ti	Boron B
EDX 1	68.9	5.2	8.0	---	4.1	0.5	---	---
EDX 2	62.2	0.0	37.8	0.0	---	---	---	---
EDX 3	46.5	0.2	17.3	36.1	0.0	---	---	---
EDX 4	74.5	7.7	10.4	0.1	6.4	1.0	---	---
EDX 5	87.6	---	12.4	---	---	---	---	---
EDX 6	72.2	7.8	11.4	0.3	7.1	1.3	---	---
EDX 7	29.0	0.0	70.8	0.0	0.2	0.1	0.0	---

4.6.5 Results SEM/EDX

4.6.5.1 Mg/Si Phase

An Mg/Si phase with a very low Mg:Si ratio was observed instead of the expected Mg_2Si in the as-cast billets. As the Mg:Si ratio is smaller than 1, it's impossible that the phase is consistent with Mg_2Si, because for Mg_2Si the Mg:Si ratio is 1.73-2.20.
In the literature [24] an $Al_8FeMg_3Si_6$ phase was found, Thermo-Calc recognizes also the existence $Al_8FeMg_3Si_6$, but our Mg/Si phase doesn't contain Fe.
The unknown Mg/Si phase occurred both in the vdc and hdc billets, but during homogenization this phase transforms to Mg_2Si or pure Si in the vdc billets, however this is not the case in the hdc billets.

4.6.5.2 Si

In the hdc billets no elemental Si was found, neither before nor after the homogenization treatment.
In the vdc billets pure Si was found in the unhomogenized and in the homogenized state, but the shape of the Si transforms during homogenization.
Before the heat treatment, the Si shows a round structure, but during the heat treatment the Si dissolves in the Al matrix and re-precipitates in an undesired elongated morphology along grain boundary.

4.6.5.3 AlFeSi

Both in the hdc and vdc billets before homogenization AlFeSi was found as plates on the grain boundary. After homogenization the AlFeSi transformed into a pearl necklace structure on the grain boundaries, but there was no significant change in chemical composition.

4.6.5.4 SEM/EDX of the DSC Sample

Sample cooled with 20°C/min in the DSC from 700°C to 50°C. There is a coarse structure with pores on the grain boundaries. There were 3 different precipitations observed in the DSC samples: AlFeSi, Mg_2Si and Si – the Mg_2Si and Si appear together in the same particle.

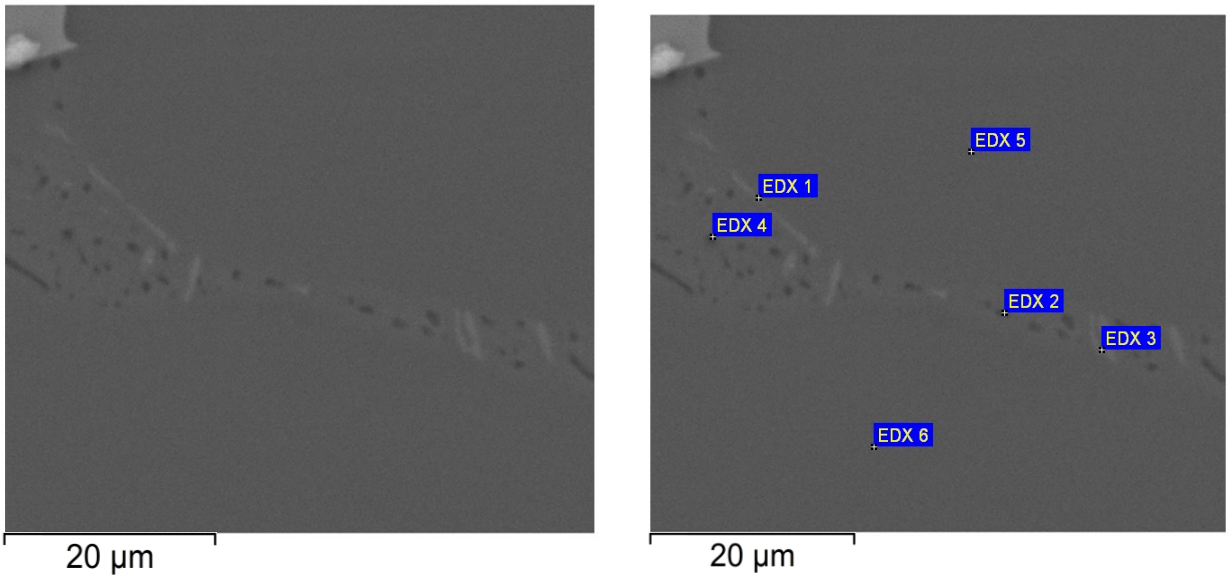

Figure 4.26 Spot EDX analysis I DSC sample

Table 4.11 EDX results I DSC sample

Element atom[%]	Magnesium Mg	Aluminium Al	Silicon Si	Iron Fe	Manganese Mn	Chromium Cr	Type
EDX 1	4.4	81.3	13.3	0.7	0.3	0.0	Mg/Si+AlFeSi
EDX 2	6.8	69.4	23.9	0.1	0.1	0.0	Mg/Si
EDX 3	7.8	74.9	15.8	1.1	0.3	0.1	Mg/Si+AlFeSi
EDX 4	3.1	73.0	23.6	0.2	0.1	0.0	Mg/Si
EDX 5	0.6	98.1	1.1	0.0	0.2	0.0	Matrix
EDX 6	0.8	97.7	1.1	0.1	0.3	0.1	Matrix

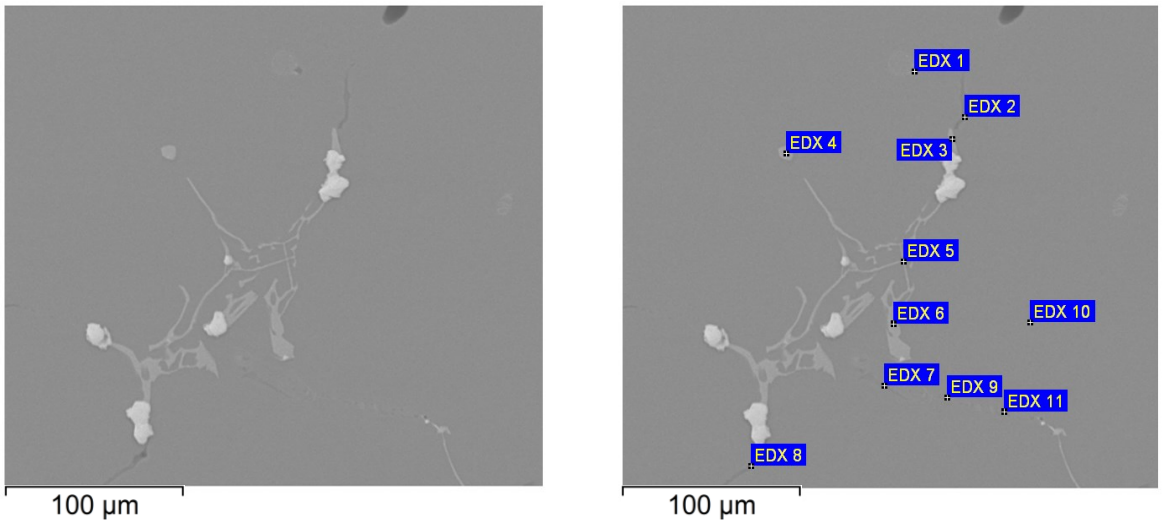

Figure 4.27 Spot EDX analysis II DSC sample

Table 4.12 EDX results II DSC sample

Element atom[%]	Magnesium Mg	Aluminium Al	Silicon Si	Iron Fe	Manganese Mn	Chromium Cr	Type
EDX 1	3.1	74.6	21.6	0.3	0.3	0.1	Mg/Si+AlFeSi
EDX 2	24.4	51.0	24.6	0.1	0.0	0.0	Mg/Si
EDX 3	0.1	72.9	12.0	6.2	6.6	2.2	AlFeSi
EDX 4	0.0	70.9	12.1	7.5	7.5	1.9	AlFeSi
EDX 5	0.6	89.8	4.5	2.6	2.2	0.3	AlFeSi
EDX 6	0.2	72.2	11.1	9.0	6.5	1.1	AlFeSi
EDX 7	2.9	84.6	12.5	0.0	0.1	0.0	Mg/Si
EDX 8	5.7	47.2	47.1	0.0	0.0	0.0	Mg/Si
EDX 9	2.0	72.3	25.5	0.1	0.2	0.0	Si
EDX 10	0.7	98.3	0.6	0.0	0.2	0.2	Matrix
EDX 11	3.3	71.8	24.7	0.0	0.1	0.1	Mg/Si

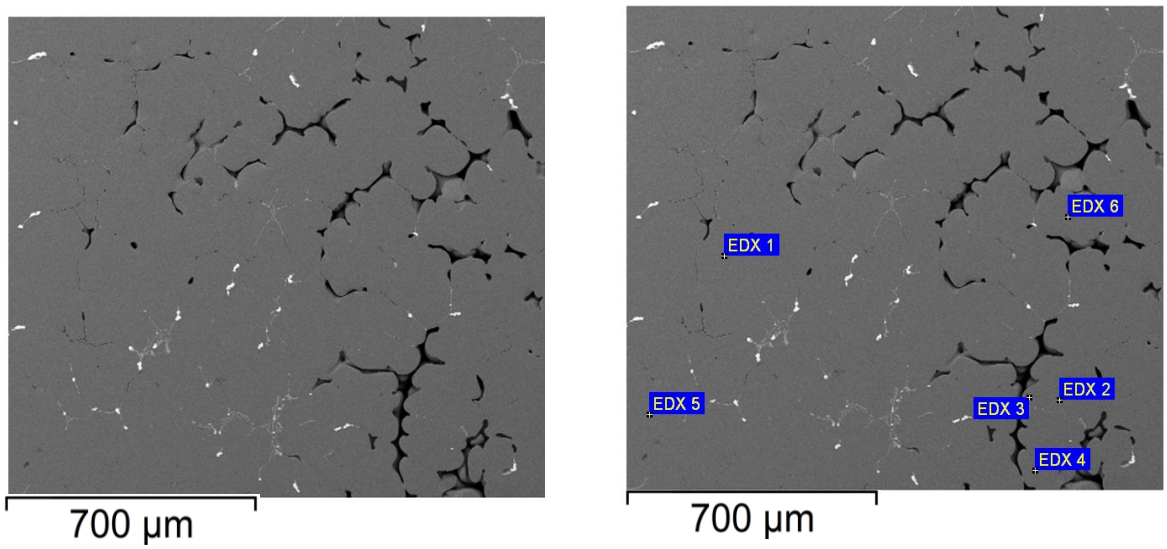

Figure 4.28 Spot EDX analysis III DSC sample

Table 4.13 EDX results III DSC sample

Element atom[%]	Magnesium Mg	Aluminium Al	Silicon Si	Iron Fe	Manganese Mn	Chromium Cr	Type
EDX 1	0.5	99.0	0.6	0.0	0.0	0.0	Matrix
EDX 2	0.7	98.5	0.4	0.0	0.2	0.2	Matrix
EDX 3	0.8	98.1	0.6	0.0	0.4	0.1	Matrix
EDX 4	0.8	98.3	0.5	0.1	0.3	0.1	Matrix
EDX 5	0.6	98.7	0.3	0.0	0.3	0.1	Matrix
EDX 6	0.6	98.6	0.4	0.1	0.2	0.0	Matrix+AlFeSi

4.7 Results of the Analysis

Only two phases, AlFeSi and Mg/Si, were found during the SEM observation, subsequently the existence of significant amounts of other phases can be excluded. The Mg/Si phase is most probably a mixture of silicon and Mg_2Si (because of the too low Mg:Si ratio).
The two temperature peaks at the DSC seem to come from the precipitation/dissolution of silicon (peak at 559°C, in good accordance with [22] (there 558°C) and non-equilibrium Thermo-Calc calculation (there 560°C)) and Mg_2Si (peak at 583°C, start at 574°C in good accordance with the non-equilibrium Thermo-Calc simulation (there start at 572°C)). The dissolution peak of the AlFeSi peak is inside the melting peak and therefore not clear visible in the DSC diagram. At the old homogenization temperature neither Si nor Mg_2Si dissolved completely, which strongly shows that the heat treatment temperature is too low. Furthermore there is no significant change of chemical composition of the coarse Mg/Si phase, which is a further evidence that the homogenization temperature of 555°C is too low.
As a result homogenization tests at a laboratory furnace were performed to test other homogenization temperatures and their effect on the microstructure and the mechanical properties.

5 Optimization of the Heat Treatment

5.1 Furnace Experiments

5.1.1 Cooling Conditions after the Laboratory Furnace

Target of these experiments was to find the right cooling conditions for small 6082 samples to mimic the conditions of the industrial homogenization furnace. The red line in diagram 5.1 and 5.2 shows the cooling conditions of the billet, the lime and dark green lines with insulation on 5 sides of the small 6082 sample show the best approximation of the industrial cooling conditions.

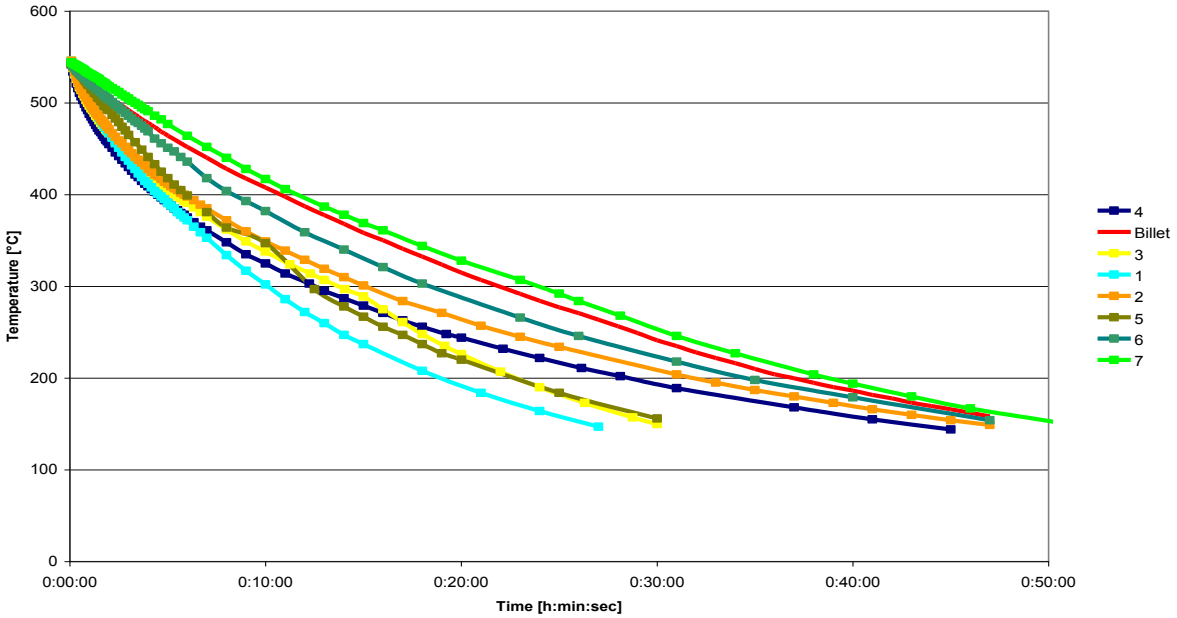

Diagram 5.1 Temperature characteristics of the billet and the samples (intersection point: 560°C)

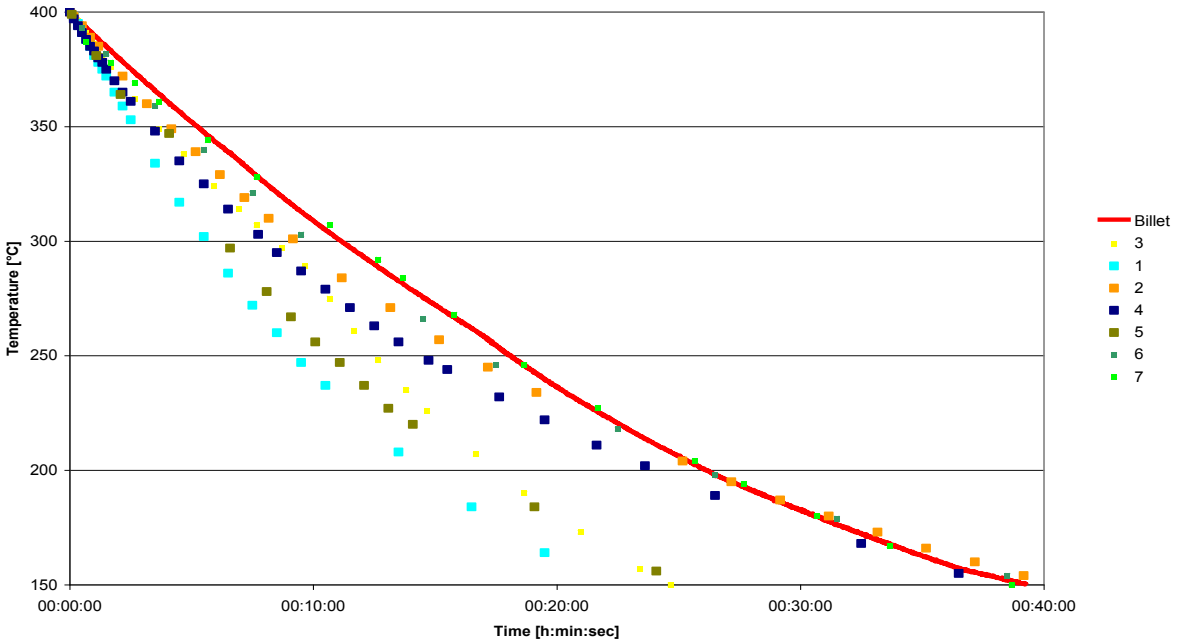

Diagram 5.2 Temperature characteristics of the billet and the samples (intersection point: 400°C)

In the following diagram we see, that Experiment 6 & 7 (see experimental methods) show a cooling rate which is almost the same as in the billet (for details about the samples/experiments see table 3.2).

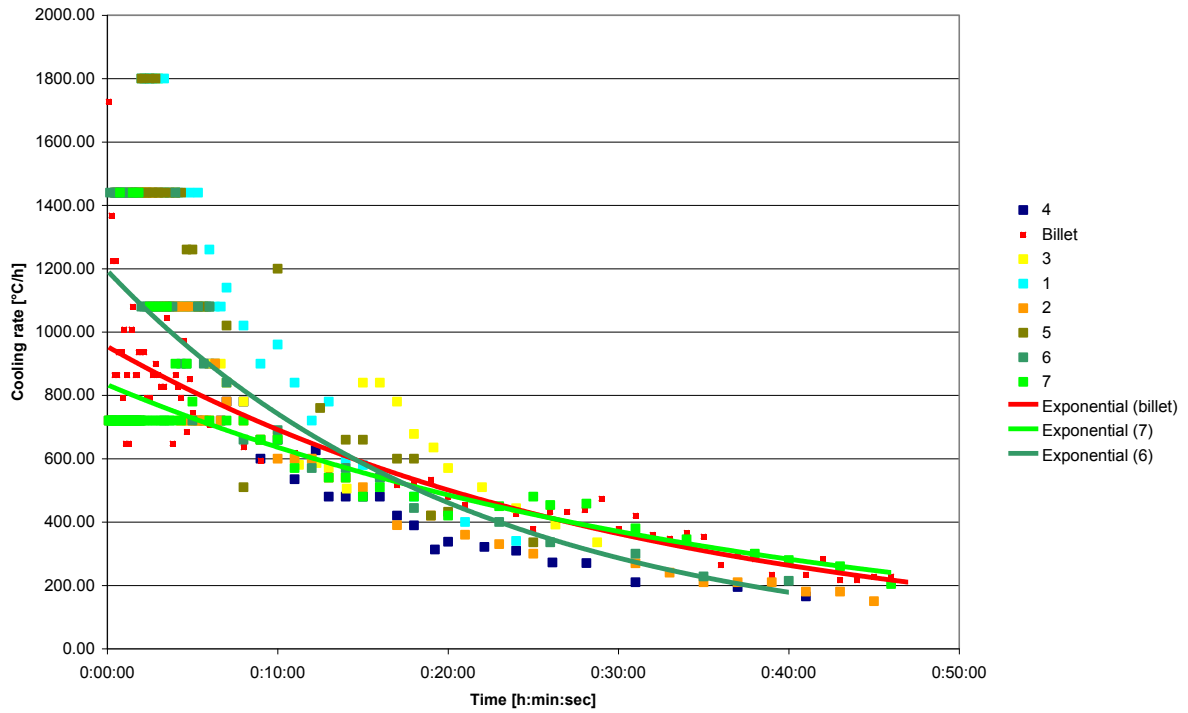

Diagram 5.3 Cooling rate plot against time

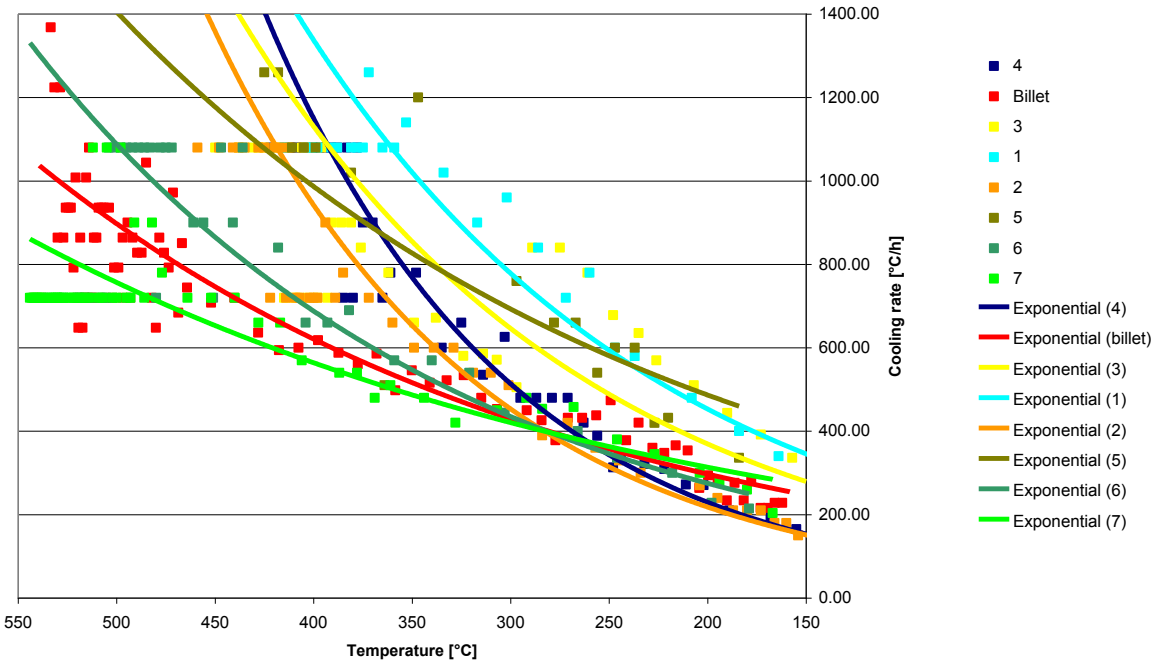

Diagram 5.4 Cooling rate plot against temperature

As a consequence of these results, for the following homogenization treatments a preheated insulation of the samples (the same insulation which was used in Experiment 6 and 7) was used to simulate the cooling conditions after the production furnace as near as possible.

The significant result was that a preheated Mg-Al-silicate insulation on 5 of 6 sides brought nearly the same cooling conditions as for the billet after the furnace with powerful fan cooling as a result of the different volume:surface ratio of the samples.
These cooling conditions are very important, because during cooling phases like Mg_2Si precipitate, and their shape and structure (coherent, semi-coherent and incoherent) are dependent on the cooling rate. Furthermore these Mg_2Si precipitations are important for the flow behaviour during billet extrusion and for the mechanical properties of the final product.

5.1.2 Homogenization Experiments in the Laboratory Furnace

For this test, samples from the unhomogenized hdc billet were prepared.

5.1.2.1 Temperature Sequence

During these experiments the temperature profile was reported (diagram 5.5).
The red line in diagram 5.5 shows the temperature chart of the billet in the industrial furnace, holding time was 4:30h, holding temperature was 555°C.
The other lines show the temperature charts of the samples in the laboratory furnace.

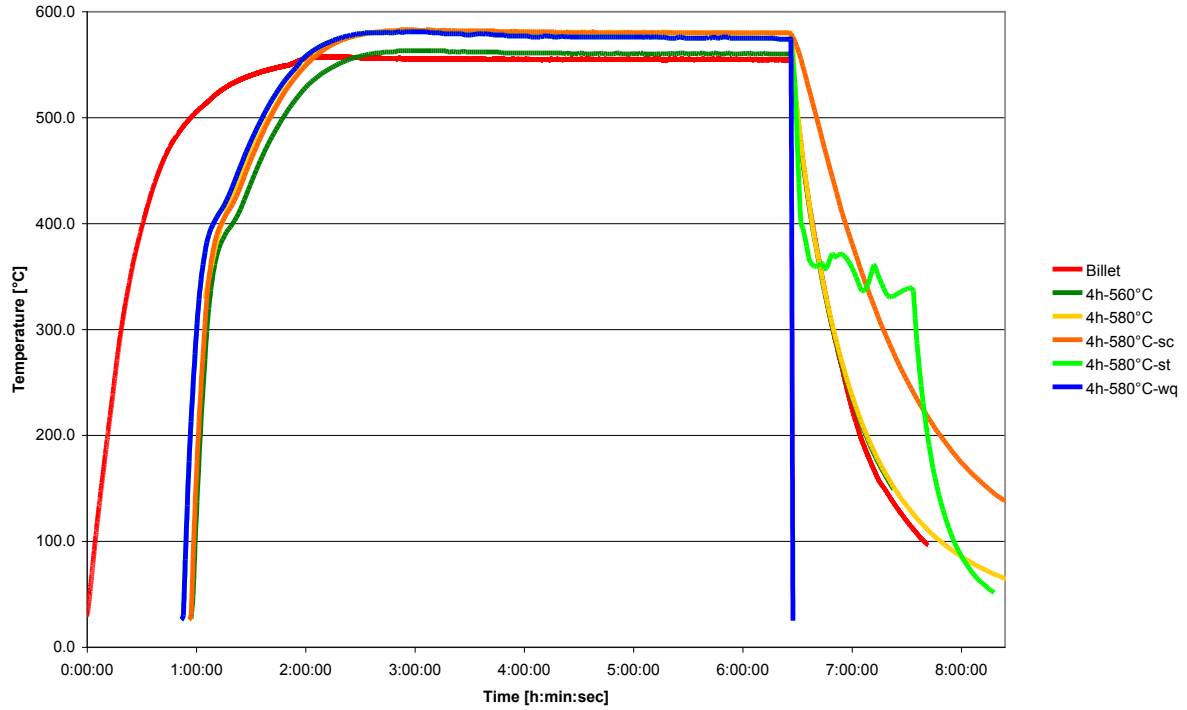

Diagram 5.5 Temperature gradation of the 5 experiments compared to the billet of the industrial process plot against time

Diagram 5.6 demonstrates the cooling sequence in detail, both of the sample of the industrial furnace and the samples of the laboratory furnace.

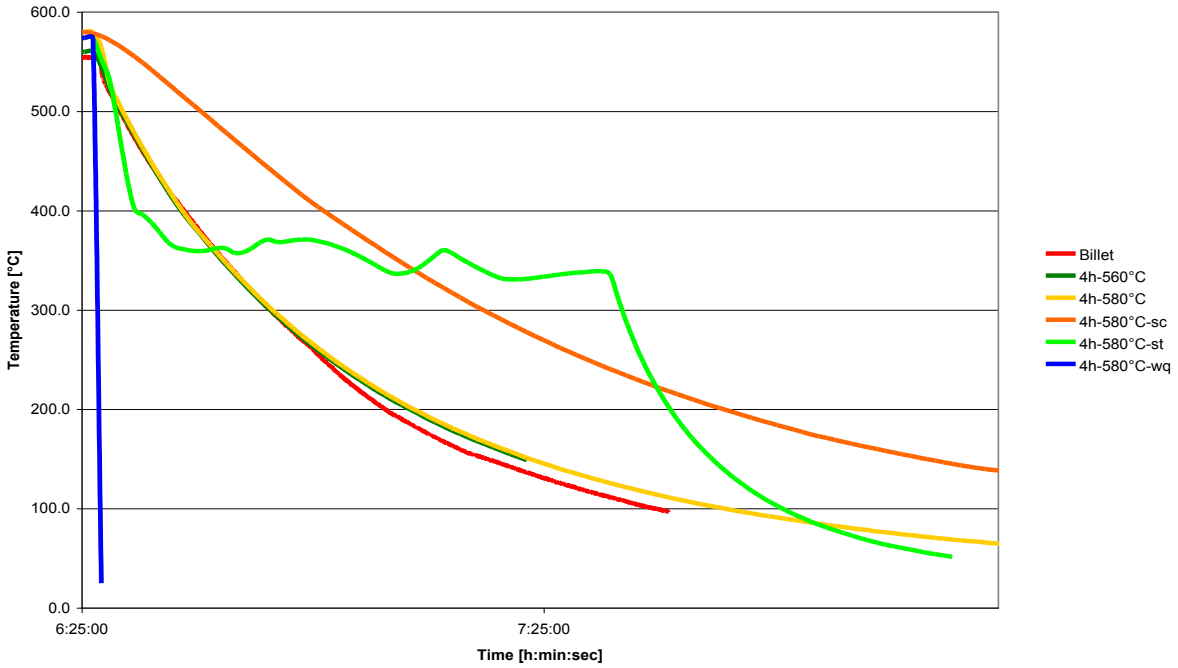

Diagram 5.6 Temperature gradation of the 5 experiments during cooling compared to the billet

After these experiments metallographic samples for LOM (checking grain growth) SEM and TEM and specimens for the PSCT were prepared.

5.2 Plain Strain Compression Test (PSCT)

5.2.1 Preheating Conditions at the Extrusion Press

In order to obtain similar heating conditions in the experiment the heating conditions before the extrusion press in the production was measured:

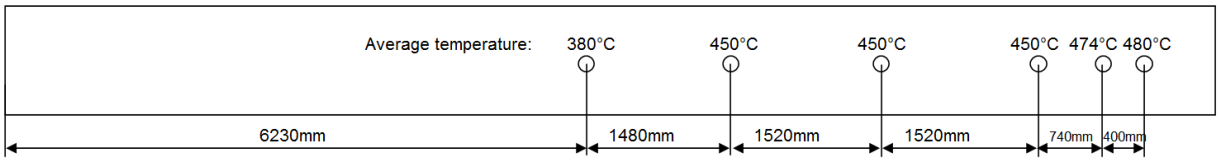

Figure 5.1 Schematic drawing of the preheating furnace

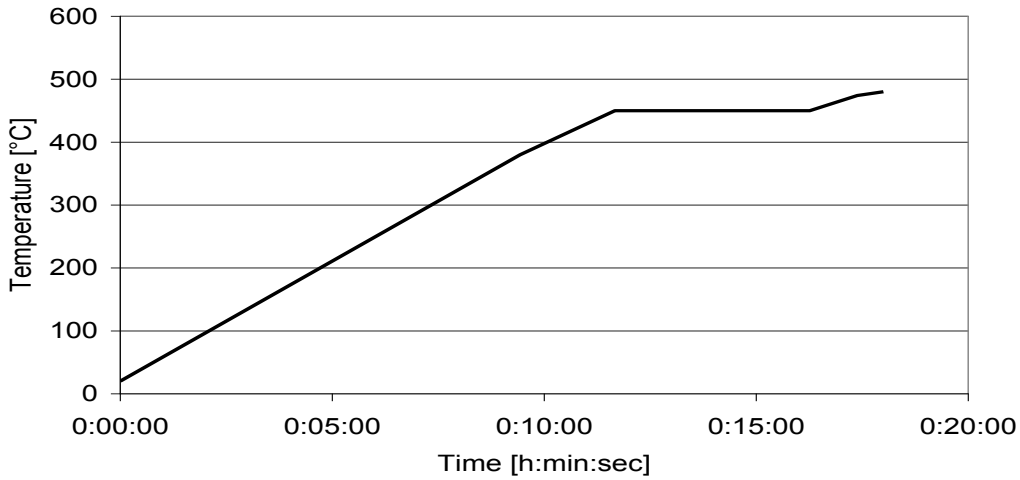

Diagram 5.7 Temperature of the billets in the preheating furnace

5.2.2 Preheating Conditions at the PSCT

During test 2-8II the temperature was not measured because this test was a pre-test to analyze the experimental set-up.
The samples were preheated to 480°C and after 6 minutes at this temperature the test was performed. The heating period (first 8 minutes) is not as essential as the holding period at 480°C. As a result all performed experiments can be compared successfully, although the curves in diagram 5.8 deviate from each other in the heating period.

Table 5.1 List of abbreviations

Abbreviation	Acceptation
6II	4.5h homogenized at 560°C in industrial furnace, standard cooling
4IIf	6h homogenized at 540°C in industrial furnace, standard cooling
8IILab	4h homogenized at 580°C in laboratory furnace, standard cooling
6IILab	4h homogenized at 560°C in laboratory furnace, standard cooling
st	4h homogenized at 580°C in laboratory furnace, step cooled
sc	4h homogenized at 580°C in laboratory furnace, slow cooled
wq	4h homogenized at 580°C in laboratory furnace, water quenched

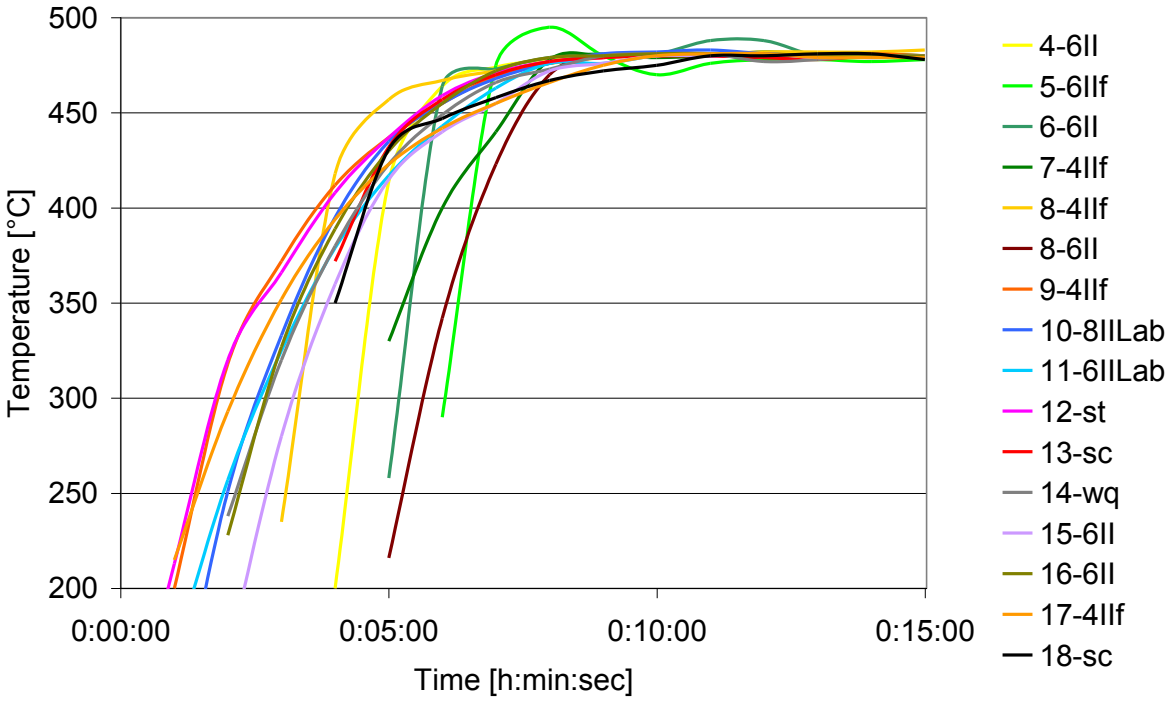

Diagram 5.8 Preheating conditions before the PSCT, sample temperature plot against time

5.2.3 Results of the PSCT

A force-displacement curve was measured and a stress-strain diagram was calculated from this data. Because of a nonlinear behaviour of all samples between 0 and 10MPa the curves were normalized to a start point of 10MPa and 30MPa. Two different start points were used, because both have their advantages: At start point 10MPa the plastic deformation is quiet small, but there are still some influences from

the set-up (e.g. settling movement). At start point 30MPa the plastic deformation is quiet large, but there are no influences from the machine set-up any more.
During test 18-sc (slow cooled) the upper tool touched the specimen during preheating, as a result this curve wasn't used for the further analysis.
Diagram 5.9 shows the raw data with settling movement of the sample, diagram 5.10 and 5.11 show the data with normalized zero-point.

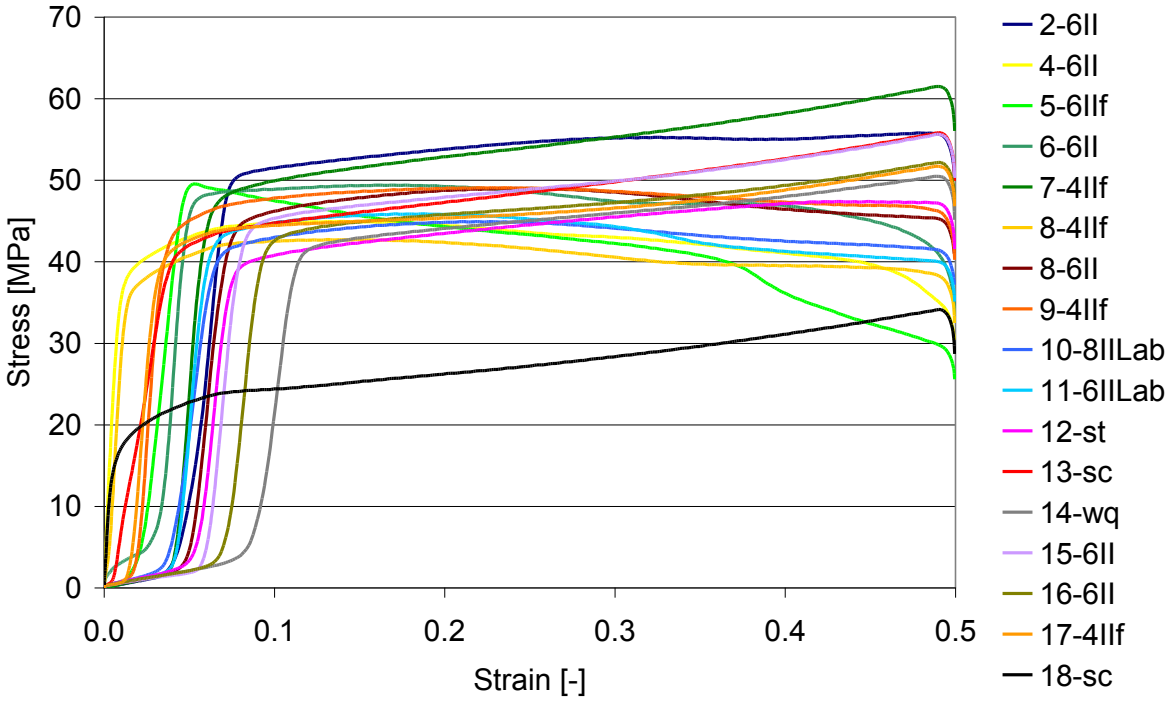

Diagram 5.9 Stress-Strain diagram

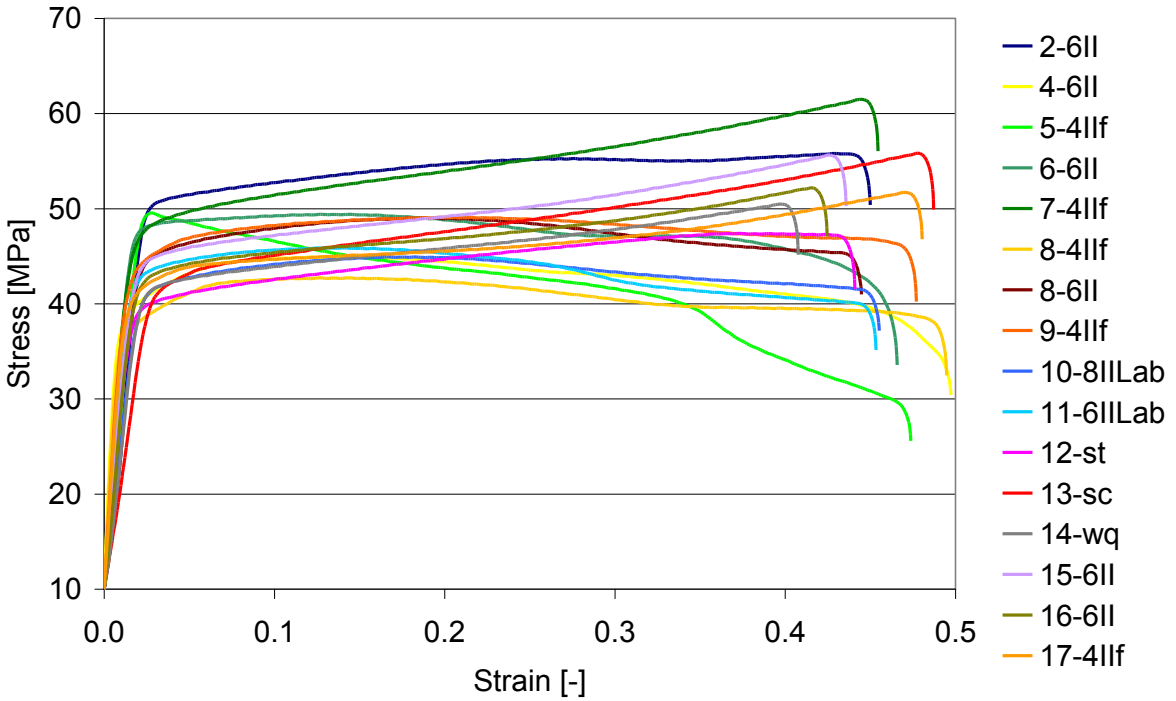

Diagram 5.10 Stress-Strain curve normalized to 10MPa

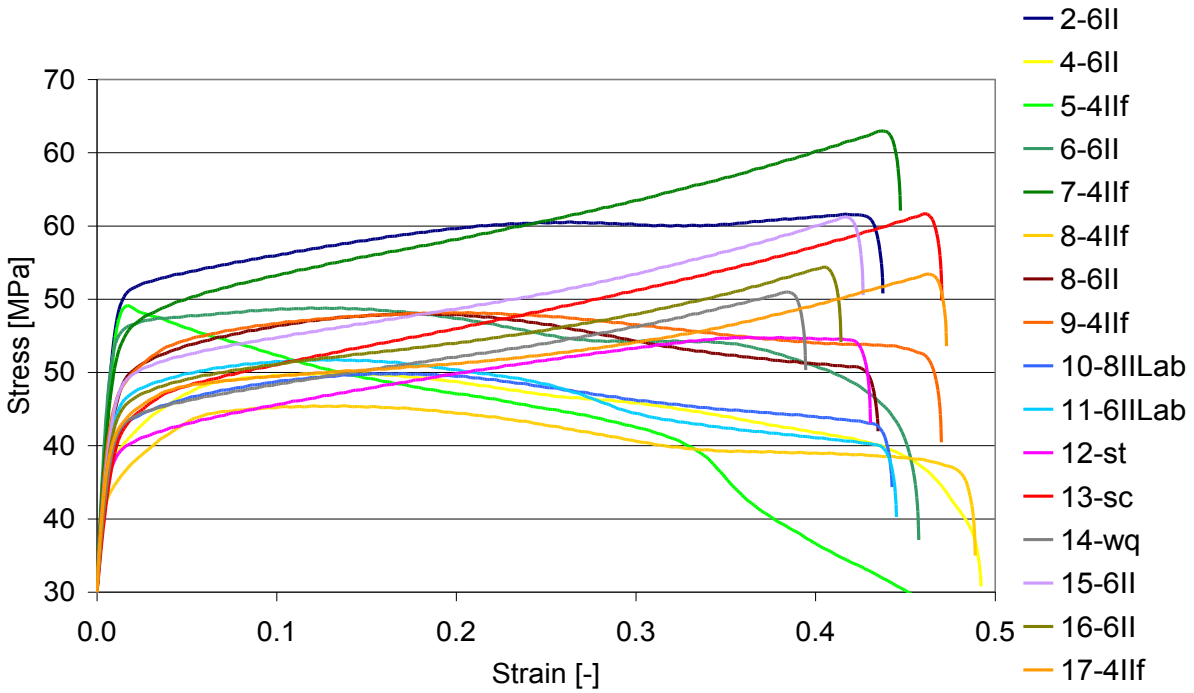

Diagram 5.11 Stress-Strain curve normalized to 30MPa

For further analysis of the flow stress only the strain range 0 - 0.05 was analysed because only this range is important for analyzing the flow stress and at higher strains most samples tilted and the stress values became dependent on the tilting angle.

5.2.4 Calculation of the Flow Stress

For details see appendix 9.1.
Diagram 5.12 shows, that the sample 4-6II (555°C, hdc) has the highest stiffness at low strain rates, samples 6-6II and 2-6II (both 555°C, hdc) have the highest stiffness at higher strain rates. Sample 13-sc (580°C, slow cooled) shows the lowest stiffness. Also 10-8IILab and 12-st show a quiet low stiffness dF/dε.

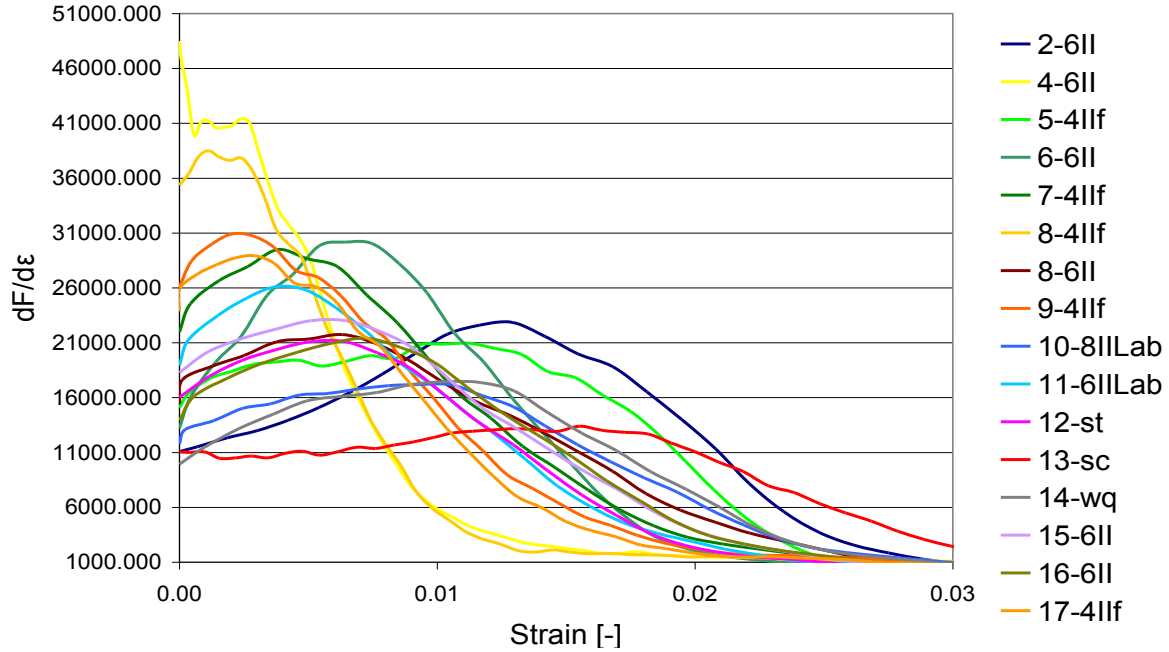

Diagram 5.12 Stiffness (dF/dε) of the material plot against strain

5.2.5 Calculated Flow Stress

The analysis shows, that the flow stress of the samples homogenized at 580°C is significant lower than the flow stress of the samples heat treated at 555°C. The difference of the flow stress is about 10%.

Table 5.2 Comparison flow stress and Stiffness of the specimens

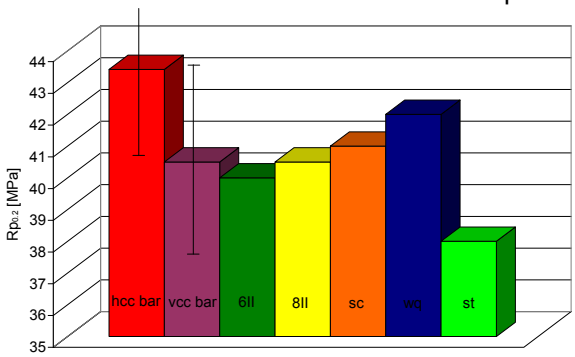

Diagram 5.13 Flow stress $R_{p0.2}$ (normalized 10MPa)

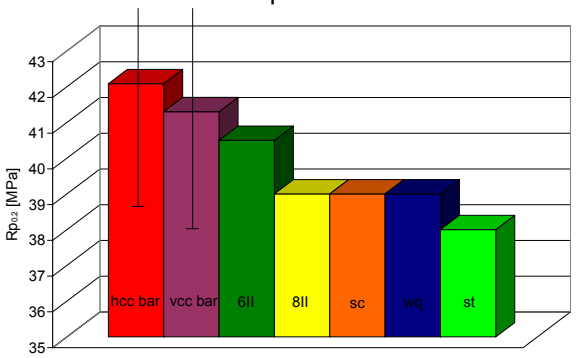

Diagram 5.14 Flow stress $R_{p0.2}$ (normalized 30MPa)

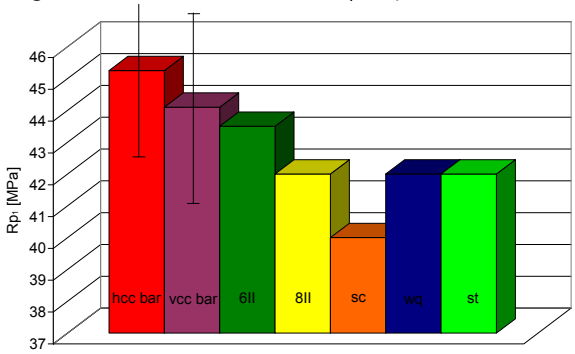

Diagram 5.15 Flow stress $R_{p1.0}$ (normalized 10MPa)

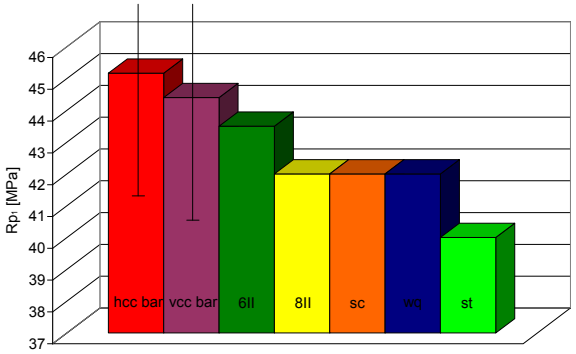

Diagram 5.16 Flow stress $R_{p1.0}$ (normalized 30MPa)

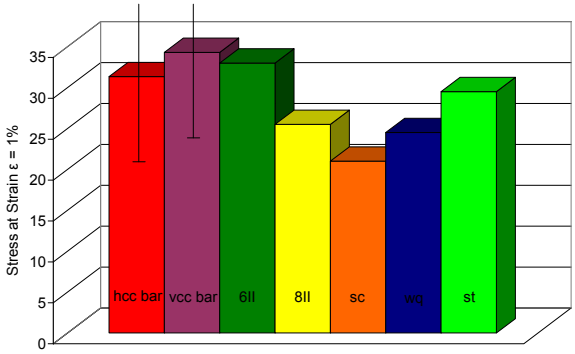

Diagram 5.17 Flow stress at strain ε=1% (n. 10MPa)

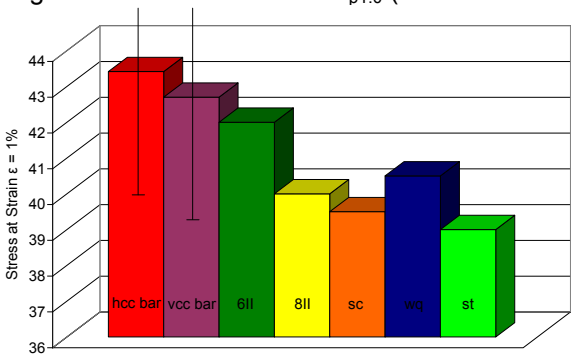

Diagram 5.18 Flow stress at strain ε=1% (n. 30MPa)

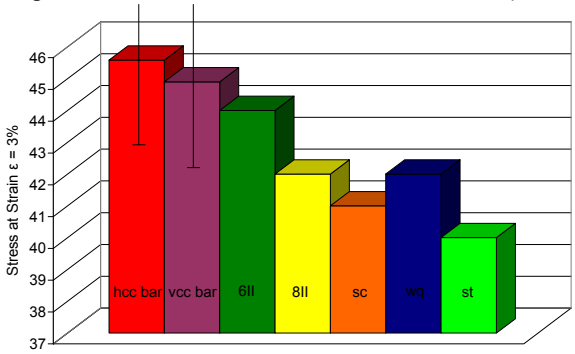

Diagram 5.19 Flow stress at strain ε=3% (n. 10MPa)

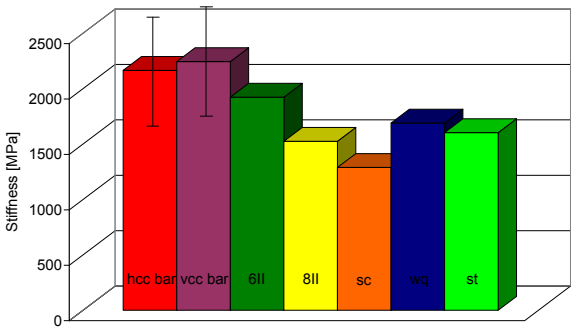

Diagram 5.20 Stiffness (dF/dε) (normalized 30MPa)

As expected in 6 of 8 cases the flow stress shows a lower value for the vdc billets compared to the hdc billets. The water quenched sample show a higher stiffness than the other samples homogenized at 580°C, caused by the higher Mg and Si

content of the matrix. Consequently the slow cooled (sc) sample shows the lowest stiffness, because most of the Mg and Si were precipitated during cooling. In conclusion the results suggest a trend of a higher cooling speed resulting in a lower stiffness. There is no error bar for the 6II, 8II, sc, wq and st samples because the number of samples was too small.

5.3 Light Optical Microscopy

As the homogenization temperature was increased to 580°C it was essential to check the grain size to keep sure that grains do not grow significantly.

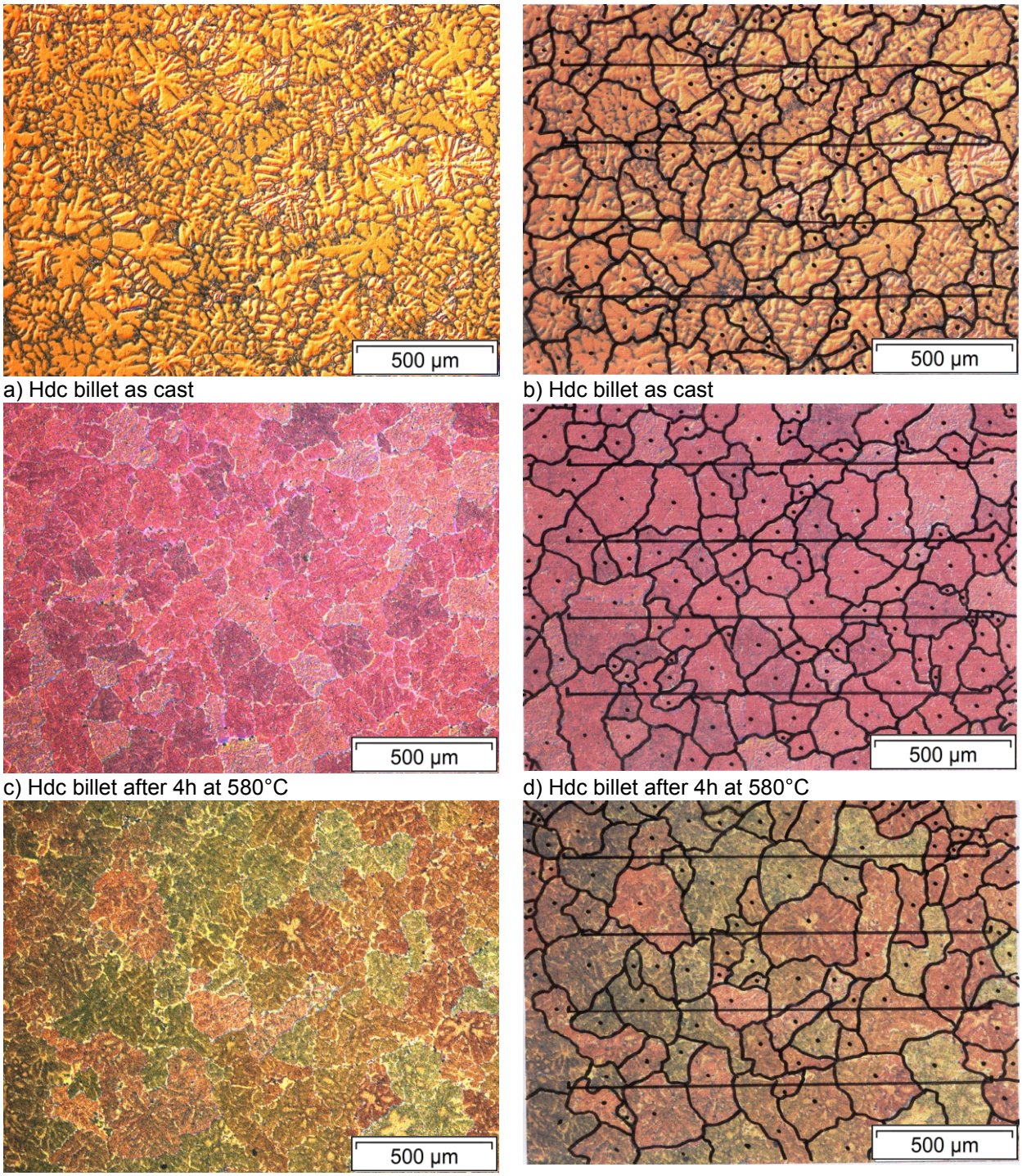

a) Hdc billet as cast
b) Hdc billet as cast
c) Hdc billet after 4h at 580°C
d) Hdc billet after 4h at 580°C
e) Hdc billet after 4h at 560°C
f) Hdc billet after 4h at 560°C

Figure 5.2 Comparison of the grain size (Barker)

Table 5.3 Grain size (line analysis)

	Grain size [µm]	
	Before homogenization	After homogenization
Hdc billet, 4h, 580°C	110	125
Hdc billet, 4h, 560°C	110	141

Table 5.4 Grain size (area analysis)

	Grain size [µm]	
	Before homogenization	After homogenization
Hdc billet, 4h, 580°C	140	140
Hdc billet, 4h, 560°C	140	162

To make sure, that grain growth does not occur a further Barker etch solution (solution 2) was performed. In Figure 5.3 the grain size is quiet similar suggesting that the difference in heat treatment temperature does not affect the grain size.
In figures 5.4 and 5.5 the microstructures at different magnifications (100x - 1000x) of samples homogenized at 560°C and 580°C show the morphology of the microstructure at low magnifications and etching pits at the highest magnification.
The black rectangles in figures 5.4 and 5.5 mark the area with a higher magnification.

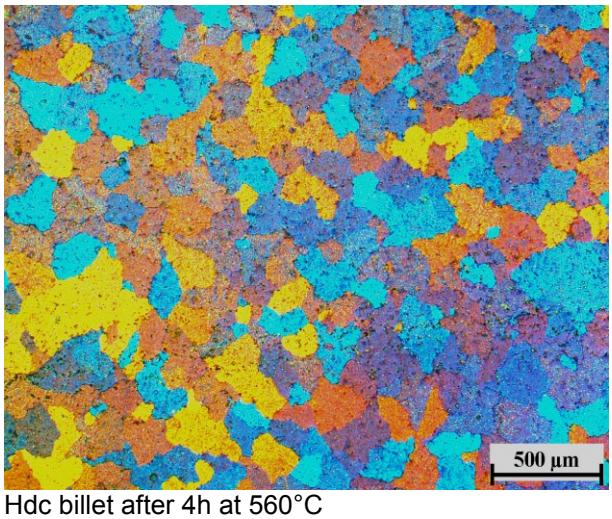

Hdc billet after 4h at 560°C

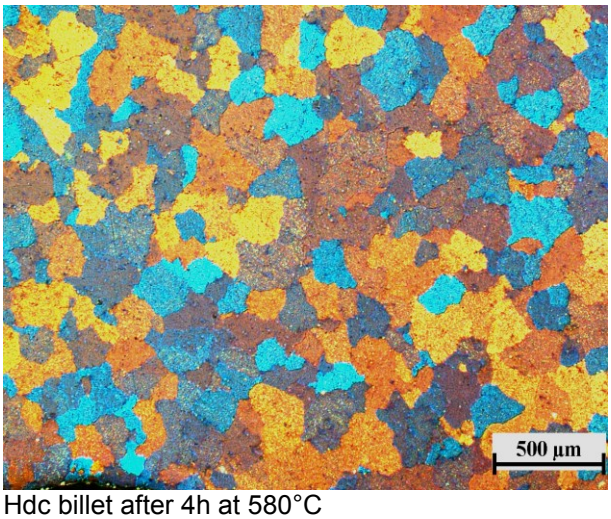

Hdc billet after 4h at 580°C

Figure 5.3 Comparison of the grain size (Barker solution 2)

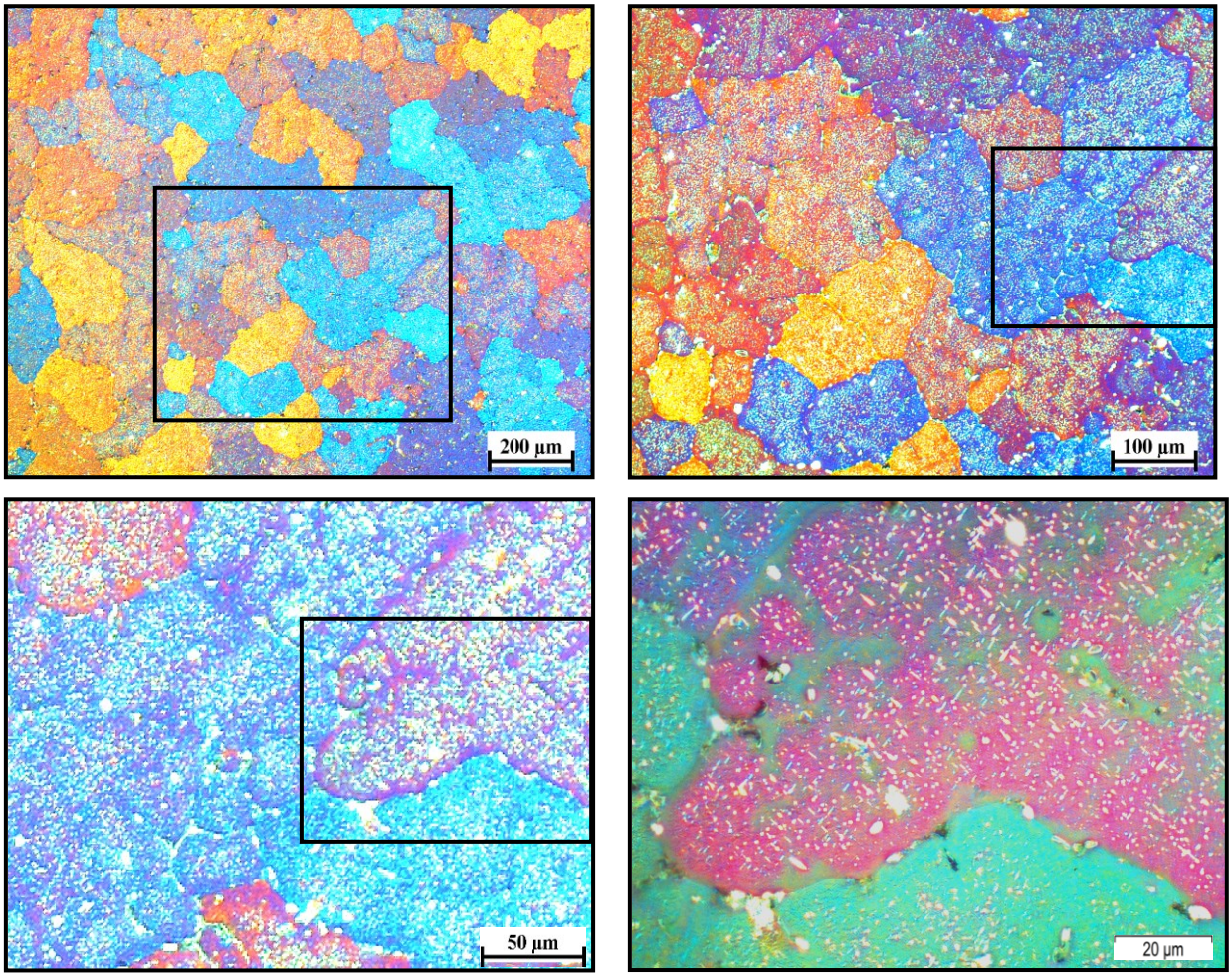

Figure 5.4 Microstructure of the samples homogenized for 4h at 560°C

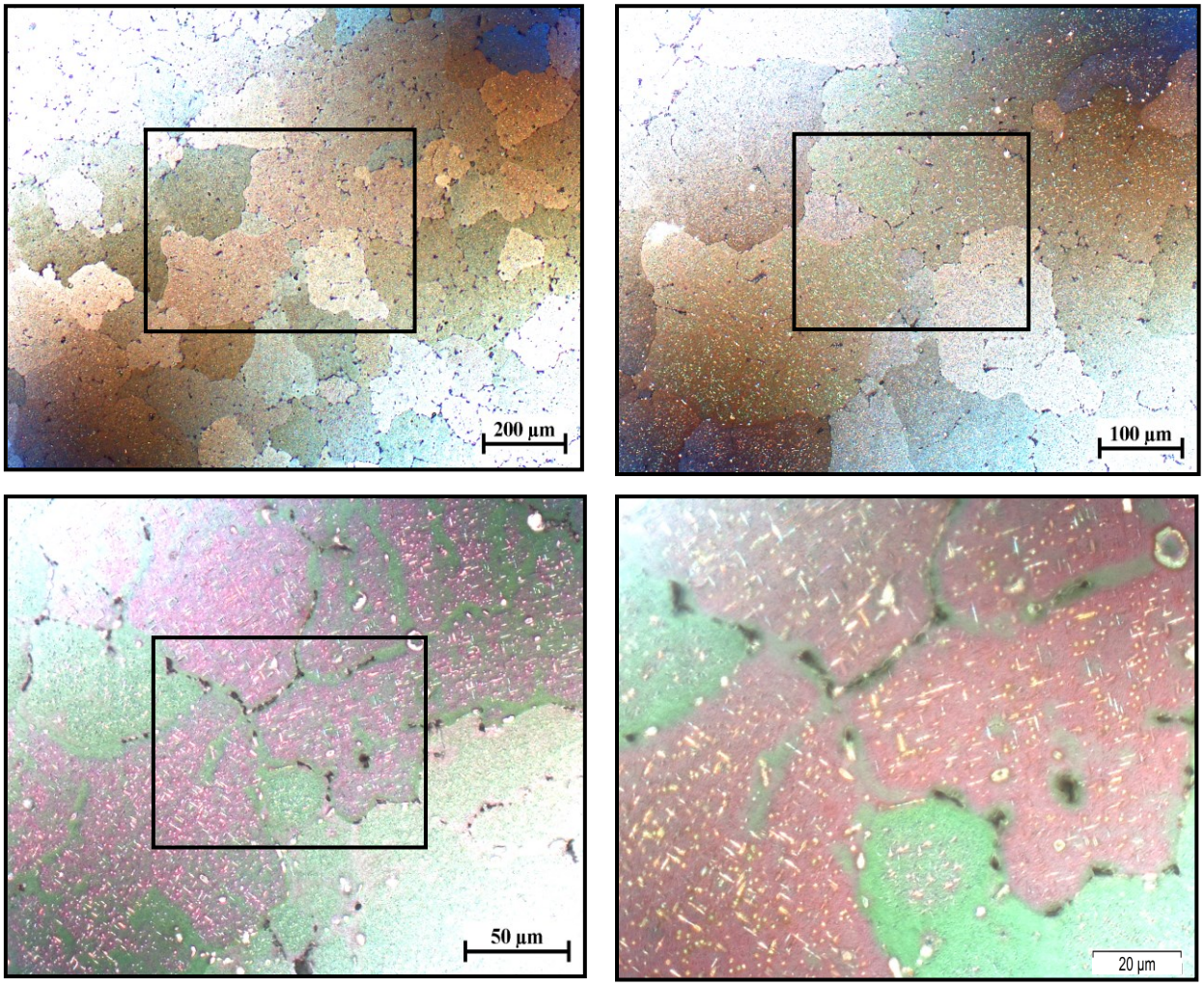

Figure 5.5 Microstructure of the samples homogenized for 4h at 580°C

At the highest magnification (1,000x) in figure 5.6 structures inside the grains become visible. The length of the white lines is on average 5µm, the width is ~500nm. The angle between the different precipitations inside a grain is 90°. Most probably these white lines originate from coherent or semi-coherent Mg_2Si precipitations along the <100>Al. These precipitations dissolved during the etching process and these white lines correspond to etching pits along the <100>Al.

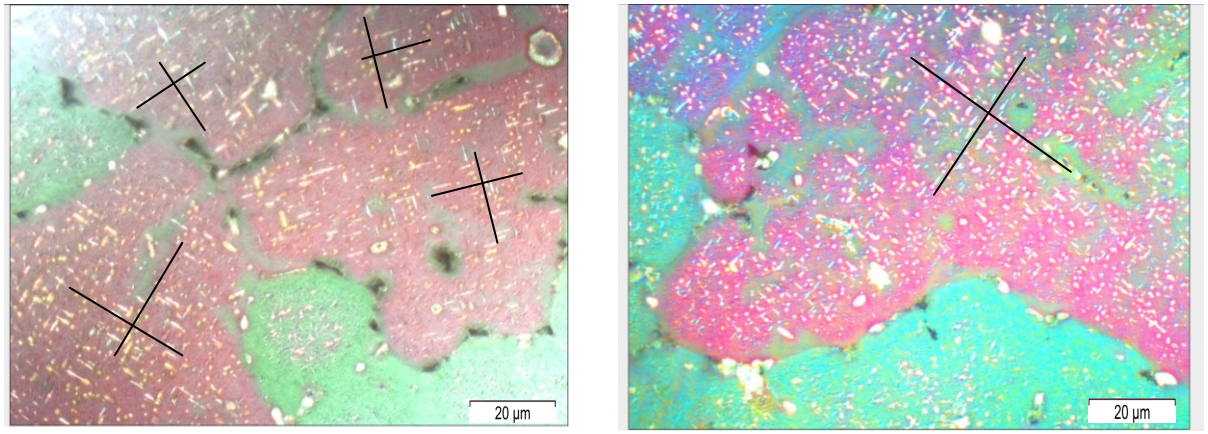

Hdc billet after 4h at 580°C Hdc billet after 4h at 560°C

Figure 5.6 Structures inside the grains

5.4 Scanning Electron Microscopy

5.4.1 Results

5.4.1.1 Sample 560°C (6II)

In the comparison in figure 5.7 and appendix 9.2 we see, that there are also Mg/Si precipitations inside the matrix. The reason for this is that the homogenization temperature is too low, the Mg/Si precipitations cannot dissolve and re-precipitate during cooling on the grain boundary.

5.4.1.2 Sample 580°C (8II)

In figure 5.7 and appendix 9.2 one can see that the transformation of the plate-like β-AlFeSi into α-AlFeSi was more completely in the 580°C than in the 560°C samples.

5.4.1.3 Slow cooled Sample (sc)

In the slow cooled sample in figure 5.7 more µm-sized Mg/Si precipitations were visible than in other samples. The reason for this is a cooling rate which is at least 50% slower than for other samples.

5.4.1.4 Step cooled Sample (st)

Inside the grains of the step cooled samples in the figure 5.7 and appendix 9.2 small (<1µm) precipitations are visible. These precipitations are most probably Mg/Si particles. These structures are also visible in the samples 8II, 6II and sc, but the structures are less significant there. These structures are not visible in the wq samples.

5.4.1.5 Water quenched Sample (wq)

In figure 5.7 there are only precipitations of AlFeSi, there are no Mg/Si particles as a consequence of fast cooling. This is a further evidence that the second DSC peak is the dissolution peak of Mg_2Si and the first DSC peak at lower temperatures is the dissolution peak of Si. As a result the matrix of the water quenched sample is rich in Mg and Si, because there are no precipitations of Si or Mg_2Si.

For further pictures see appendix 9.2.

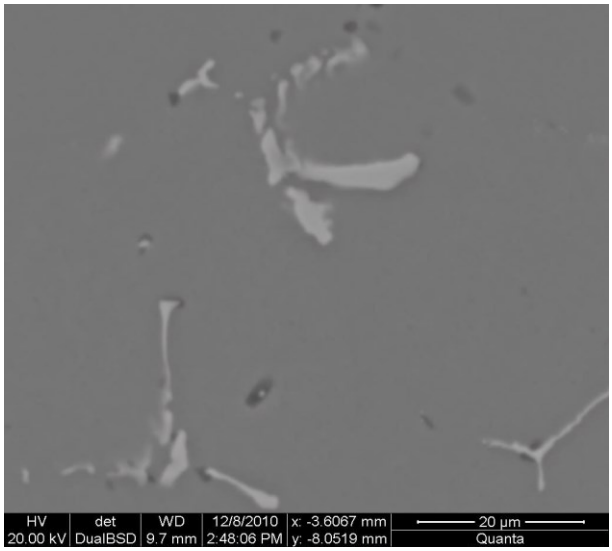

560°C, normal cooling

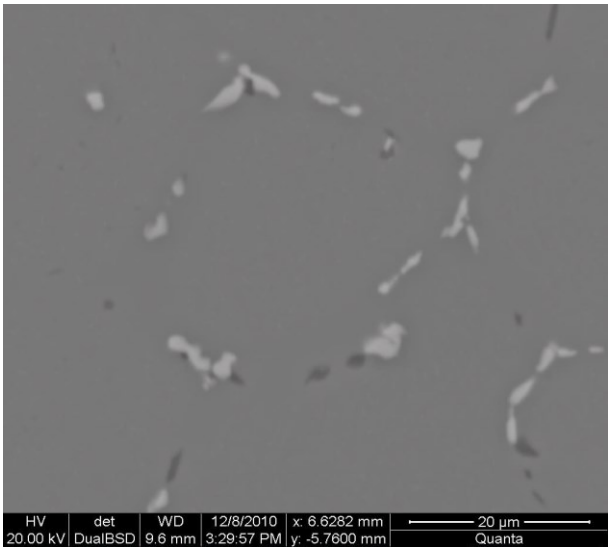

580°C, normal cooling

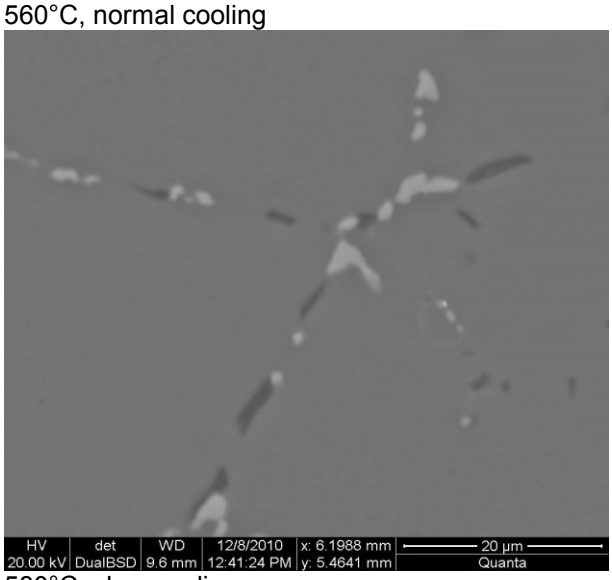

580°C, slow cooling

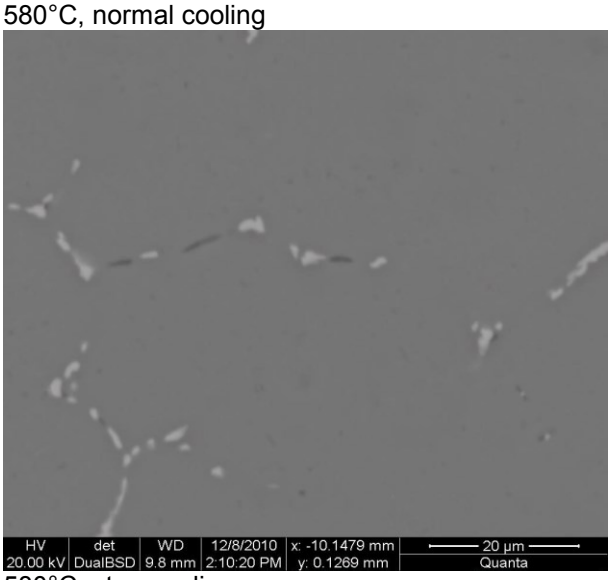

580°C, step cooling

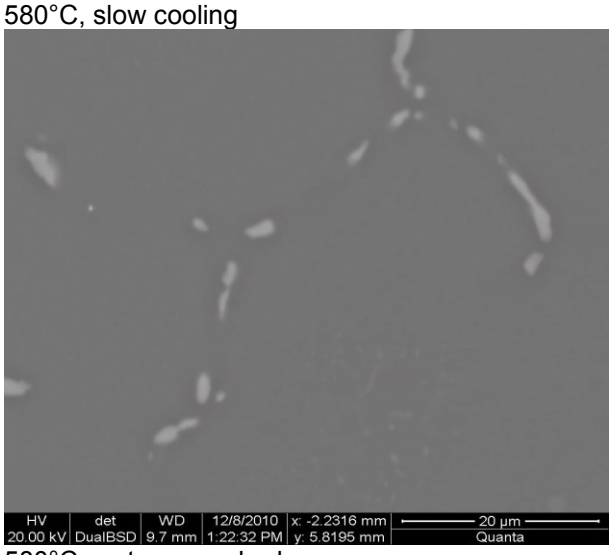

580°C, water quenched

Figure 5.7 Comparison of the five different cooling conditions

5.5 Energy Dispersive X-Ray Diffraction

5.5.1 Criteria for Selection

More than 150 EDX locations were analyzed, they were classified through the criteria in table 5.5. Each EDX spot which doesn't fit into this scheme was defined as a mixture of particles.

Table 5.5 Criteria for selection

Criteria	Matrix	Mg/Si	Si	AlFeSi
Fe	≤0.1	≤0.1	≤0.1	
Al	>95.0	≤95.0	≤95.0	≤95.0
Si	≤2.0	>2.0	>2.0	
Mg	≤2.0			≤2.0
Mg/Si		>0.1	≤0.1	

5.5.2 EDX Analysis

On each sample (8II - 580°C, 6II - 560°C, st - step cooled, sc - slow cooled and wq - water quenched) at least at 28 locations an EDX analysis was performed. Beside the particles (Mg/Si, AlFeSi) and the particular element ratios also the matrix was analysed. For details see appendix 9.3.

5.5.3 EDX Results

5.5.3.1 Characterisation of the Mg/Si Particles

At the homogenization temperature of 560°C the large Mg/Si particles consist of nearly pure Si. Because of the new implemented, higher homogenization temperature the particles have a significant higher Mg content, but the Mg/Si ratio does not agree with the composition of Mg/Si particles from the literature [26], as a result TEM analysis for further observation and particle identification was done.

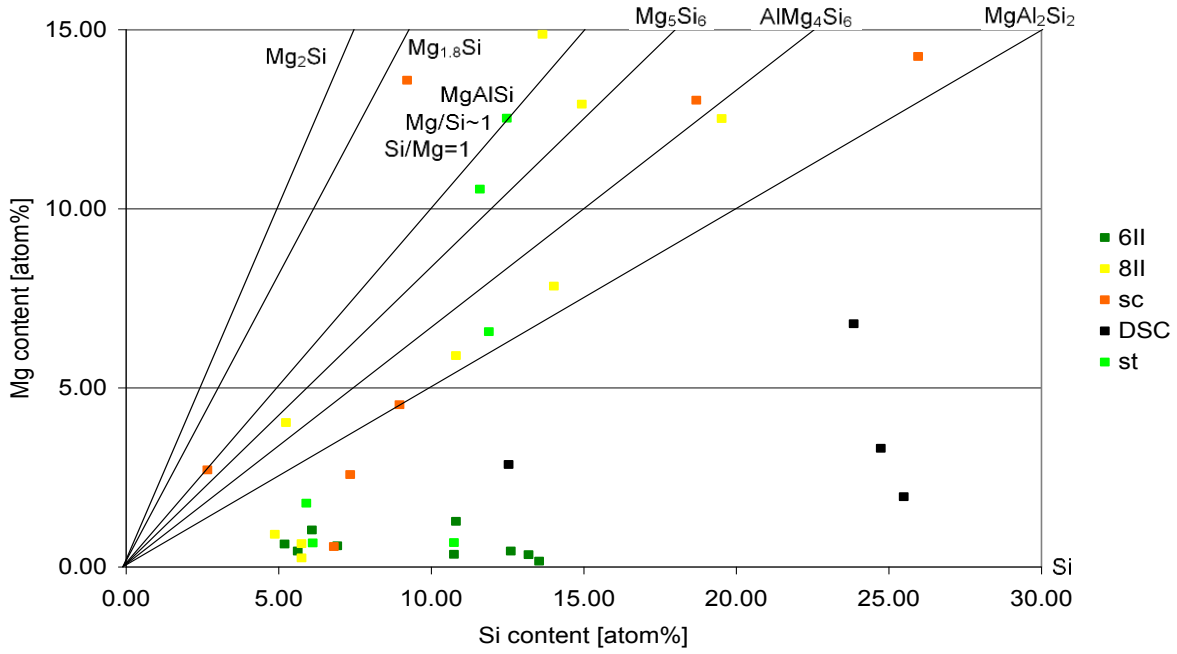

Diagram 5.21 Composition of the Mg/Si particles (Mg content plot against Si content)

5.5.3.2 Characterisation of the AlFeSi Particles

From the SEM-EDX results it appears that the transformation of the β-AlFeSi to α-AlFeSi is not complete for all different homogenization conditions, because the composition of the particles is between the composition of α- and β-AlFeSi. For further investigations TEM observations were done in section 5.6.

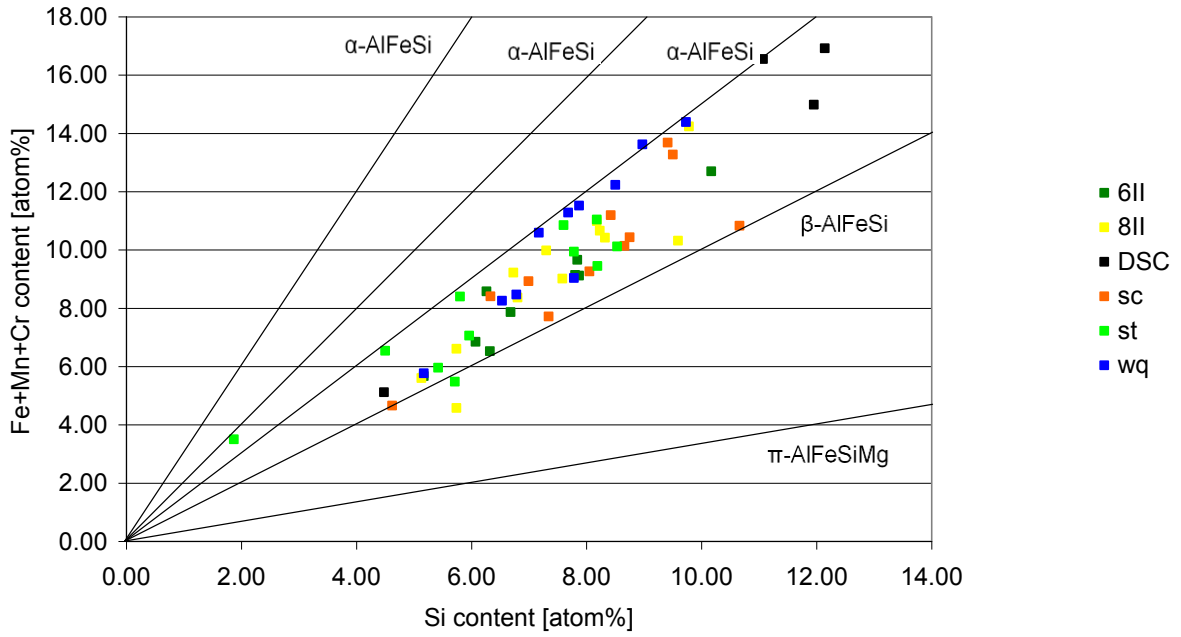

Diagram 5.22 Composition of the AlFeSi particles (Fe+Mn+Cr content plot against Si content)

5.5.3.3 Overview

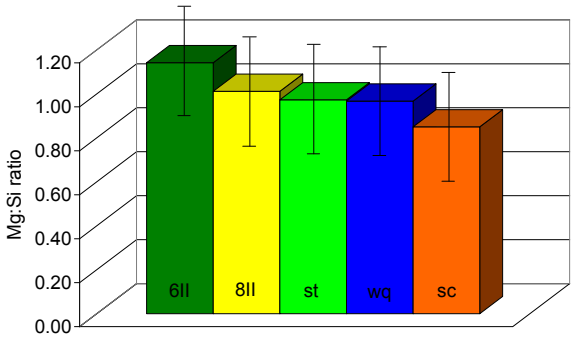

Diagram 5.23 Mg:Si ratio in the matrix

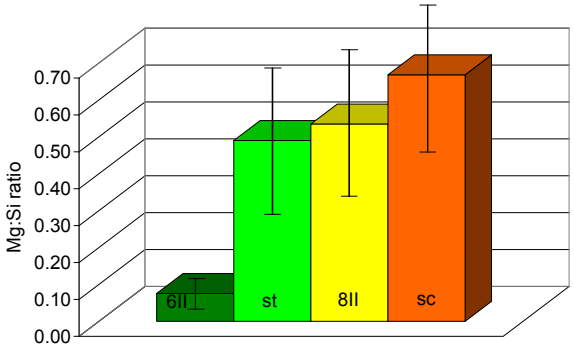

Diagram 5.24 Mg:Si ratio in the Mg-Si precipitations (no data for wq samples because there where no Mg/Si precipitations as a result of the high cooling speed)

For a heat treatment at 580°C the Mg:Si ratio (0.85 – 1.01) in the matrix was observed to be lower than at 560°C (Mg:Si ratio 1.14). On the other hand the Mg:Si ratio in the Mg/Si precipitations is much higher in the samples heat treated at 580°C (0.49 – 0.67 instead of 0.08 in the 560°C samples). The significant difference of the Mg:Si ratio in the Mg/Si particles is caused by an increase of the Mg content. In the 560°C samples most Mg/Si precipitations are pure Si, in the samples heat treated at 580°C the Mg/Si precipitations consist of Mg and Si (Mg:Si ratio of ~0.50).

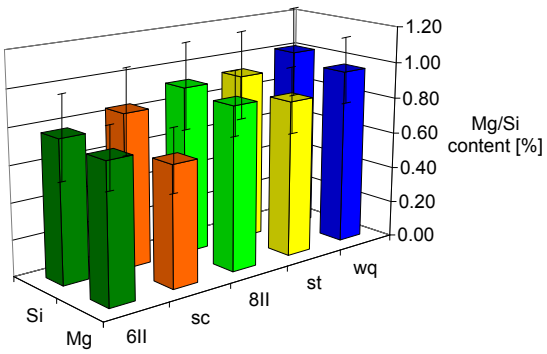

Diagram 5.25 Mg and Si content in the matrix

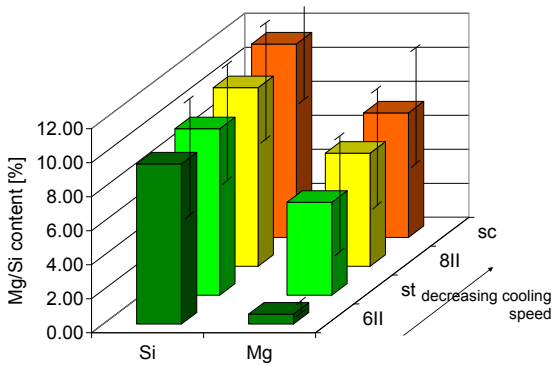

Diagram 5.26 Mg and Si content in the Mg/Si precipitations

The higher homogenization temperature facilitates that Mn from the matrix diffuses more completely into the AlFeSi particles, thereby lowering the Mn content in the matrix. In the following tables two decimal places are shown because more than 150 EDX spots were analyzed and the tables show the result of the data analysis and not only the raw data of the EDX.

Table 5.6 Matrix composition of the samples

Sample	Mg	Al	Si	Fe	Mn	Cr
6II	0.75	98.12	0.78	0.02	0.24	0.09
8II	0.90	97.90	0.92	0.04	0.16	0.08
sc	0.66	98.23	0.84	0.02	0.15	0.10
st	0.86	97.89	0.93	0.02	0.22	0.08
wq	0.97	97.73	1.01	0.02	0.20	0.08
Alloy 6082	0.85	97.06	1.14	0.24	0.54	0.17

At all samples nearly all of the Mg in the alloy remains in the matrix, about 20% of the Si precipitates. 90% of the Fe precipitates as AlFeSi. But also 63% of the Mn and 50% of the Cr precipitates as Al(Fe,Mn,Cr)Si, which means that 50% of both alloy elements are lost for AlFeSi. About 12% of the Si precipitates as AlFeSi (because of the comparison of the water quenched sample with the alloy composition). In the samples heat treated at 580°C about 10% of Si precipitates as coarse (>1µm), not the hardness affecting Mg/Si phase. Diagram 5.27 shows that the Mg and Si content of the matrix increases with the cooling speed.

Table 5.7 Chemical composition of the Mg/Si precipitations

Sample	Mg	Al	Si	Fe	Mn	Cr
6II	0.58	89.76	9.42	0.04	0.17	0.05
8II	6.65	82.71	10.51	0.02	0.10	0.03
sc	7.32	81.11	11.38	0.03	0.16	0.04
st	5.46	84.65	9.79	0.02	0.11	0.03
wq	---	---	---	---	---	---
Alloy 6082	0.85	97.06	1.14	0.24	0.54	0.17

Table 5.8 Chemical composition of the AlFeSi precipitations

Sample	Mg	Al	Si	Fe	Mn	Cr
6II	0.50	82.71	7.50	4.55	3.83	0.90
8II	0.37	83.04	7.43	4.74	3.69	0.74
sc	0.30	81.77	8.07	4.70	4.26	0.91
st	0.43	85.22	6.32	3.91	3.46	0.66
wq	0.63	81.23	7.62	5.32	4.27	0.93
Alloy 6082	0.85	97.06	1.14	0.24	0.54	0.17

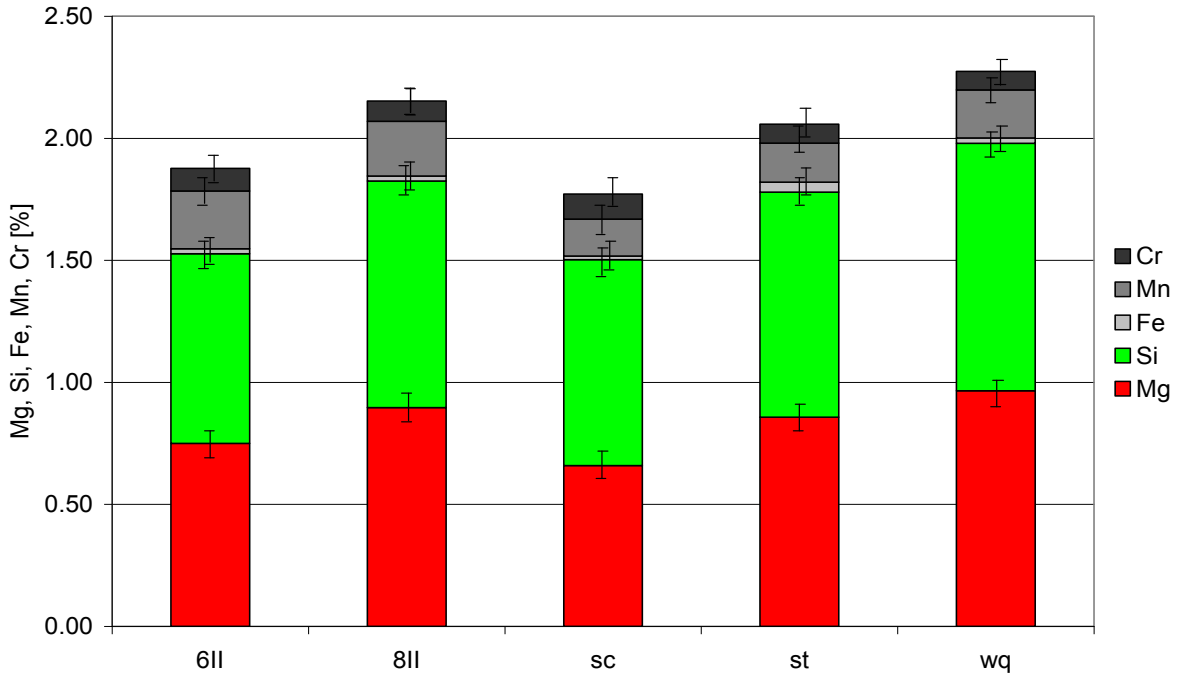

Diagram 5.27 Average matrix composition of the 5 different samples (remaining: Al)

The increase of 25°C in the homogenization temperature increases the (Fe+Mn+Cr):Si ratio by 5% (diagram 5.28). Furthermore, the cooling conditions also influence the Mg:Si ratio in the Mg:Si particles, with increasing cooling speed the Mg:Si ratio increases.

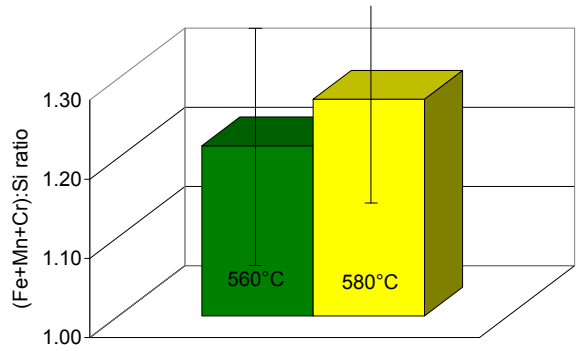

Diagram 5.28 (Fe+Mn+Cr):Si ratio in the AlFeSi particles

5.6 Transmission Electron Microscopy

Because of the large error in measurement at the EDX of the SEM also EDX measurements at TEM were performed. Furthermore selected area diffraction patterns were analysed to determine the crystal structure of the AlFeSi and the Mg/Si phase. In the following for each important particle type only some analyzed particles are shown. For all analyzed particles see appendix 9.4.

5.6.1 Mg/Si Particles

5.6.1.1 Small Mg/Si Particles inside the Grain

There are small Mg/Si particles within the grain, as a consequence of the EDX results, giving a Mg:Si ratio of 1.5-2.0, this small particles should be Mg_2Si and U2-AlMgSi particles. The diffraction patterns show that these particles are coherent with the matrix. Furthermore there were found few pure Si particles (appendix 9.4).

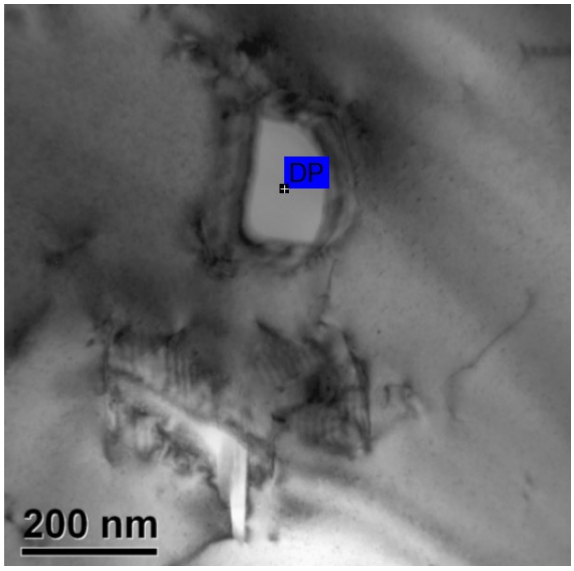

Figure 5.8 Mg_2Si particle, 200 x 150nm

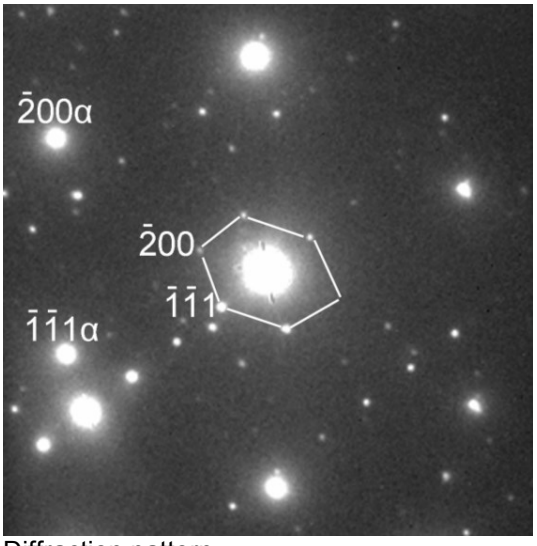

Diffraction pattern

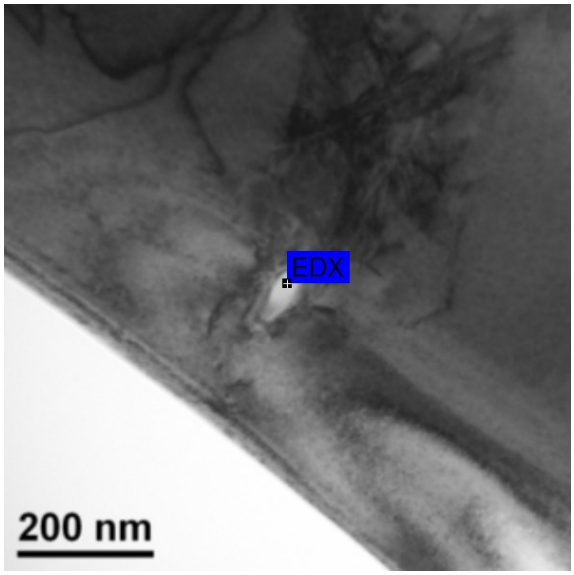

Figure 5.9 Mg_2Si particle, 100 x 50nm

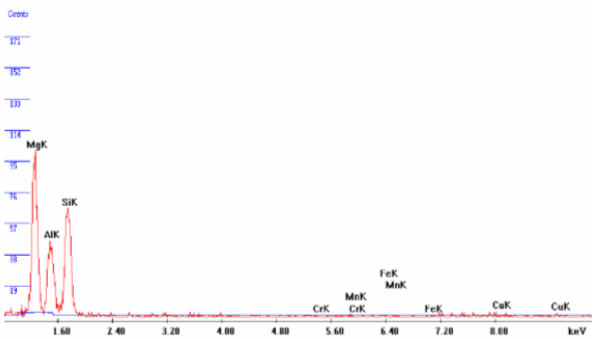

EDX-result

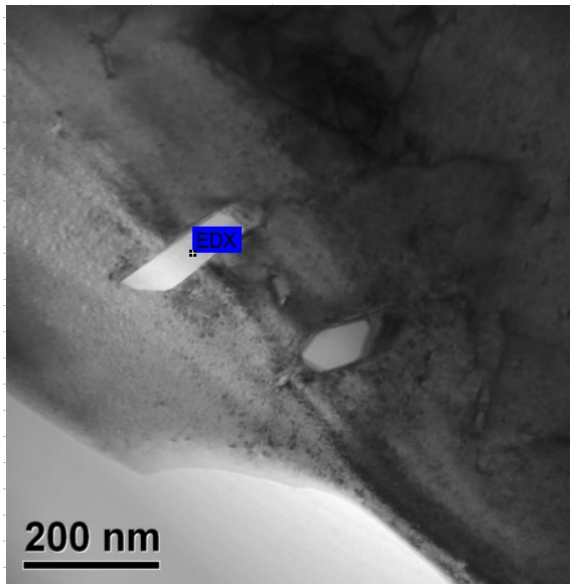

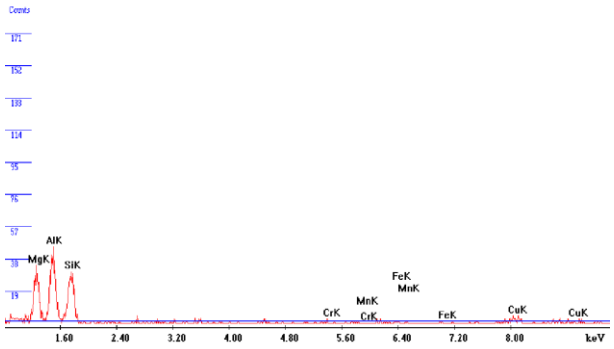

EDX-result

Figure 5.10 U2-AlMgSi particle, 200 x 50nm

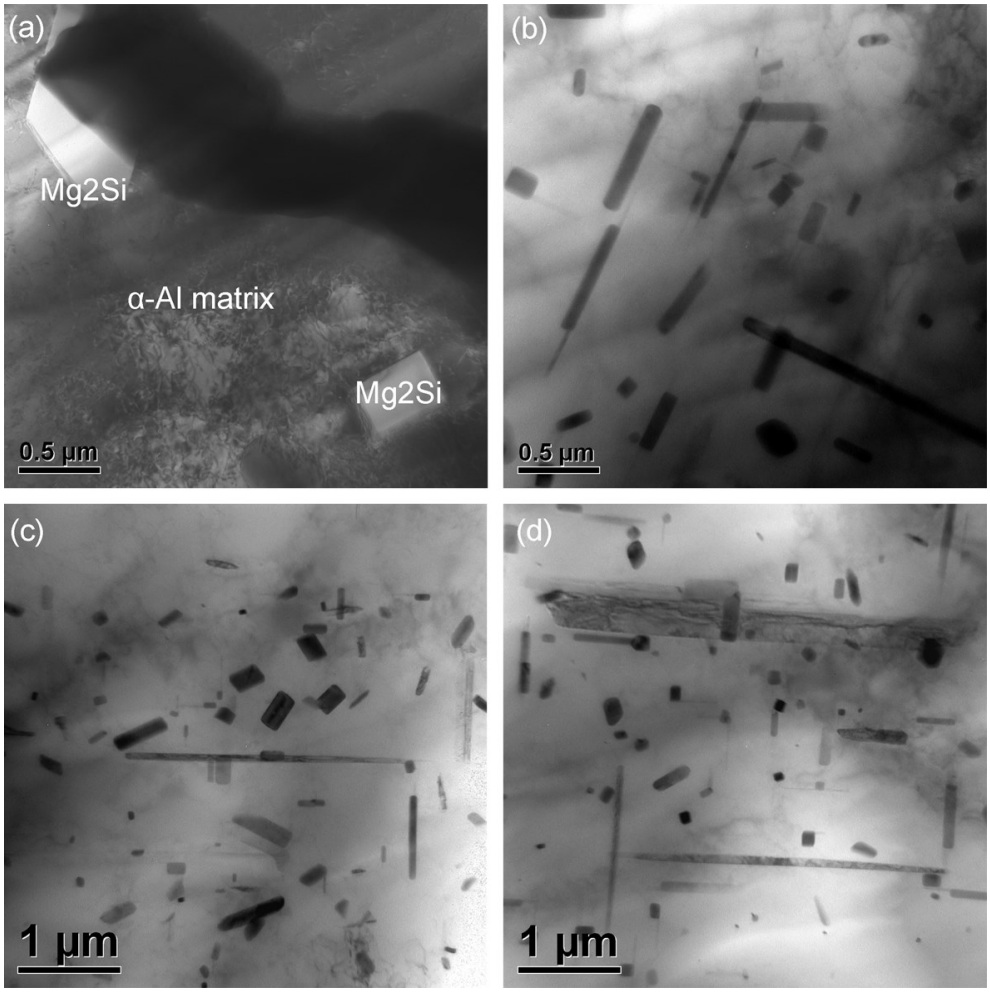

Figure 5.11 Mg_2Si, β", β' and β inside the grain (orientation relationship between particles and matrix)

5.6.1.2 Large Mg/Si Particles on the Grain Boundary

There are large, elongated particles (2-5µm) with a Mg:Si ratio of 1.48 (figure 5.12). This ratio is too low for near stoichiometric Mg_2Si, but some of the Mg is replaced by Al, as a result the (Mg+Al):Si ratio is 1.64, which is quiet near the lower range for the Mg:Si ratio of Mg_2Si. There is an orientation relationship between the matrix and the particles, e.g. <001>Al//<001>AlMgSi, {001}Al//{001}AlMgSi. There are also large, elongated particles (2-5µm) with a Mg:Si ratio of 1.89 (figure 5.13), as a consequence this is a Mg_2Si particle. The diffraction pattern verifies this.

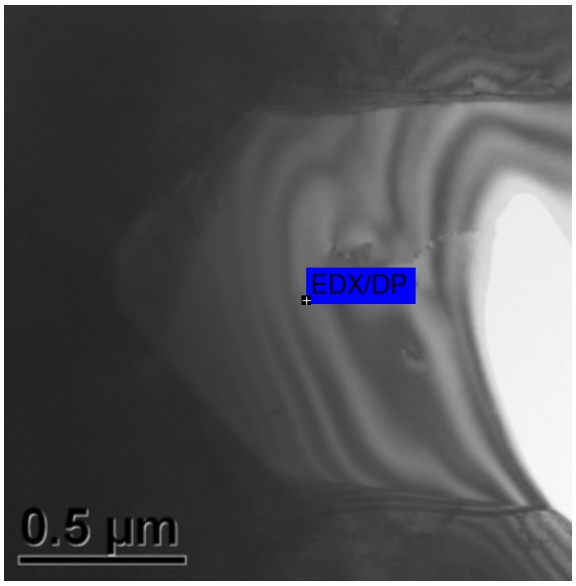

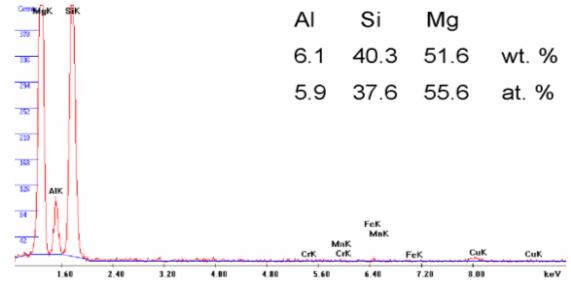

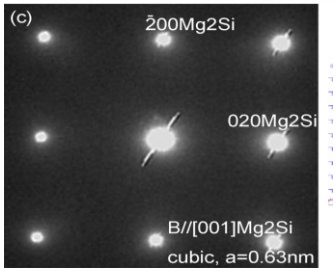

EDX-result, diffraction pattern

Figure 5.12 Mg_2Si particle, Mg:Si = 1.48, >2 x 1µm

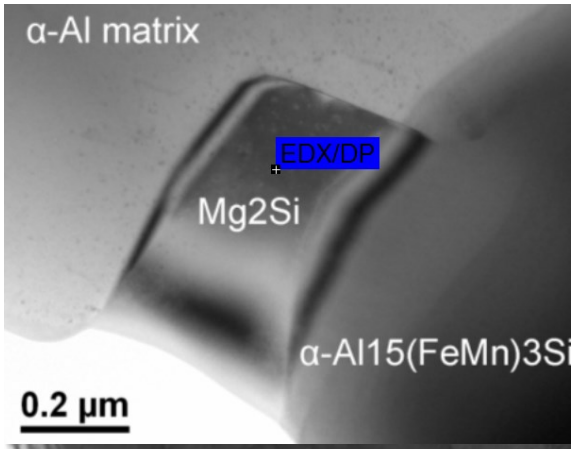

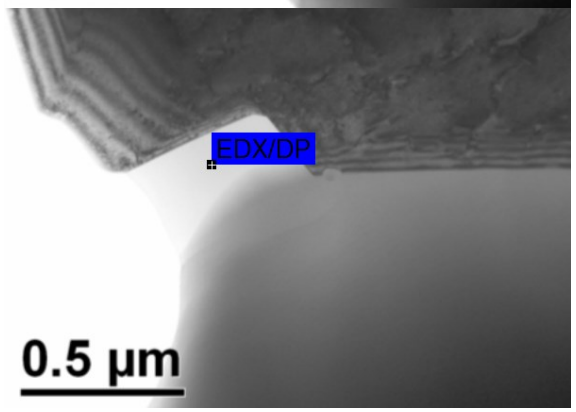

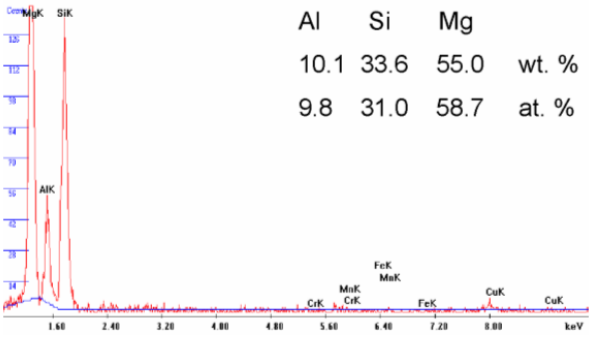

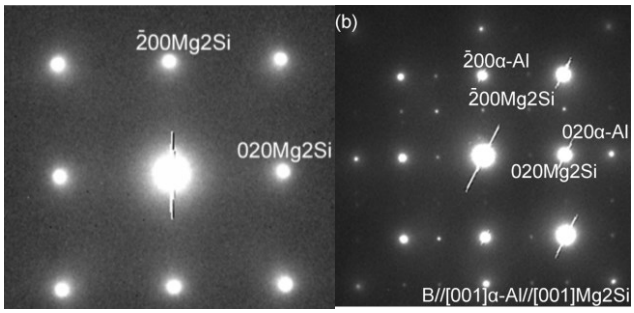

EDX-result, diffraction pattern

Figure 5.13 Mg_2Si particle, Mg:Si=1.89, 200 x 500nm

5.6.2 AlFeSi Particles

5.6.2.1 Small AlFeSi Particles inside the grain

In figures 5.14 and 5.15 there are small Al(Fe,Mn,Cr)Si particles inside the grains, the Mn content of this particles is higher than the Fe content. Only one small AlFeSi particle inside grains was identified as the brittle β-AlFeSi, all other AlFeSi particles were identified as α-AlFeSi. Because of the small size of the AlFeSi particles this particles could increase the strength of the material.

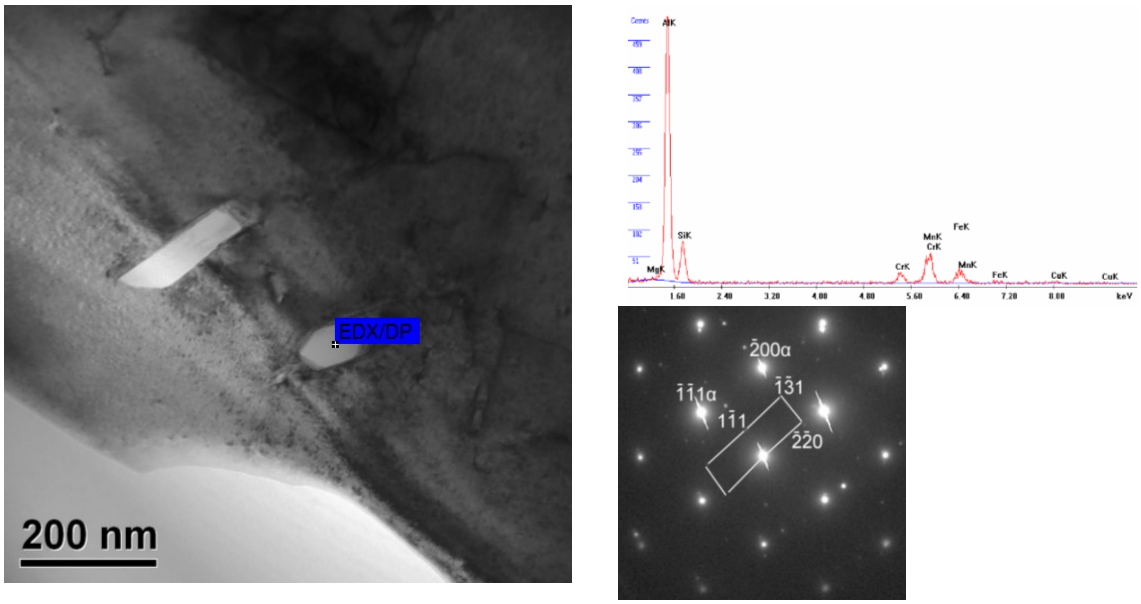

EDX-result, diffraction pattern

Figure 5.14 AlFeSi particle, Mn rich, 100 x 50nm

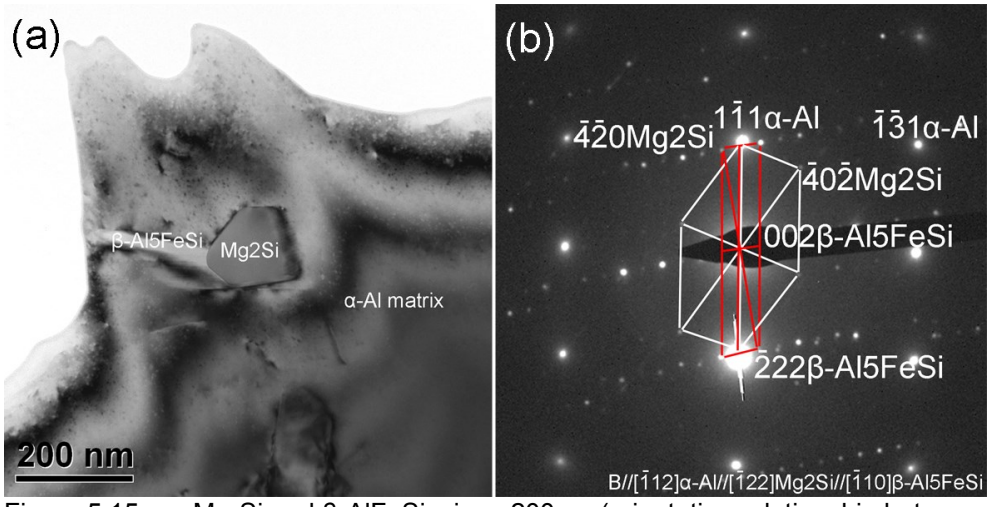

Figure 5.15 Mg_2Si and β-AlFeSi, size ~200nm (orientation relationship between Mg_2Si and matrix)

5.6.2.2 Large AlFeSi Particles on the Grain Boundary

The large AlFeSi particles on the grain boundary fully transformed into the less brittle α-AlFeSi. Contrary to the AlFeSi particles inside the grain the Fe content is higher than the Mn content (as expected).

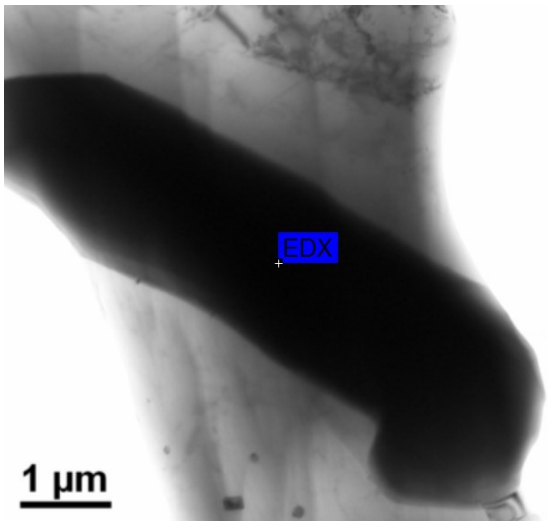

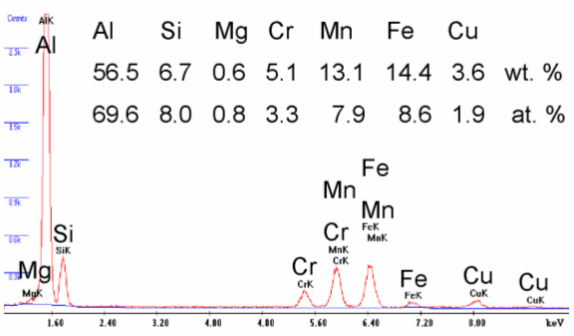

EDX-result

Figure 5.16 AlFeSi particle, >10 x 2µm

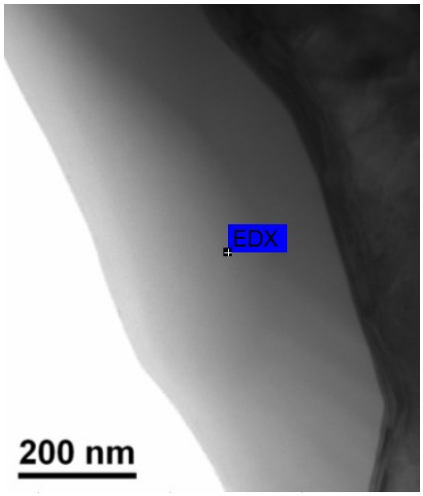

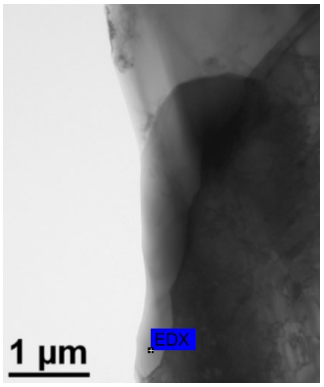

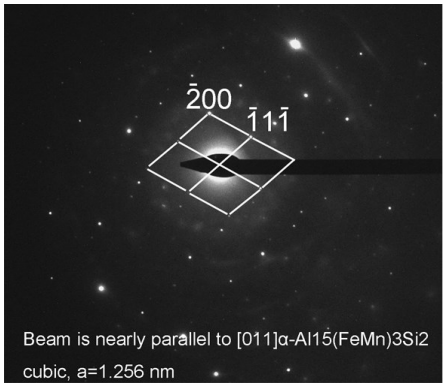

diffraction pattern

Figure 5.17 AlFeSi particle, 5 x 1µm

5.6.3 Precipitation free Zone

In figures 5.18 and 5.19 there is a precipitation free zone at the grain boundary with a thickness between 2 and 3 µm. Within this area there are no small precipitations of Mg_2Si or other Mg/Si phases. As a result, the strength of this area is lower.

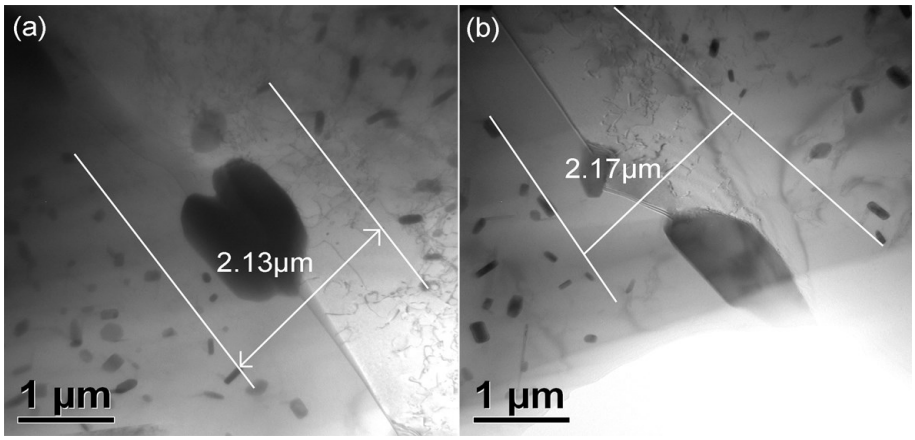

Figure 5.18 Precipitation free zone on grain boundary

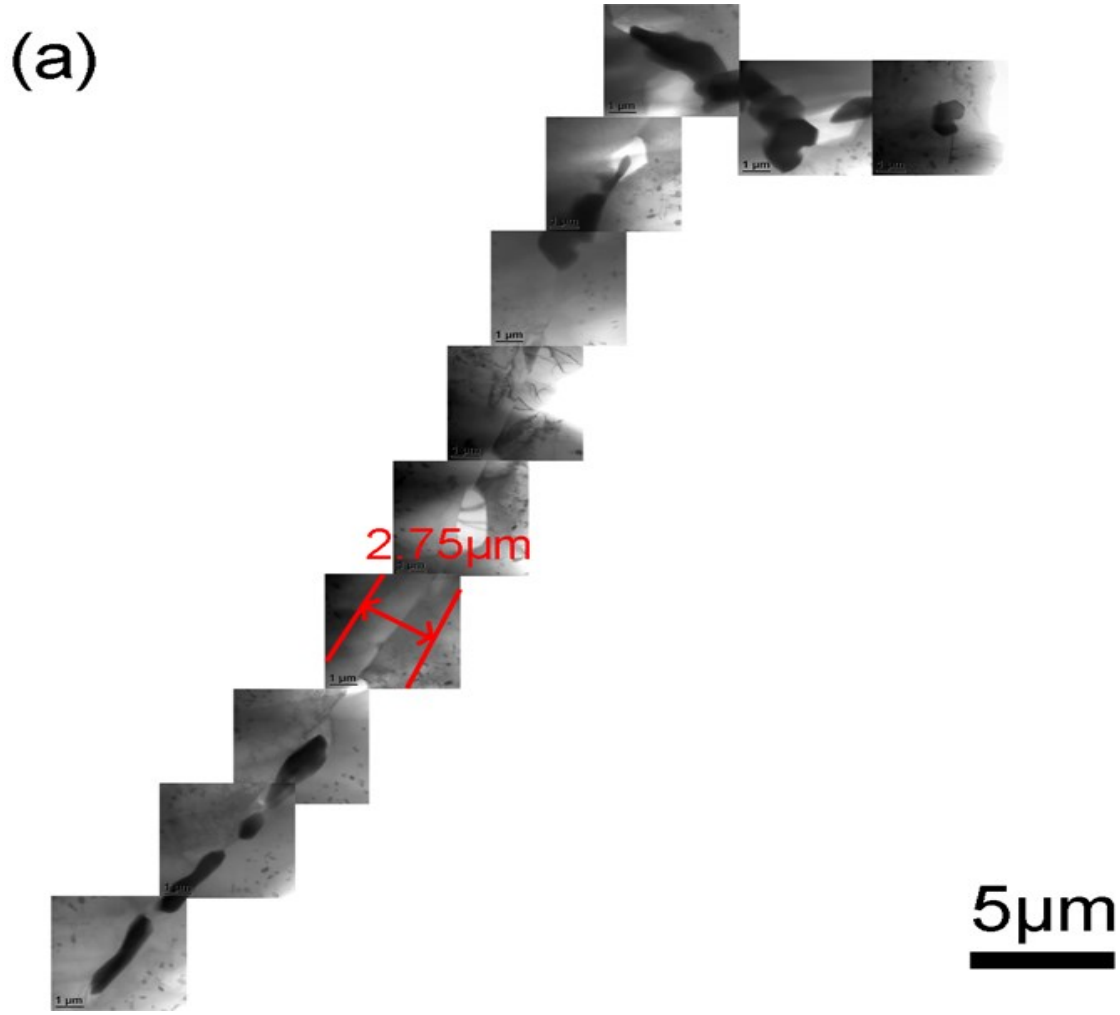

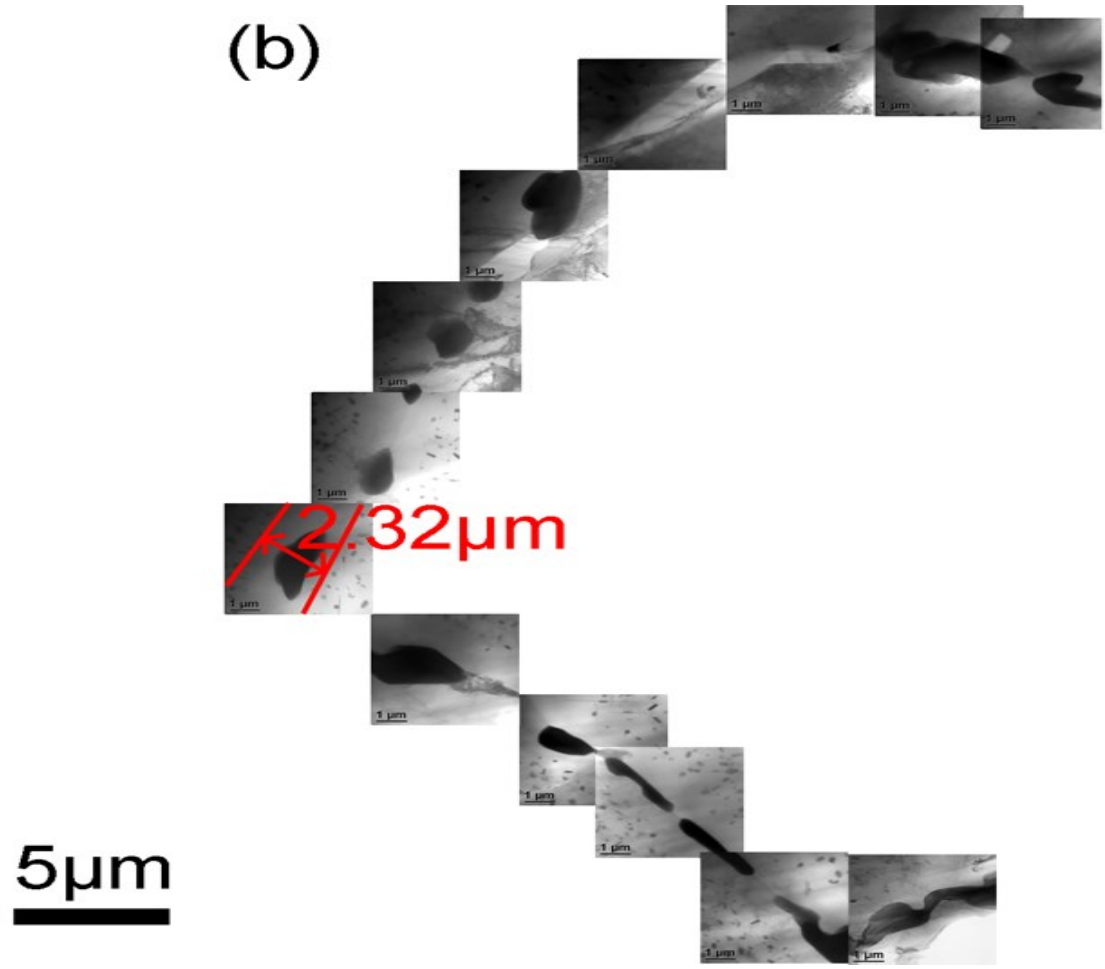

Figure 5.19 Precipitation free zone on a reconstructed grain boundary

5.6.4 TEM Results

There are two different kinds of small (100nm) Mg/Si particles inside the grains, Mg_2Si and U2-AlMgSi. Two different kinds of large (1µm) Mg/Si particles on the grain boundary were observed, one kind of particles is the expected, near stoichiometric Mg_2Si, in the other type of Mg_2Si particles some Mg is replaced by Al resulting in $(Mg,Al)_2Si$. The average Mg:Si ratio in the large Mg/Si particles is 2.3 (min. 1.6, max. 2.8), which is a evidence that these particles are Mg_2Si particles. No large Mg/Si particles with a Mg:Si ratio <1 were detected, most probably as a result of the small analyzed area, because a lot of this particles were observed in the SEM. There are small (100-200nm) AlFeSi particles inside the grains, which are rich in Mn. The large AlFeSi (4-8µm) particles are fully transformed from β- to α-AlFeSi on grain boundaries. On nearly all TEM Figures small (~50-100nm) Mg_2Si, β'', β' and β particles inside the grains are visible. These particles are essential for the mechanical properties and strength of the alloy. The Al_4Ca particle descends most probably from impurities in the scrap for the melting furnace - because of the small size of this particle there should be no negative effects on the mechanical properties. The average (Fe+Mn+Cr):Si ratio in the AlFeSi particles is 2.1 (min. 1.5, max. 2.8), the ratio for α-Al_8Fe_2Si is 2, which shows that all brittle β-Al_5FeSi particles transformed into α-AlFeSi. These EDX analysis were only performed for large particles on the grain boundary, because for small particles also the Al background is measured.

5.7 Extrusion Experiments

After checking the extrudability in the plain strain compression test two materials, one homogenized at 555°C, one homogenized with the new temperature of 580°C, were extruded. The target temperature of the billet after the preheating furnace was 500°C.

5.7.1 Pressure/Extrusion Speed Characteristics

The first 20 cycles were done with a low extrusion speed to preheat the tool. For the further analysis the last 5 cycles with a high extrusion speed were used.

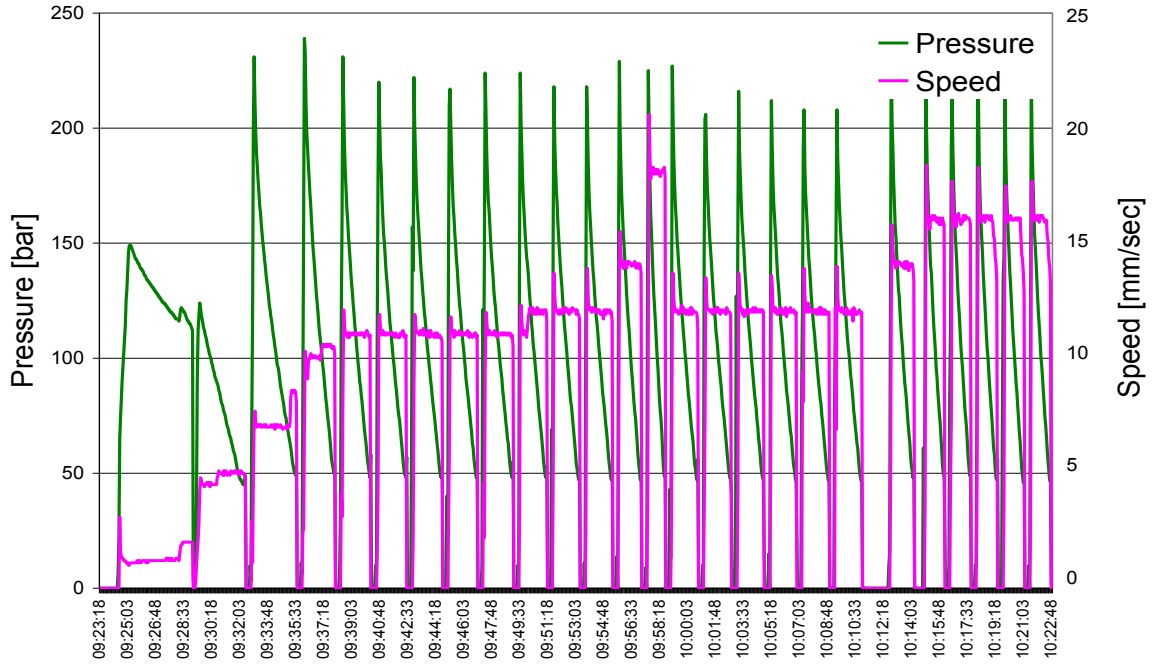

Diagram 5.29 Extrusion characteristics of the material homogenized at 555°C plot against time

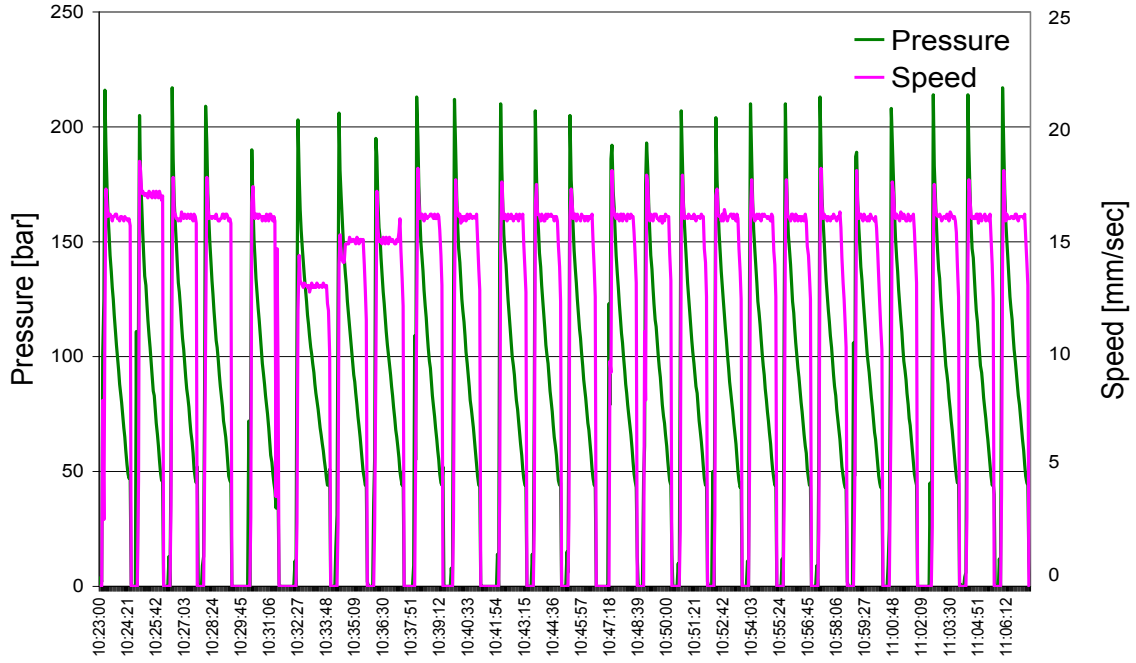

Diagram 5.30 Extrusion characteristics of the material homogenized at 580°C plot against time

In cycle number 5 the billet was not quenched, as a result hot cracks occurred, which was a result of a failure of the process and not of the new homogenization temperature. Therefore the last 5 cycles were used, to ensure stable process conditions.

5.7.2 Results

There was a reduction of extrusion pressure of 10 bar through the higher homogenization temperature (figure 5.31).

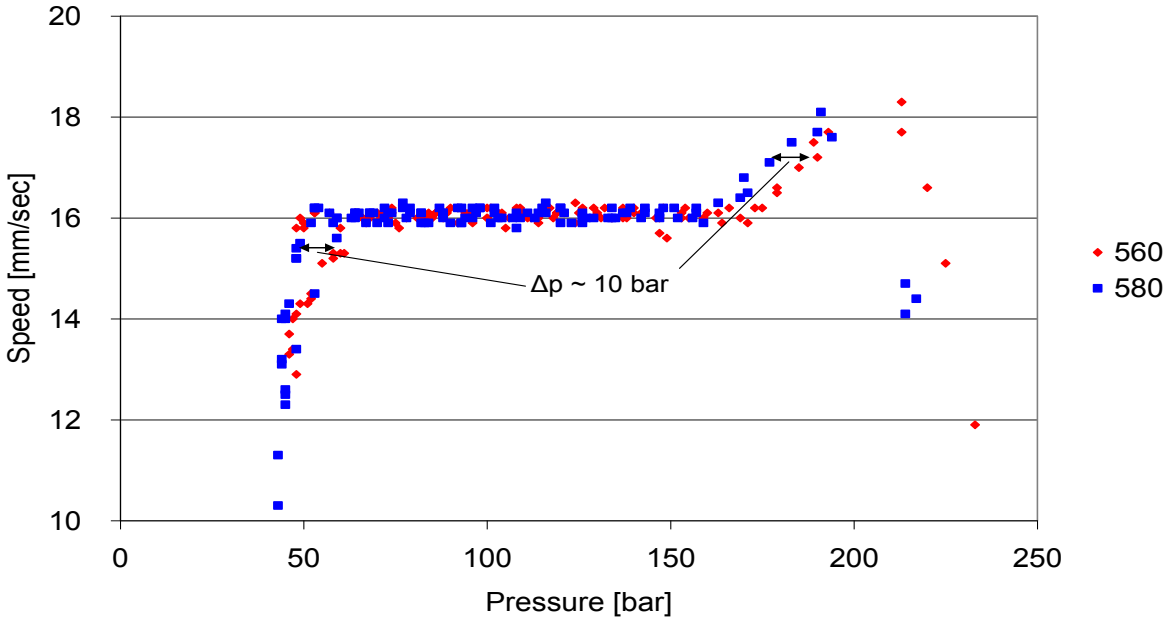

Diagram 5.31 Extrusion speed plot against extrusion pressure

Diagram 5.32 shows the significant difference in extrusion pressure. At all extrusion speeds the extrusion pressure is 10 bar lower than at the material homogenized at 580°C.

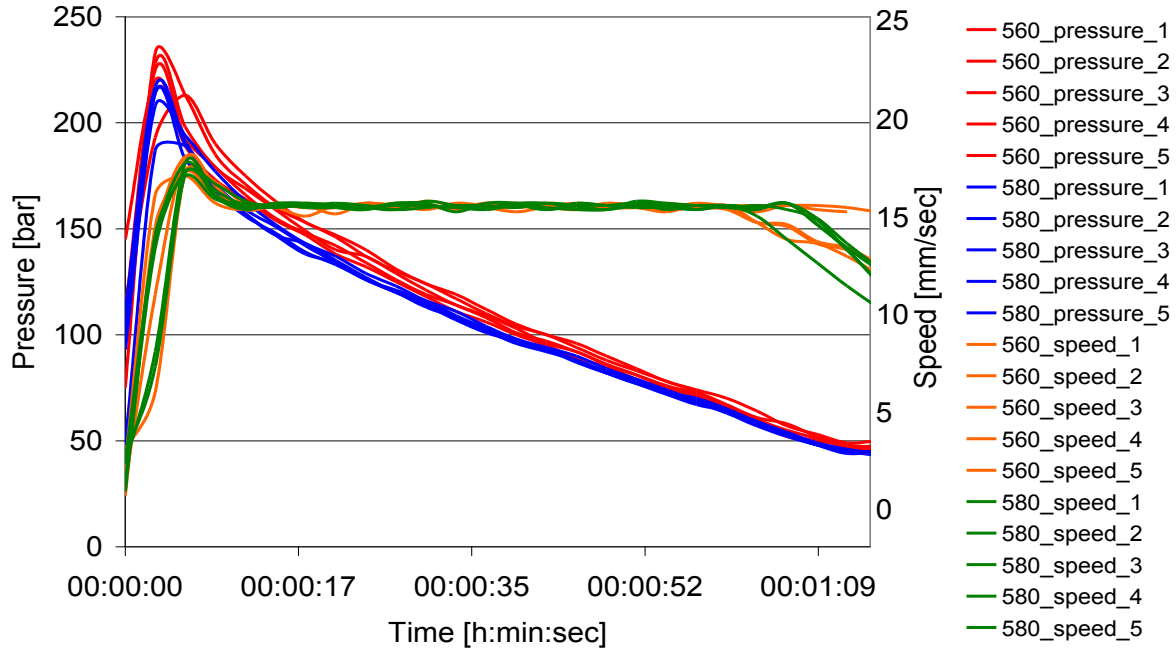

Diagram 5.32 Extrusion speed and pressure versus time

The average maximum pressure is the average of the maximum values of the 5 analysed extrusion cycles. The average pressure was calculated from the pressure at an extrusion speed between 15.5 and 16.5 mm/sec. The maximum pressure was the highest value measured during the 5 cycles.

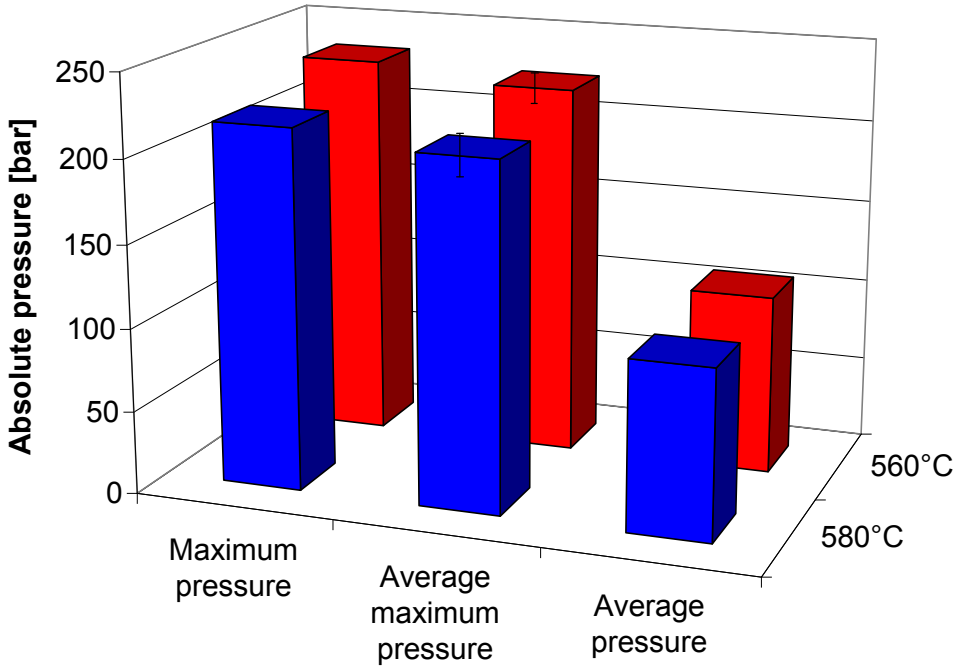

Diagram 5.33 Comparison of the extrusion results (absolute)

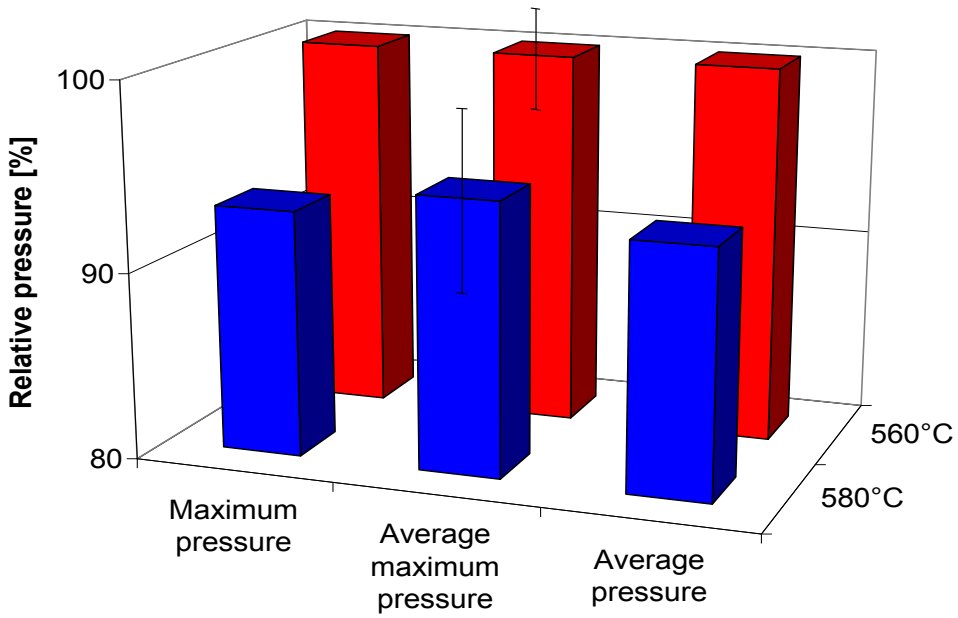

Diagram 5.34 Comparison of the extrusion results (relative)

Table 5.9 Comparison of the extrusion pressure

	560°C	580°C
Maximum pressure	233	217
Average pressure	108	102
Average max. pressure	224	208

5.7.3 Properties of the Extruded Profile

5.7.3.1 Mechanical Properties

Both, the extruded material homogenized at 560°C and 580°C, show the same mechanical properties as shown in diagram 5.35 and 5.36.

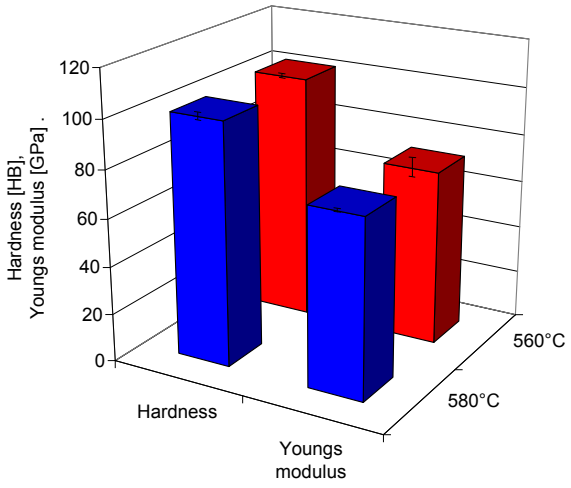

Diagram 5.35 Hardness and Young's mod. after T6

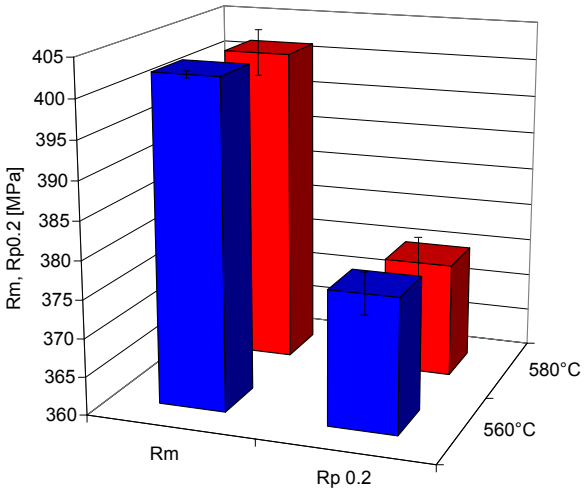

Diagram 5.36 R_m and $R_{p0.2}$ after T6

5.7.3.2 Depth of recrystallized Layer

As the extruded profiles are forged to the final product, it is essential that the depth of recrystallized area on the surface is small. It's essential for the profile RV26 that the recrystallized layer on the surface is thinner than 1mm to meet the customer's requirements. To test this required property samples from the start and the end of the billet were heat treated (540°C for 120, 240 and 360 min.) etched and the thickness of the recrystallized layer was measured with the microscope.

Table 5.10 Percentage of sample which have a Rxx layer thicker than 1mm

Homogenization temp.:		560°C	580°C
120 min	start	70%	80%
	end	0%	10%
240 min	start	80%	70%
	end	0%	10%
360 min	start	70%	60%
	end	10%	50%

This high percentage of rejections is a result of the high extrusion speed of 1.6 mm/sec (plunger speed), normally the extrusion speed is 1.1 mm/sec, about 30% lower than during the test. The samples with a homogenization temperature of 580°C and a heat treatment at 540°C for 360 min. show a significant higher percentage of samples with a recrystallized layer thicker than 1mm. But it is important to note, that the average recrystallized layer thickness of this degraded material is 1.3mm, compared to 3.5mm of the samples homogenized at 560°C. Overall the percentage of rejects and the depth of the recrystallized layer is equal in the old and the new homogenization treatment.

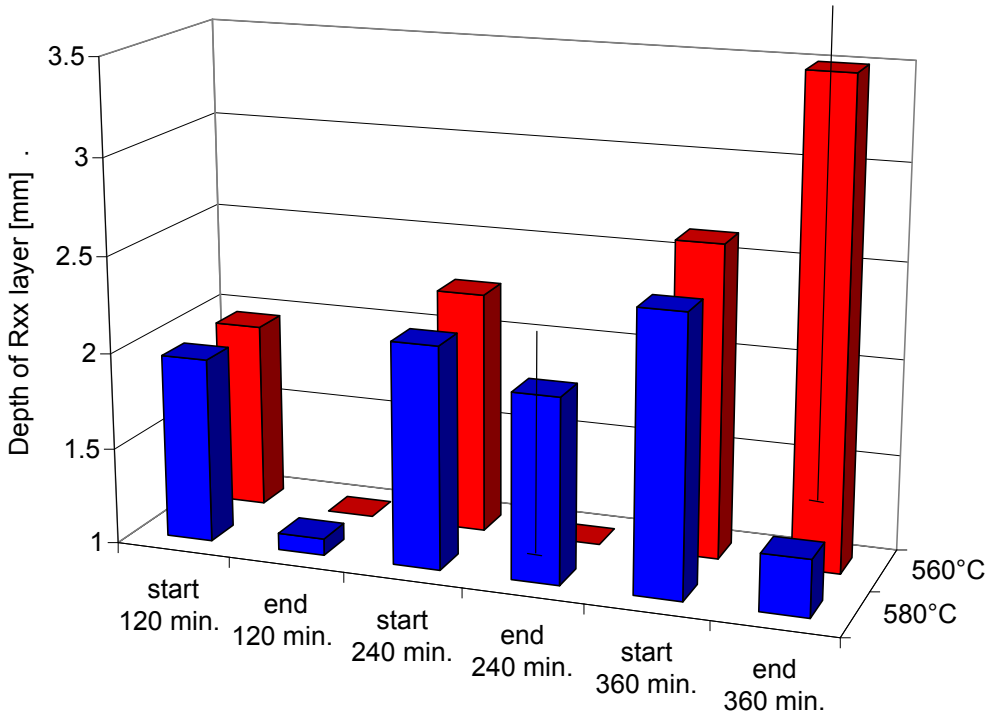

Diagram 5.37 Depth of recrystallized layer of the rejections

5.8 Results of the Optimization

There is good correlation between the results of the applied methods. The microstructure shows, that the Mg:Si ratio in the Mg/Si particles increased significant through the homogenization at 580°C instead of 555°C. Also the transformation of β-AlFeSi to α-AlFeSi is more completely through the higher homogenization temperature. As a result, in the PSCT flow stress decreased by 10% and the extrusion pressure during billet extrusion decreased by 8%.

6 Results and Discussion

This diploma thesis was divided into 3 main parts: The analysis of the homogenization treatment, the optimization of the heat treatment and implementation of the new developments in the industrial process.

6.1 Analysis of the Homogenization Treatment

Firstly a Thermo-Calc calculation was performed to determine the phases which could appear in the 6082 alloy. The calculation showed that AlFeSi, Mg_2Si, Si, $Al_{13}Cr_4Si_4$, $Al_5Cu_2Mg_8Si_6$ and a Ti-Al phase could exist in the alloy. In contrast to the calculation literature data shows AlFeSi, Mg_2Si and Si. The DSC analysis shows 2 different peaks between 550 and 600°C. On the basis of the Thermo-Calc calculation and a sample which was water quenched at 580°C these 2 peaks were identified as the dissolution peak of Si (at 559°C) and Mg_2Si (at 583°C) in good correlation to the literature [22] and the Thermo-Calc results. The furnace temperature and the cooling conditions were measured with a thermocouple. The holding temperature was 555°C, 5°C below the expected and adjusted temperature of 560°C. As a result, this temperature is too low for a successful heat treatment because both DSC peaks for dissolution are above this temperature. Samples for the LOM, SEM and EDX were taken from the center of the billets (where the heat treatment and cooling conditions were measured), by a calculation of the surface temperature (Groeber diagram) it was shown that there are no significant temperature differences between the surface and the center. As a consequence, the microstructure in the whole billet can be assumed to be constant.
The results of Thermo-Calc and DSC were verified with the LOM, SEM and EDX results. The AlFeSi phase was not transformed completely and the Mg/Si phase was not dissolved completely during the heat treatment. Consequently, there was brittle plate-like β-AlFeSi on the grain boundary and a coarse Mg/Si phase inside the grain, which does not influence the deformability. Most of the Mg/Si particles had a high Si content before and after the heat treatment, normally the Si should be dissolved during homogenization and re-precipitated as Mg_2Si during cooling.

6.2 Optimization of the Heat Treatment

Firstly the homogenization treatment of the 500kg billets was simulated in the laboratory furnace with small samples (51.5x51.5x16mm). Because of the results in the analysis of the actual situation and the literature research the homogenization temperature was increased to 580°C. Because of this rise of temperature grain growth can occur, but a grain size analysis showed that there wasn't a significant change in the grain size through the new heat treatment. Samples were homogenized in the laboratory furnace at 560°C (to compare them with the industrial furnace) and 580°C, furthermore different cooling conditions were applied (standard cooling, fast and slow cooling and water quenching). The LOM, SEM and EDX analysis show a more complete β- to α-AlFeSi transformation, furthermore the Mg/Si phase dissolved completely during the heat treatment and re-precipitated in a phase

which was richer in Mg than in the samples homogenized at 560°C. The microstructural results show an advancement, but with the SEM the Mg/Si phase could not be identified, consequently TEM observations were performed. In the TEM three different points of interest were observed: Mg/Si phase, AlFeSi and the precipitation free zone on the grain boundary. There are different Mg/Si phases: Coarse Mg_2Si, $(Mg,Al)_2Si$ (same structure like Mg_2Si, but some Mg replaced by Al) and U2-AlMgSi on the grain boundary. The first 2 phases were identified in the TEM, the last phase in the SEM. Furthermore there are small β'', β' and β-Mg_2Si, U2-AlMgSi and few Si particles inside the grain (identified in the TEM). The AlFeSi was found on the grain boundary, the diffraction pattern shows that all observed coarse AlFeSi particles were fully transformed into α-AlFeSi. However, small AlFeSi particles were found inside the grain. They were rich in Mn, the Mn content was higher than the Fe content, as a result these particles are more correctly described as AlMnSi particles. On these AlMnSi particles Mg_2Si and U2-AlMgSi precipitate during cooling. One reason for the high Mn content is the precipitation of these small particles during homogenization treatment. The matrix is richer in Mn than in Fe, as a result there is more Mn available and the Mn and Si diffuse to build AlMnSi.
The thickness of the precipitation free zone on the grain boundary is about 2-3 µm.
After this microstructural advantages a PSCT (plain strain compression test) was performed because the flow stress of the material at extrusion temperature is a dose for the extrudability of the material. The material was preheated with the parameters of the industrial process and the test was undertaken with a strain rate of $1s^{-1}$. The flow stress decreased 10% as a result of the heat treatment at 580°C instead of 555°C. The different cooling conditions brought further advantages in the reduction of the flow stress.

6.3 Implementation of the Developments

After the successful PSCT billets were homogenized at the optimized homogenization temperature and extruded in the industrial process. For the extrusion a simple profile (circular cross-section) was used to limit factors of influence. The results of the PSCT were confirmed with a reduction of extrusion pressure of 8%. This reduction in pressure results in a lower energy input during extrusion, as a result the rise of temperature will be lower and the risk of surface defects will be reduced. The mechanical properties and the depth of recrystallized layer were not influenced negatively by the change in the homogenization process.
By increasing the homogenization temperature to 580°C it was possible to reduce the time for heat treatment 30 minutes (or relative 11%), as a result the output of the homogenization furnace can be increased by more than 10%.
Because of these outstanding results for the industrial partner the homogenization temperature in the industrial process will be increased from 555°C to 580°C and the homogenization time can be decreased from 4:30h to 4:00h.

7 Conclusion

The target of this diploma thesis was the understanding of the microstructure and the effects on mechanical properties to reduce the pressure during billet extrusion.
This target was accomplished by a reduction of the extrusion pressure of 8% accompanied by a reduction of homogenization time by 11%. Experiments with step cooling show further points of improvement to reduce the pressure during extrusion – results of the PSCT show a possibility for a further reduction in pressure of 7%, which means in total a reduction of more than 15%.

There was a good correlation between the PSCT and the extrusion experiments, which verifies the theory that the flow stress is a dose for the extrusion pressure [19]. The enhancement of the extrusion properties of the material doesn't affect the properties of the extruded profile negatively.
The TEM observations show a complete transformation of the coarse β-AlFeSi on the grain boundary to α-AlFeSi. Furthermore the heat treatment at 555°C resulted in a Si rich phase on the grain boundary, the new heat treatment at 580°C produced Mg rich Mg_2Si, $(Mg,Al)_2Si$ and AlMgSi.

Unexpectedly two phases were found, which were not reported in literature up to now: Mn rich, nm-size AlFeSi were found inside the grain. In many cases the Mn content was higher than the Fe content, as a consequence it's more accurate to speak about AlMnSi particles. The size of this particles is in the range of some 100nm, accordingly this particles can lift the strength of the alloy, which could be a positive effect of the unwanted Fe content in 6xxx alloys.
Furthermore an AlMgSi phase was found, most probably U2-AlMgSi. Indeed this phase was reported in literature in the past, but only as an nm-size (<100nm) particle [26]. In the observed sample this phase was found with µm-size (>1µm).

In the LOM nm-size (~100nm), coherent Mg_2Si particles became visible through Barker etching with trench creation. This particles were also visible in the TEM, but not in the SEM.

The technological results are:

- 10% lower stress in PSCT
- 8% lower extrusion pressure
- 11% reduction of homogenization time
- Good accordance of the PSCT and extrusion experiment results
- good Rxx-stability

The microstructural results are:

- More complete transformation of β-AlFeSi to α-AlFeSi
- Mg_2Si and AlMgSi particles instead of Si rich particles on grain boundary
- Small, Mn rich Al(Fe,Mn)Si particles inside the grain
- Large AlMgSi particles alongside expected Mg_2Si on the grain boundary
- Small coherent Mg/Si particles visible in TEM and LOM (through Barker etching)

8 References

[1] N.C.W. Kuijpers, F.J. Vermolen, C. Vuik, P.T.G. Koenis, K.E. Nilsen, S. van der Zwaag, The dependence of the β-AlFeSi to α-Al(Fe,Mn)Si transformation kinetics in Al–Mg–Si alloys on the alloying elements, Materials Science and Engineering A, Volume 394, Issues 1-2, 15 March (2005), pp. 9-19.

[2] M. B. Karamış, İ. Halıcı, The effects of homogenisation and recrystallization heat treatments on low-grade cold deformation properties of AA 6063 aluminium alloy, Materials Letters, Volume 61, Issues 4-5, February (2007), pp. 944-948.

[3] Y. Birol, The effect of homogenization practice on the microstructure of AA 6063 billets, Journal of Materials Processing Technology, Volume 148, Issue 2, 15 May (2004), pp. 250-258.

[4] G. Mrówka-Nowotnik, J. Sieniawski, Influence of heat treatment on the microstructure and mechanical properties of 6005 and 6082 aluminium alloys, Journal of Material Processing Technology, Volume 162-163, (2005), pp. 367-372.

[5] H. Tanihata, T. Sugawara, K. Matsuda, S. Ikeno, Effect of casting and homogenizing treatment conditions on the formation of Al–Fe–Si intermetallic compounds in 6063 Al–Mg–Si alloys, Journal of Materials Science, Volume 34, Number 6, (1999), pp. 1205-1210.

[6] N. C. W. Kuijpers, W. H. Kool, P. T. G. Koenis, K. E. Nilsen, I. Todd, S. van der Zwaag, Assessment of different techniques for quantification of α-Al(Fe,Mn)Si and β-AlFeSi intermetallics in AA 6xxx alloys, Volume 49, Issue 5, December (2002), pp. 409-420.

[7] D. Lassance, M. Schmitz, F. Delannay, T. Pardoen, Linking microstructure and high temperature ductility in aluminium alloys AA 6xxx, 15th European Conference of Fracture, Stockholm, (2004), pp. P100.

[8] L. F. Mondolfo, A. R. Peel, A test for extrudability, Light Metal Age, Volume 36, Number 2-4, (1978), pp. 30-33.

[9] S. Zajac, B. Hutchinson, A. Johansson, L.-0. Gullman, R. Lagneborg, Microstructure control and extrudability of aluminium-Mg-Si alloys micro-alloyed with manganese, Journal de Physique IV, Colloque C7, supplement au Journal de Physique 111, Volume 3, November (1993), pp. 251-253.

[10] J. L. Cavazos, R. Colás, Precipitation in a heat-treatable aluminium alloy cooled at different rates, Materials Characterization, Volume 47, Issues 3-4, September-October (2001), pp. 175-179.

[11] O. Reiso, O. Sjøhum, U. Tundal, J. E. Hafstås, The effect of cooling rate after homogenization and billet preheating practice on extrudability and section properties Part 1: Extrudability and Mechanical Properties, 6th International

Aluminium Extrusion Technology Seminar, Volume 1, Chicago, Illinois, USA, 14-17 May (1996), pp. 1-10.

[12] O. Reiso, O. Sjøhum, U. Tundal, J. E. Hafstås, The effect of cooling rate after homogenization and billet preheating practice on extrudability and section properties Part 2: A microstructural investigation, 6th International Aluminium Extrusion Technology Seminar, Volume 1, Chicago, Illinois, USA, 14-17 May (1996), pp. 141-147.

[13] O. Reiso, Extrusion of AlMgSi alloys, Materials Forum, Volume 28, (2004), pp. 32-46.

[14] S. Zajac, B. Bengtsson, A. Johansson, L.-O. Gullman, Optimisation of Mg_2Si phase for extrudability of AA 6063 and AA 6005 alloys, Materials Science Forum, Volumes 217 - 222, Number 1, (1996), pp. 397-402.

[15] S. Zajac, Controlling extrudability in Al-Mg-Si alloys, Thermo-Mechanical Processing in Theory, Modelling and Practice [TMP] exp 2; Stockholm; Sweden, 4-6 Sept. (1996), pp. 307-322.

[16] L. Lodgaard, N. Ryum, Precipitation of dispersoids in a 6082 alloy, EUROMAT 97: 5th Conference of Advanced Materials and Processes and Applications, Volume 4, Characterisation and Production/Design, Maastricht, Netherlands, 21-23 April (1997), pp. 69-72.

[17] T. Johnsen, N. Dahl, B. R. Henriksen, E. K. Jensen, Precipitation of Mg_2Si in Al-Mg-Si- alloys during cooling from homogenization temperature, ET 96: Profiles of Change. 6th International Aluminium Extrusion Technology Seminar, Volume 1, Chicago, Illinois, USA, 14-17 May (1996), pp. 529-533.

[18] S.R. Claves, D.L. Elias, W. Z. Misiolek, Analysis of the intermetallic phase transformation occurring during homogenization of 6xxx aluminum alloys, Materials Science Forum, Volumes 396 - 402, Part 2, (2002), pp. 667-674.

[19] J. van de Langkruis, R. Bergwerf, S. van der Zwaag, W.H. Kool, Linking plane strain compression tests on AA 6063 to laboratory scale extrusion via constitutive equations, Materials Science Forum, Volumes 331 - 337, Number 1, (2000), pp. 565-570.

[20] K. B. S. Couto, M. Concalves, W. H. Van Geertruyden, W. Z. Misiolek, Homogenization and hot ductility of aluminium alloy AA 6063, Materials Forum, Volume 28, (2004), pp. 1388-1393.

[21] K. B. S. Couto, S.R. Claves, W. H. Van Geertruyden, W. Z. Misiolek, M. Concalves, Effects of homogenisation treatment on microstructure and hot ductility of aluminium alloy 6063, Materials Science and Technology, Volume 21, Number 2, (2005), pp. 263-268.

[22] H. Gjestland, A. L. Dons, O. Lohne, O. Reiso, Aluminium alloys: their physical and mechanical properties, International Conference at University of Virginia, Volume 1, Charlottesville, Virginia, USA, (1986), pp. 359-370.

[23] R. A. Ricks, N. C. Parson, H. L. Yiu, S. A. Court, Microstructural optimisation for extrusion of 6063 alloys, 5th International Aluminium Extrusion Seminar, Volume 2, (1992), pp. 57-69.

[24] M.A. Cooksey, N. Danilova, B. Rinderer, M. J. Couper, Process performance of continuous billet homogenisers, 6th Australian Asian Pacific Conference on Aluminium Cast House Technology, The Minerals, Metals and Materials Society, (1999), pp. 309-318.

[25] G. Lang, A. F. Castle, Effect of rate of cooling after homogenization on direct-extrusion parameters of 6063 (Al-Mg-Si) billets, Metals Technology, Volume 5, (1978), pp. 434-438.

[26] S. Camero, E. S. Puchi, G. Gonzalez, Effect of 0.1% vanadium addition on precipitation behaviour and mechanical properties of Al-6063 commercial alloy, J Mater Sci, Volume 41, (2006), pp. 7361-7373.

[27] R. A. Siddiqui, H. A. Abdullah, K. R. Al-Belushi, Influence of aging parameters on the mechanical properties of 6063 aluminium alloy, Journal of Materials Processing Technology, Volume 102, Issues 1-3, (2000), pp. 234-240.

[28] Y. Birol, The effect of processing and Mn content on the T5 and T6 properties of AA6082 profiles, Journal of Materials Processing Technology, Volume 173, Issue 1, (2006), pp. 84-91.

[29] H. Raupenstrauch, Script "Wärmetechnik", University of Leoben, (2011), pp. 64-65.

[30] B. Buchmayr, Script "Umformtechnik", University of Leoben, (2011), pp. 18.

9 Appendix

9.1 Flow Stress Calculation PSCT

9.1.1 Flow Stress from start point 10MPa

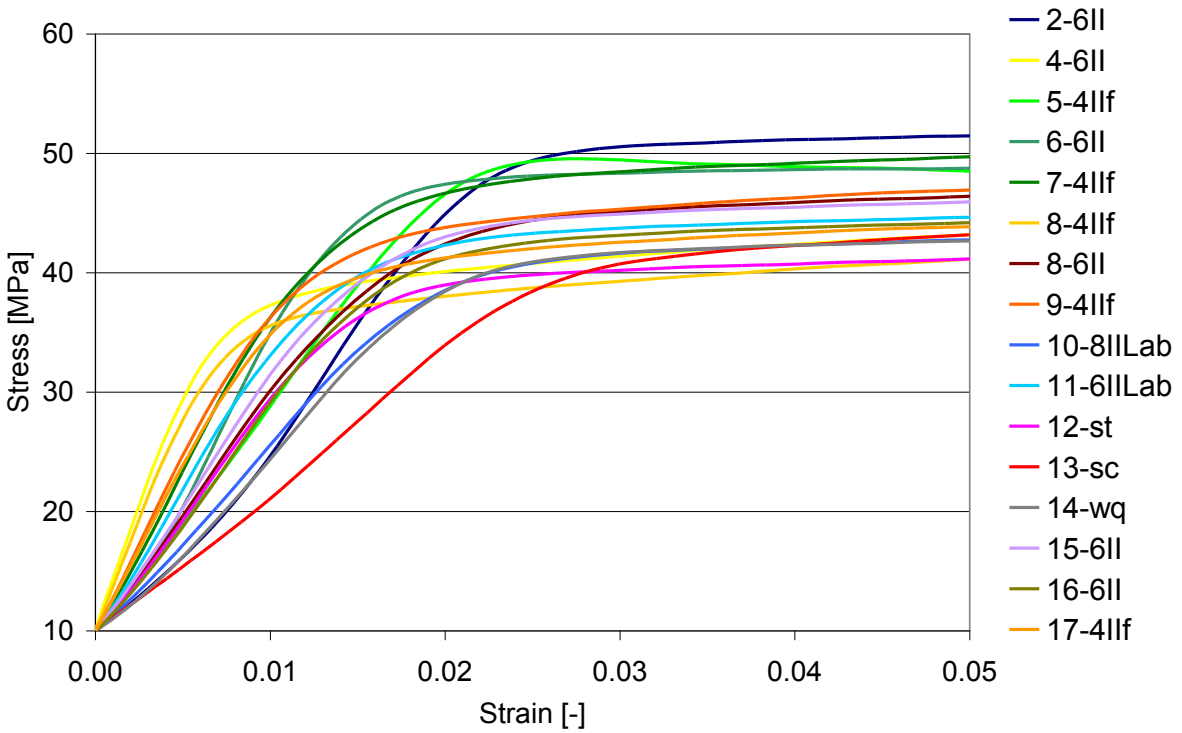

Diagram 9.1 Detail Stress-Strain curve (normalized to 10MPa)

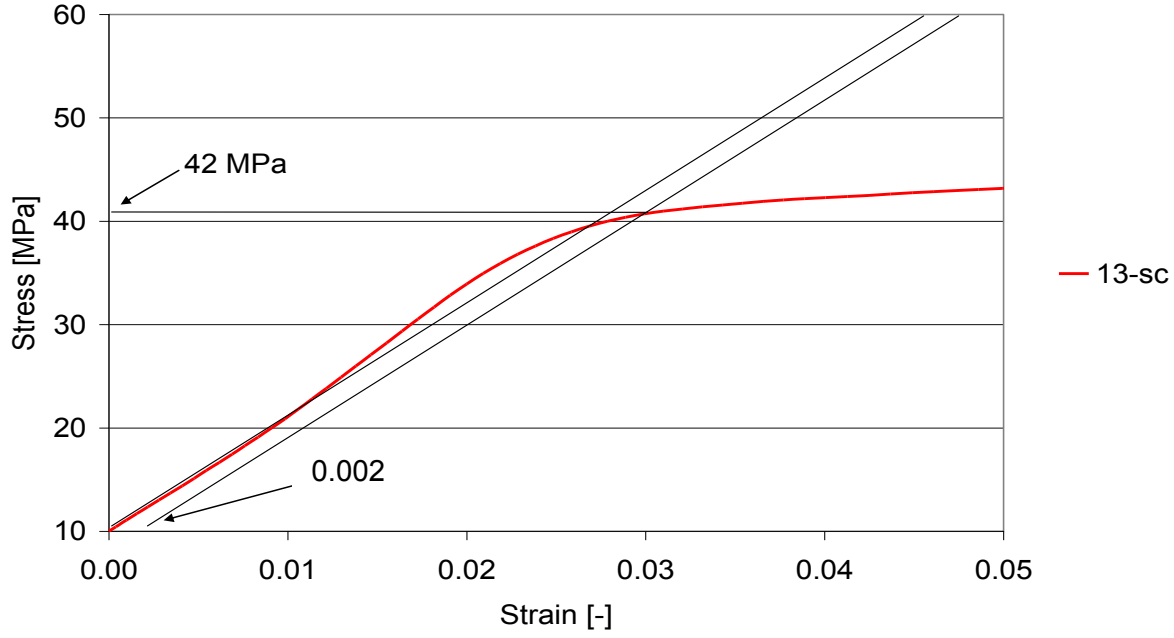

Diagram 9.2 Procedure to obtain the flow stress (e.g. $R_{p0.2}$)

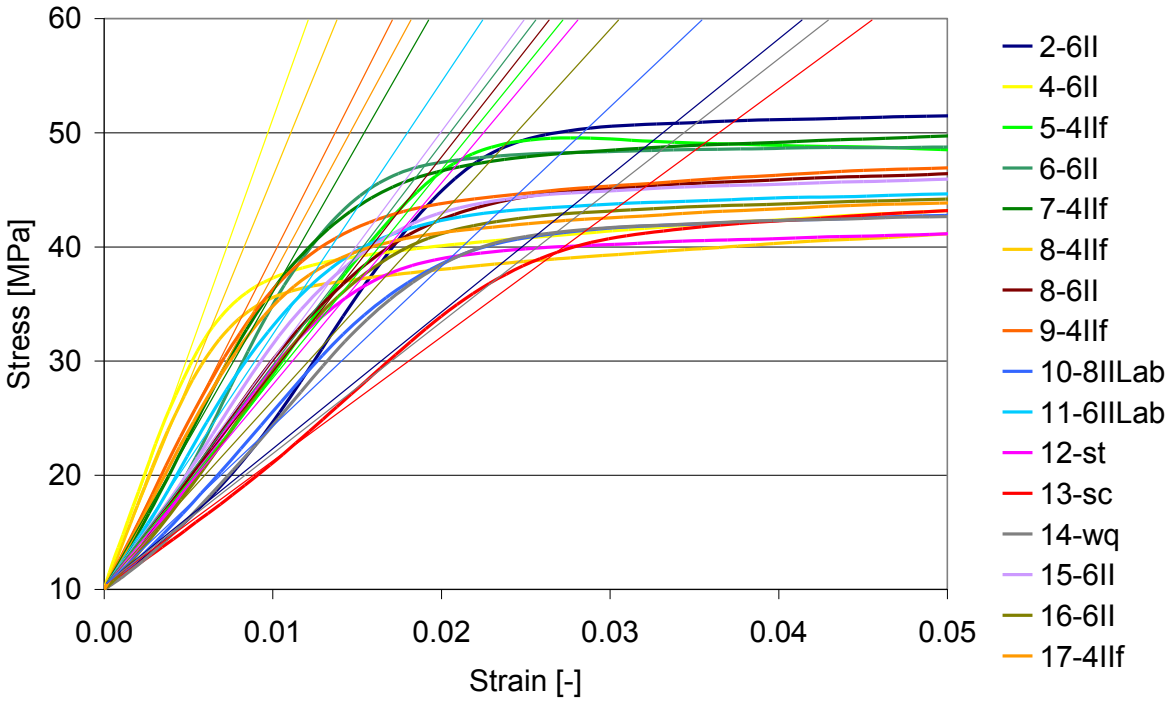

Diagram 9.3 Identifikation of $R_{p0.2}$

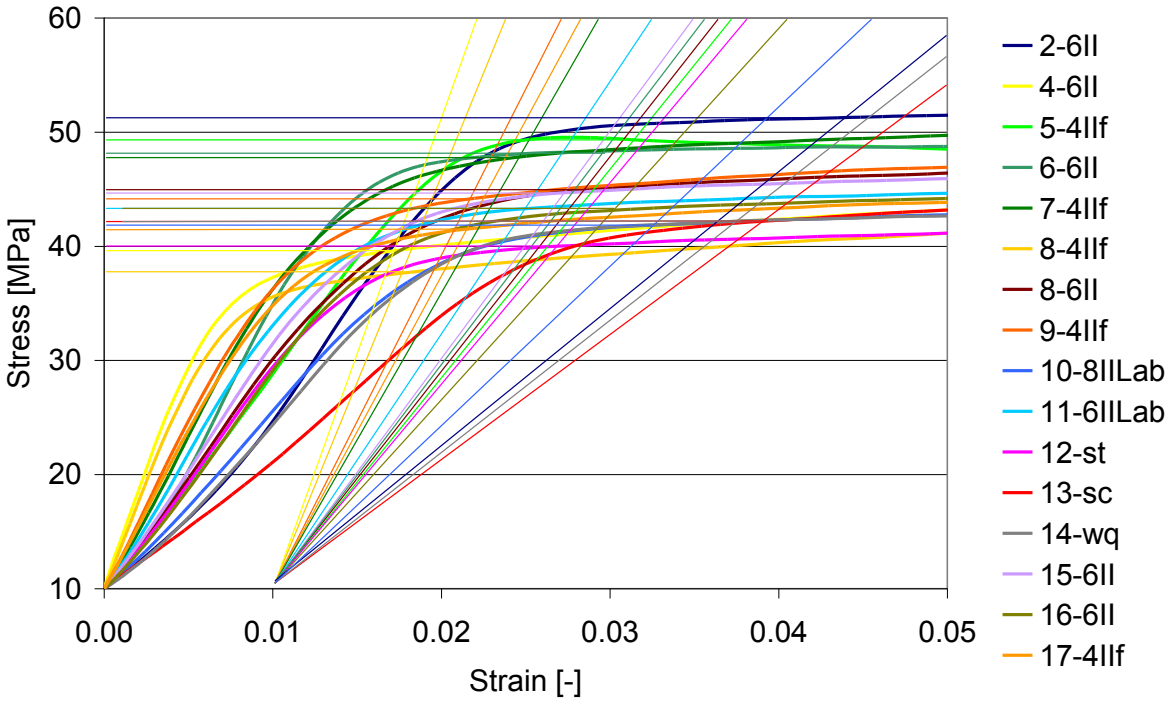

Diagram 9.4 Identification of $R_{p1.0}$

9.1.2 Flow Stress from start point 30MPa

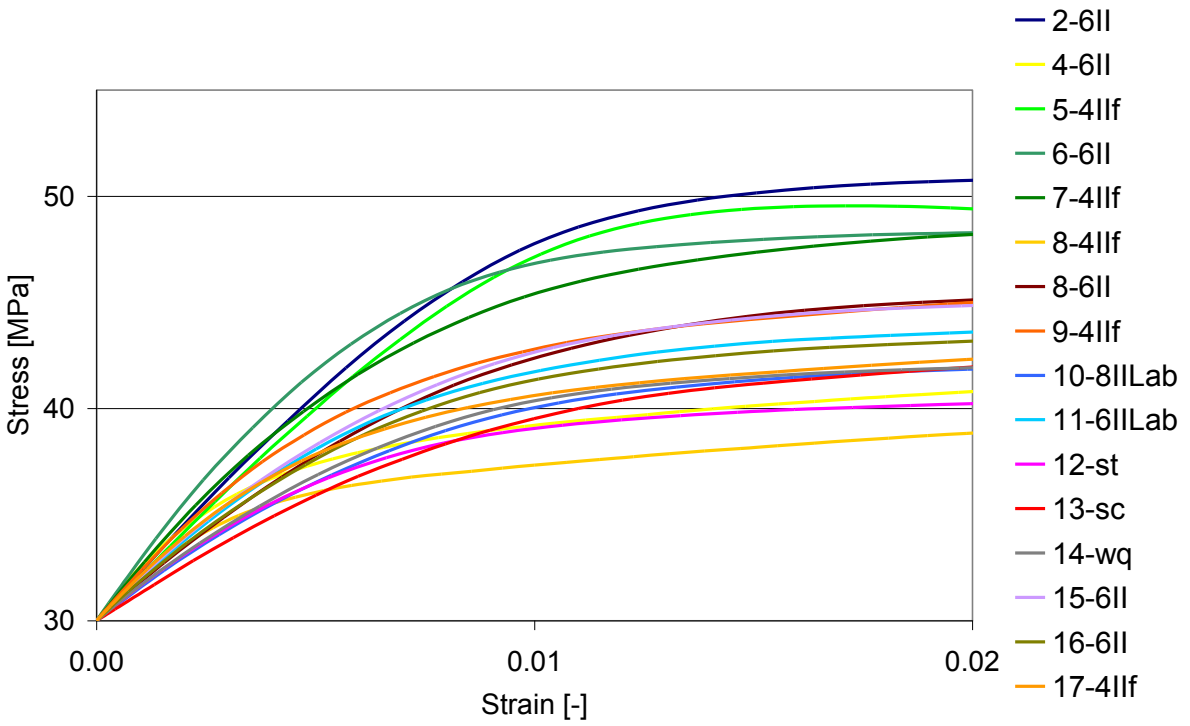

Diagram 9.5 Detail Stress-Strain curve (normalized to 30MPa)

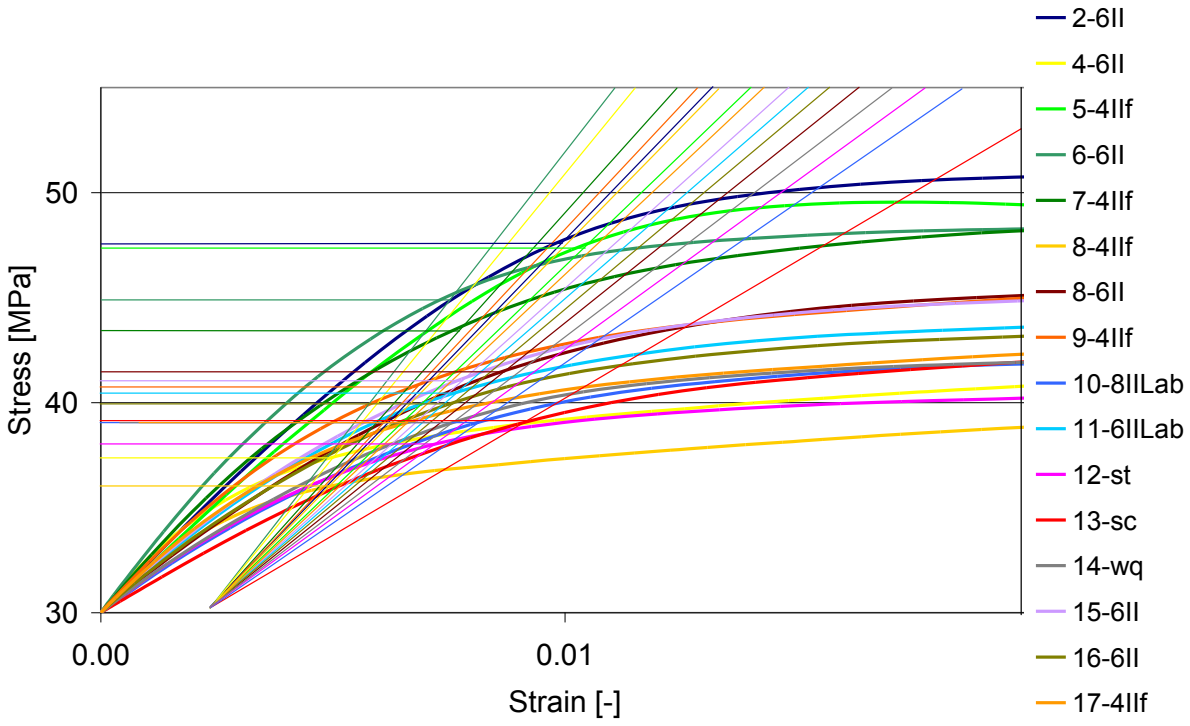

Diagram 9.6 Identification of $R_{p0.2}$

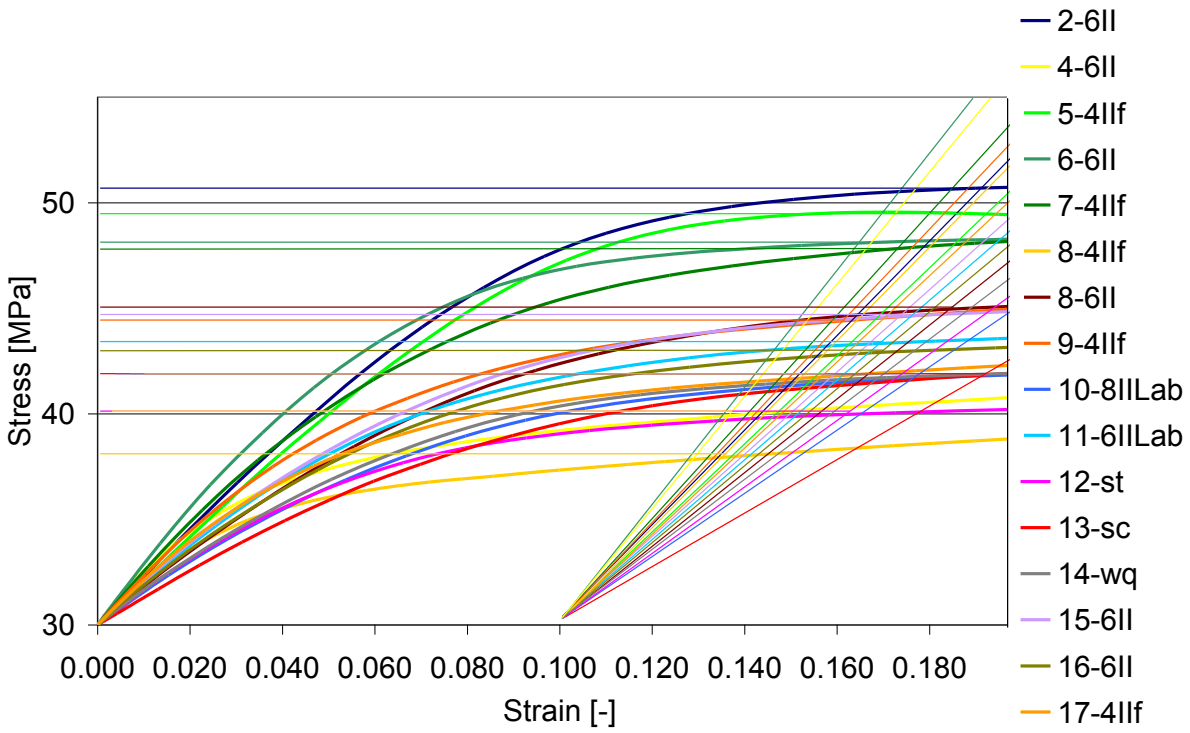

Diagram 9.7 Identification of $R_{p1.0}$

9.2 SEM Analysis

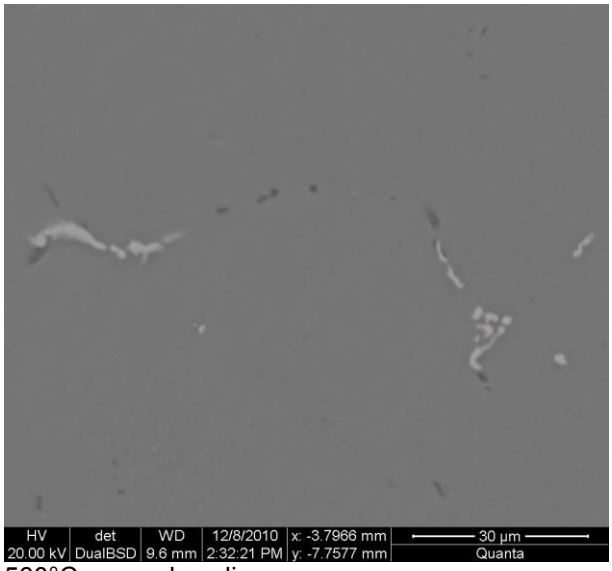

560°C, normal cooling

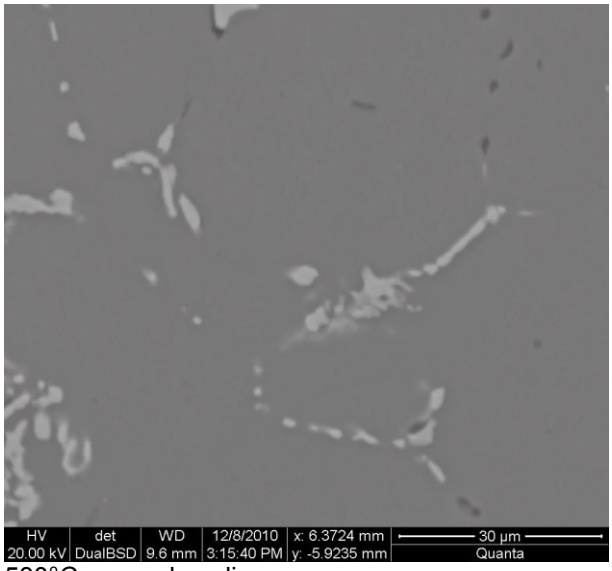

580°C, normal cooling

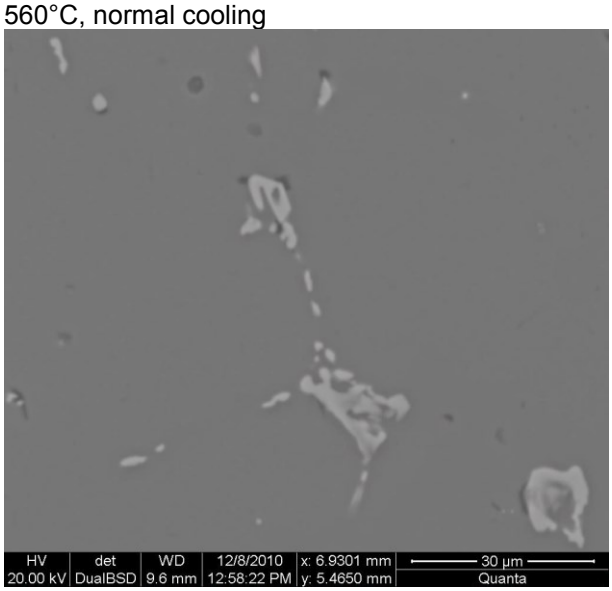

580°C, slow cooling

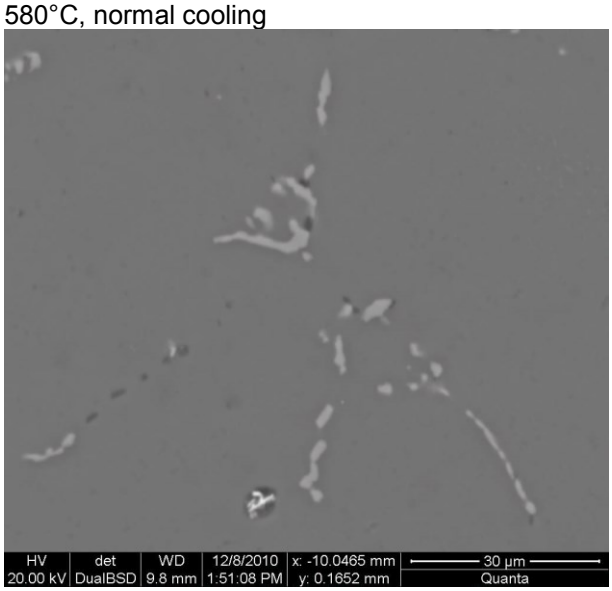

580°C, step cooling

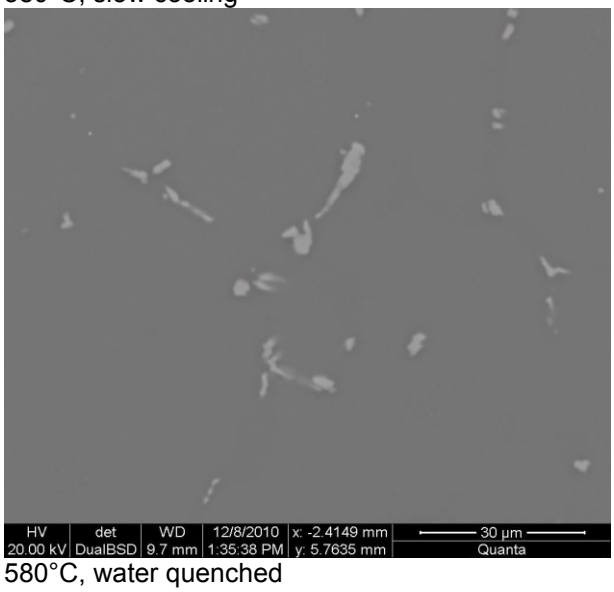

580°C, water quenched

Figure 9.1 Comparison 2 of the five different cooling conditions

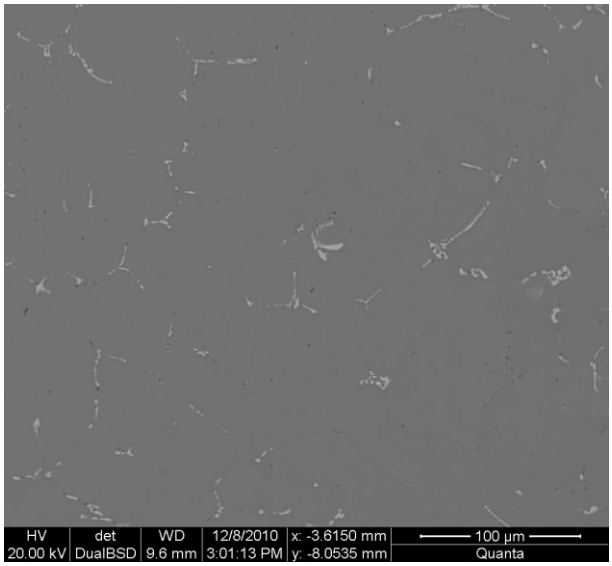

560°C, normal cooling

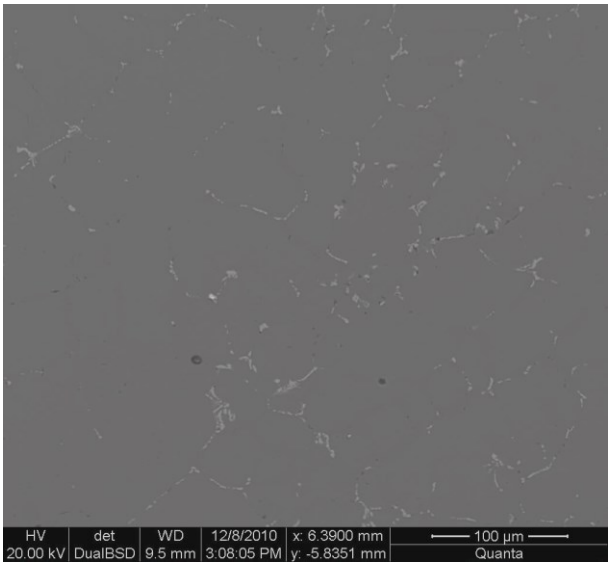

580°C, normal cooling

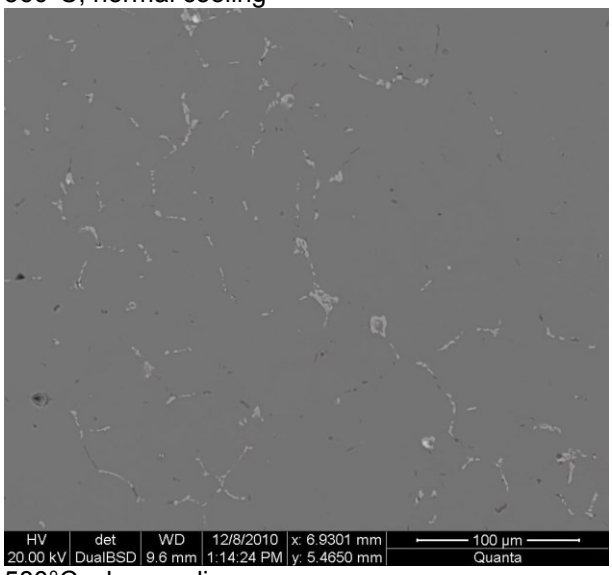

580°C, slow cooling

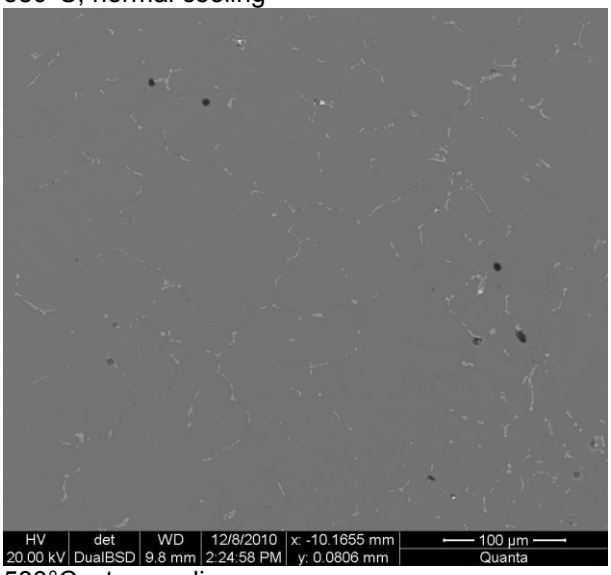

580°C, step cooling

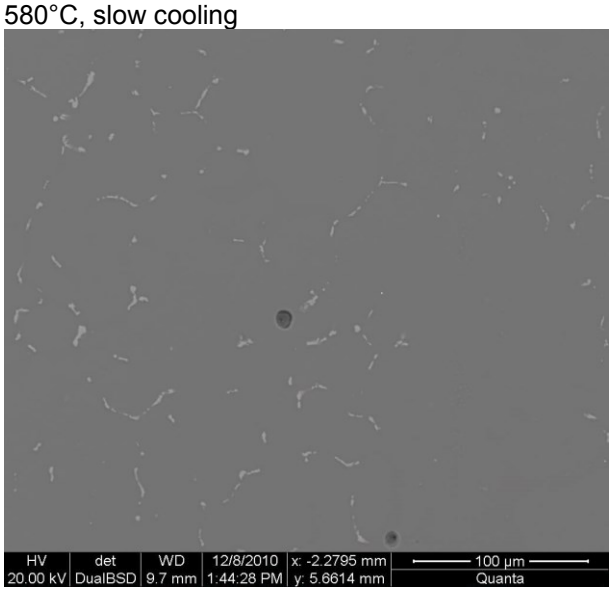

580°C, water quenched

Figure 9.2 Comparison 3 of the five different cooling conditions

9.3 EDX Analysis (SEM)

9.3.1 Sample 560°C (6II)

Temperature: 560°C
Duration: 4h
Cooling: normal (600 K/h)

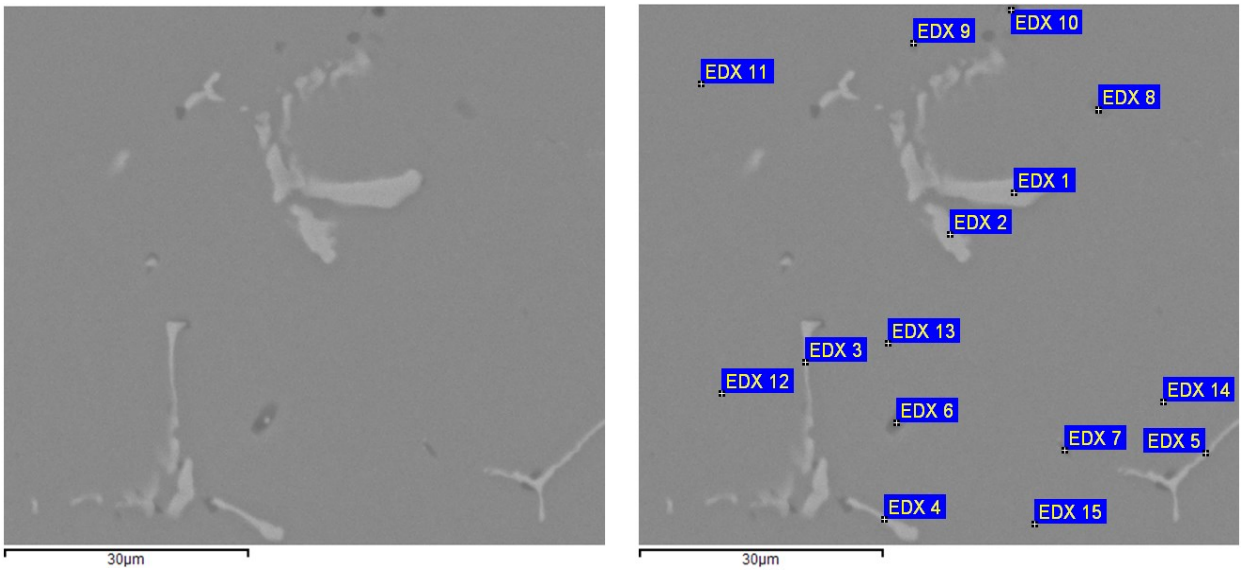

Figure 9.3 Spot EDX analysis I sample 6II

Table 9.1 EDX results I sample 6II

Element atom[%]	Magnesium Mg	Aluminium Al	Silicon Si	Iron Fe	Manganese Mn	Chromium Cr	Type
EDX 1	0.4	72.1	10.9	7.2	7.4	2.1	AlFeSi
EDX 2	0.2	77.0	10.2	6.1	5.3	1.4	AlFeSi
EDX 3	0.4	86.7	6.3	2.8	2.8	0.9	AlFeSi
EDX 4	0.8	86.3	6.1	3.5	2.8	0.6	AlFeSi
EDX 5	0.4	88.7	5.2	2.7	2.5	0.5	AlFeSi
EDX 6	0.4	86.5	12.6	0.1	0.3	0.1	Si
EDX 7	1.0	92.9	6.1	0.0	0.0	0.0	Mg/Si
EDX 8	0.4	88.6	10.8	0.1	0.3	0.0	Si
EDX 9	0.3	86.2	13.2	0.0	0.2	0.1	Si
EDX 10	0.6	92.4	6.9	0.0	0.1	0.0	Si
EDX 11	1.1	97.9	0.8	0.1	0.1	0.0	Matrix
EDX 12	1.3	97.5	1.0	0.0	0.2	0.1	Matrix
EDX 13	0.6	98.7	0.4	0.0	0.3	0.0	Matrix
EDX 14	0.6	98.2	0.8	0.0	0.3	0.1	Matrix
EDX 15	0.6	98.1	0.8	0.1	0.3	0.1	Matrix+AlFeSi

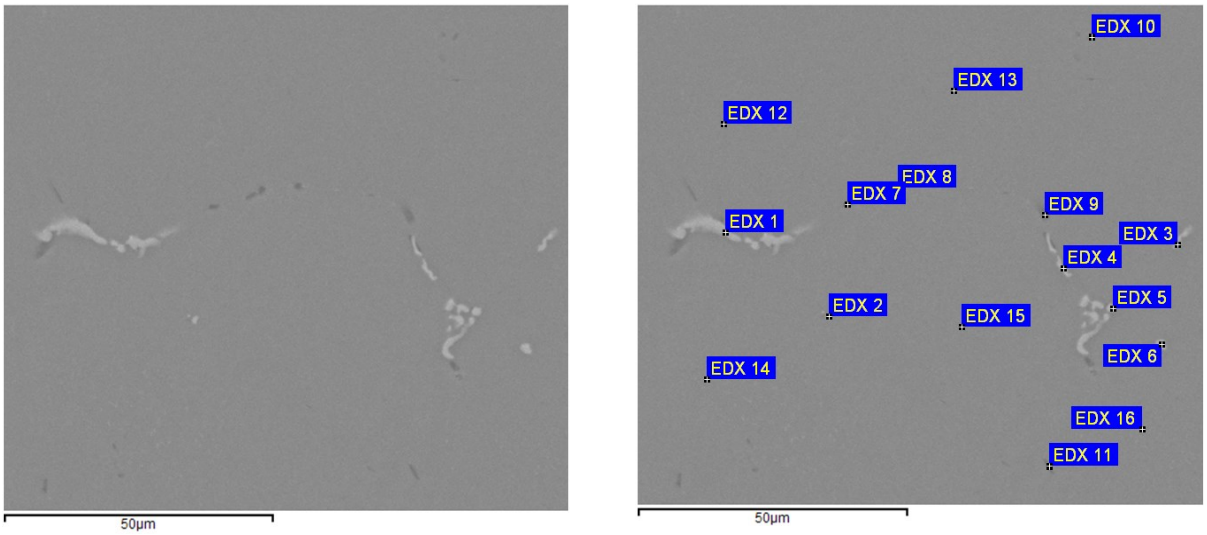

Figure 9.4 Spot EDX analysis II sample 6II

Table 9.2 EDX results II sample 6II

Element atom[%]	Magnesium Mg	Aluminium Al	Silicon Si	Iron Fe	Manganese Mn	Chromium Cr	Type
EDX 1	0.4	82.6	7.9	4.5	3.8	0.9	AlFeSi
EDX 2	4.8	85.1	6.0	1.2	2.1	0.9	Mg/Si+AlFeSi
EDX 3	1.0	82.1	7.8	4.6	3.8	0.7	AlFeSi
EDX 4	0.4	84.7	6.3	4.6	3.4	0.7	AlFeSi
EDX 5	0.3	85.2	6.7	4.2	3.1	0.5	AlFeSi
EDX 6	0.8	81.7	7.8	5.3	3.6	0.8	AlFeSi
EDX 7	0.4	93.7	5.6	0.0	0.2	0.0	Si
EDX 8	2.5	83.3	13.9	0.1	0.2	0.0	Mg/Si+AlFeSi
EDX 9	1.3	87.7	10.8	0.1	0.0	0.1	Mg/Si
EDX 10	0.6	93.7	5.2	0.0	0.4	0.1	Mg/Si
EDX 11	0.2	86.2	13.5	0.0	0.1	0.0	Si
EDX 12	0.5	97.1	1.7	0.1	0.5	0.1	Matrix
EDX 13	0.5	98.4	0.7	0.0	0.3	0.1	Matrix
EDX 14	0.8	98.2	0.4	0.1	0.3	0.2	Matrix
EDX 15	0.9	97.6	1.1	0.1	0.1	0.1	Matrix
EDX 16	0.7	98.6	0.4	0.0	0.2	0.1	Matrix

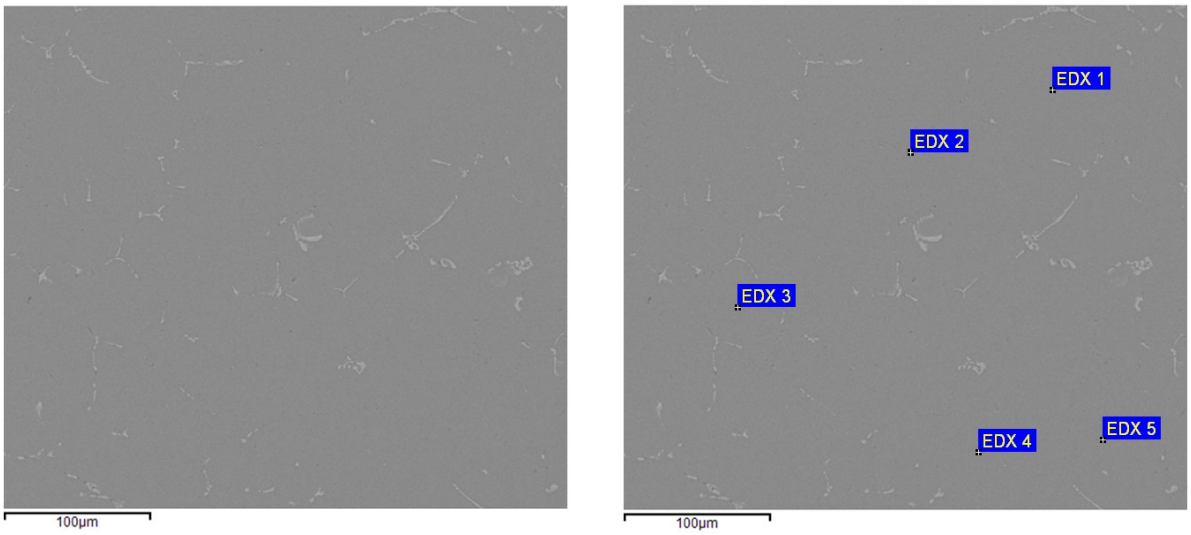

Figure 9.5 Spot EDX analysis III sample 6II

Table 9.3 EDX results III sample 6II

Element atom[%]	Magnesium Mg	Aluminium Al	Silicon Si	Iron Fe	Manganese Mn	Chromium Cr	Type
EDX 1	0.7	98.4	0.7	0.0	0.3	0.0	Matrix
EDX 2	0.8	97.8	1.0	0.0	0.3	0.2	Matrix
EDX 3	0.7	98.8	0.4	0.0	0.1	0.0	Matrix
EDX 4	0.7	98.0	0.9	0.0	0.2	0.1	Matrix
EDX 5	0.5	98.7	0.6	0.0	0.1	0.1	Matrix

9.3.2 Sample 580°C (8II)

Temperature: 580°C
Duration: 4h
Cooling: normal (1h)

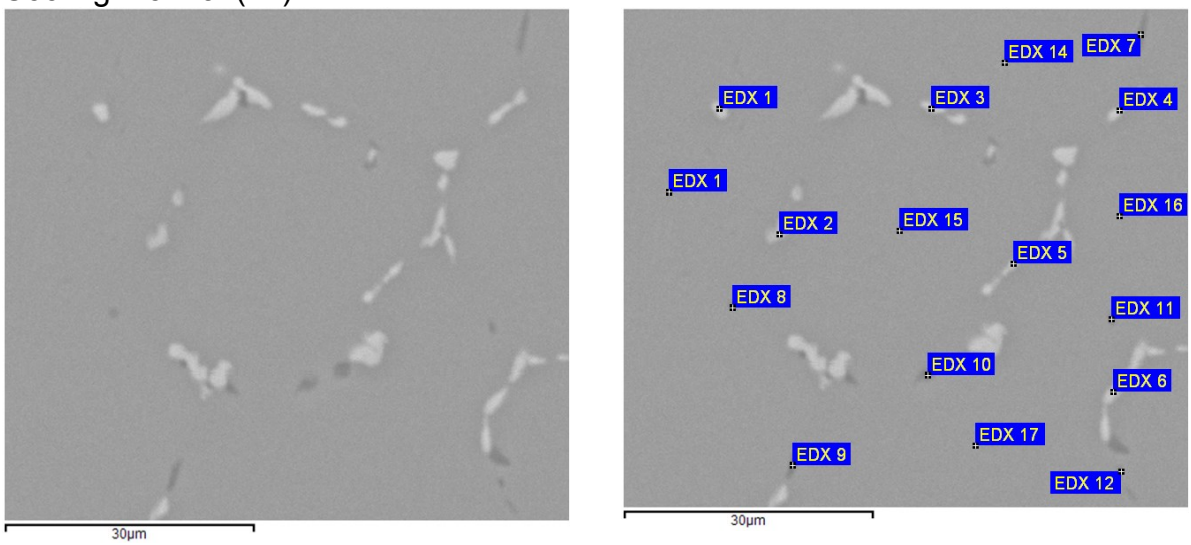

Figure 9.6 Spot EDX analysis I sample 8II

Table 9.4 EDX results I sample 8II

Element atom[%]	Magnesium Mg	Aluminium Al	Silicon Si	Iron Fe	Manganese Mn	Chromium Cr	Type
EDX 1	0.7	82.0	7.3	5.3	4.0	0.7	AlFeSi
EDX 2	0.7	88.9	5.7	2.5	1.6	0.5	AlFeSi
EDX 3	0.4	84.5	6.8	4.2	3.5	0.7	AlFeSi
EDX 4	0.3	89.0	5.1	2.6	2.5	0.5	AlFeSi
EDX 5	0.4	87.3	5.7	3.3	2.8	0.6	AlFeSi
EDX 6	0.5	82.9	7.6	4.7	3.7	0.7	AlFeSi
EDX 7	7.8	78.0	14.0	0.0	0.1	0.1	Mg/Si
EDX 8	4.0	90.5	5.2	0.1	0.1	0.0	Mg/Si
EDX 9	12.5	67.7	19.5	0.0	0.2	0.1	Mg/Si
EDX 10	14.9	71.4	13.7	0.0	0.1	0.0	Mg/Si
EDX 11	0.3	93.9	5.8	0.0	0.0	0.1	Si
EDX 12	0.7	93.4	5.8	0.0	0.2	0.0	Mg/Si
EDX 13	1.6	96.2	1.9	0.1	0.2	0.1	Matrix
EDX 14	1.0	97.5	1.2	0.1	0.2	0.0	Matrix
EDX 15	0.7	98.1	0.7	0.1	0.3	0.1	Matrix
EDX 16	0.8	98.4	0.6	0.0	0.2	0.0	Matrix
EDX 17	0.8	97.9	1.0	0.0	0.1	0.1	Matrix

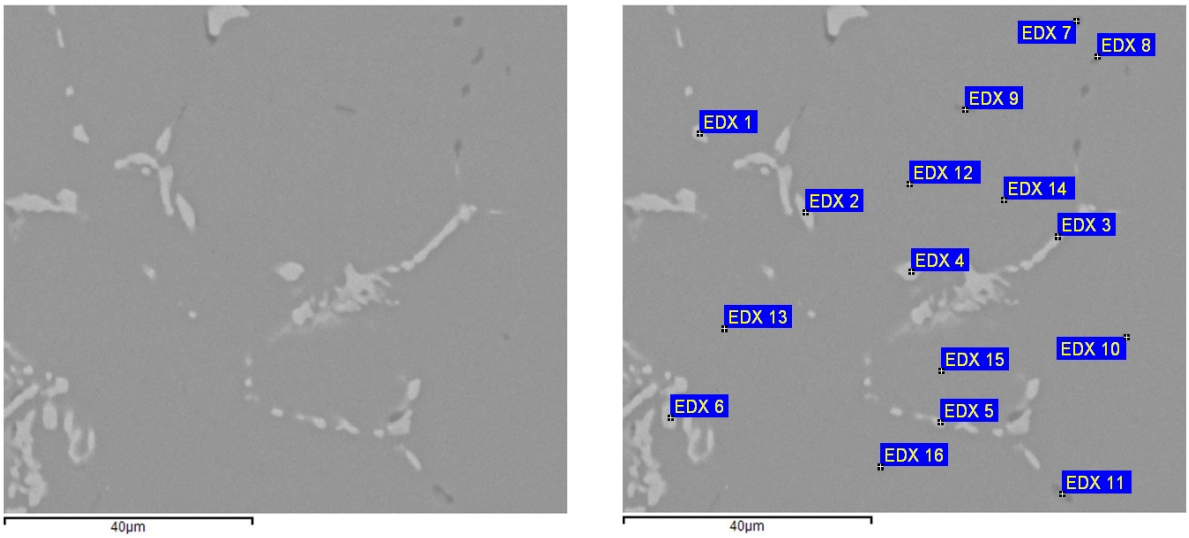

Figure 9.7 Spot EDX analysis II sample 8II

Table 9.5 EDX results II sample 8II

Element atom[%]	Magnesium Mg	Aluminium Al	Silicon Si	Iron Fe	Manganese Mn	Chromium Cr	Type
EDX 1	0.3	80.9	8.2	5.5	4.2	1.0	AlFeSi
EDX 2	0.2	81.1	8.3	5.7	4.0	0.7	AlFeSi
EDX 3	0.3	80.6	8.2	5.7	4.4	0.9	AlFeSi
EDX 4	0.0	76.0	9.8	7.4	5.8	1.1	AlFeSi
EDX 5	0.3	83.7	6.7	4.6	3.8	0.8	AlFeSi
EDX 6	0.4	79.7	9.6	5.5	3.9	0.9	AlFeSi
EDX 7	5.9	83.2	10.8	0.1	0.0	0.0	Mg/Si
EDX 8	12.9	72.0	14.9	0.0	0.2	0.0	Mg/Si
EDX 9	0.9	94.1	4.9	0.0	0.1	0.0	Mg/Si
EDX 10	0.3	96.9	2.7	0.0	0.0	0.0	Matrix+Mg/Si
EDX 11	8.1	74.1	13.7	2.3	1.5	0.3	Mg/Si+AlFeSi
EDX 12	0.8	98.2	0.8	0.0	0.2	0.0	Matrix
EDX 13	1.1	96.5	2.1	0.0	0.1	0.2	Matrix+Mg/Si
EDX 14	1.0	98.0	0.7	0.1	0.2	0.1	Matrix
EDX 15	0.4	98.9	0.6	0.1	0.0	0.0	Matrix
EDX 16	0.7	98.4	0.6	0.0	0.1	0.1	Matrix

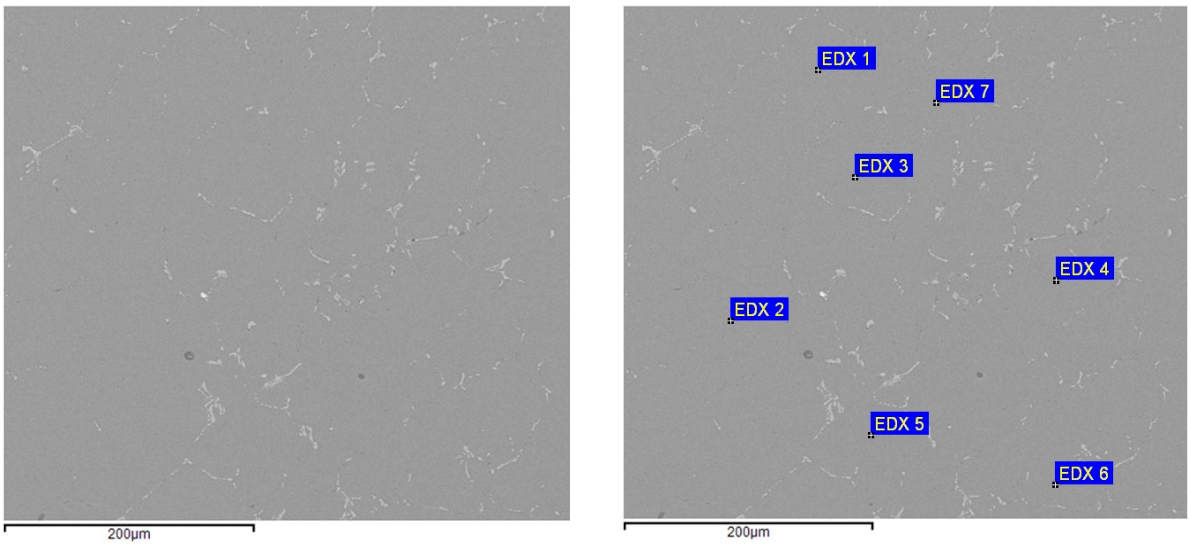

Figure 9.8 Spot EDX analysis III sample 8II

Table 9.6 EDX results III sample 8II

Element atom[%]	Magnesium Mg	Aluminium Al	Silicon Si	Iron Fe	Manganese Mn	Chromium Cr	Type
EDX 1	0.6	98.6	0.6	0.0	0.2	0.0	Matrix
EDX 2	0.6	98.6	0.6	0.0	0.2	0.1	Matrix
EDX 3	1.2	96.5	1.9	0.0	0.3	0.1	Matrix
EDX 4	0.5	98.5	0.6	0.1	0.1	0.1	Matrix
EDX 5	1.7	97.0	1.2	0.0	0.0	0.1	Matrix
EDX 6	1.1	97.8	0.8	0.0	0.1	0.1	Matrix
EDX 7	0.6	98.1	0.9	0.1	0.2	0.2	Matrix+AlFeSi

9.3.3 Slow cooled Sample (sc)

Temperature: 580°C
Duration: 4h
Cooling: slow cooling (2h)

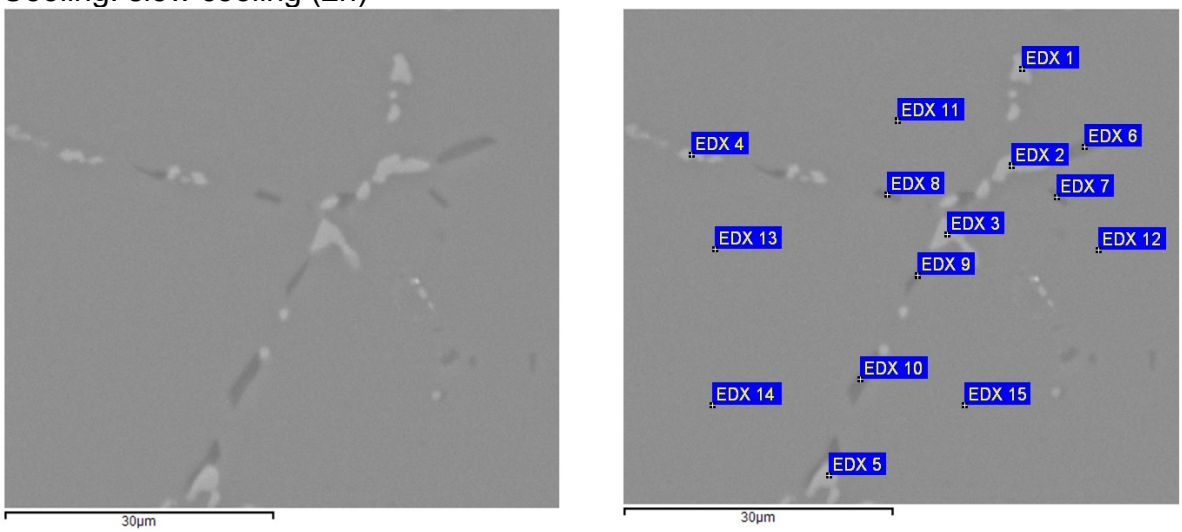

Figure 9.9 Spot EDX analysis I sample sc

Table 9.7 EDX results I sample sc

Element atom[%]	Magnesium Mg	Aluminium Al	Silicon Si	Iron Fe	Manganese Mn	Chromium Cr	Type
EDX 1	0.3	80.6	8.8	4.8	4.8	0.9	AlFeSi
EDX 2	0.4	76.8	9.5	6.1	5.8	1.3	AlFeSi
EDX 3	0.0	76.9	9.4	6.6	5.9	1.2	AlFeSi
EDX 4	0.2	83.9	7.0	4.4	3.9	0.7	AlFeSi
EDX 5	3.0	70.7	14.0	6.8	4.3	1.2	Mg/Si+AlFeSi
EDX 6	14.3	59.7	26.0	0.0	0.1	0.0	Mg/Si
EDX 7	2.7	94.3	2.7	0.1	0.2	0.0	Mg/Si
EDX 8	4.5	86.3	9.0	0.0	0.2	0.0	Mg/Si
EDX 9	2.6	90.0	7.4	0.0	0.1	0.0	Mg/Si
EDX 10	0.6	92.4	6.8	0.0	0.3	0.0	Si
EDX 11	0.9	96.8	2.1	0.0	0.1	0.2	Matrix+Mg/Si
EDX 12	0.6	98.6	0.6	0.0	0.1	0.1	Matrix
EDX 13	0.6	98.3	0.8	0.0	0.3	0.0	Matrix
EDX 14	1.0	97.8	0.9	0.0	0.2	0.2	Matrix
EDX 15	0.8	98.3	0.8	0.0	0.1	0.1	Matrix

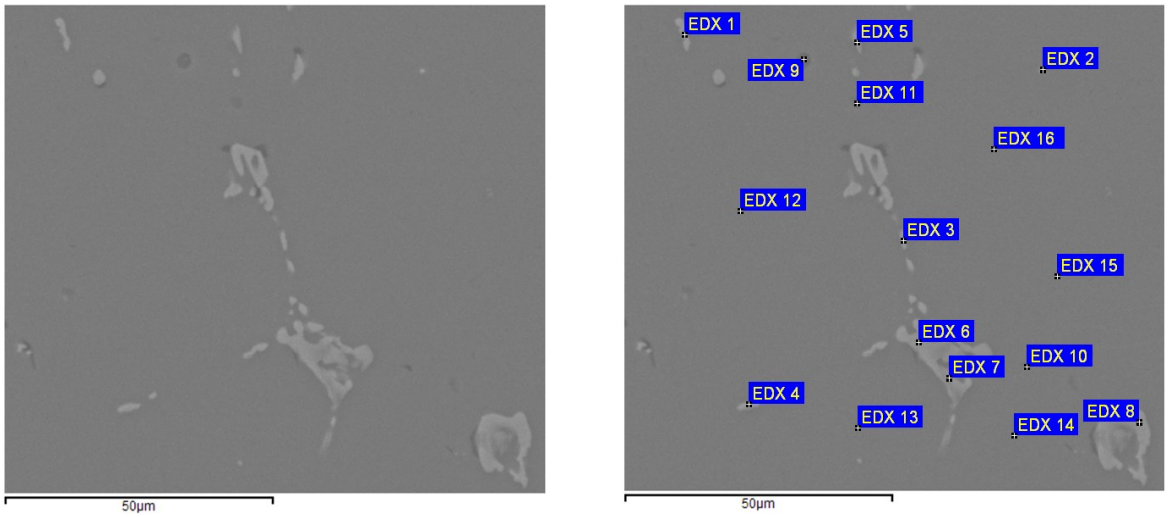

Figure 9.10 Spot EDX analysis II sample sc

Table 9.8 EDX results II sample sc

Element atom[%]	Magnesium Mg	Aluminium Al	Silicon Si	Iron Fe	Manganese Mn	Chromium Cr	Type
EDX 1	0.3	82.4	8.1	3.4	4.6	1.2	AlFeSi
EDX 2	2.5	95.7	1.5	0.0	0.3	0.1	Mg/Si+0.70Pb*
EDX 3	0.7	84.6	6.3	4.5	3.3	0.7	AlFeSi
EDX 4	0.2	80.2	8.4	5.9	4.3	1.0	AlFeSi
EDX 5	0.6	90.1	4.6	1.6	2.5	0.6	AlFeSi
EDX 6	0.3	80.9	8.7	5.6	4.0	0.6	AlFeSi
EDX 7	0.0	84.9	7.3	3.8	3.4	0.60	AlFeSi
EDX 8	0.4	78.2	10.7	5.1	4.5	1.3	AlFeSi
EDX 9	13.0	67.8	18.7	0.1	0.2	0.2	Mg/Si
EDX 10	0.4	97.7	1.8	0.0	0.0	0.1	Matrix
EDX 11	13.6	77.1	9.2	0.0	0.1	0.1	Mg/Si
EDX 12	0.7	98.4	0.7	0.1	0.2	0.0	Matrix
EDX 13	0.8	98.3	0.8	0.0	0.1	0.1	Matrix
EDX 14	0.4	99.0	0.5	0.0	0.1	0.1	Matrix
EDX 15	0.9	97.8	0.9	0.1	0.2	0.2	Matrix+AlFeSi
EDX 16	0.6	98.4	0.7	0.0	0.2	0.1	Matrix

*The particle EDX 2 contains lead, source of this is most probably scrap.

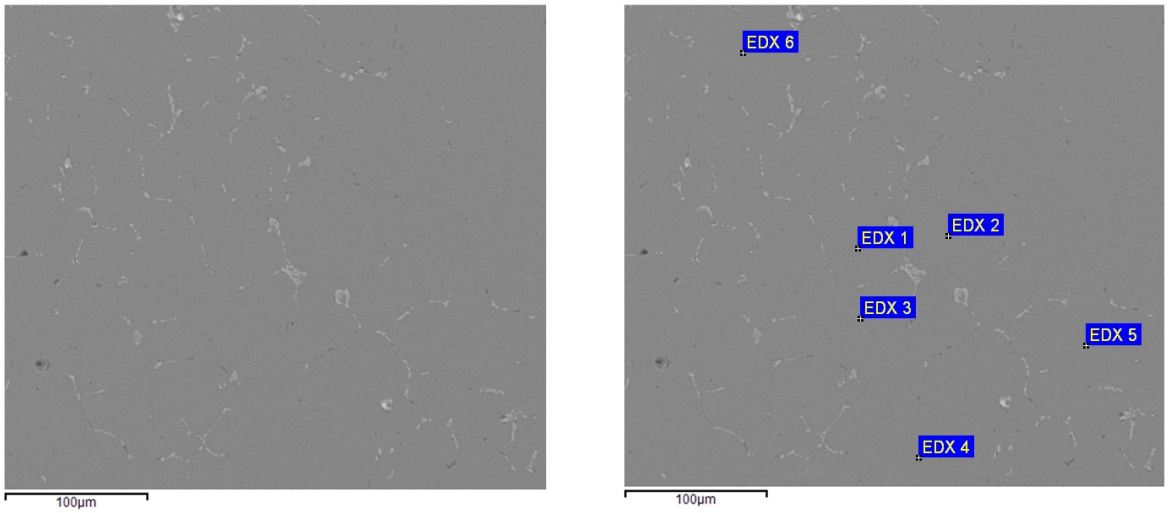

Figure 9.11 Spot EDX analysis III sample sc

Table 9.9 EDX results III sample sc

Element atom[%]	Magnesium Mg	Aluminium Al	Silicon Si	Iron Fe	Manganese Mn	Chromium Cr	Type
EDX 1	0.7	98.2	0.7	0.1	0.3	0.2	Matrix
EDX 2	0.5	98.4	0.7	0.0	0.2	0.2	Matrix
EDX 3	0.7	97.8	1.1	0.0	0.2	0.1	Matrix
EDX 4	0.9	97.8	1.1	0.0	0.1	0.2	Matrix
EDX 5	0.6	98.1	0.7	0.2	0.3	0.1	Matrix+AlFeSi
EDX 6	0.9	98.0	0.8	0.1	0.2	0.0	Matrix+AlFeSi

9.3.4 Step cooled Sample (st)

Temperature: 580°C
Duration: 4h
Cooling: air quenched to ~350°C, 1h holding, air quenching to room temperature

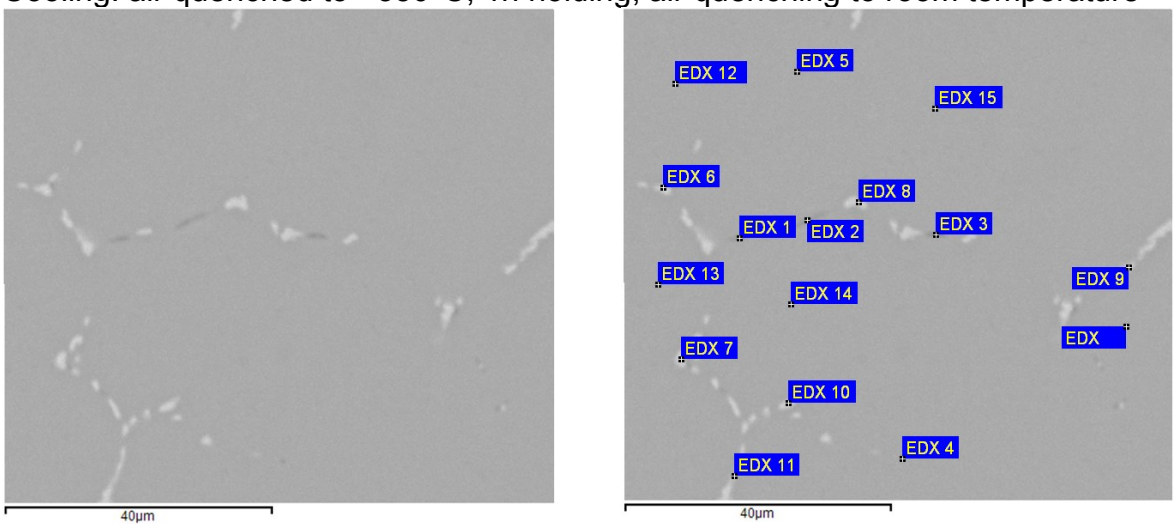

Figure 9.12 Spot EDX analysis I sample st

Table 9.10 EDX results I sample st

Element atom[%]	Magnesium Mg	Aluminium Al	Silicon Si	Iron Fe	Manganese Mn	Chromium Cr	Type
EDX 1	6.6	81.4	11.9	0.0	0.2	0.0	Mg/Si
EDX 2	12.5	74.8	12.5	0.1	0.1	0.0	Mg/Si
EDX 3	0.7	88.5	10.8	0.0	0.1	0.0	Si
EDX 4	1.8	92.1	5.9	0.0	0.1	0.1	Mg/Si
EDX 5	0.6	97.4	1.6	0.0	0.3	0.2	Matrix
EDX 6	0.5	81.8	8.2	4.4	4.2	0.9	AlFeSi
EDX 7	0.9	80.4	8.5	4.8	4.5	0.8	AlFeSi
EDX 8	0.3	85.5	5.8	4.2	3.5	0.7	AlFeSi
EDX 9	0.4	88.6	4.5	2.9	3.1	0.6	AlFeSi
EDX 10	0.3	88.3	5.4	2.9	2.6	0.5	AlFeSi
EDX 11	0.4	94.3	1.9	1.6	1.6	0.3	AlFeSi
EDX 12	0.9	97.9	1.0	0.0	0.2	0.0	Matrix
EDX 13	0.8	98.3	0.6	0.0	0.2	0.0	Matrix
EDX 14	0.6	98.3	0.8	0.0	0.2	0.1	Matrix
EDX 15	0.9	97.8	1.0	0.1	0.1	0.1	Matrix
EDX 16	1.4	96.4	1.6	0.2	0.3	0.2	Matrix+AlFeSi

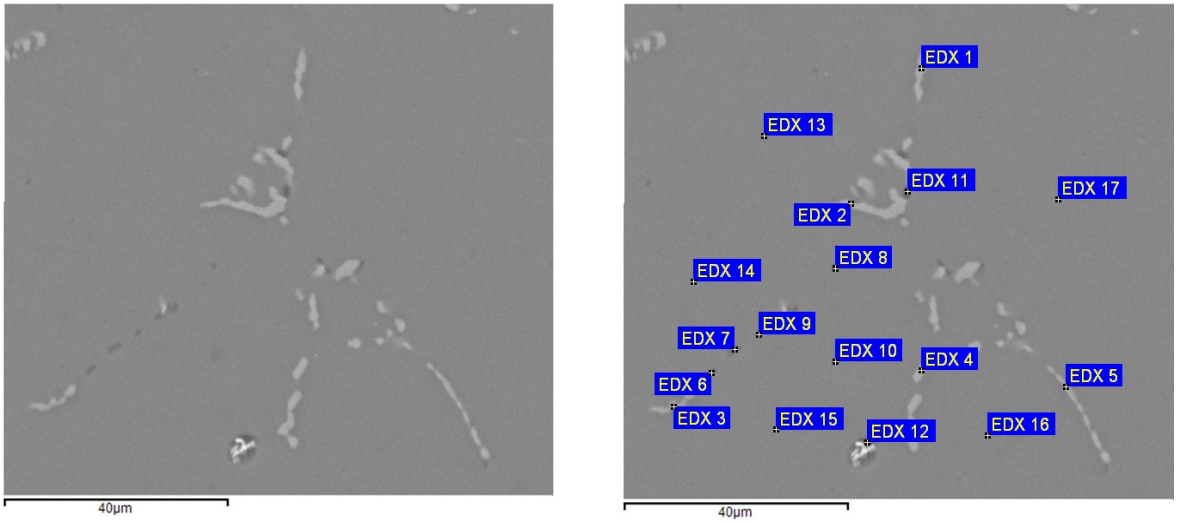

Figure 9.13 Spot EDX analysis II sample st

Table 9.11 EDX results II sample st

Element atom[%]	Magnesium Mg	Aluminium Al	Silicon Si	Iron Fe	Manganese Mn	Chromium Cr	Type
EDX 1	0.5	81.1	7.6	6.1	3.9	0.9	AlFeSi
EDX 2	0.4	81.9	7.8	4.7	4.6	0.6	AlFeSi
EDX 3	0.4	88.5	5.7	1.9	2.8	0.8	AlFeSi
EDX 4	0.2	80.6	8.2	5.9	4.5	0.7	AlFeSi
EDX 5	0.4	86.6	6.0	3.8	2.8	0.5	AlFeSi
EDX 6	0.4	95.9	3.6	0.0	0.1	0.0	Matrix+Mg/Si
EDX 7	10.6	77.7	11.6	0.0	0.2	0.0	Mg/Si
EDX 8	0.7	93.1	6.1	0.0	0.1	0.0	Mg/Si
EDX 9	0.0	94.8	5.0	0.1	0.1	0.0	Si+AlFeSi
EDX 10	0.7	98.3	0.8	0.0	0.2	0.0	Matrix
EDX 11	0.1	79.7	18.8	0.7	0.7	0.0	Si+AlFeSi
EDX 12	0.4	98.2	1.3	0.2	0.0	0.0	Matrix+AlFeSi
EDX 13	1.5	96.8	1.2	0.0	0.3	0.1	Matrix
EDX 14	0.6	98.6	0.5	0.2	0.1	0.1	Matrix+AlFeSi
EDX 15	0.7	98.1	0.9	0.0	0.3	0.1	Matrix
EDX 16	0.7	98.1	0.9	0.1	0.1	0.1	Matrix
EDX 17	0.7	98.4	0.7	0.0	0.2	0.1	Matrix

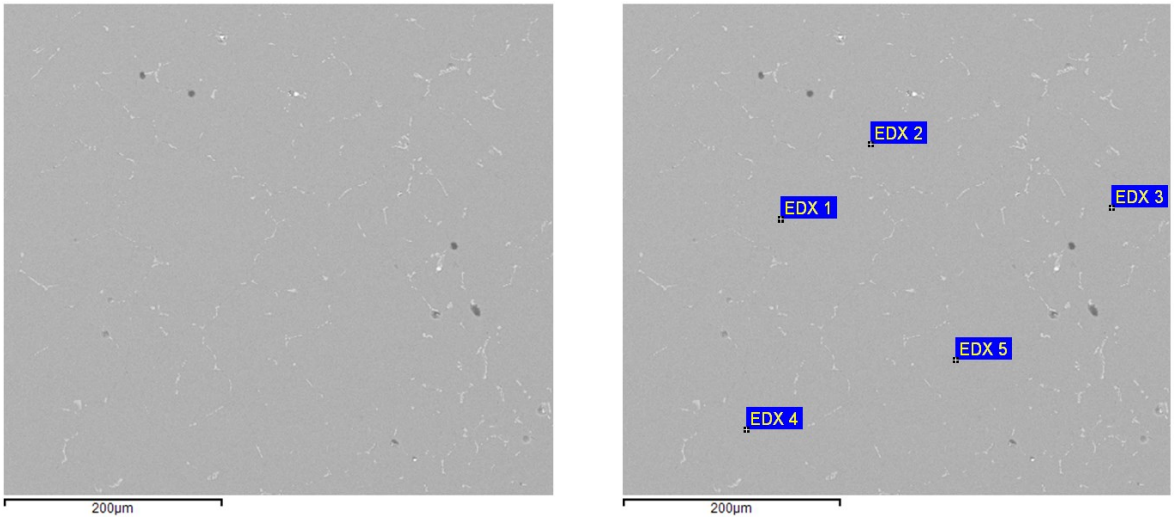

Figure 9.14 Spot EDX analysis III sample st

Table 9.12 EDX results III sample st

Element atom[%]	Magnesium Mg	Aluminium Al	Silicon Si	Iron Fe	Manganese Mn	Chromium Cr	Type
EDX 1	0.9	98.0	0.6	0.0	0.3	0.1	Matrix
EDX 2	0.9	98.0	0.7	0.0	0.3	0.2	Matrix
EDX 3	1.2	97.6	1.1	0.0	0.2	0.0	Matrix
EDX 4	0.8	97.7	1.2	0.0	0.3	0.1	Matrix
EDX 5	0.9	97.8	1.0	0.0	0.2	0.1	Matrix

9.3.5 Water quenched Sample (wq)

Temperature: 580°C
Duration: 4h
Cooling: water quenched

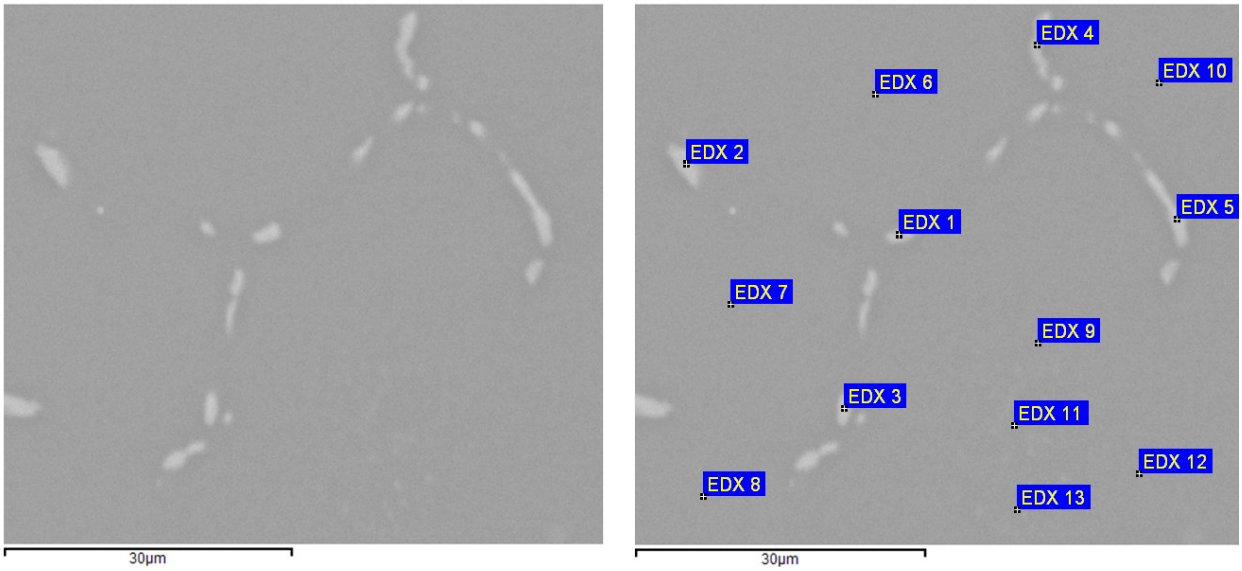

Figure 9.15 Spot EDX analysis I sample wq

Table 9.13 EDX results I sample wq

Element atom[%]	Magnesium Mg	Aluminium Al	Silicon Si	Iron Fe	Manganese Mn	Chromium Cr	Type
EDX 1	0.7	81.9	7.2	5.4	4.2	1.0	AlFeSi
EDX 2	0.5	80.1	7.9	6.5	4.3	0.7	AlFeSi
EDX 3	0.7	84.5	6.5	4.5	3.2	0.6	AlFeSi
EDX 4	0.9	88.2	5.2	3.1	2.1	0.5	AlFeSi
EDX 5	0.8	82.4	7.8	4.8	3.5	0.7	AlFeSi
EDX 6	1.1	97.7	0.9	0.1	0.1	0.2	Matrix+AlFeSi
EDX 7	0.9	97.5	1.1	0.0	0.2	0.2	Matrix
EDX 8	1.1	97.8	0.8	0.1	0.2	0.0	Matrix
EDX 9	1.0	97.6	1.0	0.1	0.2	0.0	Matrix
EDX 10	1.0	97.6	1.1	0.0	0.3	0.1	Matrix
EDX 11	1.0	96.6	1.7	0.1	0.5	0.1	Matrix+AlFeSi
EDX 12	0.9	98.0	1.0	0.1	0.1	0.0	Matrix
EDX 13	1.0	97.8	1.1	0.0	0.1	0.0	Matrix

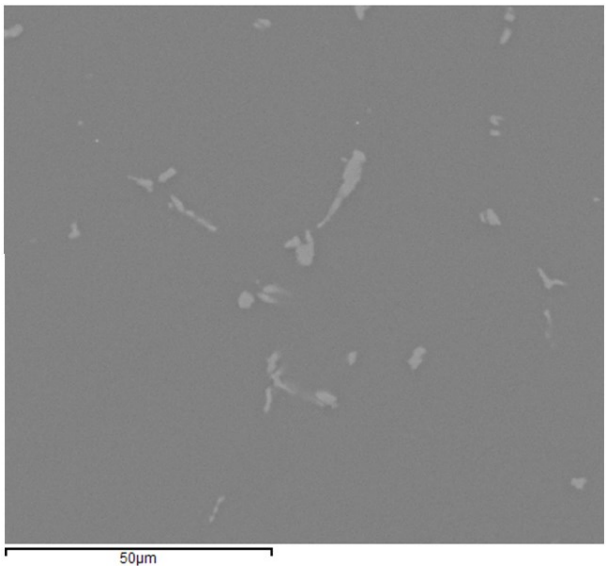

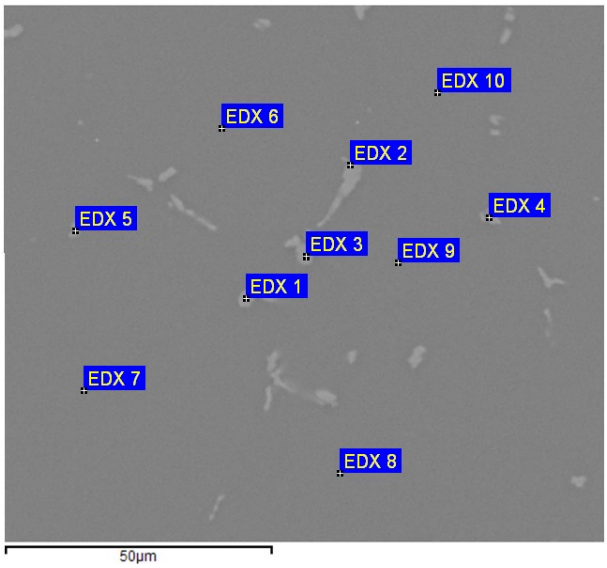

Figure 9.16 Spot EDX analysis II sample wq

Table 9.14 EDX results II sample wq

Element atom[%]	Magnesium Mg	Aluminium Al	Silicon Si	Iron Fe	Manganese Mn	Chromium Cr	Type
EDX 1	0.6	80.5	7.7	6.2	4.2	0.9	AlFeSi
EDX 2	0.4	75.5	9.7	7.1	6.2	1.1	AlFeSi
EDX 3	0.5	76.9	9.0	7.4	5.1	1.1	AlFeSi
EDX 4	0.5	78.8	8.5	5.2	5.5	1.5	AlFeSi
EDX 5	0.8	84.0	6.8	3.2	4.3	1.0	AlFeSi
EDX 6	1.0	97.7	1.0	0.0	0.2	0.1	Matrix
EDX 7	0.8	97.7	1.1	0.0	0.2	0.2	Matrix
EDX 8	1.0	97.8	0.9	0.0	0.3	0.1	Matrix
EDX 9	1.0	97.6	1.1	0.0	0.1	0.1	Matrix
EDX 10	1.0	97.6	1.0	0.1	0.3	0.1	Matrix

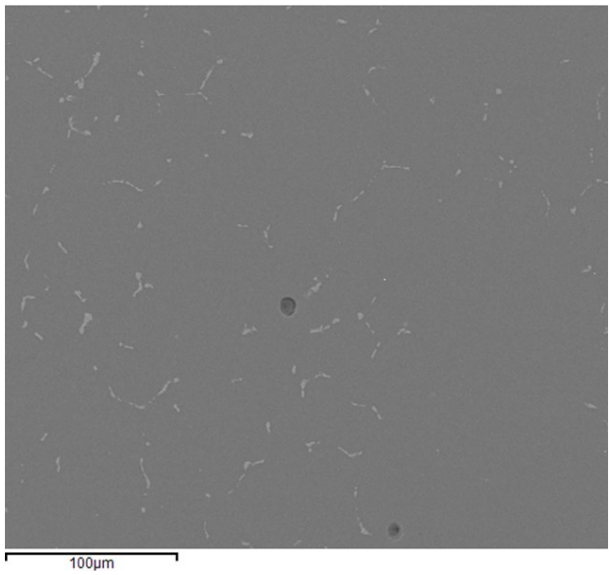

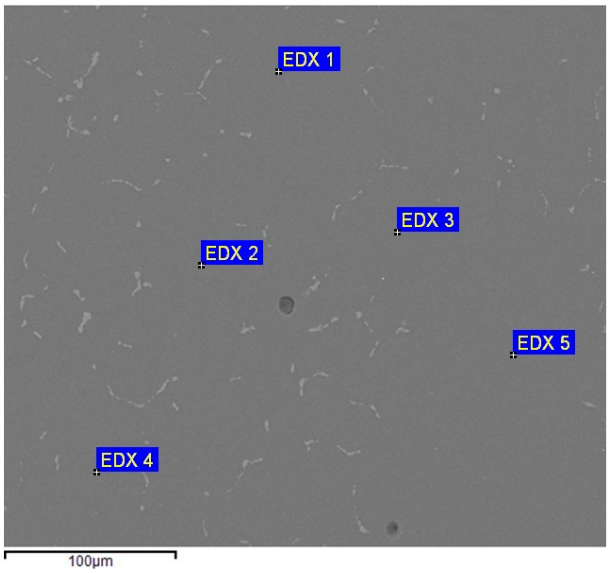

Figure 9.17 Spot EDX analysis III sample wq

Table 9.15 EDX results III sample wq

Element atom[%]	Magnesium Mg	Aluminium Al	Silicon Si	Iron Fe	Manganese Mn	Chromium Cr	Type
EDX 1	0.8	98.2	0.9	0.0	0.0	0.0	Matrix
EDX 2	1.0	97.7	0.9	0.0	0.2	0.2	Matrix
EDX 3	1.0	97.6	1.2	0.0	0.2	0.0	Matrix
EDX 4	1.1	97.5	1.0	0.2	0.1	0.1	Matrix+AlFeSi
EDX 5	1.0	97.6	1.0	0.0	0.3	0.1	Matrix

9.4 TEM Analysis

9.4.1 Mg/Si Particles

9.4.1.1 Small Mg/Si Particles inside the Grain

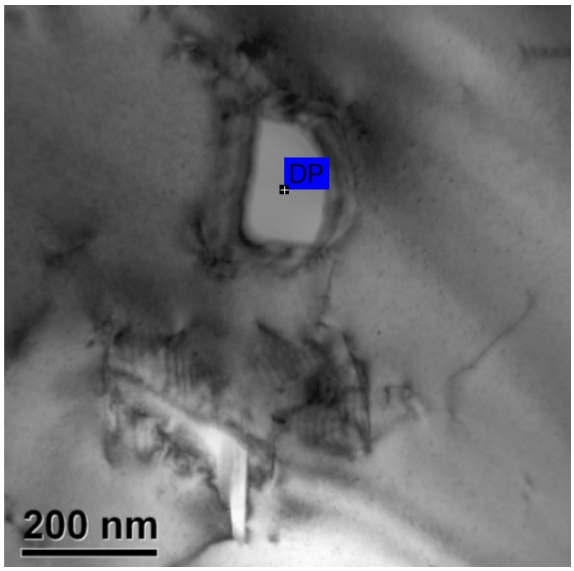

Figure 9.18 Mg_2Si particle, 200 x 150nm

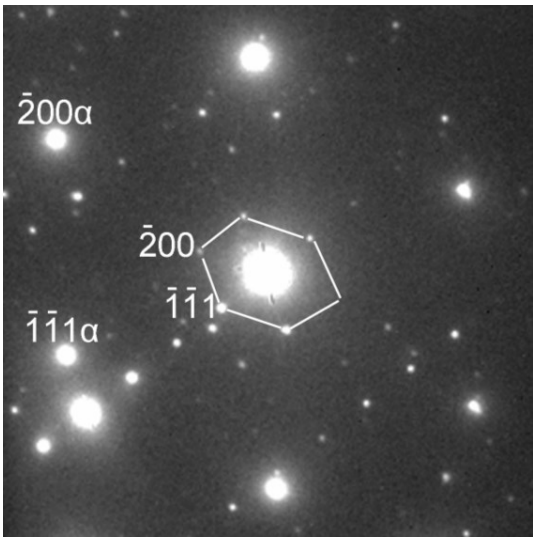

Diffraction pattern

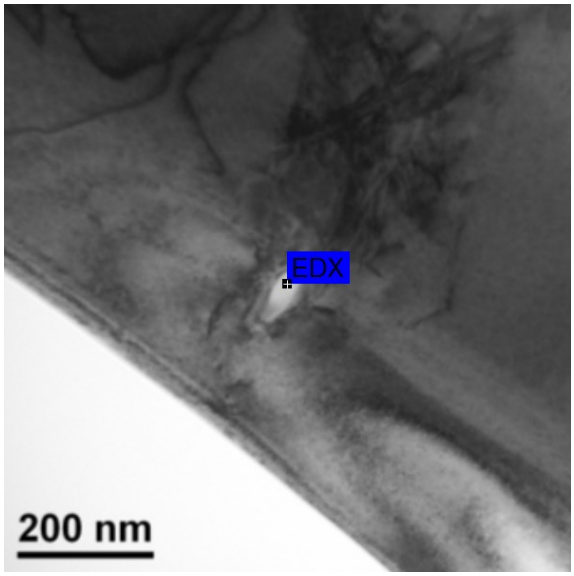

Figure 9.19 Mg_2Si particle, 100 x 50nm

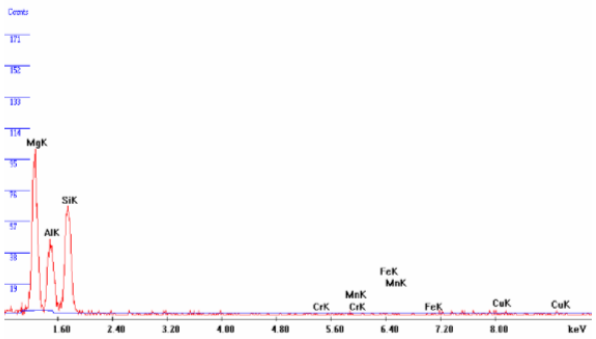

EDX-result

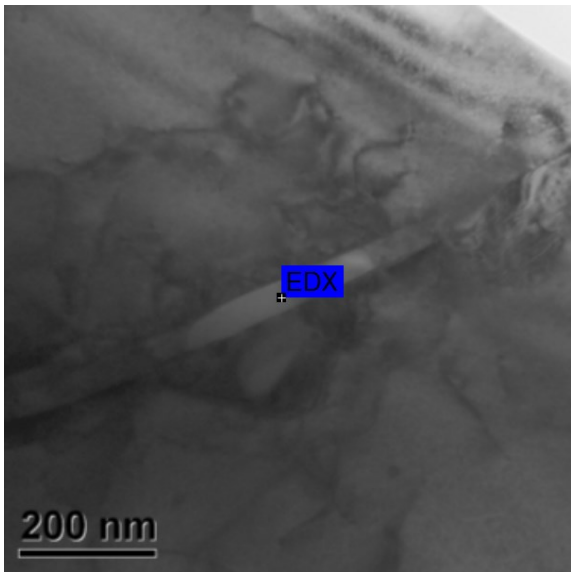

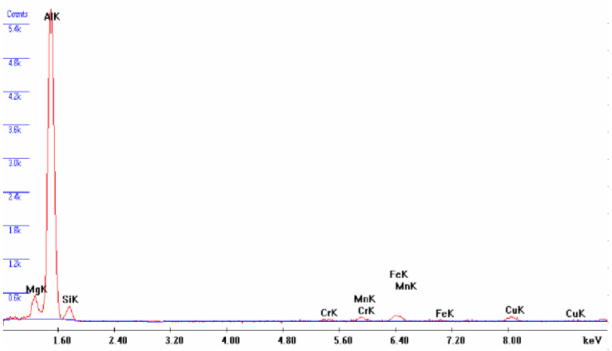

EDX-result

Figure 9.20 Mg_2Si particle, 1000 x 40nm

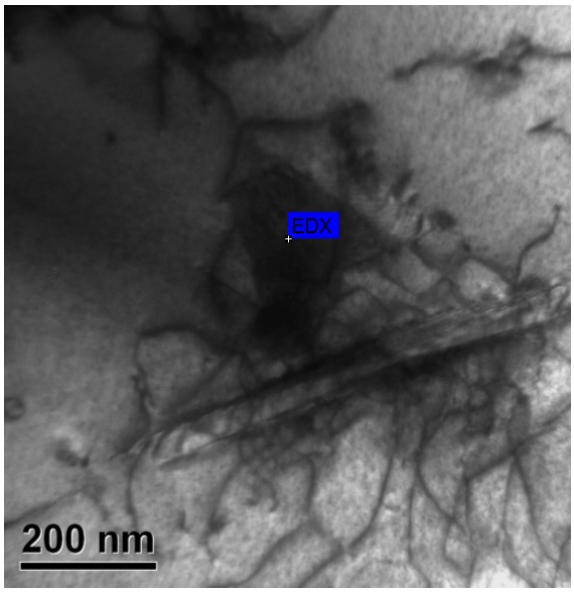

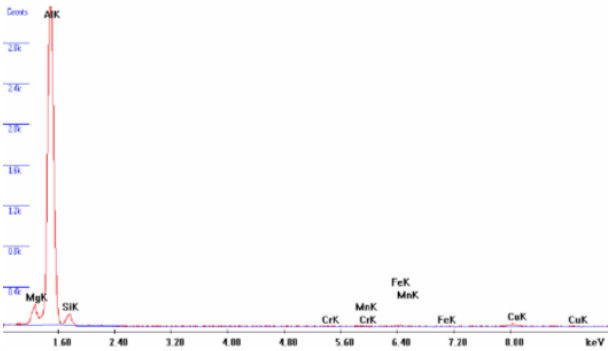

EDX-result

Figure 9.21 Mg_2Si particle, 150 x 150nm

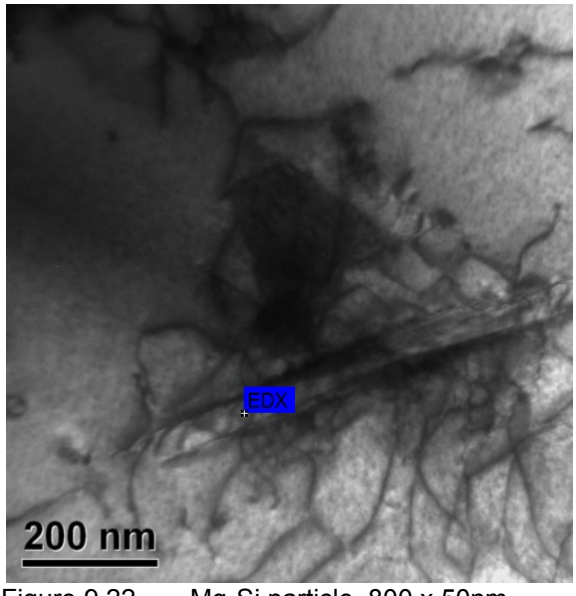

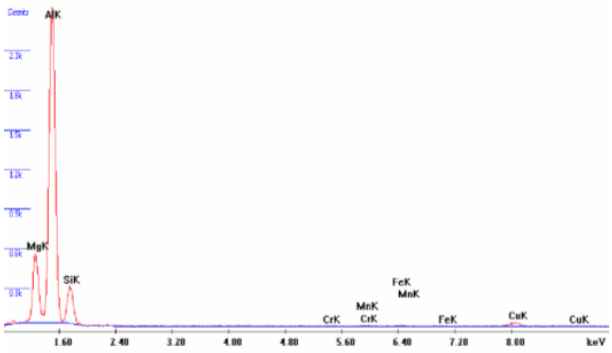

EDX-result

Figure 9.22 Mg_2Si particle, 800 x 50nm

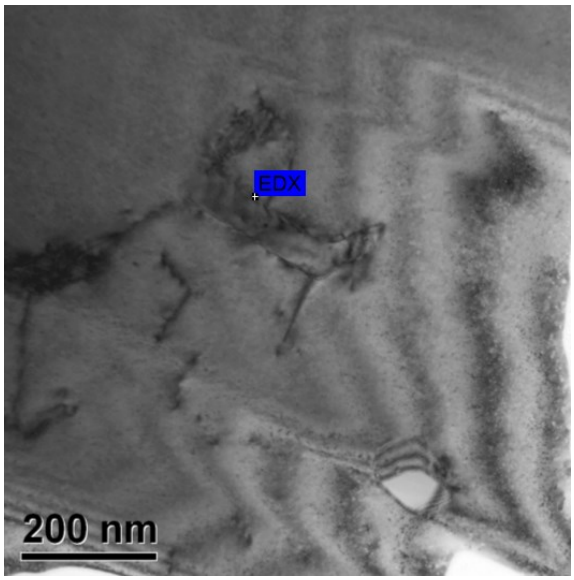

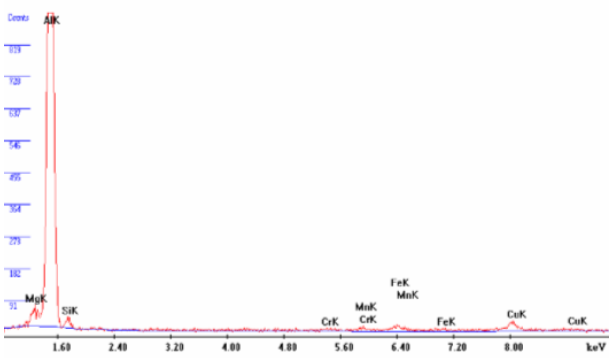

EDX-result

Figure 9.23 Mg_2Si particle, 300 x 150nm

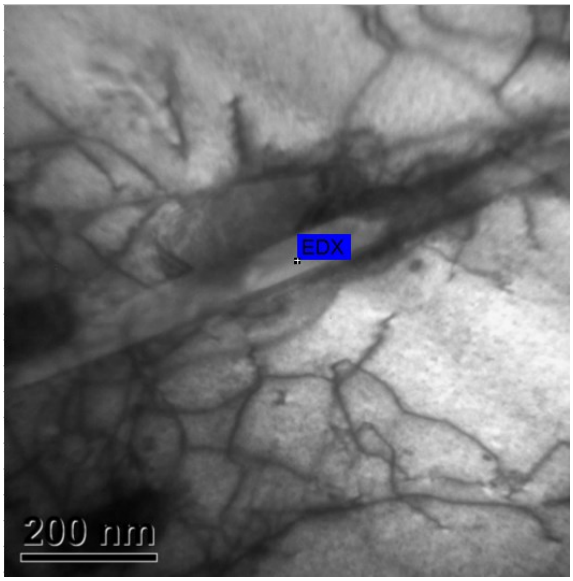

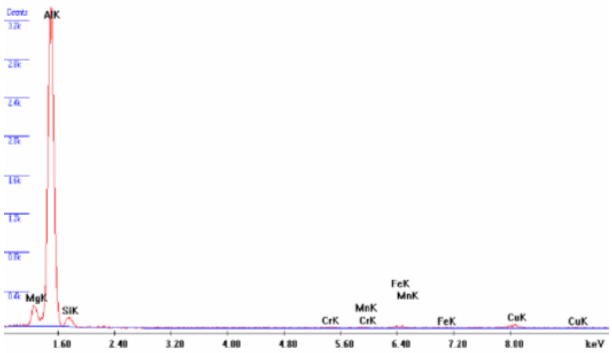

EDX-result

Figure 9.24 Mg_2Si grown on AlFeSi, 800 x 50nm

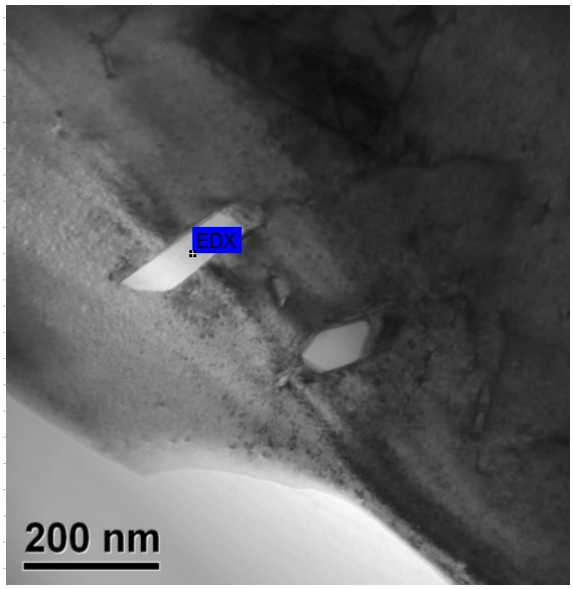

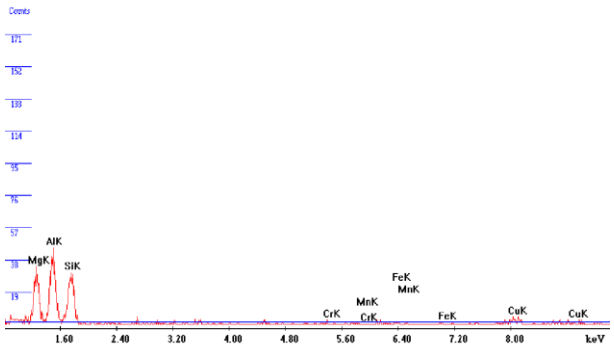

EDX-result

Figure 9.25 U2-AlMgSi particle, 200 x 50nm

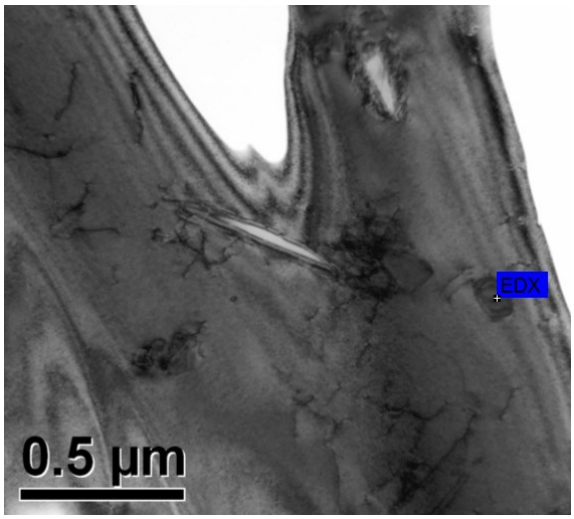

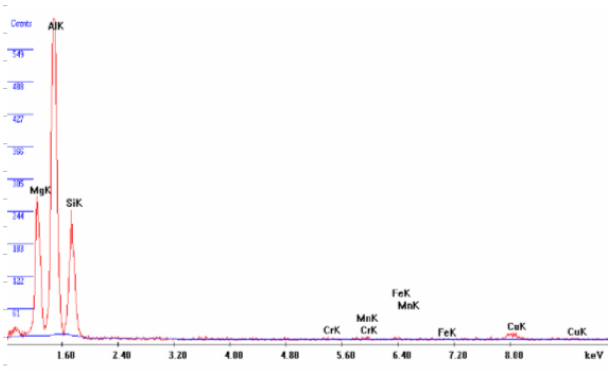

EDX-result

Figure 9.26 U2-AlMgSi particle, 100 x 100nm

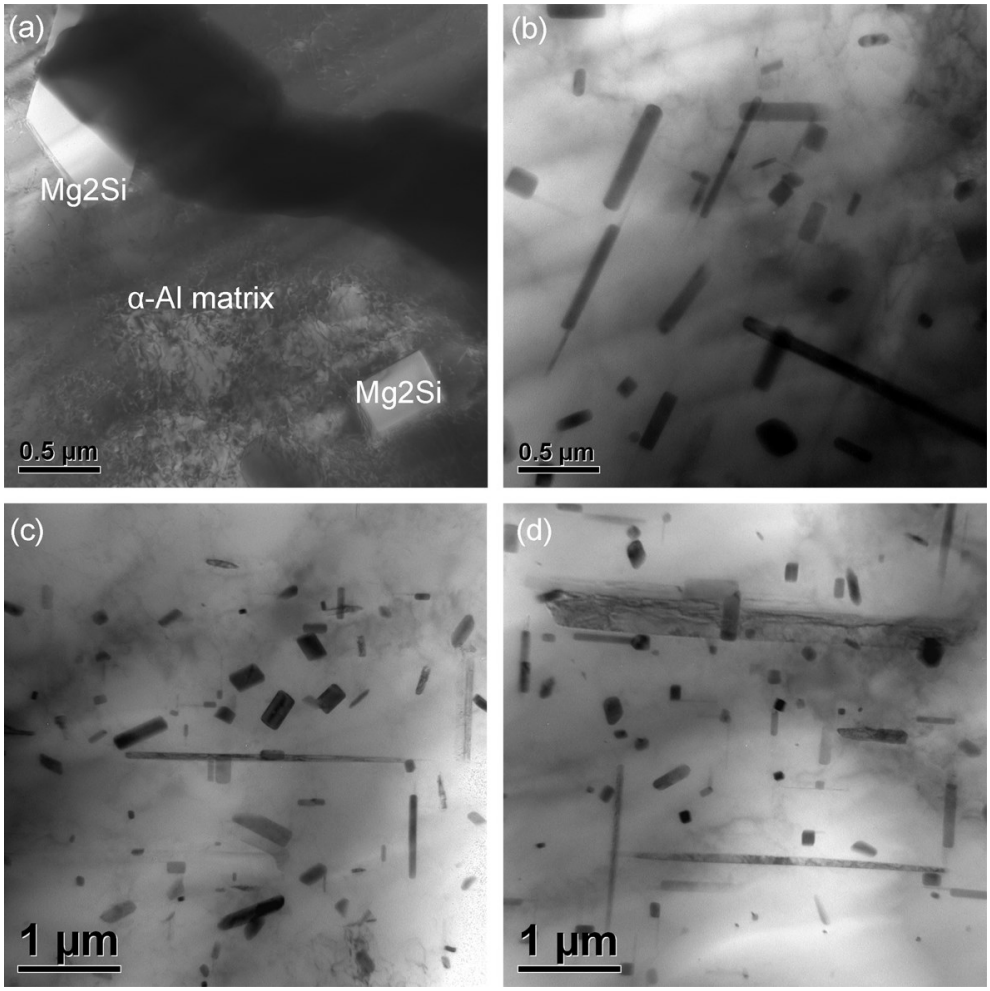

Figure 9.27 Mg_2Si, β'', β' and β inside the grains

9.4.1.2 Large Mg/Si Particles on the Grain Boundary

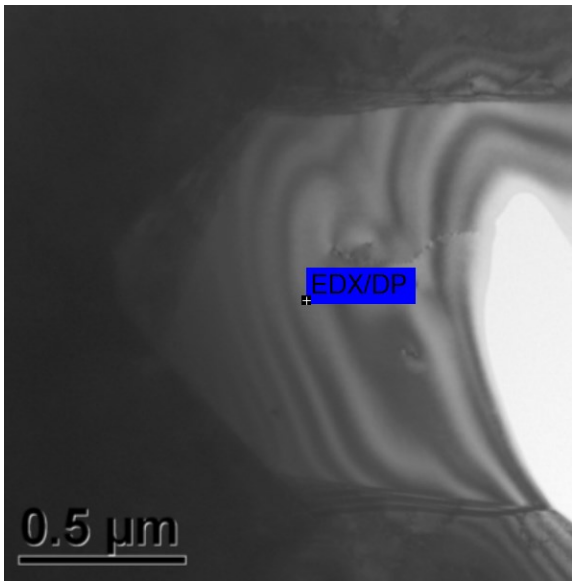

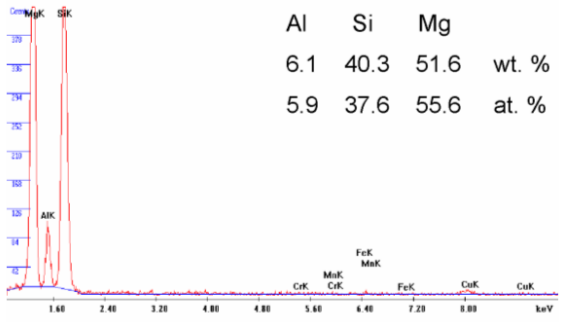

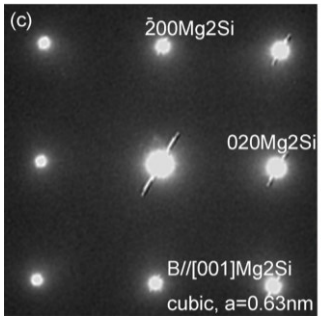

EDX-result, diffraction pattern

Figure 9.28 Mg_2Si particle, Mg:Si = 1.48, >2 x 1µm

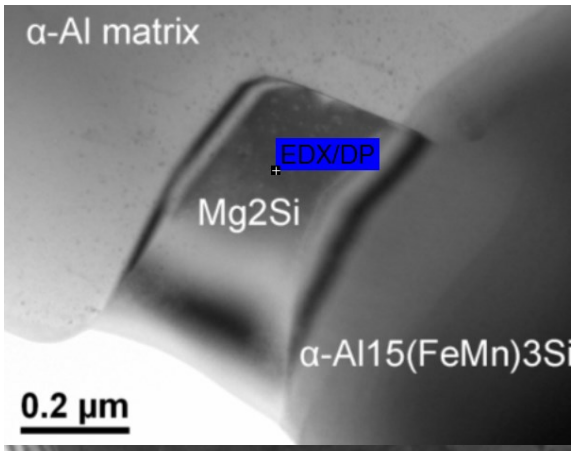

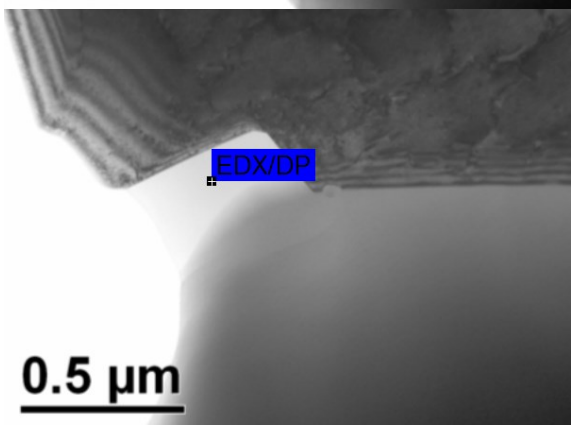

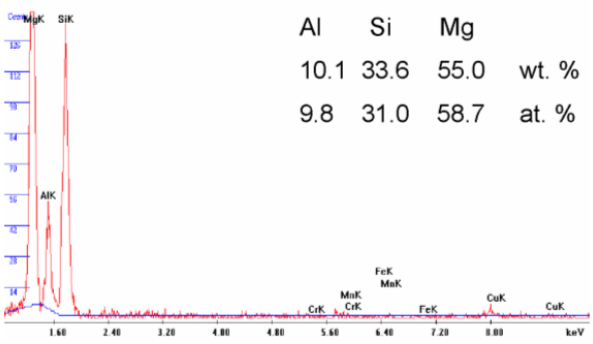

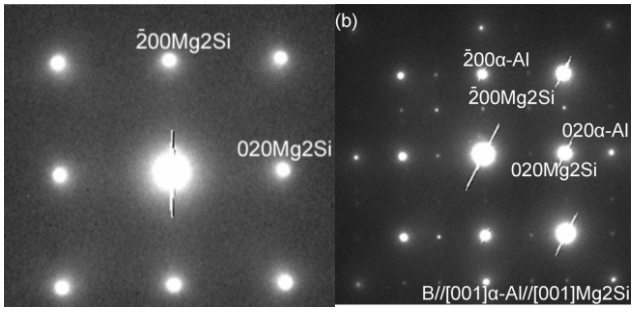

EDX-result, diffraction pattern

Figure 9.29 Mg_2Si particle, Mg:Si=1.89, 200 x 500nm

9.4.2 AlFeSi Particles

9.4.2.1 Small AlFeSi Particles inside the Grain

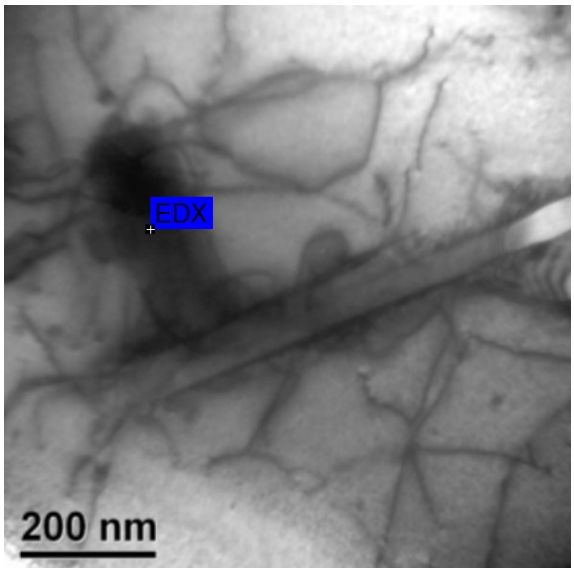

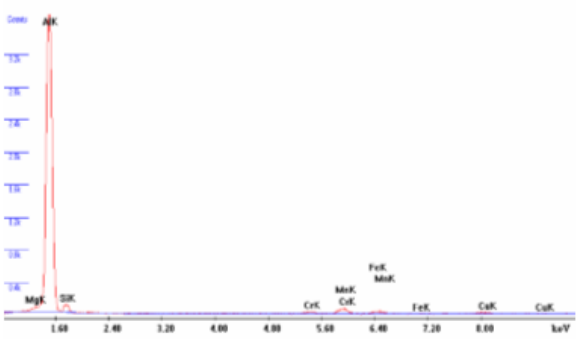

EDX-result

Figure 9.30 AlFeSi particle, Mn rich, 300 x 100nm

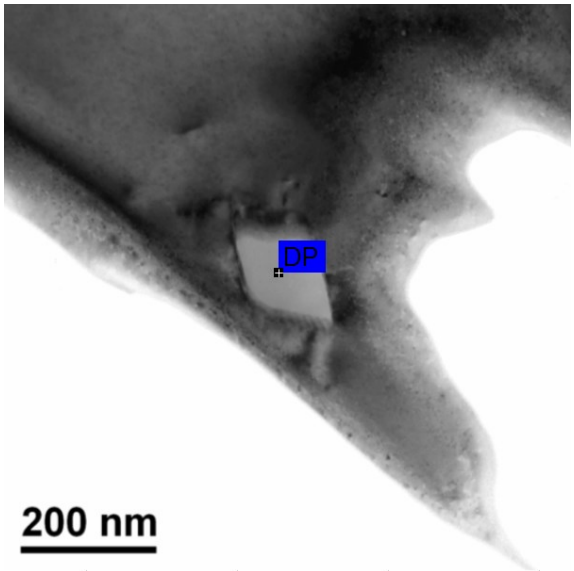

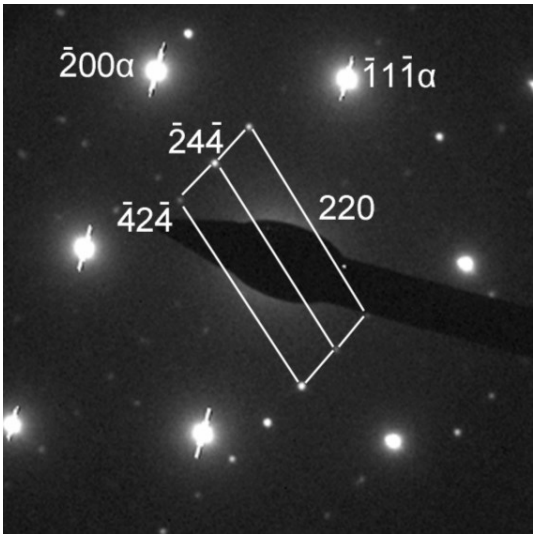

Diffraction pattern

Figure 9.31 α-AlFeSi particle, 150 x 150nm

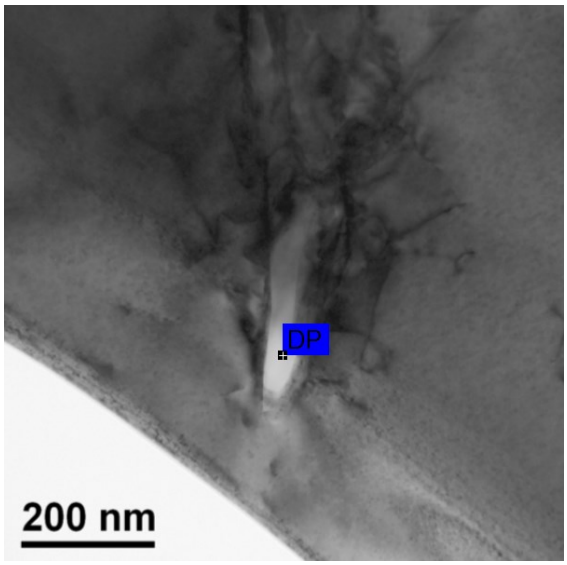

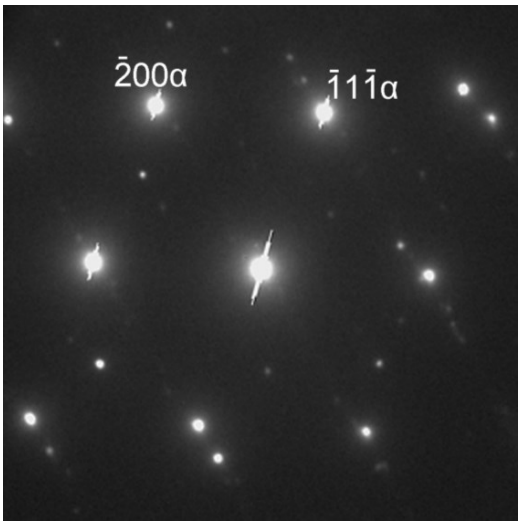

Diffraction pattern

Figure 9.32 α-AlFeSi particle, 300 x 50nm

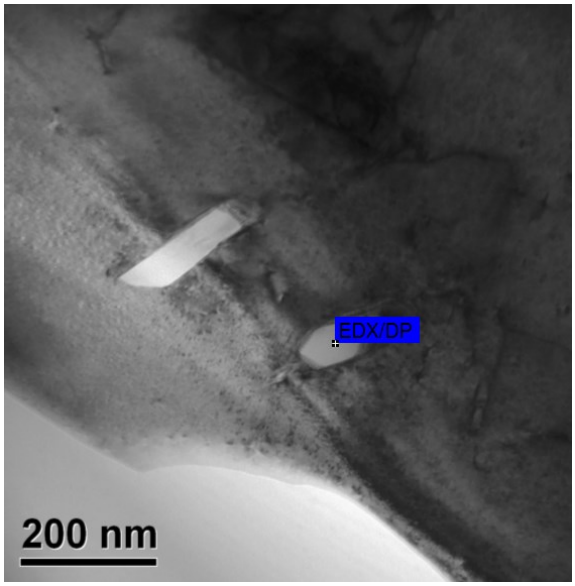

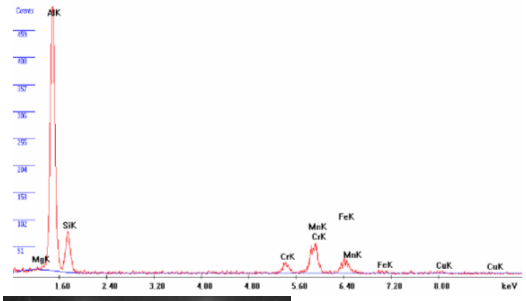

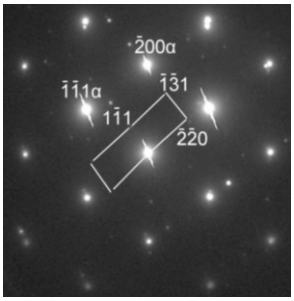

EDX-result, diffraction pattern

Figure 9.33 α-AlFeSi particle, Mn rich, 100 x 50nm

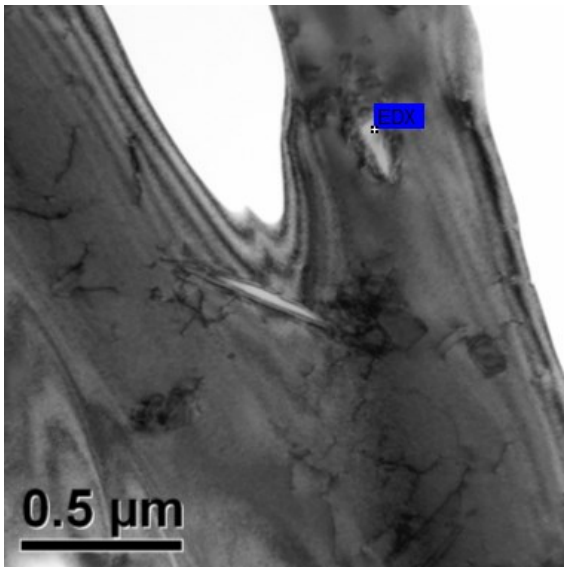

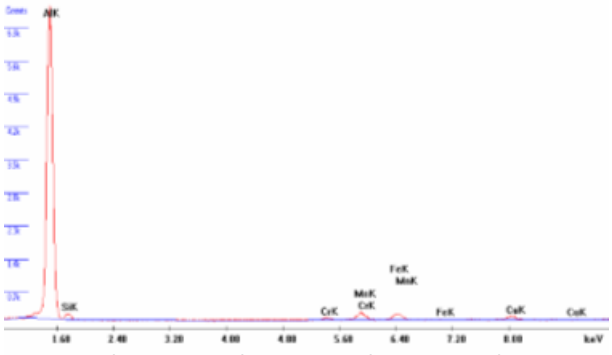

EDX-result

Figure 9.34 AlFeSi particle, Mn rich, 200 x 100nm

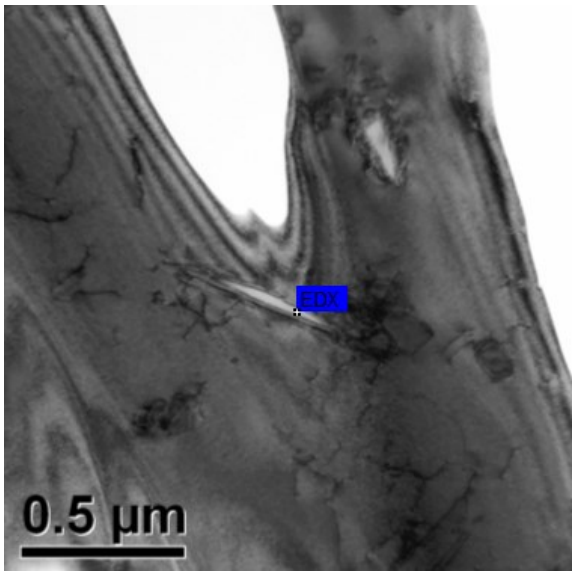

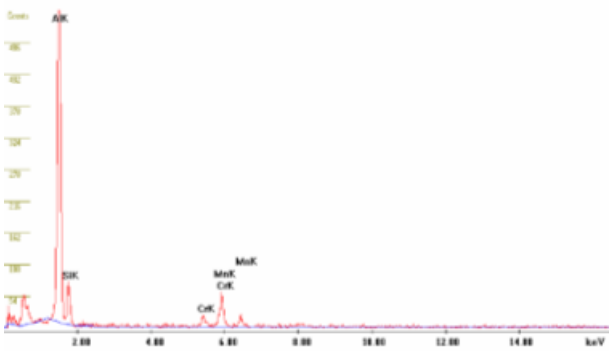

EDX-result

Figure 9.35 AlFeSi particle, Mn rich, 500 x 50nm

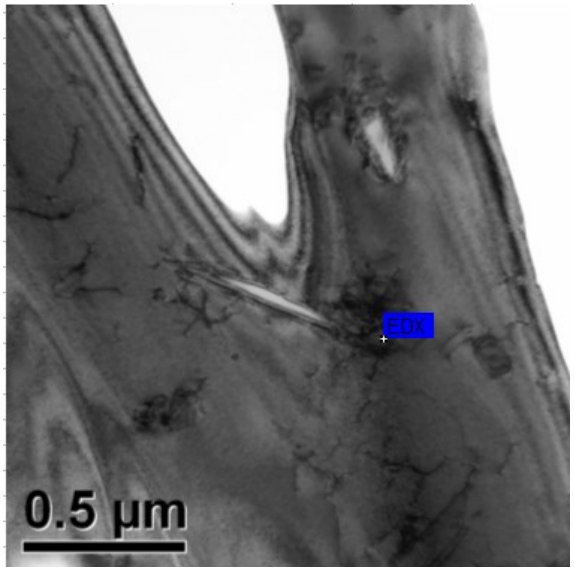

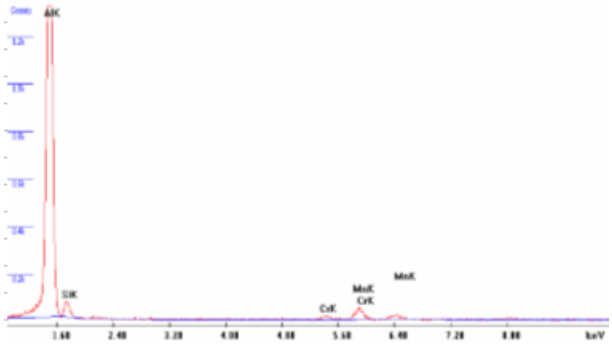

EDX-result

Figure 9.36 AlFeSi particle, Mn rich, 100 x 100nm

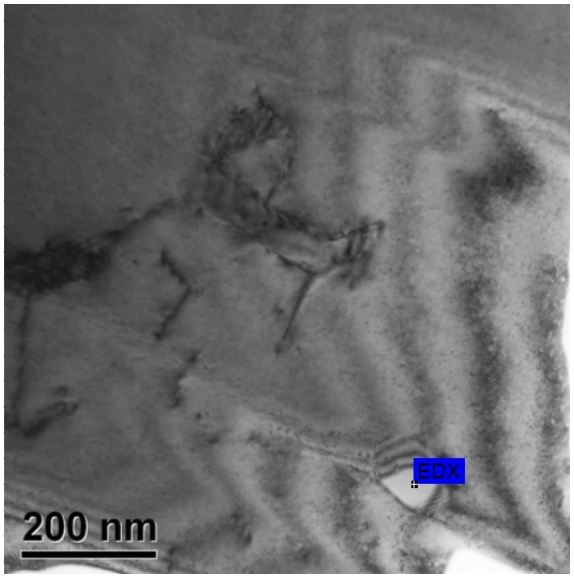

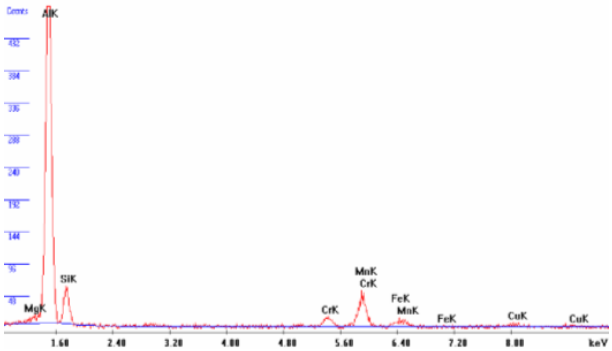

EDX-result

Figure 9.37 AlFeSi particle, Mn rich, 100 x 100nm

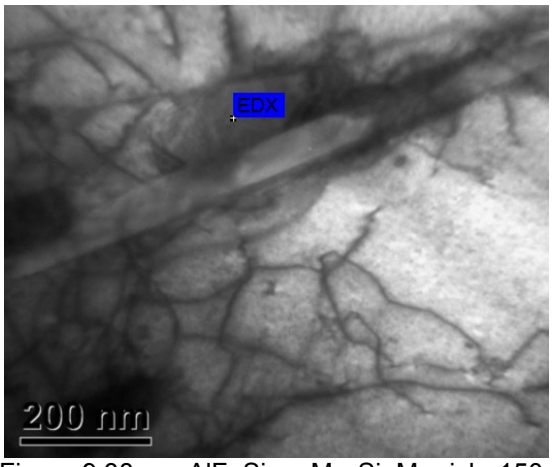

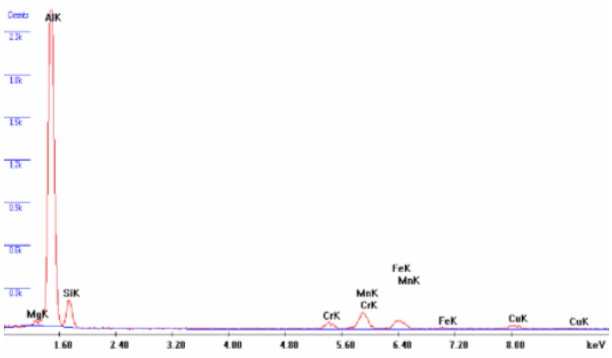

EDX-result

Figure 9.38 AlFeSi on Mg_2Si, Mn rich, 150 x 100nm

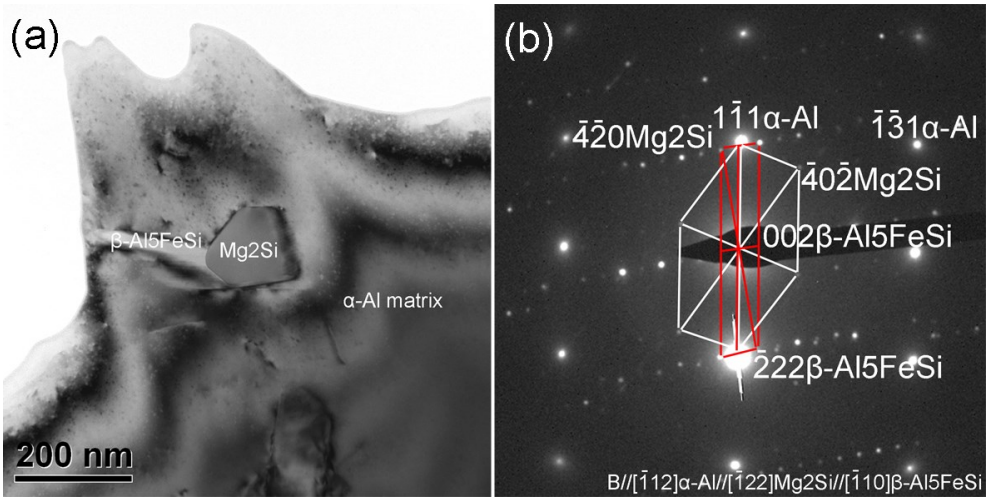

Figure 9.39 Mg_2Si and β-AlFeSi, size ~200nm

9.4.2.2 Large AlFeSi Particles on the Grain Boundary

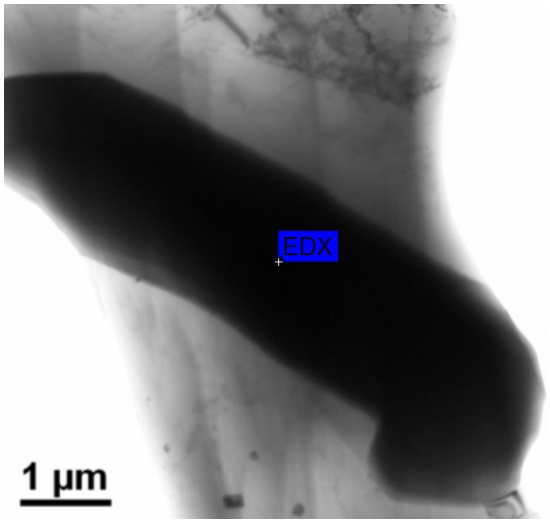

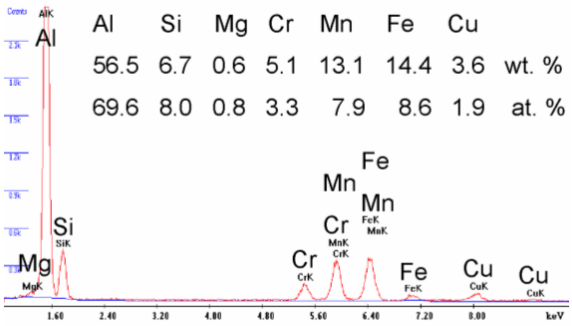

EDX-result

Figure 9.40 α-AlFeSi particle, >10 x 2µm

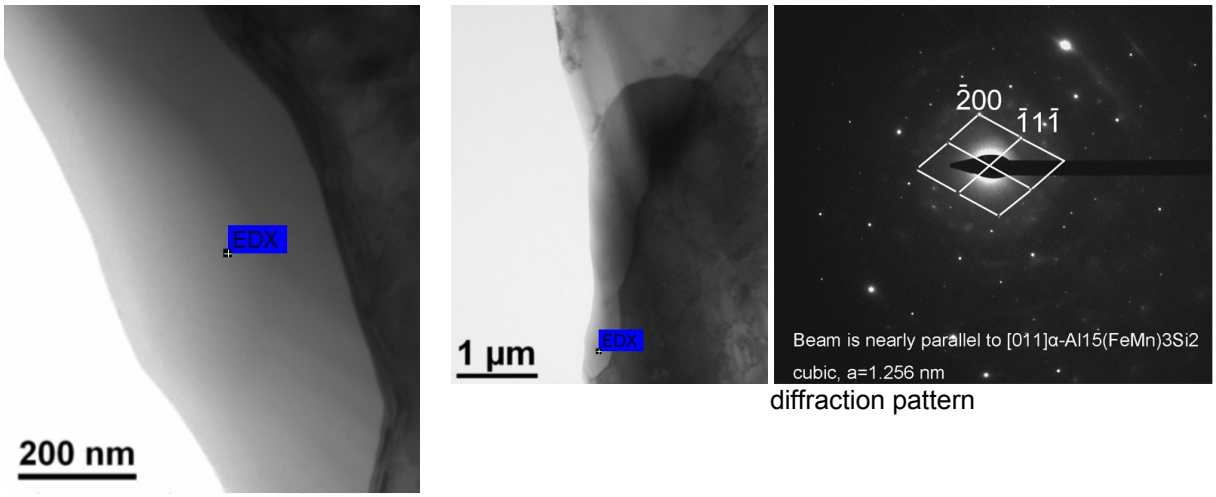

diffraction pattern

Figure 9.41 α-AlFeSi particle, 5 x 1µm

9.4.3 EDX Analysis (TEM)

For further information about the particles on the grain boundary 40 particles were analyzed. 24 AlFeSi, 11 Mg_2Si, two Si, one $(Al,Mg)_2Si$, one Al_4Ca and one U2-AlMgSi were detected.

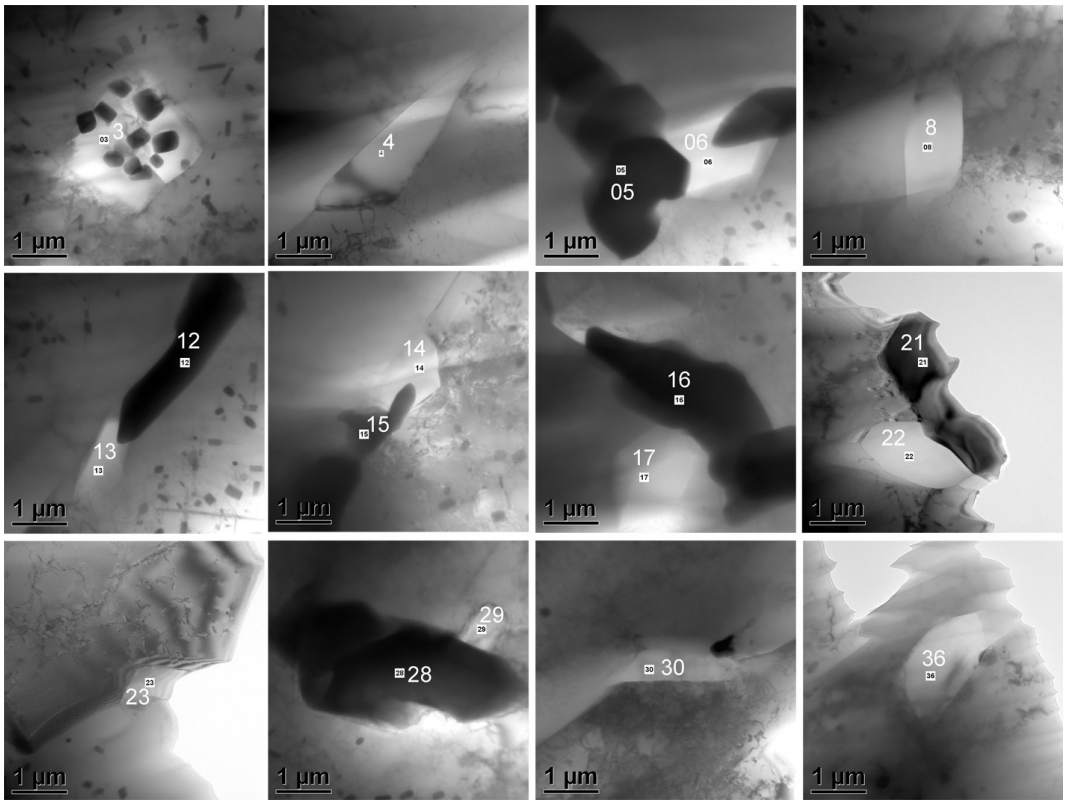

Figure 9.42 Mg_2Si particles, size 1-5µm

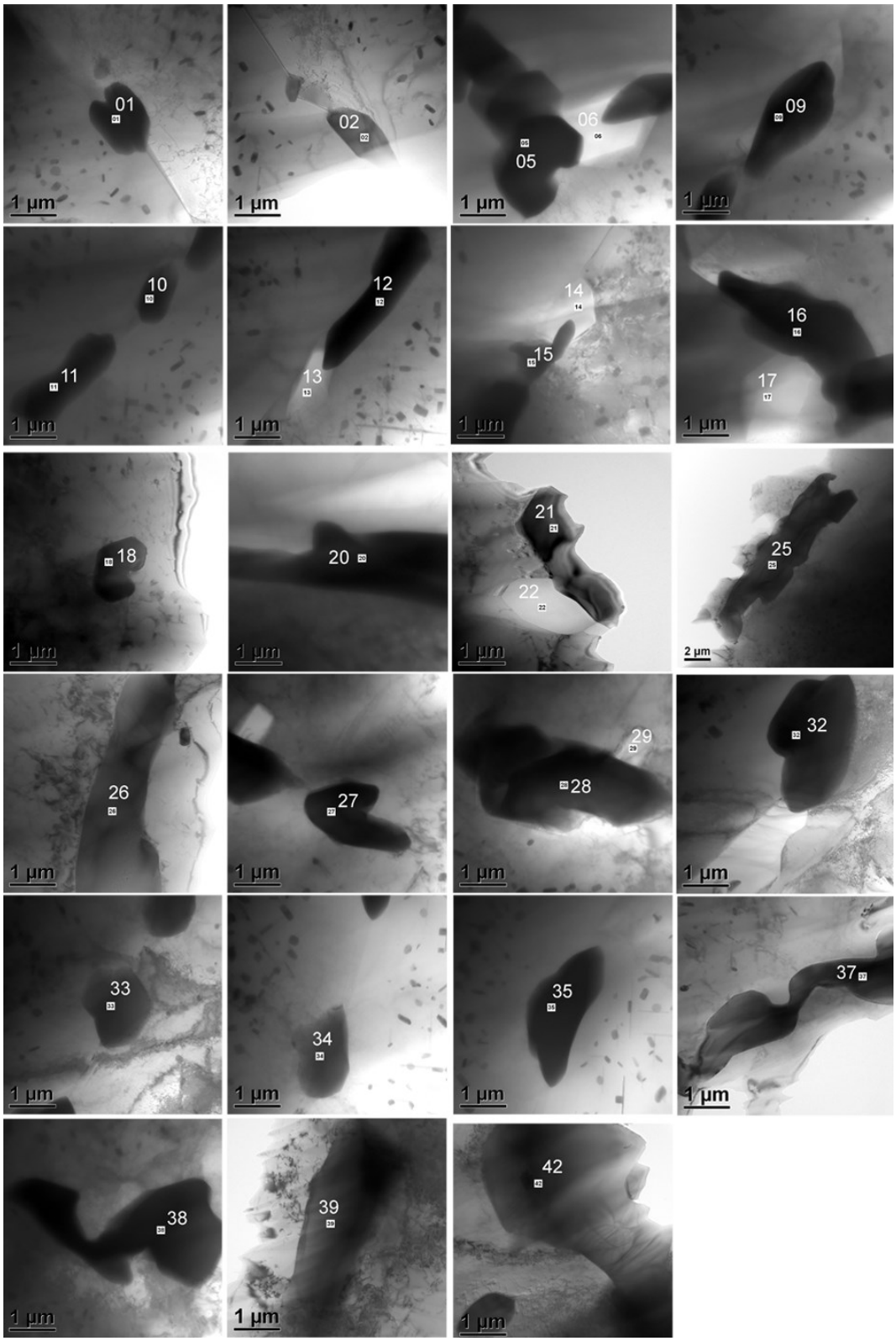

Figure 9.43 $Al_{15}Fe_3Si_2$ particles, size 1-10µm

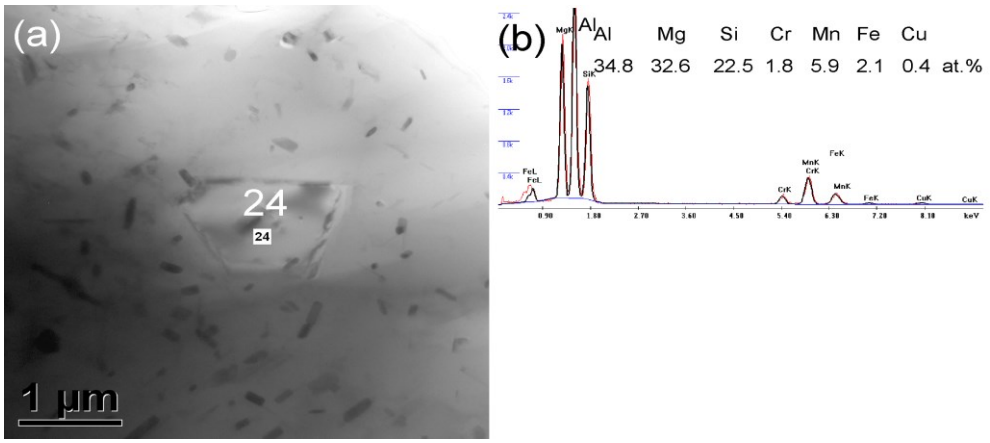

Figure 9.44 U2-AlMgSi particle, 1 x 2µm

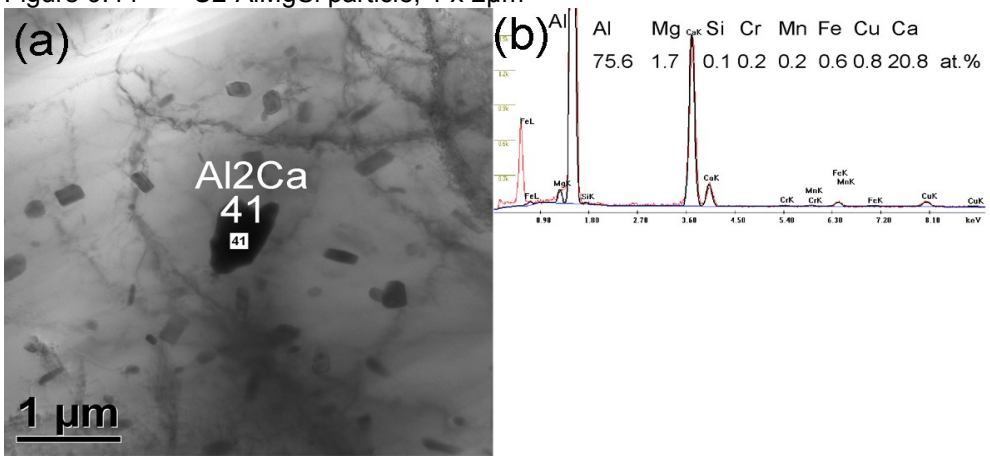

Figure 9.45 Al_4Ca particle, 500 x 500nm

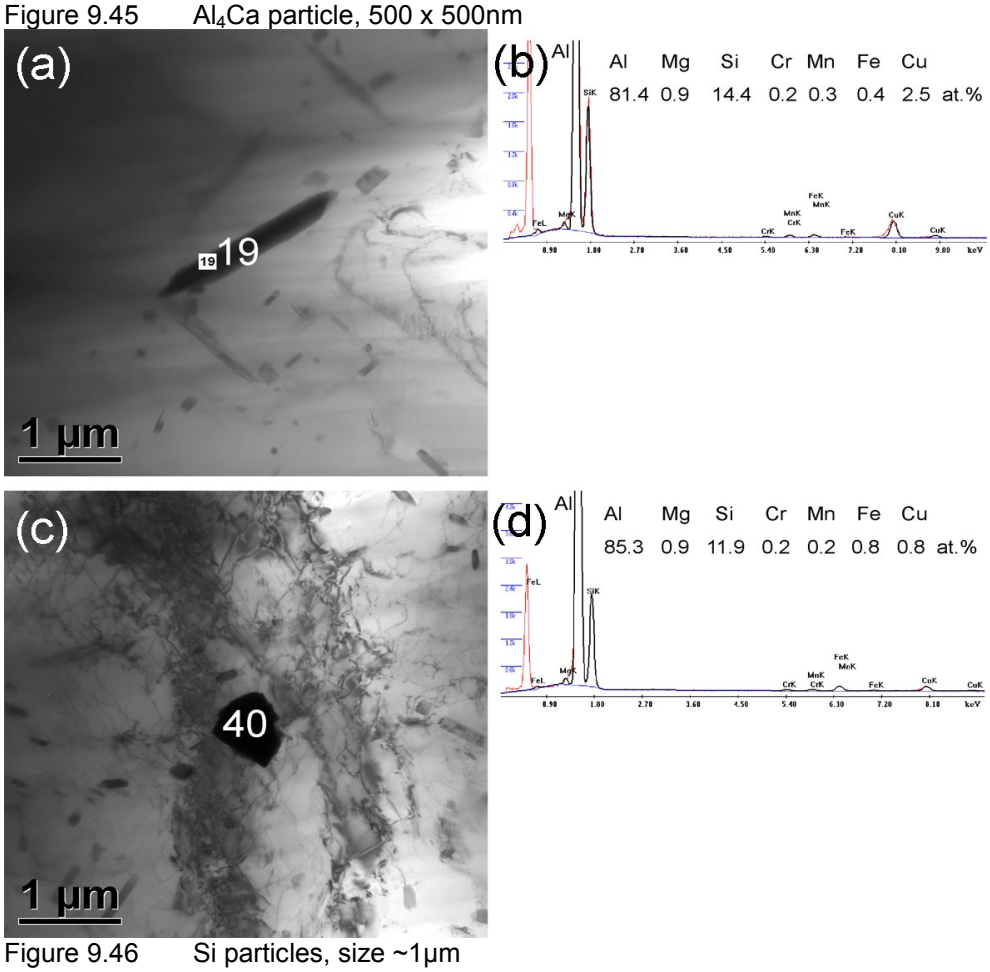

Figure 9.46 Si particles, size ~1µm

Table 9.16 EDX results TEM

Element atom[%]	Magnesium Mg	Aluminium Al	Silicon Si	Chromium Cr	Manganese Mn	Iron Fe	Type
EDX 1	1.6	69.0	8.8	1.5	7.5	11.6	$Al_{15}Fe_3Si_2$
EDX 2	0.7	69.7	11.9	2.0	8.4	7.3	$Al_{15}Fe_3Si_2$
EDX 3	63.1	7.5	28.5	0.2	0.1	0.5	Mg_2Si
EDX 4	64.5	3.5	31.4	0.1	0.2	0.3	Mg_2Si
EDX 5	0.8	71.5	7.3	1.7	8.5	10.1	$Al_{15}Fe_3Si_2$
EDX 6	69.9	4.5	25.2	0.1	0.1	0.2	Mg_2Si
EDX 7	1.3	97.7	0.4	0.1	0.2	0.3	Matrix
EDX 8	67.9	3.0	28.9	0.1	0.0	0.1	Mg_2Si
EDX 9	1.0	74.4	7.3	1.5	6.3	9.5	$Al_{15}Fe_3Si_2$
EDX 10	7.4	68.9	8.9	1.4	6.2	7.3	$Al_{15}Fe_3Si_2$
EDX 11	1.0	77.7	6.9	1.2	5.7	7.6	$Al_{15}Fe_3Si_2$
EDX 12	0.9	79.4	5.5	1.7	6.8	5.8	$Al_{15}Fe_3Si_2$
EDX 13	61.6	13.8	23.9	0.1	0.1	0.4	Mg_2Si
EDX 14	60.5	14.2	24.1	0.2	0.2	0.8	Mg_2Si
EDX 15	1.1	84.8	5.1	0.9	3.8	4.3	$Al_{15}Fe_3Si_2$
EDX 16	1.0	71.3	8.2	2.3	9.4	7.8	$Al_{15}Fe_3Si_2$
EDX 17	62.6	12.9	23.6	0.2	0.2	0.4	Mg_2Si
EDX 18	1.2	69.4	9.6	1.4	7.0	11.5	$Al_{15}Fe_3Si_2$
EDX 19	0.9	83.4	14.8	0.2	0.3	0.4	Si
EDX 20	0.7	72.6	7.6	1.4	6.9	10.8	$Al_{15}Fe_3Si_2$
EDX 21	0.5	71.1	10.9	1.2	5.6	10.7	$Al_{15}Fe_3Si_2$
EDX 22	47.9	12.7	39.0	0.0	0.1	0.3	$(Mg,Al)_2Si$
EDX 23	63.9	5.0	30.6	0.2	0.1	0.2	Mg_2Si
EDX 24	32.7	34.8	22.6	1.8	5.9	2.1	U2-AlMgSi
EDX 25	0.7	78.1	6.6	1.1	5.3	8.1	$Al_{15}Fe_3Si_2$
EDX 26	0.7	71.7	10.1	1.4	6.0	10.2	$Al_{15}Fe_3Si_2$
EDX 27	0.8	72.0	8.8	1.3	6.6	10.5	$Al_{15}Fe_3Si_2$
EDX 28	0.8	73.2	8.3	1.5	6.8	9.3	$Al_{15}Fe_3Si_2$
EDX 29	66.1	7.0	26.8	0.0	0.0	0.1	Mg_2Si
EDX 30	59.7	14.2	25.0	0.2	0.2	0.7	Mg_2Si
EDX 31	1.7	97.3	0.2	0.1	0.2	0.5	Matrix
EDX 32	0.7	71.2	9.8	2.1	9.3	6.8	$Al_{15}Fe_3Si_2$
EDX 33	0.7	70.7	10.1	2.2	9.0	7.2	$Al_{15}Fe_3Si_2$
EDX 34	0.8	77.1	8.3	1.6	6.5	5.6	$Al_{15}Fe_3Si_2$
EDX 35	0.9	72.0	8.3	2.3	8.7	7.7	$Al_{15}Fe_3Si_2$
EDX 36	64.5	4.7	30.4	0.1	0.1	0.2	Mg_2Si
EDX 37	0.6	71.8	9.7	1.9	6.9	9.1	$Al_{15}Fe_3Si_2$
EDX 38	0.9	71.5	8.1	1.6	7.0	10.9	$Al_{15}Fe_3Si_2$
EDX 39	0.9	71.1	10.8	2.1	7.0	8.0	$Al_{15}Fe_3Si_2$
EDX 40	0.9	85.9	12.0	0.2	0.2	0.8	Si
EDX 41	1.7	76.4+20.8Ca	0.1	0.2	0.2	0.6	Al_4Ca
EDX 42	0.6	71.8	8.5	2.1	7.3	9.6	$Al_{15}Fe_3Si_2$